THE ROLE OF NUCLEAR ARCHITECTURE IN DNA REPAIR

by

Kathleen Attwood

Submitted in partial fulfillment of the requirements
for the degree of Doctor of Philosophy

at

Dalhousie University
Halifax, Nova Scotia
July 2016

TABLE OF CONTENTS

LIST OF TABLES

LIST OF FIGURES

viii

ABSTRACT

Precise replication of genetic material and the maintenance of genome integrity by DNA repair mechanisms are critical processes in all organisms. The inaccurate repair or accumulation of unrepaired errors can overwhelm the cell resulting in senescence, apoptosis or cancer development. DNA lesions must be identified and efficiently repaired in the context of a highly compartmentalized nucleus, consisting of discrete chromosome territories interspersed among many specialized, functionally distinct subnuclear domains. Disruption of some of these domains or of nuclear structural components is known to result in increased genomic instability. To further understand the contributions of nuclear architecture and organization to the maintenance of genomic integrity, I investigated the roles of polymerized nuclear actin, the nuclear lamina and PML nuclear bodies on DNA repair efficiency.

I identified a novel role for nuclear actin in the non-homologous end-joining pathway of DNA repair. Altering the polymerization state of nuclear actin was found to negatively impact the retention of the GFP-tagged damage-sensing protein Ku80 at sites of DNA damage in live cells. Additionally, I examined DNA repair efficiency at the nuclear lamina in relation to chromatin ultrastructure using electron microscopy, finding that the delay in DNA repair at this nuclear compartment was due to associated heterochromatin. Finally, I investigated the role of PML isoforms and PML nuclear bodies in DNA repair. Using genome engineering, I created versatile cell lines containing a single copy of a DNA repair reporter integrated at defined nuclear locations. Using these cell lines, homologous recombination was found to be decreased when a DNA break occurred within chromatin significantly associated with PML nuclear bodies compared to an unassociated DNA break. Additionally, using these cell lines along with wild-type U2OS and a U2OS PML knockout cell line, I demonstrated that PML isoform overexpression, notably that of PML I, II and IV, leads to significant inhibition of both homologous recombination and non-homologous end joining, suggesting an early role for PML/PML nuclear bodies in DNA repair.

Collectively, these results demonstrate a complex involvement of nuclear organization and DNA repair, and that the maintenance of genomic stability is intimately linked to nuclear architecture.

LIST OF ABBREVIATIONS USED

γ-H2AX   phosphorylated H2AX

53BP1   p53-binding protein 1

ALT   alternative lengthening of telomeres

APB   ALT-associated PML nuclear bodies

APLF   Aprataxin-and-PNK-like factor

ATM   ataxia-telangiectasia mediated

ATR   ATM and Rad3-related

ATRIP   ATR-interacting partner

BARD1   BRCA1-associated RING domain 1

BCL2   B-cell lymphoma 2

BIR   break-induced replication

BLM   Bloom syndrome helicase

BRCA1   breast cancer 1, early onset

BRCA2   breast cancer 2, early onset

BSA   bovine serum albumin

BSK   pBluescript

Cas9   CRISPR-associated protein-9

CDK   cyclin-dependent kinase

CHD3   chromodomain helicase DNA-binding protein 3

CHD4   chromodomain helicase DNA-binding protein 4

CHK1   checkpoint effector kinase 1

CHK2   checkpoint effector kinase 2

Chr15	chromosome 15
CMV	cytomegalovirus
CRISPR	clustered regularly interspaced short palindromic repeats
CtIP	carboxy-terminal binding protein-interacting protein
CV	coefficient of variation
DAPI	4'6-diamidino-2-phenylindole
DAXX	death domain-associated protein
DDR	DNA damage response
dH_2O	distilled water
DIG	digoxigenin
D-loop	displacement loop
DMEM	Dulbecco's modified Eagle's medium
DMSO	dimethyl sulfoxide
DNA-PKcs	DNA-dependent protein kinase, catalytic subunit
DSB	double-strand break
DSBR	double-strand break repair
EDTA	ethylenediaminetetraacetic acid
EM	electron microscopy
ESI	electron spectroscopic imaging
FAR	fraction of activity released
FBS	fetal bovine serum
FHA	forkhead-associated
FISH	fluorescence in-situ hybridization

FRT	FLP recombination target
gRNA	guide RNA
HDAC1	histone deacetylase 1
HDAC2	histone deacetylase 2
HERC2	HECT and RLD domain containing E3 ubiquitin protein ligase 2
HJ	Holliday junction
HR	homologous recombination
IR	ionizing radiation
JMJD2A	jumonji domain 2A
JMY	junction-mediating and regulatory protein
KAP1	KRAB domain-associated protein 1
LacI	Lac repressor
LacO	Lac operator array
LIG4	DNA Ligase IV
LOH	loss of heterozygosity
loxP	locus of X(cross)-over in P1
MDC	mediator of DNA damage checkpoint 1
MHC	major histocompatibility complex
MMS	methyl methanosulfate
MRE11	meiotic recombination 11
MRN	MRE11/RAD50/NBS1
NBS1	Nijmegen breakage syndrome 1
NHEJ	non-homologous end-joining

NLS	nuclear localization signal
NuRD	nucleosome remodeling deacetylase
PAR	poly(ADP-ribose)
PARP1	poly(ADP-ribose) polymerase 1
PARP2	poly(ADP-ribose) polymerase 2
PAXX	paralog of XRCC4 and XLF
PB	PiggyBac
PCR	polymerase chain reaction
PFA	paraformaldehyde
PGK	phosphoglycerate kinase 1
PI	propidium iodide
PIAS1	protein inhibitor of activated STAT 1
PIAS4	protein inhibitor of activated STAT 4
PIKK	phosphatidylinositol 3-kinase-related kinase
PML	promyelocytic leukemia
PNPK	polynucleotide kinase/phosphatase
RAP80	receptor-associated protein 80
RBCC	ring finger, B-box and coiled coil
RNF168	ring finger protein 168
RNF8	ring finger protein 8
ROS	reactive oxygen species
RPA	replication protein A
RPMI	Roswell Park Memorial Institute

SD	standard deviation
SDS	sodium dodecyl sulphate
SDSA	synthesis-dependent strand annealing
SIM	SUMO-interacting motif
SSB	single-strand break
SSC	saline sodium citrate
SUMO	small ubiquitin-like modifier
TAP1	transporter associated with antigen processing 1
TOPBP1	topoisomerase binding partner 1
TR	terminal repeats
TRIM	tripartite motif
TSA	trichostatin A
UV	ultraviolet
WRN	Werner syndrome RecQ like helicase/nuclease
XLF	XRCC4-like factor
XRCC4	X-ray cross-complementing protein 4

ACKNOWLEDGEMENTS

CHAPTER 1. INTRODUCTION

This chapter contains material (section 1.3, 1.3.1, 1.3.5) originally published in:

"Pinder JB, Attwood KM, and Dellaire G. 2013. Reading, writing, and repair: the role of ubiquitin and the ubiquitin-like proteins in DNA damage signaling and repair. Frontiers in Genetics. 4:45"

1.1 Endogenous and exogenous sources of DNA damage

DNA is the carrier of genetic information and as such its structural maintenance and faithful replication are critical processes in all organisms. However, DNA integrity is continuously being threatened by insults arising from both exogenous (environmental) and endogenous (metabolic) sources. The result can be a variety of DNA lesions including damaged or modified bases, inter- and intra-strand cross-links, as well as single-strand breaks (SSBs) and double-strand breaks (DSBs) (1).

DNA can be damaged by exposure to a variety of exogenous physical and chemical agents. Ionizing radiation (IR) for instance, causes extensive base damage and produces free radicals that attack the sugar-phosphate backbone, generating SSBs and, at high doses, DSBs, while ultraviolet (UV) radiation can induce a variety of bulky chemical adducts in addition to strand breaks. Some other well-characterized exogenous DNA damaging agents are chemotherapeutic drugs, including DNA cross-linking agents such as mitomycin C and cisplatin, DNA alkylating agents like methyl methanosulfonate (MMS), and topoisomerase inhibitors such as camptothecin and etoposide (2).

Although exogenous agents can cause extensive difficult-to-repair lesions, the majority of DNA damage arises intrinsically as a result of normal cellular metabolism. Metabolic byproducts such as reactive oxygen and nitrogen species, estrogen metabolites, lipid peroxides, endogenous alkylating agents and reactive carbonyl species all cause damage to DNA (3). Most notable are reactive oxygen species (ROS), which produce one of the most common oxidative DNA adducts 8-oxoguanine as well as a multitude of other

oxidative base and sugar products. Hydroxyl free radicals can also react with DNA to cause SSBs and, if two such lesions are in close proximity on different strands, DSBs (3). Another major endogenous source of DNA damage is spontaneous hydrolysis, a direct consequence of the chemical instability of DNA in an aqueous environment. The glycosidic bond in DNA is particularly labile, and hydrolytic cleavage can lead to abasic sites (3). DNA bases are also susceptible to hydrolytic deamination, although at a much lower frequency (1).

These assaults on the genome can result in a cell suffering up to 10^5 DNA lesions per day (4), with one of the most cytotoxic being DSBs. DSBs can be caused directly by some of the exogenous agents listed above, however more commonly they occur indirectly as a result of endogenous sources like ROS or replication-associated errors, such as collapsed replication forks. DSBs are also intentionally generated in a site-specific manner during several physiologically and developmentally important processes such as V(D)J recombination in immune system development (5) and the generation of genetic diversity in meiosis (6). Failure to properly sense or repair these breaks can lead to loss of sequence information around the break site, or large-scale genomic rearrangements which can in turn fuel senescence, apoptosis or carcinogenesis (7). Therefore, DSBs present a unique challenge to cells in that their formation is required for physiologically vital processes, yet misrepair can promote genome instability.

1.2 Mechanisms of DSB repair

To prevent the potentially cytotoxic effects of unwanted DSBs while promoting the constructive effects of programmed breaks, two major repair pathways have evolved in eukaryotes: non-homologous end-joining (NHEJ) and homologous recombination (HR). NHEJ and HR are mechanistically distinct pathways that function in both a competitive and collaborative manner to maintain genomic stability by repairing DSBs.

2

1.2.1 Non-homologous end-joining

NHEJ is a highly efficient pathway that plays an essential role in repairing not only pathologic DSBs but also intentional DSBs created during V(D)J and class-switch recombination (8). As such, patients lacking, or carrying mutations in certain NHEJ components are not only sensitive to DNA-damaging agents like IR, but are also severely immunodeficient (9). NHEJ mediates the direct ligation of two broken DNA strands, irrespective of the sequence at either end, and without the use of a repair template (10). Due to the fact that NHEJ requires no sequence homology to direct repair, it is active at all stages of the cell cycle and is the predominant DSB repair pathway in mammalian cells (10, 11). Frequently, nucleotides next to the broken ends are damaged or lost and the two broken ends are directly ligated which can lead to small deletions, and therefore loss of sequence information at the break site. Consequently, NHEJ although efficient, is a more error-prone form of DSB repair. This is in direct contrast to HR, which requires extensive regions of DNA homology in the form of a sister chromatid to accurately repair DSBs and is primarily limited to the S and G2 phases of the cell cycle when such homologous templates are available (11).

The canonical NHEJ pathway consists of four key steps: i) DNA-end binding and NHEJ complex assembly ii) DNA-end juxtaposition iii) DNA-end processing and iv) DNA ligation and NHEJ complex dissolution (**Figure 1.1**). As a first step in NHEJ, the broken DNA ends are recognized and bound by a heterodimer of two highly related subunits, Ku70 and Ku80 (also known as Ku86). The Ku heterodimer is one of the first proteins recruited to DNA breaks, being shown to localize within seconds to tracks of DNA damage caused by laser-induced micro-irradiation (12, 13). The rapid response of Ku to DSBs is likely due to its high abundance (estimated at 400,000 molecules/cell) and its ability to bind DNA ends in a sequence-independent manner with strong affinity (binding constant of 2×10^9 M^{-1}) (14-17). The crystal structure of Ku70/80 reveals that the heterodimer forms a ring, allowing it to slide onto broken DNA ends. After binding to DSBs, the Ku heterodimer then serves as a scaffold for the recruitment or retention of several key NHEJ factors to the damage site including the catalytic subunit of DNA-dependent protein kinase (DNA-PKcs) (18), X-ray cross-complementing protein 4 (XRCC4), DNA ligase IV (LIG4) (12, 19, 20), XRCC4-like factor (XLF), (21)

Aprataxin-and-PNK-like factor (APLF) (22-24), and the newly identified paralog of XRCC4 and XLF (PAXX) (25, 26).

The interaction of Ku70/80 with DNA-PKcs in particular is of note. DNA-PKcs is a member of the phosphatidylinositol 3-kinase-related kinase family (PIKK) which also includes two other key members of the DNA damage response, ataxia-telangiectasia mutated (ATM) and ATM and Rad3-related (ATR) kinases (27). DNA-PKcs binding to DSBs causes the Ku heterodimer to move one helical turn inward from the break, allowing access of other factors to the break ends to conduct repair (28). In addition, DNA-PKcs itself appears to form a distinct structure with a large central channel through which DNA is threaded, mediating the formation of a synaptic complex that bridges and stabilizes the two broken ends (29, 30). Binding to DSBs also results in activation of the serine/threonine kinase activity of DNA-PKcs. Important phosphorylation targets of DNA-PKcs include itself (DNA-PKcs contains more than 15 autophosphorylation sites), Artemis endonuclease as well as XRCC4 and LIG4 (which form a complex at DSBs) (27).

DSBs, depending on how they were generated, can vary with respect to the chemical composition of the DNA ends. For instance ROS can cause base and sugar damage while IR generates DNA ends that are not in a directly ligatable form (do not contain 3'-hydroxyl and 5'-phosphate groups). Therefore, once the DNA ends have been brought together and stabilized by the combined action of Ku70/80 and DNA-PKcs, the next step, if necessary, is processing of the DNA ends to create a substrate suitable for LIG4 (7). Depending on the nature of the break, several different types of DNA end-processing enzymes may be required. Damaged nucleotides or incompatible ends can be resected back by nucleases such as Artemis, Werner syndrome RecQ-like helicase/nuclease (WRN) and APLF, with each enzyme being capable of processing an array of different types of damaged overhangs and possessing various nucleolytic activities. (31-34). Additional end-processing factors include polynucleotide kinase/phosphatase (PNKP), which is both a kinase and phosphatase dually capable of removing 3' phosphates and adding phosphate to 5' hydroxyl groups (35), and Aprataxin, which catalyzes the removal of adenylate groups at DNA ends (36). Finally, three different DNA polymerases are implicated in NHEJ end processing: terminal

deoxynucleotidyl transferase, DNA polymerase μ and DNA polymerase λ, capable of adding untemplated nucleotides to DNA ends or filling any gaps that may exist following processing (37). Each of these enzymatic components exhibits remarkable flexibility in the diverse range of substrate DNA upon which they can act. In fact, the NHEJ nucleases, polymerases and ligase are the most multifunctional and mechanistically flexible enzymes in each of their respective classes (10).

Once DNA ends have been sufficiently processed (if required), the final step in the repair of a DSB by NHEJ is ligation of the broken ends by LIG4. LIG4 is recruited to DSBs by Ku70/80, and forms a complex with a dimer of XRCC4. This XRCC4 dimer and an XRCC4-like protein, XLF (also known as Cernunnos), are required to stabilize LIG4 at the break site and stimulate its adenylation and ligase activity (38, 39). Following ligation, NHEJ components must dissociate from the former break site. DNA-PKcs autophosphorylation likely leads to its release from DNA, while the Ku heterodimer (which is thought to remain on DNA ends throughout the entire repair process) may be released *via* ubiquitination and be subsequently degraded (10).

The prevailing model of NHEJ has been this sequential recruitment of repair factors to the break site: Ku70/80 end binding followed by DNA-PKcs recruitment and activation resulting in end juxtaposition, processing and finally ligation by LIG4. However, while it was once thought that DNA-PKcs was the secondary factor at DNA breaks and was required for subsequent localization of NHEJ factors, it has been shown that XRCC4, LIG4 and XLF can be localized to breaks independently of DNA-PKcs (40). It was also demonstrated that a number of factors besides just Ku70/80 and DNA-PKcs, namely XRCC4 and APLF, may play a role in NHEJ complex assembly and retention of LIG4 and XLF at breaks (22, 41). The repair pathway appears to be far more flexible than previously thought, and the order of repair factor recruitment after the Ku heterodimer (which is unequivocally the first factor at DSBs) may depend on the actual complexity of the DNA damage (42). Simple DNA breaks may only require the action of Ku and the XRCC4-LIG4-XLF complex, while more complicated breaks may require DNA-PKcs and a variety of processing enzymes. Additionally, each end of the DSB may have different processing requirements, potentially leading to a unique assembly of NHEJ components at either break end. This complexity leads to the idea that there may be a

rapid exchange of NHEJ factors at DSBs, with Ku functioning as a "tool belt," recruiting or stabilizing interactions between only those enzymes whose activities are necessary for the repair of a specific break (10).
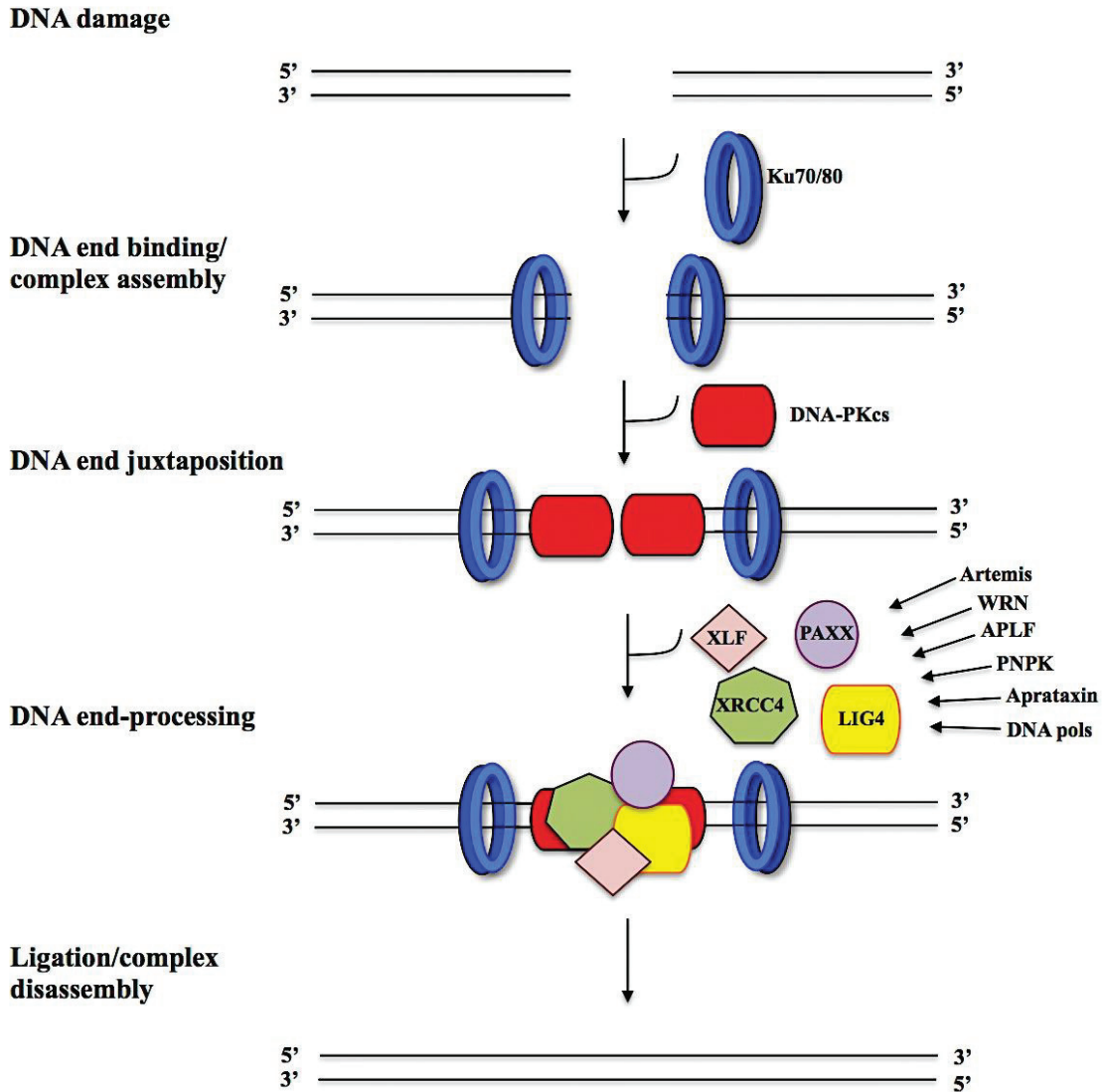
Figure 1.1. The canonical NHEJ pathway of DSB repair. Following a DSB, broken ends are bound by a heterodimer of Ku70 and Ku80, leading to recruitment and activation of DNA-PKcs and end juxtaposition. If no end-processing is required, NHEJ can proceed with just the core components Ku70/80, DNA-PKcs, XRCC4, XLF, LIG4 and the newly identified PAXX. If one or both broken DNA ends are damaged or modified, a combination of versatile end-processing factors is recruited to create ligatable ends for LIG4. However, the NHEJ pathway may be more versatile than previously thought, with the order of factor recruitment to the break site being flexible and dependent on the nature of the break itself. Ku is proposed to function as a "tool belt," recruiting and retaining only those factors necessary for the repair of a specific break.

1.2.2 Homologous recombination

The HR pathway uses information encoded on undamaged sister chromatids as a template to direct repair of DNA DSBs. This method of DSB repair is highly accurate, as identical or highly homologous sequences are used as templates, allowing the original undamaged sequence to be restored (43). HR thus maintains genomic integrity by repairing deleterious lesions like DSBs and inter-strand crosslinks, as well as damaged replication forks and incomplete telomeres. HR also plays a critical role at Spo11-induced DSBs during meiosis, ensuring proper chromosome segregation (43, 44). Mutations in genes encoding key HR factors lead to extreme sensitivity to DNA-damaging agents, and increased cancer predisposition (45). Due to reliance on sequence homology, HR occurs predominantly in the S and G2 phases of the cell cycle, peaking in mid-S phase (46) when sister chromatids are more readily available. HR therefore represents the less predominant DSB repair pathway relative to NHEJ in mammalian cells (11).

HR can be divided into three major stages: pre-synapsis, synapsis and post-synapsis. During pre-synapsis, regions around the 5' end of the break are resected to generate stretches of 3' single-stranded DNA. A protein complex comprising meiotic recombination 11 (MRE11), RAD50 and Nijmegen breakage syndrome 1 (NBS1) (the MRN complex) is one of the earliest repair factors present at a DSB and is responsible for tethering the two DNA ends together and for initiating this 5'-to-3' nucleolytic processing (47-49). The MRN complex further recruits the main endonuclease responsible for resection, carboxy-terminal binding protein-interacting protein (CtIP) (50). Additionally, a key HR component, breast cancer 1, early onset (BRCA1) has been shown to interact with both MRN and CtIP at break sites (51, 52). Although its exact role in HR has not been elucidated, it is thought that BRCA1 serves to accelerate CtIP-mediated DNA end resection (53). If more extensive resection is required, this is carried out by the combined action of the exonucleases EXOI and DNA2 along with the Bloom syndrome helicase (BLM) (54). DNA end resection serves as a key control point for DSB repair pathway determination during S/G2 phase, as NHEJ components cannot be assembled on single-stranded DNA (43). A critical function of the Ku heterodimer may be to physically protect the DNA ends from the resection machinery, with the XRCC4-

LIG4 complex aiding in its stabilization at break sites (55). Consistent with this notion, mutation of Ku or XRCC4-LIG4 results in increased resection intermediates and increased levels of overall HR (56).

The single-stranded DNA generated following resection is a target for binding by replication protein A (RPA). RPA is a heterotrimeric complex (RPA1, RPA2, RPA3) with an extremely high affinity for single-stranded DNA that plays both a stimulatory and inhibitory role in HR (57). RPA stimulates early stages of HR by removing secondary structure in single-stranded DNA to allow recombinase-coated nucleoprotein filament formation. Additionally at later stages of HR, RPA serves to bind and sequester single-stranded DNA generated during homologous DNA pairing and strand exchange (58, 59). However, for HR to proceed, RPA must first be replaced by a recombinase protein (homolog of bacterial RecA, RAD51, for somatic DSBs and DMC1 for meiotic DSBs) to form a nucleoprotein filament (known as the presynaptic filament), which then facilitates HR by searching for regions of DNA homology (43). RAD51 is a DNA-dependent ATPase and serves as the main mediator of HR by catalyzing homology search and DNA-strand exchange. RAD51 assembles cooperatively on resected single-stranded DNA, forming a right-handed helical filament with a stoichiometry of one RAD51 protomer per three or four nucleotides (60). However, RAD51 has a lower affinity and specificity for single-stranded DNA than does RPA (61), making the removal of RPA in favour of RAD51 onto single-stranded DNA a rate-limiting process. Several RAD51 cofactors, collectively termed recombination mediators, are involved in enhancing presynaptic filament formation and stability. An important recombination mediator is breast cancer 2, early onset (BRCA2). The C-terminal end of BRCA2 has a single-stranded DNA-binding motif (akin to that in RPA), as well as a helix-turn-helix double-stranded DNA-binding motif, and may therefore play a role in presynaptic filament assembly by binding at single- to double-stranded DNA transitions and aiding RAD51 nucleation (62, 63). Five human paralogs of RAD51 (RAD51B, RAD51C, RAD51D, XRCC2 and XRCC3) have also been identified as recombination mediators, functioning in different subassemblies to support RAD51 filament formation. Although the exact mechanisms are unknown, the potential functions of RAD51 cofactors include binding and anchoring the non-growing filament end, or binding the filament laterally (64, 65).

Following formation of the presynaptic filament, the next stage of HR, synapsis, proceeds.

Synapsis is characterized by homology search and strand invasion leading to displacement loop (D-loop) formation by displacement of the identical strand and base-pairing with the complementary donor strand (43). The exact mechanism of homology search has yet to be elucidated but it is thought that the presynaptic filament is stretched to an extended conformation, with a double-stranded DNA-binding site being made available to contact and test potential templates for homologous sequence (66-68). This homology search is greatly stimulated through another recombination mediator, RAD54. RAD54 is a double-stranded DNA translocase that may enhance homology search through the topological opening of the target DNA duplex or by sliding the presynaptic filament along the target duplex (69-71). Once a suitable homologous sequence has been identified, the presynaptic filament then invades the undamaged duplex generating a D-loop with the invading 3' end providing a primer for repair synthesis (43). Following strand invasion, depending on the type of initial DSB substrate and intermediates encountered by the recombination machinery, repair can be channeled into one of three related post-synaptic subpathways: double-strand break repair (DSBR), synthesis-dependent strand annealing (SDSA) or break-induced replication (BIR) (43) (see **Figure 1.2** for a depiction of pre-synapsis and synapsis and **Figure 1.3** for the post-synaptic subpathways).

In DSBR, following strand invasion and repair synthesis, the second end of the DSB is captured through DNA annealing to the extended D-loop, or by a second invasion event. This results in the formation of two crossed strands, or Holliday junctions (HJs). Resolution of HJs by the combined action of BLM helicase and TOPOIIIα topoisomerase leads to non-crossover products while dissolution of double HJ structures by the structure-specific endonucleases GEN1, MUS81/EME1 or SLX1/SLX4 leads to crossover products (a process that occurs predominantly during meiotic recombination) (72-76). SDSA is the major sub-pathway for repair of somatic DSBs. Following DNA synthesis, the D-loop is dissolved by the combined action of BLM and WRN helicases, the invading strand is displaced and reannealed with the second resected DSB end, leading to the generation of non-crossover products exclusively (73, 77, 78). This is a key

aspect for repair in somatic cells, as crossover products can lead to genomic rearrangements and large-scale loss of heterozygosity (LOH). Lastly, BIR is a sub-pathway for the repair of one-sided DSBs formed at broken replication forks or telomeres. Here, the DSB ends are resected as in the other HR sub-pathways; however, invasion by the pre-synaptic filament on a homologous DNA template is followed directly by extensive DNA synthesis that may continue as far as the next replication fork (79). While the pre-synaptic filament can invade a homologous sequence such as a sister chromatid, it can sometimes also invade a repeated sequence on a different chromosome which can result in non-reciprocal translocation or LOH (73).

These HR sub-pathways working in concert are critical in maintaining genomic stability by repairing deleterious DSBs, supporting replication after fork collapse and maintaining telomeres.
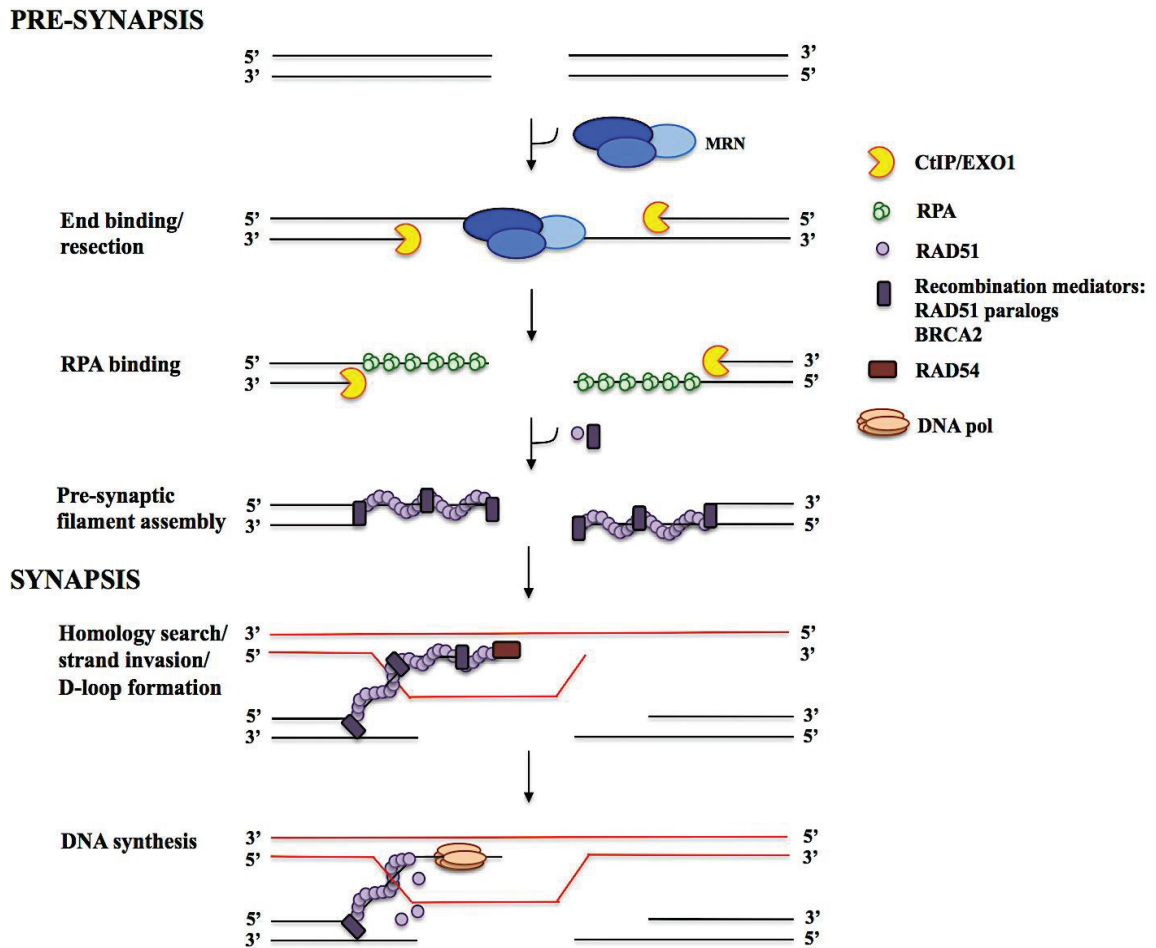
Figure 1.2. **Pre-synaptic and synaptic stages of homologous recombination.** In pre-synapsis, following DSB formation, MRN complex recruitment leads to DNA end tethering and initiation of 5'-3' nucleolytic processing. The resulting single-stranded DNA is stabilized by RPA, which is then replaced by RAD51 recombinase with assistance of various recombination mediators, forming the pre-synaptic filament. In synapsis, the pre-synaptic filament in conjunction with RAD54 undergoes DNA homology search, strand invasion and D-loop formation. From here HR branches into 3 distinct post-synaptic subpathways: DSBR, SDSA and BIR.
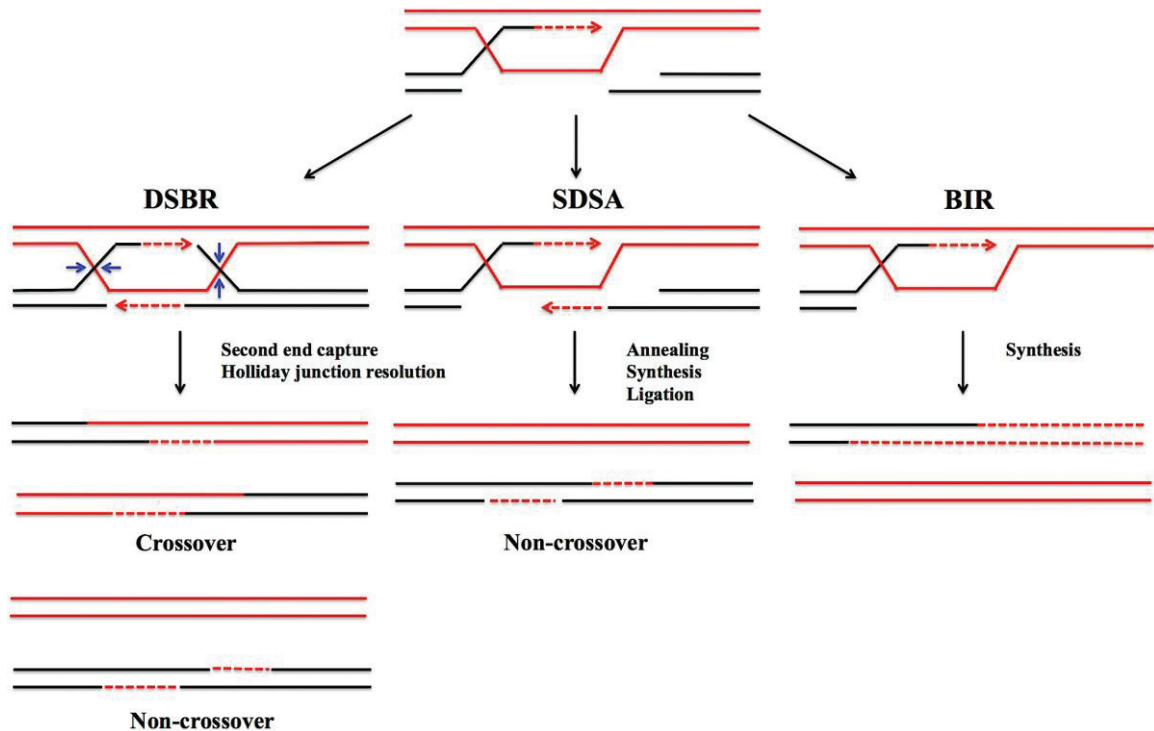
Figure 1.3. Post-synaptic subpathways of HR. DSBR, SDSA, and BIR subpathways all undergo end-resection, RAD51 pre-synaptic filament formation, homology search and strand invasion, but diverge when it comes to resolution of the resulting D-loop structure. In DSBR, second-end capture leads to double HJ formation. Alternate D-loop resolution (indicated by the blue arrows) can lead to either crossover or non-crossover products. In SDSA the invading strand is displaced from the D-loop and reannealed with the second resected DSB end. Ligation then leads to the formation of non-crossover products. BIR is primarily used to repair one-ended breaks resulting from replication-fork collapse. Strand invasion is followed by extensive DNA synthesis, which may continue as far as the next replication fork. Newly synthesized DNA is depicted as dashed lines in the same colour as the template; arrowheads indicate 3' ends.

1.3 The DNA damage response

DSBs are among the most cytotoxic DNA lesions. If not properly repaired by either NHEJ or HR, DNA DSBs can lead to a spectrum of mutations that can trigger cell death if normal checkpoint function is intact, or induce cellular transformation by activating oncogenes or disrupting tumor suppressor function (7). As a consequence, to maintain genomic stability a multi-branched, highly coordinated signaling cascade is initiated following the induction of even a single DNA DSB (80). This signaling cascade, termed the DNA damage response (DDR) integrates several cellular responses including DNA repair, chromatin remodeling, cell cycle checkpoint activation, transcriptional regulation, or apoptosis if damage proves too severe (81).

1.3.1 DNA repair foci

One of the hallmarks of the cellular response to DNA DSBs is the focal accumulation of many of the DDR proteins at the break site. This assembly of repair factors on DNA DSBs occurs in a highly regulated manner according to a strict hierarchy resulting in the formation of cytologically distinct foci in the nucleus, termed repair foci (82). The assembly of DDR factors to form repair foci is achieved using a broad spectrum of post-translational modifications including phosphorylation, ubiquitination, sumoylation, acetylation, poly(ADP-ribosyl)ation and methylation that regulates protein-protein interactions at the break site (83). These post-translational modifications not only promote assembly of repair factors into foci after DNA damage but also regulate protein stability and activity without the need for significant transcriptional upregulation of DDR factors (82). Formation of repair foci at DSBs is reliant on the phosphorylation of the key histone variant H2AX (termed γ-H2AX) (84, 85). Following DNA DSB induction, H2AX is rapidly phosphorylated by a set of kinases, ATM, ATR or DNA-PK (86, 87), and is crucial for rapid amplification of the DNA damage signal. Mediator of DNA damage checkpoint 1 (MDC1), a key mediator of the DDR, binds directly to γ-H2AX and recruits the MRN complex to break sites (88, 89). The MRN complex in turn can further stimulate ATM activity leading to rapid spreading of γ-H2AX up to 1-2 megabases around the DNA break in mammalian cells (90-92), and therefore the amplification of the

DDR signal (93, 94). In addition, γ-H2AX is crucial for the effective recruitment and retention of many DNA repair factors at DNA DSBs, including p53-binding protein 1 (53BP1), BRCA1, and RAD51 (95, 96) as well as chromatin-remodeling complexes such as NuA4, SWR1 and INO80 (97-99), resulting in the accumulation of a high concentration of repair factors in the vicinity of a break, as discussed in greater detail in the following sections. Repair foci can therefore be viewed as affinity platforms, bringing together a variety of DDR factors that work in a combinatorial manner to elicit certain cellular responses to DNA damage (82). In fact it has been demonstrated that even in the absence of DNA damage, tethering of certain DDR components to chromatin is sufficient to form repair foci and mount a full DDR (100, 101).

1.3.2 DDR initiation - sensing DNA damage

The DDR is a complex signaling cascade, requiring the coordinated actions of various proteins. At the molecular level its constituents can be grouped into three major categories: 1) sensors that recognize the lesion and initiate the signaling response 2) mediators that transduce and amplify the damage signal and 3) effectors that are responsible for carrying out various cellular responses to damage including DNA repair, cell cycle checkpoint activation and chromatin remodeling.

The first proteins at DSBs are molecular sensors of DNA damage: proteins capable of directly recognizing breaks and binding broken DNA in a sequence-independent manner. These sensors include the Ku70/80 heterodimer, the MRN complex and the poly(ADP-ribose) polymerases-1 and -2 (PARP1 and PARP2) (83). As discussed in section 1.2.1, the Ku heterodimer is responsible for initiating NHEJ by binding DNA non-discriminately through a ring-shaped structure capable of sliding onto broken DNA ends. Ku competes for DNA-end binding with PARP1, PARP2 and the MRN complex. PARP1 and PARP2 are very early sensors of DNA damage, being able to directly recognize both SSBs and DSBs. Binding to breaks triggers the enzymatic activities of PARP1 and PARP2, resulting in the synthesis of large amounts of poly(ADP-ribose) (PAR) polymers in the vicinity of the break. PARP1 and PARP2 have been shown to be important for initial recruitment of MRE11 of the MRN complex to DNA breaks (102).

The MRN complex is a major sensor of DNA breaks, binding DNA through a dimer of MRE11, while a dimer of RAD50 serves to stabilize the two DNA ends (47). As discussed in section 1.2.2, the MRN complex is important for initiating end resection in the early stages of HR; however, it also plays a critical role in DDR-signal initiation by recruiting the main DDR kinase ATM to DNA breaks (93,94).

The DDR signaling cascade is primarily coordinated by the serine/threonine protein kinases of the PIKK family: ATM, ATR and DNA-PK (83). ATM and DNA-PK are both activated in response to DSBs with ATM being considered the master kinase of the DDR, targeting hundreds of substrates (103). ATM is primarily recruited to DSBs through an interaction at the C-terminal end of the MRN component NBS1, promoting ATM autophosphorylation, monomerization and activation (93,94). However, there is evidence that ATM can also be activated in response to disrupted chromatin structure caused by break formation (104). DNA-PK catalytic activity is stimulated by Ku70/80-mediated DNA binding and primarily regulates a small group of proteins involved in DNA end-joining (27). Unlike ATM and DNA-PK, ATR is activated in response to single-stranded DNA generated at stalled replication forks during S phase or following HR-mediated DNA-end resection of DSBs that occur during S or G2 phase (105). Specifically, RPA bound to single-stranded DNA recruits and activates ATR through its interaction partners ATR-interacting partner (ATRIP) and topoisomerase-binding partner 1 (TOPBP1) (106, 107). In the case of DSBs that are destined for repair by HR, ATM is the initial kinase activated immediately after break formation; however, the RPA-coated single-stranded DNA generated during end resection eventually promotes a switch to ATR activation (108) (see **Figure 1.4A**). Together these three kinases are responsible for phosphorylating a wide range of target proteins to effectively signal the presence of DNA breaks.

Figure 1.4. The signaling cascade of the DNA damage response. **(A)** Initial sensing and downstream signaling of a DNA break is dependent on the nature of the break and the cell cycle phase in which it occurs. Breaks can be sensed by the Ku heterodimer, signaled by ATM or DNA-PK and repaired by NHEJ in all cell cycle phases. Breaks that occur as a result of collapsed replication forks in S phase are sensed by RPA, signaled by ATR kinase and repaired by HR. DSBs occurring in S/G2 phases are sensed by either Ku70/80 or the MRN complex and, depending on the resection state of the two DNA ends, are repaired by either NHEJ or HR. **(B)** The amplification of the DNA damage signal. For simplicity, signaling through ATM kinase only is shown. A key event in signaling a DSB is phosphorylation of histone H2AX on serine 139 by one of the kinases of the PIKK family. MDC1 binding in turn leads to recruitment of the MRN complex through an interaction with NBS1. NBS1 in turn promotes the recruitment and activation of additional copies of ATM resulting in amplification of the DNA damage signal. **(C)** A secondary wave of protein accumulation at DSBs is reliant on post-translational modification by ubiquitination and sumoylation. ATM phosphorylates MDC1, generating a binding site for the E3 ubiquitin ligase RNF8. The ligase activity of RNF8 is required for RNF168 localization to DSBs through an unknown mechanism (depicted by a question mark). RNF168 monoubiquitinates H2A type histones on lysine 13 and 15. RNF8 then catalyzes the addition of lysine 63-linked ubiquitin chains through association with the E2 ubiquitin-conjugating enzyme UBC13. Interaction between RNF8 and UBC13 is stabilized by HERC2, which is phosphorylated by ATM following DNA damage. 53BP1 or BRCA1 are then differentially recruited to DNA breaks to promote repair by either NHEJ or HR, respectively.

A
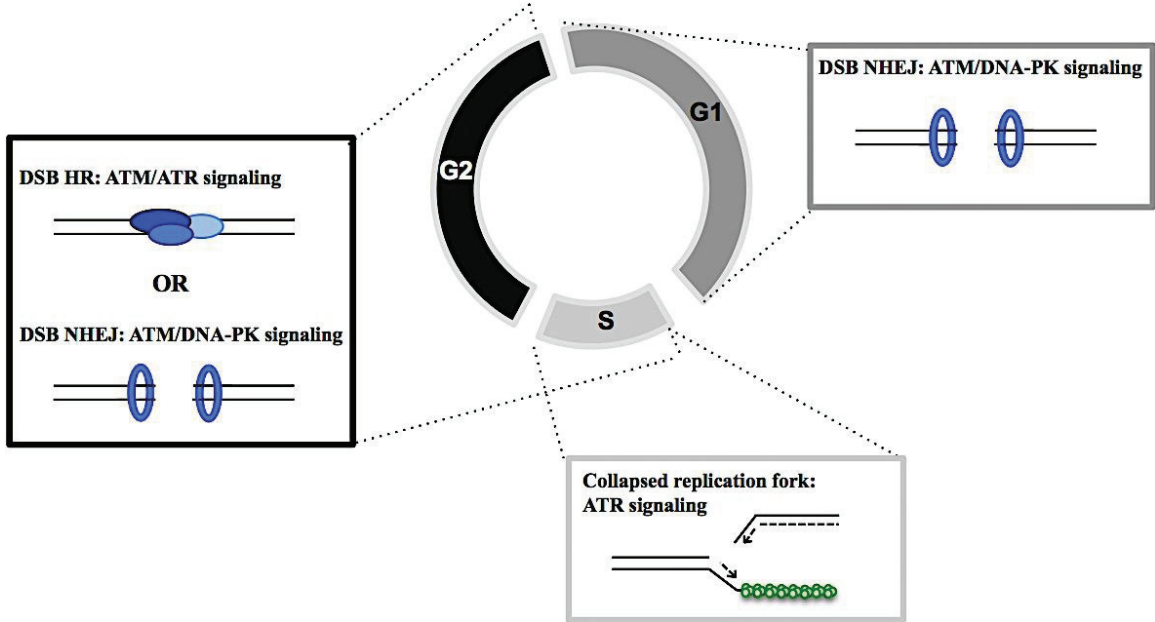
B
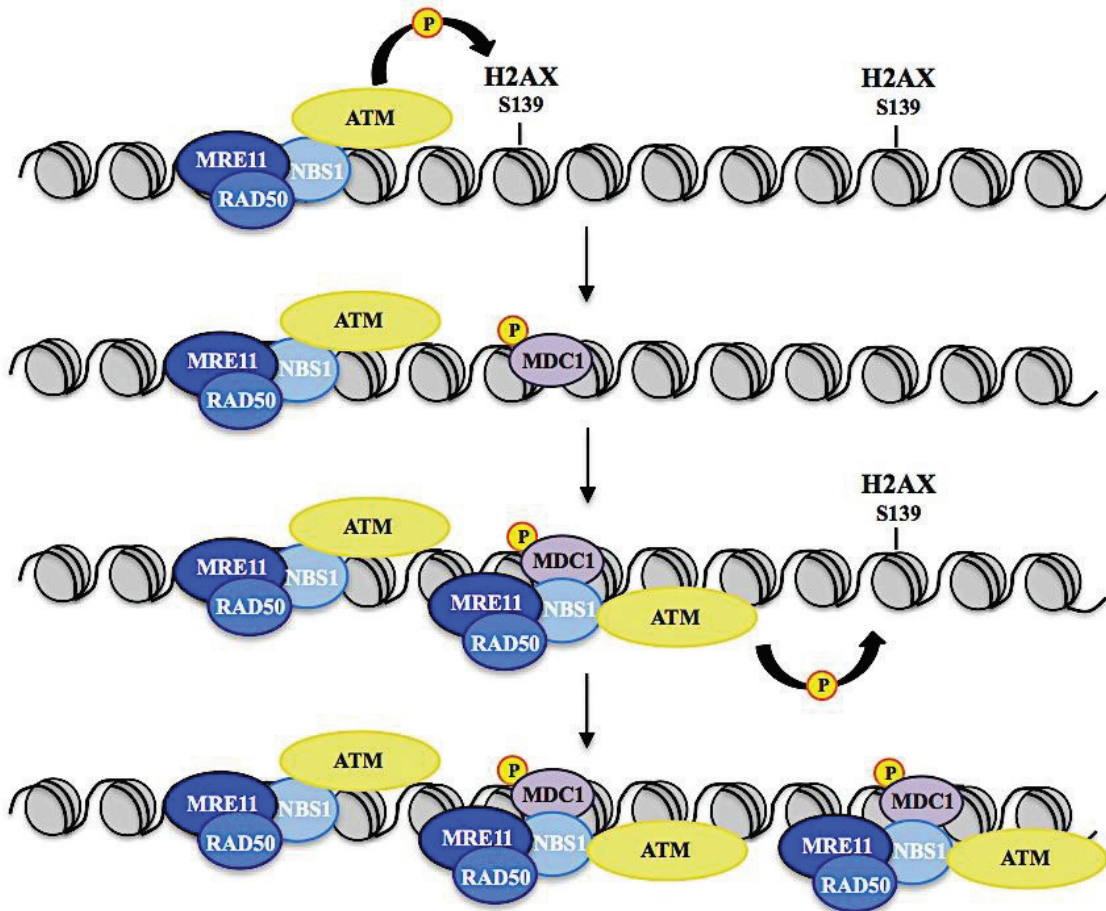
C
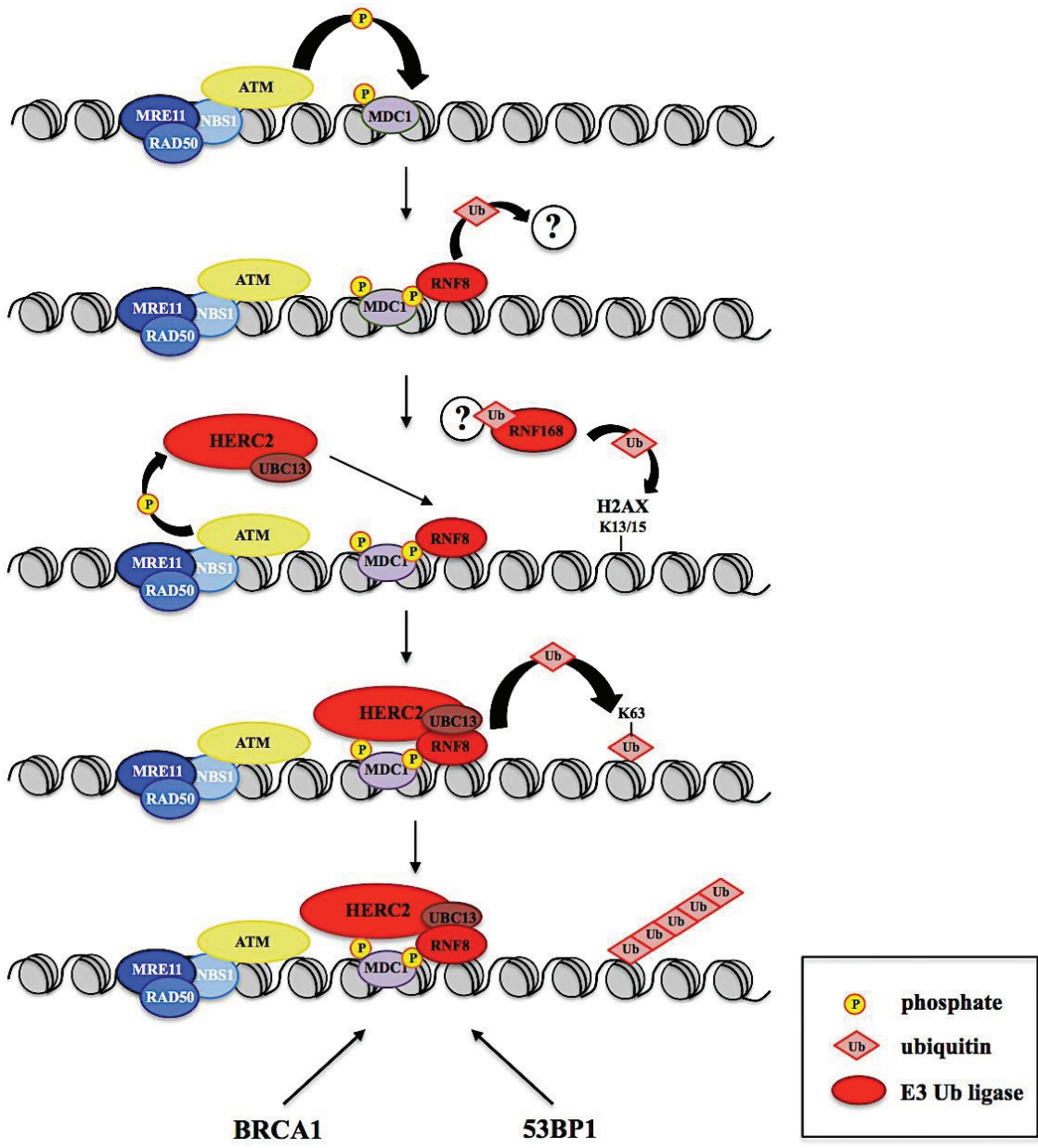
1.3.3 Amplification of the DNA damage signal during the DDR

A critical early step in the DDR is the phosphorylation of the H2AX on serine 139, forming γ-H2AX. H2AX is a variant of histone H2A, comprising 10-15% of total cellular H2A in mammalian cells (84, 85). Phosphorylation of H2AX is carried out largely by ATM although functional redundancy exists with ATR and DNA-PK (87). γ-H2AX provides a high-affinity binding site for a key mediator protein of the DDR, MDC1 (89). MDC1 is constitutively phosphorylated by casein kinase 2 at multiple conserved acidic sequence motifs near its N terminus. These motifs allow MDC1 to interact with the N-terminal phospho-binding motif on NBS1, the forkhead-associated (FHA) domain, resulting in the additional recruitment of MRN and hence activated ATM to DSBs (109). This recruitment results in a positive feedback loop as additional copies of ATM lead to extension of γ-H2AX outwards from the break site and amplification of the DDR signal (83, 91, 92, 110) (illustrated in **Figure 1.4B**).

This MRN-ATM- γ-H2AX-MDC1 recruitment loop represents the first wave of protein accumulation at repair foci induced by phosphorylation-mediated protein interactions. MDC1 then serves as a binding platform for what is considered the second wave of protein recruitment- one that is mediated by ubiquitination and sumoylation (83). Once recruited to DSBs, MDC1 is phosphorylated within a conserved motif by ATM or related kinases, generating a binding site for the FHA domain of ring finger protein 8 (RNF8) E3 ubiquitin ligase (111, 112). The ligase activity of RNF8 is required to recruit another ubiquitin ligase, ring finger protein 168 (RNF168), which is responsible for initiating a non-proteolytic ubiquitin cascade by mono-ubiquitinating histones H2A or H2AX at lysine residues 13 and 15 (113-116). RNF8 then catalyzes the addition of lysine 63-linked ubiquitin chains to H2A/H2AX following this initial ubiquitination by RNF168, through association with the E2 ubiquitin-conjugating enzyme UBC13 (115-117). Recently, another E3 ubiquitin ligase, HECT and RLD domain containing E3 ubiquitin protein ligase 2 (HERC2), had been identified as playing a crucial role in promoting histone poly-ubiquitination at DSBs. HERC2 is an extremely large (460 kDa) protein that is phosphorylated by ATM and related kinases on its C terminus following DNA damage, providing a strong binding site for the FHA domain of RNF8 (118). RNF8

has an intrinsic ability to dimerize or oligomerize, allowing it to simultaneously interact with MDC1 and HERC2, resulting in the formation of a ternary MDC1-RNF8-HERC2 complex at break sites (118). Due to its large size, attempts at addressing whether the E3 ligase activity of HERC2 itself is required for DDR signaling have been unsuccessful. However, HERC2 has been shown to play a role in stabilizing the interaction between RNF8 and UBC13, thereby ensuring formation of lysine 63-linked ubiquitin chains at sites of DNA damage (118).

The ubiquitination of the H2A type histones is critical for the recruitment of a variety of other DDR factors to the DNA break, chief among these being 53BP1, BRCA1, and BRCA1-associated RING domain 1 (BARD1) (119). Recruitment of 53BP1 to DSBs involves binding of its tudor domain to dimethylated histone H4 (H4K20me2) (120). This is a constitutive histone modification and in the absence of DNA damage is bound by Jumonji domain 2A (JMJD2A) with a higher affinity than 53BP1. Following DNA damage, RNF8 and RNF168 can trigger proteasomal degradation of JMJD2A by catalyzing the addition of lysine 48-linked ubiquitin chains (121). Additionally, recent studies have shown that 53BP1 can also bind to RNF168-ubiquitinated H2A at DSBs (116). 53BP1 promotes the NHEJ pathway of break repair through a number of mechanisms that include blocking 5'-end resection, mediating synapsis of DNA ends and increasing mobility of damaged chromatin to allow DNA ends to find each other for productive ligation (122-125). In contrast to 53BP1, recruitment of BRCA1 to DSBs promotes DNA-end resection and therefore the HR pathway of break repair as discussed in section 1.2.2. BRCA1 is recruited to breaks through one of its interaction partners, receptor-associated protein 80 (RAP80), which binds directly to lysine 63-linked ubiquitin chains generated by RNF8 and RNF168 (112, 119, 126) (as depicted in **Figure 1.4C**). Therefore a competitive relationship exists between 53BP1 and BRCA1, with 53BP1 promoting DNA repair by NHEJ and BRCA1 stimulating HR repair. The mechanisms promoting preferential recruitment of 53BP1 over BRCA1 or *vice versa* to DSBs are not fully understood and remain an area of intense research.

More recently, yet another layer of regulation in the DDR cascade has emerged: sumoylation (81). Small ubiquitin like-modifier (SUMO) E3 ligases, termed protein inhibitor of activated STAT1 and STAT4 (PIAS1 and PIAS4) have been shown to be

recruited to repair foci where they were found to be required for recruitment and retention of BRCA1 and 53BP1. PIAS4 was reported to stimulate the ubiquitin ligase activity of RNF8, while PIAS1 has been shown to directly sumoylate BRCA1 (127, 128).

1.3.4 Integration of the DNA damage signal with cell cycle control

To maintain genomic stability, DNA repair must be tightly coordinated with cell cycle progression. In response to DNA damage, the cell cycle must be temporarily paused at important stages such as before or during DNA replication (the G1/S and intra-S checkpoints respectively) and before cell division (the G2/M checkpoint). This pausing grants the cell time to properly repair DNA thereby preventing duplication or segregation of damaged DNA (129). Transition from one cell cycle phase to the next is governed by the temporal activation of cyclin-dependent kinases (CDKs), which promote cell cycle progression by inducing degradation of cell cycle inhibitory proteins in association with specific partner cyclins. CDK activation is dependent on cycles of phosphorylation and dephosphorylation: specifically, inhibitory phosphorylation of CDKs by the WEE1 protein kinase family and CDC25-mediated dephosphorylation of WEE1-mediated phosphorylation events (130). In parallel to contributing to the focal accumulation of repair factors at DNA damage sites, ATM and ATR kinases are also responsible for activating key cell cycle checkpoint effector kinases in response to damage. ATM responds to non-resected DSBs and is responsible for the phosphorylation and activation of the serine/threonine checkpoint effector kinase 2 (CHK2), while ATR responds to RPA-coated single-stranded DNA and activates checkpoint effector kinase 1 (CHK1) with assistance from two mediators, TOPBP1 and Claspin (131-136). Once activated, CHK1 and 2 dissociate from sites of damage and disperse throughout the nucleus where they phosphorylate substrates involved in CDK activation, promoting their degradation, CDK inhibition and cell cycle arrest (137). In this fashion, through ATM and ATR kinases, the cell integrates DNA repair with cell cycle regulation in response to DNA damage.

1.3.5 Integration of the DNA damage signal with chromatin remodeling

The recruitment of DDR factors to the site of DNA DSBs is complicated by the fact that the physiological substrate upon which repair must occur is not naked DNA, but rather DNA complexed with histone proteins in the form of chromatin. Furthermore, the compaction of eukaryotic chromatin is variable, with DNA being packaged as either euchromatin or heterochromatin (81). Euchromatin represents loosely packed, transcriptionally active gene-rich regions, while heterochromatin is generally characterized by highly repetitive regions that are tightly compacted and are transcriptionally silent (138). The differential compaction of DNA into either euchromatin or heterochromatin thus serves to control access of various proteins to the underlying DNA, regulating key cellular processes such as transcription, DNA replication, and repair (139, 140). Accordingly, the interplay between chromatin and DNA repair factors plays a central role in the cellular response to DSBs, and modulation of chromatin structure is critical for mediating access of repair proteins to underlying DNA lesions. To overcome the physical barrier posed by chromatin structure, a variety of histone-modifying enzymes and chromatin-remodeling complexes are recruited to break sites following DNA damage to facilitate binding of DNA repair proteins (141). Histones are also subject to a vast array of post-translational modifications including phosphorylation, methylation, acetylation, ubiquitination, and sumoylation (142). Together, these modifications can influence the structure of chromatin directly, for example by impacting the stability of individual nucleosomes, or indirectly by creating or eliminating binding sites for non-histone proteins, such as ATP-dependent chromatin remodelers that can in turn facilitate changes in chromatin organization (143).

As discussed above, one of the most well-characterized DNA damage-induced histone modifications is the massive phosphorylation of H2AX surrounding DSBs. Another critical early event for the cellular response to DNA damage is the rapid acetylation of histones H2A and H4 at DSBs by Tip60 acetyltransferase, a component of the NuA4 remodeling complex (144-146). Tip60 as well as other components of the NuA4 complex are recruited to DSBs immediately following damage where they can extend the acetylation of H2A and H4 along chromatin in a similar manner to γ-H2AX spreading (145-148). This increase in acetylation promotes chromatin relaxation to a less

compact conformation which is more permissive to DNA repair. In fact, inactivation of Tip60 prevents the formation of open chromatin structures at DSBs and subsequently impairs accumulation of repair factors at breaks (146). Another component of the NuA4 complex, the ATPase p400, when recruited to DNA breaks (through interaction with MDC1), plays a role in regulating nucleosome stability and RNF8-mediated chromatin ubiquitination (149). p400 mediates a decrease in nucleosome stability by promoting the exchange of H2A with the histone variant H2AZ in an active process that requires the ATPase activity of p400 in addition to the histone-acetylation activity of Tip60 (150). This histone exchange, in addition to acetylation events in the vicinity of DNA breaks, combines to create an even more relaxed, flexible chromatin structure at DSBs (151). This open conformation exposes RNF8 ubiquitination targets as well as histone-methylation sites such as H4K20me2, facilitating recruitment of PIAS1/PIAS4, BRCA1, and 53BP1 to DNA DSBs (81, 149, 152).

These histone modifications and chromatin restructuring are typically associated with DNA repair in euchromatic regions. The situation differs however, in the highly compact and often highly repetitive heterochromatic regions of the genome. DSBs occurring in heterochromatin generally display slower repair kinetics than those occurring in euchromatin (153, 154). Several studies have demonstrated that γ-H2AX foci assemble preferentially in euchromatin or localize at the boundary of heterochromatin but can rarely be detected microscopically within actual heterochromatic regions (153-155). Additionally, the genomic distribution of H2AX does not appear to be equal, with H2AX showing a marked preference for gene-rich areas and a lower overall distribution in heterochromatin, which may explain the inability to detect γ-H2AX in these regions (91, 92, 156). For effective repair to occur within heterochromatin, dynamic alterations to chromatin structure are required. A main contributor to chromatin remodeling in heterochromatin is KRAB domain-associated protein 1 (KAP1). KAP1 is a transcriptional co-repressor involved in the maintenance of heterochromatin structure in conjunction with the nucleosome-remodeling deacetylase (NuRD) complex. NuRD is a multi-subunit complex that couples ATPase chromatin-remodeling activities (through chromodomain helicase DNA-binding proteins 3 and 4 (CHD3 and CHD4)) with histone deacetylation (through histone deacetylase 1 and 2 (HDAC1/HDAC2) subunits),

interacting with KAP1 through the CHD3 component (81, 157, 158). Due to its role in chromatin compaction, KAP1 poses a substantial barrier to DNA DSB repair in heterochromatin. Phosphorylation of KAP1 on serine 824 by ATM has been shown to be essential for DSB repair in heterochromatic regions (153), and to enhance cellular survival following IR (154, 159). Following DNA damage, ATM induces the phosphorylation of KAP1, resulting in dispersion of CHD3 from DNA DSBs, and also triggering a relaxation of chromatin structure (158).

It is clear that the context in which a break occurs can impact its subsequent repair, and an important aspect of the DDR is the initiation of multiple chromatin-remodeling events in response to DNA DSBs. Whether they all function simultaneously or are evoked in response to different stimuli to mediate alternative repair pathways (NHEJ or HR for instance) remains to be determined (81).

1.4 DNA repair in the context of nuclear architecture

As discussed above, DNA within eukaryotic cells is highly organized and compacted into chromatin. Likewise, there is a strict spatial organization of chromatin within the nucleus as a whole. The nucleus itself is a highly compartmentalized structure consisting of discrete chromosome territories interspersed among many specialized, functionally distinct subnuclear compartments (160). These subnuclear compartments or domains are important parts of the nuclear landscape as they serve to structurally organize the nucleus by each occupying a discrete position, creating distinct environments to perform specific nuclear functions (161). It has been shown that the structure, behavior and biochemical constituents of many of these subdomains can be altered following genotoxic stress and as such many have been implicated as playing roles in DNA damage signaling and repair (162).

1.4.1 Nuclear actin

Actin is one of the most abundant cellular proteins. It is found predominantly in the cytoplasm where it plays critical roles in cell motility, division and signaling as well

as in the maintenance of cellular structure. However, actin is also present in the nucleus, and although nuclear actin does not form a nuclear body or domain *per se*, it has been found to participate in an ever-growing number of nuclear functions (163). Actin can exist in two forms: free monomeric G-actin (globular) or as part of polymeric microfilament known as F-actin (filamentous) which is a highly dynamic, flexible structure. Like cytoplasmic actin, nuclear actin serves as an important structural component, existing in both G- and F-actin forms (163). Nuclear actin interacts with components of the nuclear lamina: lamin A and emerin (which is discussed in further detail in the following section) (164, 165). It has been suggested that a protein complex consisting of actin, emerin and lamin A at the nuclear periphery provides structural support to the nucleus and stabilizes the nuclear membrane against mechanical stress (166, 167). In addition, similar to actin in the cytoplasm, actin in the nucleus plays a role in motility. Specifically, actin has been implicated in the intra-nuclear movement of certain chromosomal loci as well as in the movement of nuclear subdomains such as promyelocytic leukemia (PML) nuclear bodies (which are discussed extensively in following sections) (168-170). Besides structural support and intra-nuclear motility, nuclear actin, either alone or in association with a variety of actin-related proteins, is also involved in a diverse array of nuclear processes. Actin promotes transcription through an interaction with all three eukaryotic RNA polymerases, and also regulates the activity of specific transcription factors (171-176). Additionally, actin is involved in chromatin-remodeling, as actin and actin-related proteins are components of various chromatin-remodeling and modifying complexes. For instance, actin was shown to be necessary for the chromatin remodeling activity of the SWI/SNF complex and to be involved in its association with various nuclear structures (177-179). Nuclear actin has also been shown to participate in pre-mRNA splicing and export (180). Finally, nuclear actin has been implicated in DNA repair. For instance, junction-mediating and regulatory protein (JMY), a protein cofactor that promotes nuclear actin filament assembly, has been shown to be a DNA damage responsive protein, accumulating following damage induction and promoting p53-induced apoptosis. In addition, over-expression of an actin depolymerization factor, cofilin, was shown to alter nuclear actin dynamics following

DNA damage and to sensitize cells to IR (181-183).

1.4.2 The nuclear lamina

The nuclear lamina is a dense fibrillar meshwork closely associated with the inner nuclear membrane in mammalian nuclei, where it not only provides mechanical support to the nuclear envelope, but also facilitates overall genome organization (184). The major structural components of the nuclear lamina are the type V intermediate-filament proteins, the nuclear lamins. Lamins are composed of a short N-terminal 'head' domain, a long central α-helical coiled-coil rod domain and a globular C-terminal 'tail' domain (185, 186). Lamins self-assemble into higher order filamentous structures, with the rod domain mediating lamin dimerization and the N- and C-terminal domains facilitating head-to-tail polymer assembly (184). Lamins are classified as either A or B types based on their biochemical and functional properties. There are four A-type lamins (A, C, C2, and a minor isoform AΔ10) that are derived by the alternative splicing of a single gene, *LMNA*. A-type lamins are expressed in a tissue-specific manner, and only after the onset of cell differentiation (187-189). In contrast, two B-type lamins (B1 and B2) have been characterized, each encoded by different genes (*LMNB1* and *LMNB2*, respectively). B-type lamins are essential for cell viability and are expressed in all cells throughout all stages of development (190, 191).

In addition to providing the structural framework of the nuclear lamina, lamins also act as a scaffold for organizing chromatin at the nuclear periphery. Lamins make direct contact with DNA, specifically gene-poor heterochromatic regions, leading to the accumulation of a thick layer of chromatin and creation of a transcriptionally repressive environment at the nuclear lamina (160, 192-194). Lamins are important for overall genomic organization and integrity, as evidenced by the fact that *LMNA*-/- cells lack this dense chromatin layer at the nuclear periphery and consequently exhibit increased genomic instability (195-197). In addition to chromatin, the A- and B-type lamins interact directly or indirectly with many known inner nuclear membrane proteins including emerin, lamin-B receptor, and lamin-associated polypeptides 1 and 2β as well as a variety of other nuclear proteins including several components of the RNA polymerase II

transcriptional machinery and DNA replication complexes (184). Therefore, by providing binding sites for a wide variety of different proteins spanning a broad functional spectrum, the nuclear lamina has been implicated as playing roles in cell proliferation and differentiation, transcription, DNA replication, chromatin-remodeling, and DNA repair, to name a few (184, 197-200).

In terms of DNA repair, as mentioned above, cells defective in A-type lamins exhibit an increased level of genomic instability. This genomic instability is characterized by a higher level of chromatid breaks, increased sensitivity to IR, and defects in repair foci assembly. Additionally, the repair foci that do form have a greatly reduced positional stability in these cells (197, 201). It has also been demonstrated that depletion of A-type lamins results in transcriptional repression of *BRCA1* and *RAD51* genes, suggesting a possible regulatory role in HR. Interestingly, it was postulated that this decrease in *BRCA1* and *RAD51* transcription may be due to altered chromosomal positioning in a *LMNA*-/- background (202). It is therefore postulated that a role of the nuclear lamina and lamins may be through regulation of chromatin movement in the nucleus. Chromatin movement could be restricted to avoid inappropriate recombination events such as those that could easily occur in the highly repetitive heterochromatin associated with the lamina; or conversely, repositioning of certain DNA damage sites to more favorable repair environments could be promoted (203).

1.4.3 Promyelocytic leukemia nuclear bodies

PML nuclear bodies are nuclear matrix-associated proteinaceous domains that are present in most mammalian cell lines and tissues. PML nuclear bodies range in size between 0.1-1.0 μm and typically number between 5 and 30 bodies per nucleus depending on tissue and cell type, cell cycle phase and differentiation stage. Many proteins (in the range of 100) are known to be recruited to PML bodies, associating either constitutively or transiently (but more often transiently) (204). As such, PML bodies are structurally dynamic and functionally heterogeneous subnuclear domains (205). Due to the diversity of associated proteins, PML bodies have been implicated in a wide range of cellular functions, including induction of apoptosis, activation of cell cycle checkpoints

and senescence, inhibition of proliferation, transcriptional regulation, antiviral responses, hormone signaling, protein degradation and post-translational modification, chromatin-remodeling, DNA damage response and DNA repair (162, 205-209).

The primary structural component of PML bodies is the PML protein itself. PML is not essential for cell survival; however, PML-null mice display an increased risk of tumor development, and decreased PML expression has been linked to tumor progression in several cancer types, all of which may be tied to the diverse tumor-suppressing roles of PML nuclear bodies (210-212). PML is a member of the tripartite motif (TRIM) family of proteins (213, 215). The *PML* gene is comprised of nine exons that are alternatively spliced to produce seven isoforms (PMLI-VII) (215, 216). All isoforms share an N terminus that consists of a RING finger domain, two B-boxes and an α-helical coiled-coil (RBCC region) but vary in the central and C-terminal regions, differences which confer each isoform with specific protein-binding capabilities (see **Figure 1.5**) (215). All but one PML isoform (PMLVII) contain a nuclear localization signal (NLS), while only PMLI contains a nuclear export signal that allows all isoforms to shuttle between the nucleus and cytoplasm through heterodimer formation (217, 218). Upon individual PML isoform expression in *PML* -/- cells, PML nuclear bodies vary in size and in composition, demonstrating that isoform-specific sequences are responsible for contacting specific nuclear components, influencing body formation (217-219). However, the identity of exact PML isoform interaction partners, as well as the cellular function of each individual isoform remains poorly understood (218).

PML is subject to a variety of post-translational modifications, but arguably the most significant is sumoylation, a modification that is important for both nuclear body biogenesis and subsequent protein recruitment (220). PML directly binds the SUMO E2 ligase UBC9 that permits conjugation of SUMO on three lysine residues in the N-terminal RBCC region of PML (221). PML also contains a SUMO-interacting motif (SIM), which allows SUMO-mediated PML multimerization and nuclear body biogenesis. This also allows PML to interact with a variety of seemingly unrelated proteins that are either sumoylated themselves, or contain a SIM, thereby contributing to nuclear body formation, diversity and integrity (205, 222). This is illustrated by the fact that expression of a PML mutant incapable of being sumoylated fails to recruit

constitutively associated PML nuclear body proteins such as the transcriptional regulators Sp100 and death domain-associated protein (DAXX), and that sumoylation-defective *UBC9-/-* cells show defects in PML nuclear body formation (206, 223).

The overall structure of PML nuclear bodies consists of an outer shell of PML protein, with the various PML interaction partners residing within the interior. PML bodies are proteinaceous in nature and in general do not contain nucleic acids (224). However, electron-microscopic studies have demonstrated that PML bodies make extensive contact with chromatin fibers at their periphery (225). The position of PML nuclear bodies in the nucleus as well as the chromatin sequences that they contact are not random. Immunofluorescence *in situ* hybridization experiments have shown that PML bodies associate preferentially with several particularly gene-rich and transcriptionally active genomic regions including the major histocompatibility complex (MHC) class 1 gene-cluster region and the p53 gene locus (226-230). This may point to a necessary role of PML bodies in the transcriptional regulation of these regions (228). These chromatin contacts at the periphery of PML nuclear bodies are mediated through protein-based threads emanating from the body core and are important for maintaining both the positional stability and structural integrity of PML bodies in the nucleus (205, 225). Due to the intimate association of PML bodies with chromatin, PML nuclear body number and structural integrity are highly sensitive to any topological changes in chromatin structure, such as those occurring during the cell cycle. For instance, in early S phase when DNA is being replicated, PML nuclear bodies become distorted and eventually undergo a fission event, being pulled apart into what are termed 'PML microbodies.' Consequently, the number of PML-containing structures roughly doubles during G2 phase before finally being fully restored in both size and number upon cell division and completion of the cell cycle (231-233). It should be noted that the increase in PML body number during G2 is not due to an increase in PML protein level in G2; instead, it is due to loss of structural integrity owing to altered chromatin structure during the previous S phase (231). Similarly, alterations in chromatin structure resulting from various genotoxic stresses like heat shock, heavy metals, and DNA damaging agents such as UV and cisplatin have all been demonstrated to cause dispersal of PML nuclear bodies into numerous PML microbodies (234-238). PML nuclear bodies, in addition to their various

other potential functions, have been postulated as being sensors of cellular stress, monitoring the topological state and integrity of chromatin and releasing appropriate protein factors in response.

In addition to the increase in body number and subcellular distribution observed following DNA damage, several lines of evidence have pointed to PML and PML nuclear bodies as being heavily involved in the DNA damage response. Firstly, many DDR factors have been shown to display altered subcellular distributions with respect to PML nuclear bodies following DNA damage. Several DDR factors associate with PML bodies in unstressed cells (ATR, BLM, RAD51, MRE11, RPA) with some of them (ATR and MRE11) dissociating from bodies at early time points after DNA damage with subsequent relocalization at later time points. Additionally, some DDR proteins are not found in association with PML bodies in unstressed cells but are recruited specifically in response to DNA damage (ATM, WRN, TOPBP1, BRCA1) (236, 239, 240). The exact mechanism of this DDR factor sequestration to or release from PML bodies is not well characterized for many of these factors, but may rely on post-translational modification (particularly sumoylation and phosphorylation) of participating proteins (205, 241). The PML protein itself has also been implicated in DNA repair, as it has been shown to be phosphorylated by several DNA damage-activated kinases including ATM, ATR and CHK2 (205, 242). This DNA damage-dependent phosphorylation event is thought to regulate PML protein stability, PML nuclear body integrity and partner association. In this way PML and PML nuclear bodies may play a role in the temporal regulation of the DDR, sequestering or releasing specific DDR factors as needed following DNA damage. Exactly how this is accomplished is not fully understood. In addition to this, it is now becoming increasingly clear that PML and PML bodies may be playing a more active role in the actual process of DNA repair. This has come from observations that following damage, PML bodies often partially colocalize with DNA repair foci as well as with regions of single-stranded DNA (236, 243). PML has also been found to be required for the proper localization of RAD51 to repair foci following DSB induction (244-246). Additionally, *PML* -/- cells display high rates of sister chromatid exchange and demonstrate an inability to progress through S phase in the presence of DNA damage, implying that PML plays some type of regulatory role in HR (243, 247). Despite these

observations, the extent to which HR is dependent on the PML protein itself or PML nuclear bodies is not fully understood, nor are the individual contributions of specific PML isoforms to DNA repair. Additionally the role of PML on the NHEJ pathway of DSB repair has not been extensively examined.
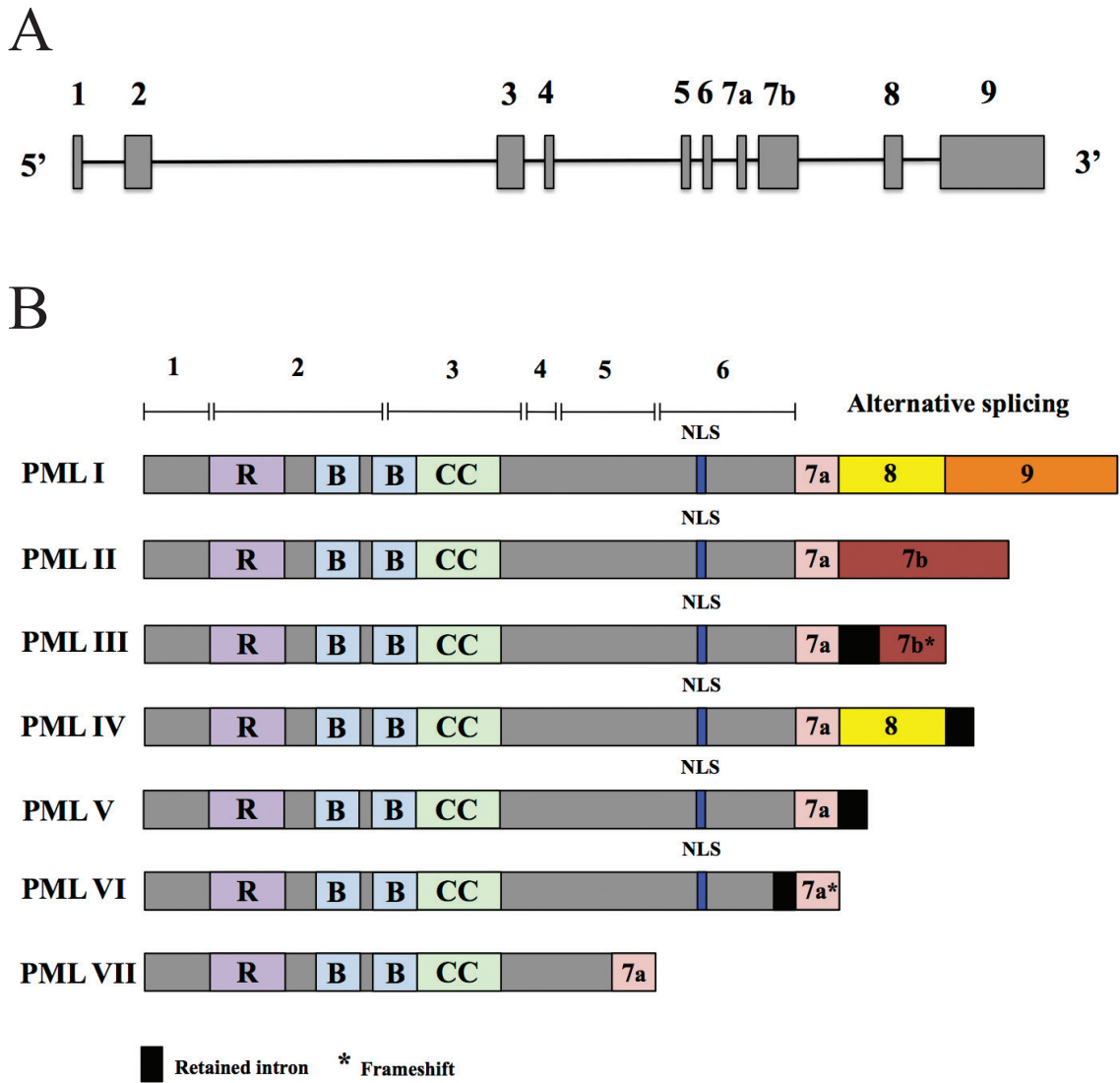
Figure 1.5. **Schematic diagram of the *PML* gene and PML isoforms**. **(A)** The *PML* gene consists of 9 exons. **(B)** All PML isoforms share an N-terminal domain consisting of a RING finger (R) motif, two B-box zinc finger motifs and an α-helical coiled-coil. Alternative splicing at the C-terminus yields seven different PML isoforms. All isoforms except for PML VII have an NLS. Adapted from (270).

1.5 Overview

In this thesis, I present the results of my studies aimed at understanding the influence of nuclear architecture on DSB repair. I demonstrate a role for nuclear actin in NHEJ, showing that polymeric nuclear actin is important for retention of the sensor protein Ku80 at DNA break sites. I show that delay in DSB repair at the nuclear lamina by HR is due to the compact heterochromatin structure associated with this nuclear subdomain. Additionally, I created versatile cell lines containing single defined insertions of either NHEJ or HR reporter DNA using a combination of different genomic engineering techniques. Using these cell lines, the effect of DSB position with respect to PML nuclear bodies on repair is examined, finding that HR is impacted when DSBs occur in close proximity to PML bodies. I also investigate the impact of individual PML isoforms on DNA repair, demonstrating a role in early stages of repair by both NHEJ and HR. Collectively these findings demonstrate a complex interaction between DNA repair and the nuclear environment, as the specific location of a DNA break within the nucleus can impact subsequent repair.

CHAPTER 2. MATERIALS AND METHODS

2.1 Cell culture

All cell lines used or generated in this study are based on human osteosarcoma U2OS cells (American Type Culture Collection) and are listed in **Table 2.1**. All cell lines were cultured in Dulbecco's modified Eagle's medium (DMEM) (Sigma-Aldrich) supplemented with 10% fetal bovine serum (FBS) (Thermo Fisher Scientific) and 1% penicillin/streptomycin (Thermo Fisher Scientific) under various selection conditions at 37°C with 5% CO_2.

Table 2.1. Cell lines used and/or generated in this study

Cell line(s)	Selection	Source
U2OS	None	ATCC
U2OS CRISPR PML knockout (ΔPML) clone 4	None	J. Salsman*
U2OS pFlexible PB 1:2 col.1-12	1µg/mL puromycin	This study
U2OS pFlexible PB 1:5 col.1-12	1µg/mL puromycin	This study
U2OS pFlexible PB 1:10 col.1-12	1µg/mL puromycin	This study
U2OS Chr15 5' px330 pFlexible col.1-6	1µg/mL puromycin	This study
U2OS Chr15 3' px330 pFlexible col.1-6	1µg/mL puromycin	This study
U2OS Chr15 5' 3' px335 pFlexible col.1-6	1µg/mL puromycin	This study
U2OS TAP 5' px330 pFlexible col.1-6	1µg/mL puromycin	This study
U2OS TAP 3' px330 pFlexible col.1-6	1µg/mL puromycin	This study
U2OS TAP 5'3' px335 pFlexible col.1-6	1µg/mL puromycin	This study
U2OS Chr15 5'px330 pFlexible col.6 FLP	5µg/mL ganciclovir	This study
U2OS TAP 5' px330 pFlexible col.1 FLP	5µg/mL ganciclovir	This study
U2OS Chr15 pFlexible Cre-NHEJ col.1-6	200µg/mL G418	This study
U2OS Chr15 pFlexible Cre-HR col.1-6	1µg/mL puromycin	This study
U2OS TAP pFlexible Cre-NHEJ col.1-6	200µg/mL G418	This study
U2OS TAP pFlexible Cre-HR col.1-6	1µg/mL puromycin	This study
U2OS Chr15 pFlexible CRISPR NHEJ col.1-6	200µg/mL G418	This study
U2OS Chr15 pFlexible CRISPR HR col.1-6	1µg/mL puromycin	This study
U2OS TAP pFlexible CRISPR NHEJ col.1-6	200µg/mL G418	This study
U2OS TAP pFlexible CRISPR HR col.1-6	1µg/mL puromycin	This study

*Dalhousie University

2.2 Microscopy

2.2.1 Microirradiation and live cell imaging

U2OS cells were grown to a confluency of 60-70% on sterile glass coverslips (Thermo Fisher Scientific) and co-transfected with 100 ng of a Ku80-GFP expression vector and either 100 ng of NLS-actin wild-type or NLS-G13R actin expression vectors along with 1800 ng pBluescript (BSK) as a carrier (2 µg total DNA). Each vector was driven by a cytomegalovirus (CMV) promoter. Transfections were performed with lipofectamine 2000 (Thermo Fisher Scientific) according to the manufacturer's protocol. For live-cell imaging, cells were visualized on a custom-built Zeiss Axioobserver Z1 inverted microscope (Intelligent Imaging Innovations), equipped with a 37°C incubator (ASI, USA), a CSU-M1 spinning-disk confocal scanner and 4 laser lines (405, 488, 560 and 633 nm). The cells were observed using a 40X objective (1.3 N.A) lens and images were recorded using an Evolve cooled charge-coupled device (CCD) camera (Photometrics) and Slidebook 5.0 software (Intelligent Imaging Innovations). UV-laser induced DNA damage was performed as described by Kruhlak *et al*., 2006 (248). Briefly, 24 h post-transfection, U2OS cells were photosensitized with 2 µM Hoechst 33342 (Thermo Fisher Scientific) for 5 min and in the case of cytochalasin D treatment, cells were incubated with 1 µg/mL cytochalasin D (Sigma-Aldrich) for 2 h prior to Hoechst treatment. Coverslips were then washed three times in PBS for 5 min per wash and immediately imaged. For the duration of imaging, cells were incubated in phenol red-free Roswell Park Memorial Institute (RPMI) media (Thermo Fisher Scientific) supplemented with 10% FBS and maintained at 37°C. DNA DSBs were induced in transfected cells using a 405 nm UV laser and the recruitment of GFP-tagged Ku80 to sites of damage was followed in real time. Images were processed and analyzed using Slidebook and Adobe Photoshop. Quantification of fluorescence intensity was measured within laser track regions and compared to regions outside of the laser track for 30 cells at every time point in a 40 sec time course. Statistical analyses (two-tailed t-test) were conducted using Excel 2007 software (Microsoft).

36

2.2.2 Electron spectroscopic imaging (ESI) of chromatin structure and variation

U2OS cells were grown to 80-90% confluence on 18-mm glass coverslips (Thermo Fisher Scientific) and were treated with either vehicle (0.1% dimethyl sulfoxide (DMSO) (Sigma-Aldrich)) or with 500 nM trichostatin A (TSA) (InvivoGen) for 4 h before being fixed in 4% paraformaldehyde (PFA) (Electron Microscopy Sciences) for 10 min at room temperature. Cells were washed three times in PBS for 5 min, permeabilized in 0.5% Triton X-100 (Sigma-Aldrich) for 5 min, and washed again in PBS. Cells were then "post-fixed" in 1% glutaraldehyde (Electron Microscopy Sciences) for 5 min at room temperature to maintain chromatin structure during resin embedding. Following fixation, cells were washed three times in PBS for 5 min each wash, followed by three 10 min washes with electron microscopy (EM) grade water (Gibco). Cells were then dehydrated in an ethanol series (2 h in 30%, 1 h in 50%, 1 h in 70%, 1 h in 90% and 20 min in 100% anhydrous ethanol) and embedded in Quetol 651 (Electron Microscopy Sciences) before being processed, sectioned and imaged by ESI as previously described (249) using a Tecnai 20 transmission electron microscope (FEI) equipped with an energy-filtering spectrometer (Gatan). Energy-filtered electron micrographs of nitrogen (N) and phosphorus (P) were collected, and non-chromosomal protein was segmented by subtracting the N from the P ESI micrograph, which was then false coloured in cyan and combined in a composite image with the P ESI micrograph false colored in yellow in Adobe Photoshop to highlight chromatin. The composite elemental maps of N-P (cyan) and P (yellow) were then analyzed for thickness of nuclear-lamina-associated chromatin using Image J v1.48k software (NIH). Pixel measurements (50 measurements taken from 10 cells) were converted into microns (μm) and then averaged per cell, and the data was represented as mean chromatin thickness ± standard error of the mean (SEM) (n=10). Statistical significance between cell lines was generated using the Student's t test in Excel (Microsoft). The mean coefficient of variation (CV) in chromatin density was calculated for chromatin within the nucleus of vehicle- and TSA-treated U2OS cells (n=5), using phosphorus-enriched 155 keV electron micrographs as previously described by the Dellaire lab (251). Briefly, the mean and standard deviation (SD) pixel intensities were first determined from 5 X 10 pixel-wide line scans per cell using Image J. Then for each

cell the CV was determined by dividing the mean pixel intensity by the SD, after which the CVs were averaged for vehicle- or TSA-treated cells and represented as a percentage ± SEM.

2.3 Generation of cell lines

2.3.1 Cloning

All plasmids used and/or generated in this study are listed in **Table 2.2**.

Table 2.2. Plasmids used and/or generated in this study. Intermediate as well as final constructs are noted.

Plasmid	Notes	Source
pBluescript II KS (-) (pBSK)	Empty cloning vector	Addgene
pFlexible Purotk 10X P/FRT	FRT/loxP recombination sites with selectable puroΔTK marker	(251)
pJRC49	128X LacO array	J. Chubb‡
pBLR5	PB TR sites	Sanger Institute
pBLR5-AflII	pBLR5 with added AflII site	This study
pBLR5-LacO	Intermediate-128XLacO flanked by PB TRs	This study
BSK-loxP	Intermediate-loxP site in BSK	This study
BSK-loxPM	Intermediate-loxPM site in BSK	This study
pFlexible-loxPM	Intermediate-loxPM in place of 3' loxP site in pFlexible	This study
pFlexible-SceI-loxPM	Intermediate-I-SceI recognition site between 5' FRT and PGK promoter	This study
pFlexible-LacO-pBLR5	Final construct-modified pFlexible sequence and 128X LacO array flanked by PiggyBac TRs	This study
pEJ	NHEJ reporter	J. Dahm-Daphi¥
BSK-pEJ1	Intermediate-2184bp fragment of pEJ	This study
BSK-pEJ1-loxP	Intermediate- loxP site 5' to fragment 1 of pEJ	This study
BSK-loxP-pEJfull	Intermediate-loxP site 5' to full NHEJ reporter sequence from pEJ	This study
Floxed-pEJ	Final-NHEJ reporter flanked by loxP-loxPM sites	This study
pcDNA3.1(-)	Empty cloning vector	Addgene

Plasmid	Notes	Source
pGC	HR reporter	J. Dahm-Daphi¥
pcDNA3.1-loxPM	Intermediate-loxPM site in pcDNA3.1	This study
pcDNA3.1-loxP-loxPM	Intermediate-loxP and loxPM sites in pcDNA3.1	This study
pcDNA3.1-loxP-pGC1-loxPM	Intermediate-2868bp pGC fragment flanked by loxP-loxPM sites	This study
Floxed-pGC	Final-HR reporter flanked by loxP-loxPM sites	This study
Chr15-TOPO4	5' and 3' Chr15 homology arms separated by AflII/MluI restriction sites	This study
TAP-TOPO4	5' and 3' TAP homology arms separated by AflII/MluI restriction sites	This study
Chr15-pFlexible-LacO-pBLR5-TOPO4	Chr15 pFlexible-LacO-pBLR5 CRISPR donor vector	This study
TAP-pFlexible-LacO-pBLR5-TOPO4	TAP1 pFlexible-LacO-pBLR5 CRISPR donor vector	This study
pFlexible-TOPO2.1 (N)	5' and 3' pFlexible homology arms separated by SalI/SacII restriction sites	This study
pFlexible-TOPO2.1 (H)	5' and 3' pFlexible homology arms separated by AvrII/SspI restriction sites	This study
pFlexible-pEJ-TOPO2.1	pFlexible-LacO-pBLR5 NHEJ CRISPR donor vector	This study
pFlexible-pGC-TOPO2.1	pFlexible-LacO-pBLR5 HR CRISPR donor vector	This study
px330-U6-Chimeric_BB-CBh-hSpCas9	Cas9/gRNA expression vector	Addgene
px335-U6-Chimeric_BB-CBh-hSpCas9n(D10A)	Cas9 nickase/gRNA expression vector	Addgene
px330-Chr15 5' gRNA	Chr15 Cas9/5'gRNA	This study
px330-Chr15 3' gRNA	Chr15 Cas9/3'gRNA	This study
px335-Chr15 5' gRNA	Chr15 Cas9nickase/5'gRNA	This study
px335-Chr15 3' gRNA	Chr15 Cas9nickase/3'gRNA	This study
px330-TAP 5' gRNA	TAP1 Cas9/5'gRNA	This study
px330-TAP 3' gRNA	TAP1 Cas9/3'gRNA	This study
px335-TAP 5' gRNA	TAP1 Cas9nickase/5'gRNA	This study
px335-TAP 3' gRNA	TAP1 Cas9nickase/3'gRNA	This study
px330-pFlex gRNA	pFlexible-LacO-pBLR5 Cas9/gRNA	This study
pPGK-FLPobpA	FLP recombinase expression	Addgene
mPB	PB recombinase expression	(252)
pBS513 EF1 alpha-cre	Cre recombinase expression	Addgene
px330-Lamin 5' gRNA	Lamin Cas9/5'gRNA	J. Pinder*
Clover-lamin donor	Clover-lamin CRISPR donor	J. Pinder*
EJ5-GFP	NHEJ reporter	Addgene
β-actin SceI	I-SceI expression	M. Jasin†
pKu80-GFP	GFP tagged Ku80 expression	M. Hendzel Δ

Plasmid	Notes	Source
NLS-actin WT	WT actin expression	M. Hendzel Δ
NLS-G13R actin	G13R mutant actin expression	M. Hendzel Δ
pNLS-IRFP670	far-red protein expression	Addgene
pMD35	Southern blot high-copy control probe: human telomere-associated repeat	M. Dobson*
CMV-FLAG-J1	FLAG-tag expression	J. Salsman*
FLAG-PMLI-J1	FLAG-tagged PMLI expression	J. Salsman*
FLAG-PMLII-J1	FLAG-tagged PMLII expression	J. Salsman*
FLAG-PMLIII-J1	FLAG-tagged PMLIII expression	J. Salsman*
FLAG-PMLIV-J1	FLAG-tagged PMLIV expression	J. Salsman*
FLAG-PMLV-J1	FLAG-tagged PMLV expression	J. Salsman*
FLAG-PMLVI-J1	FLAG-tagged PMLVI expression	J. Salsman*

‡MRC Laboratory for Molecular Cell Biology University College of London
¥University Medical Centre Hamburg-Eppendorf
*Dalhousie University
†Memorial Sloan Kettering Cancer Center
ΔUniversity of Alberta

2.3.1.1 Generation of the 14-kb plasmid construct pFlexible-LacO-pBLR5

The pBLR5 vector containing the terminal repeats (TR) for PiggyBac (PB) transposition was used as the backbone for the generation of a large targeting construct to be integrated into human cells (**Figure 2.1A**). To facilitate future cloning, an AflII restriction site was inserted into EcoRV/NheI-digested (unless otherwise indicated all restriction enzymes were from New England Biolabs) pBLR5 (near the 5' TR) as an annealed oligonucleotide linker with compatible ends (AflII linker- see **Table 2.3** for the oligonucleotide sequences). A 128x Lac operator array (LacO) was then isolated from the plasmid pJRC49 (**Figure 2.1B**) as a BamHI/XhoI fragment and ligated into BamHI/XhoI-digested pBLR5 (between the two TRs) to generate pBLR5-LacO. pFlexible is a generic targeting vector containing FLP recombinase target (FRT) and locus of X(cross)-over in P1 (loxP) recombination sites as well as the positive/negative selectable marker puroΔTK (**Figure 2.1C**). To modify this vector for directional Cre-lox recombination, the asymmetric 8-bp spacer region of the 3' canonical loxP site was mutated to generate the alternate loxP2272 site (253). A 500-bp fragment containing the

loxP site was amplified from pFlexible by polymerase chain reaction (PCR) using loxP EcoRI and loxP R primers (primer sequences are presented in **Table 2.4)** and subcloned between EcoRI and NotI sites in pBSK to generate BSK-loxP. BSK-loxP was then digested with XbaI and PstI and an oligonucleotide linker containing the alternative loxP2272 sequence (termed loxPM in this study) and was inserted with compatible overhangs (loxPM linker- see **Table 2.3** for oligonucleotide linker sequence; base pairs differing from canonical loxP are indicated in bold). The loxPM site was then re-cloned into pFlexible using BclI and NotI to generate pFlexible-loxPM. The 18-bp recognition site for the homing endonuclease I-SceI was subsequently incorporated as an oligonucleotide linker (I-SceI linker, **Table 2.3**) into HindIII/PacI-digested pFlexible-loxPM between the 5' FRT site and the phosphoglycerate kinase 1 (PGK) promoter, generating pFlexible-SceI-loxPM. The entire region of pFlexible-SceI-loxPM between loxP and loxPM (approximately 2700 bp) was amplified with flanking AflII and NheI restriction sites by PCR using primers pFlex AflII F and pFlex NheI R (**Table 2.4**), and cloned into pBLR5-LacO between the 5' TR and 128x LacO array to generate the final 14-kb targeting construct pFlexible-LacO-pBLR5 (**Figure 2.1D**).

PCR amplifications were performed using Phusion high-fidelity DNA polymerase (New England Biolabs). PCR reaction mixtures were set up according to the manufacturer's protocol and the amplification protocol was as follows: denaturation (95°C for 5 min), 30 amplification cycles (95°C for 30 s; 60°C for 30 s (annealing temperature varied slightly depending on primer composition); 72°C for 30 s) and final extension (72°C for 10 min). For amplification of longer products (greater than 2000 bp) the GC-rich Phusion protocol was followed. Briefly, PCR reactions were prepared as above with the addition of 3% (final concentration) DMSO. The amplification protocol was composed of: denaturation (98°C for 1 min), 5 preliminary amplification cycles (98°C for 30 s, 58°C for 30 s, 72°C for 1.3 min), 25 amplification cycles (98°C for 30 s, 60°C for 30 s (annealing temperature varied slightly depending on primer composition), 72°C for 1 min) and a final extension (72°C for 10 min). All cloning steps to generate pFlexible-LacO-pBLR5 were done in MAX efficiency Stbl2 competent *E. coli* cells (Thermo Fisher Scientific) to prevent recombination across highly homologous sequences in this vector. All cloning intermediates as well as the final product were

verified at every stage by Sanger sequencing (Genewiz, South Plainfield, NJ).

Table 2.3. Sequence of oligonucleotides annealed to create linkers used in this study

Linker		Oligonucleotide sequence (5'-3')
AflII linker	F	ATCGATCATGGCATCTTAAGCCATGAACAG
	R	CTAGCTGTTCATGGCTTAAGATGCCATGATCGCT
loxPM linker	F	CTAGAAAGTATAGGAACTTCATAACTTCGTAT**AA**AGTAT**CC**TATACGAAGTTATATGCA
	R	TATAACTTCGTATA**GG**ATACT**TT**ATACGAAGTTATGAAGTTCCTATACTTT
I-SceI linker	F	AGCTTAGTTACGCTAGGGATAACAGGGTAATATAGTTAAT
	R	TAACTATATTACCCTGTTATCCCTAGCGTAACTA
pEJ loxP linker	F	CGCAAGTATAACTTCGTATAATGTATGCTATACGAAGTTATGCTTACATGCA
	R	TGTAAGCATAACTTCGTATAGCATACATTATACGAAGTTATACTTGCGGGCC
pEJ loxPM linker	F	GGTAGACCATAACTTCGTAT**AA**AGTAT**CC**TATACGAAGTTATGGACTTGAGCT
	R	CAAGTCCATAACTTCGTATA**GG**ATACT**TT**ATACGAAGTTATGGTCTACCGC
pGC loxPM linker	F	AATTCTAGACCATAACTTCGTAT**AA**AGTAT**CC**TATACGAAGTTATGGACTTA
	R	AGCTTAAGTCCATAACTTCGTATA**GG**ATACT**TT**ATACGAAGTTATGGTCTAG
pGC loxP linker	F	AATTGGCAAGATAACTTCGTATAATGTATGCTATACGAAGTTATGCTTACTCG
	R	CGAGTAAGCATAACTTCGTATAGCATACATTATACGAAGTTATCTTGCC

* base pairs in the loxPM oligonucleotide sequences differing from canonical loxP are indicated in bold
F and R oligonucleotides were annealed to create double-stranded linkers

Table 2.4. Primers used for cloning in this study

Primer	Sequence (5'-3')*
loxP EcoRI F	CTGAGGAATTCGCTCGCTGATCAGCCTCGACT
loxP R	CGACTCACTATAGGGCGAATTGG
pFlex AflII F	TTACGCCTTAAGCAAGCTCGAAATTAACCCTCACTA
pFlex NheI R	GCGCCGCTAGCCGTGACCGCTACACTTGCCA
pEJ1 ApaI F	GCAATAGGGCCCGTGGATAACCGTATTACCGCCAT
pEJ1 R	CGTGACCGCTACACTTGCCA
pEJ2 F	CTGAGCAAAGACCCCAACGA
pEJ2 EcoRV R	GCCTACGATATCCGAGGTATGTAGGCGGTGCT
pGC1 NruI F	ACCATGTCGCGAGGCTGCGTTATCCCCTGATTCTGT
pGC1 MluI R	GCATTAACGCGTGACCCACACCTTGCCGAT
pGC2 F	CCCAGTTCCGCCCATTCT
pGC2 MluI R	GGTATCACGCGTCGTCCCATTCGCCATTCA
C15 5H FWD2	GGCTCTGATGACCACCTGAACC
C15 5H REV	TACGCGTTTTGTGCGACTTAAGAAGGAATAGGCTGGGATCCCCAC
C15 3H FWD	TCTTAAGTCGCACAAAACGCGTAGTTCTCCCTGAGCCTGTGGATAC
C15 3H REV1	ATCCAAGCCCATTCCTCAGC
TAP 5H FWD2	TCTCGCCGACTGGGTGCT
TAP 5H REV1	TACGCGTTTTGTGCGACTTAAGAGTTTTCGCTCTTGGAGCCAA
TAP 3H FWD3	TCTTAAGTCGCACAAAACGCGTACGAGAGCTGATCTCATGGGGA
TAP 3H REV2	AAGCCGACGCACAGGGTTT
pFlex 5H FWD1	CAAGCTCGAAATTAACCCTCACT
pFlex pEJ 5H REV1	TCCGCGGTTTGTGCGAGTCGACAGCGCCTTTTTTGTTTAAACTTTT
pFlex pGC 5H REV1	TCCTAGGTTTGTGCGAAATATTAGCGCCTTTTTTGTTTAAACTTTT
pFlex pEJ 3H FWD1	TGTCGACTCGCACAAACCGCGGACGCCCTATAGTGAGTCGTATTACAA
pFlex pGC 3H FWD1	TAATATTTCGCACAAACCTAGGACGCCCTATAGTGAGTCGTATTACAA
pFlex 3H REV1	CTTACAATTTCCATTCGCCATT
pEJ SalI F	GTAACTGTCGACCCCTGATTCTGTGGATAACCGT
pEJ SacII R	CCATGACCGCGGGTATTGTCTCCTTCCGTGTTTCAGT

*5' primer extensions that do not match template are underlined
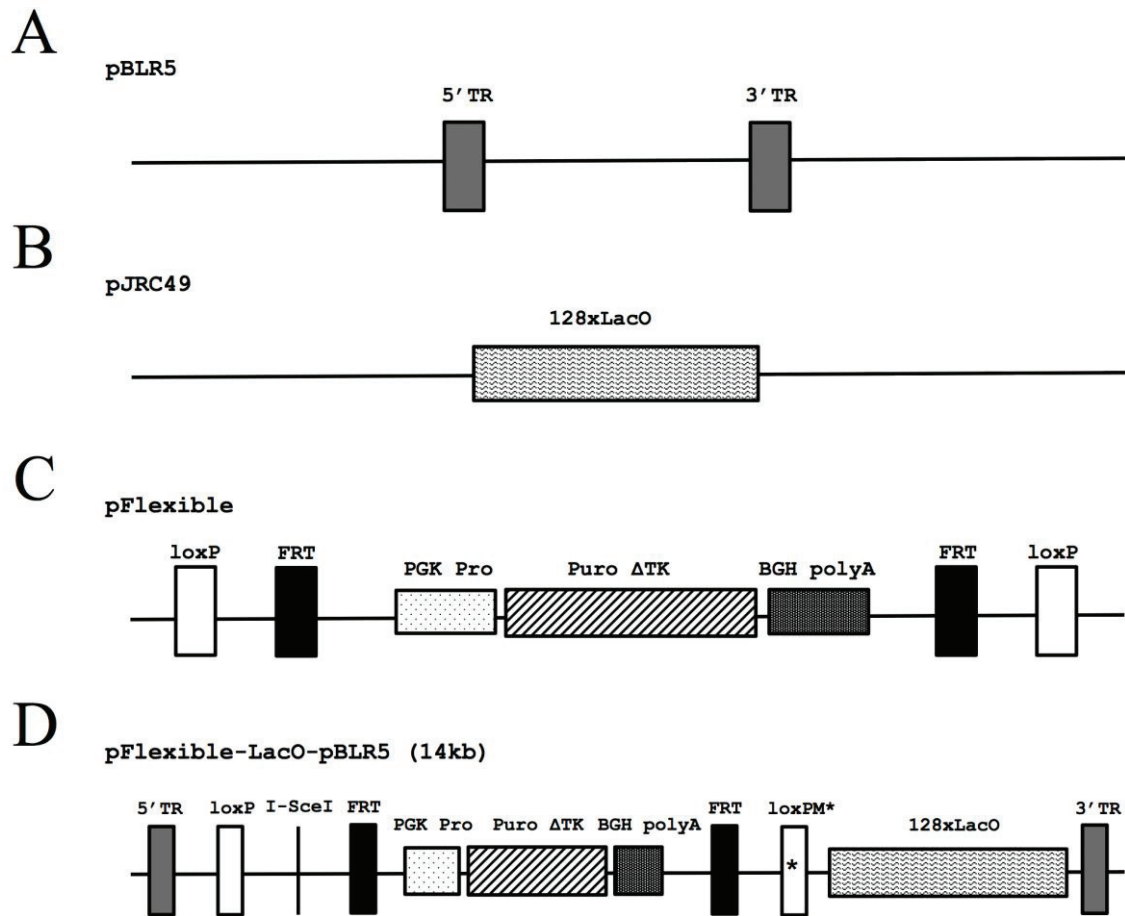
Figure 2.1. Linearized depiction of pBLR5, pJRC49, pFlexible and pFlexible-LacO-pBLR5 vectors. (A) pBLR5 contains two identical PB TRs for genomic insertion of intervening sequence by PB transposition **(B)** pJRC49 contains 128 repeats of a Lac operator sequence **(C)** pFlexible contains a puroΔTK positive/negative selectable marker under the control of a PGK promoter flanked by FRT and loxP recombination sites. All components of the pFlexible vector were used and/or modified in the creation of pFlexible-LacO-pBLR5 **(D)** pFlexible-LacO-pBLR5 is a 14-kb targeting vector created for integration into human U2OS cells. The PB vector pBLR5 was used as a backbone for the generation of this construct. pFlexible-LacO-pBLR5 contains a puroΔTK positive/negative selectable marker flanked by FRT sites and an I-SceI recognition sequence. These components are flanked by a canonical loxP site and a mutated version of loxP, termed loxPM. A 128x LacO array is located upstream to the loxPM site. Flanking this entire region are the PB TR sequences. The actual length of the construct integrated into the genome is 11082 bp.

2.3.1.2 NHEJ and HR reporter plasmids

Well-characterized reporter plasmids based on the reconstitution of a defective GFP gene were used to study DNA repair by NHEJ and HR. pEJ and EJ5-GFP reporter plasmids were used in the generation of cell lines or to study extrachromosomal DNA repair by NHEJ as previously described (254, 255). Briefly, these NHEJ reporters consist of two 18-bp I-SceI recognition sites separating a GFP gene from a CMV promoter by either an out-of-frame start codon (pEJ) or a puromycin-resistance gene (EJ5-GFP). When the I-SceI endonuclease is expressed, it cleaves DNA on either side of the out-of-frame start codon or puromycin-resistance gene, generating a DSB. Direct re-ligation of broken DNA ends by NHEJ results in GFP expression (see **Figure 2.2A**; only the pEJ reporter is depicted for simplicity). The pGC reporter plasmid was used in the generation of cell lines to study DNA repair by HR (254). This reporter contains two truncated GFP fragments separated by a puromycin-resistance gene, with the upstream GFP fragment containing an I-SceI recognition site (**Figure 2.2B**). Upon I-SceI expression, a DSB is created which, when repaired by HR using homologous sequence from the 3' truncated GFP fragment as a template to direct repair, results in full reconstitution of the GFP gene. HR repair events are then be detected by measuring fluorescence due to GFP expression.
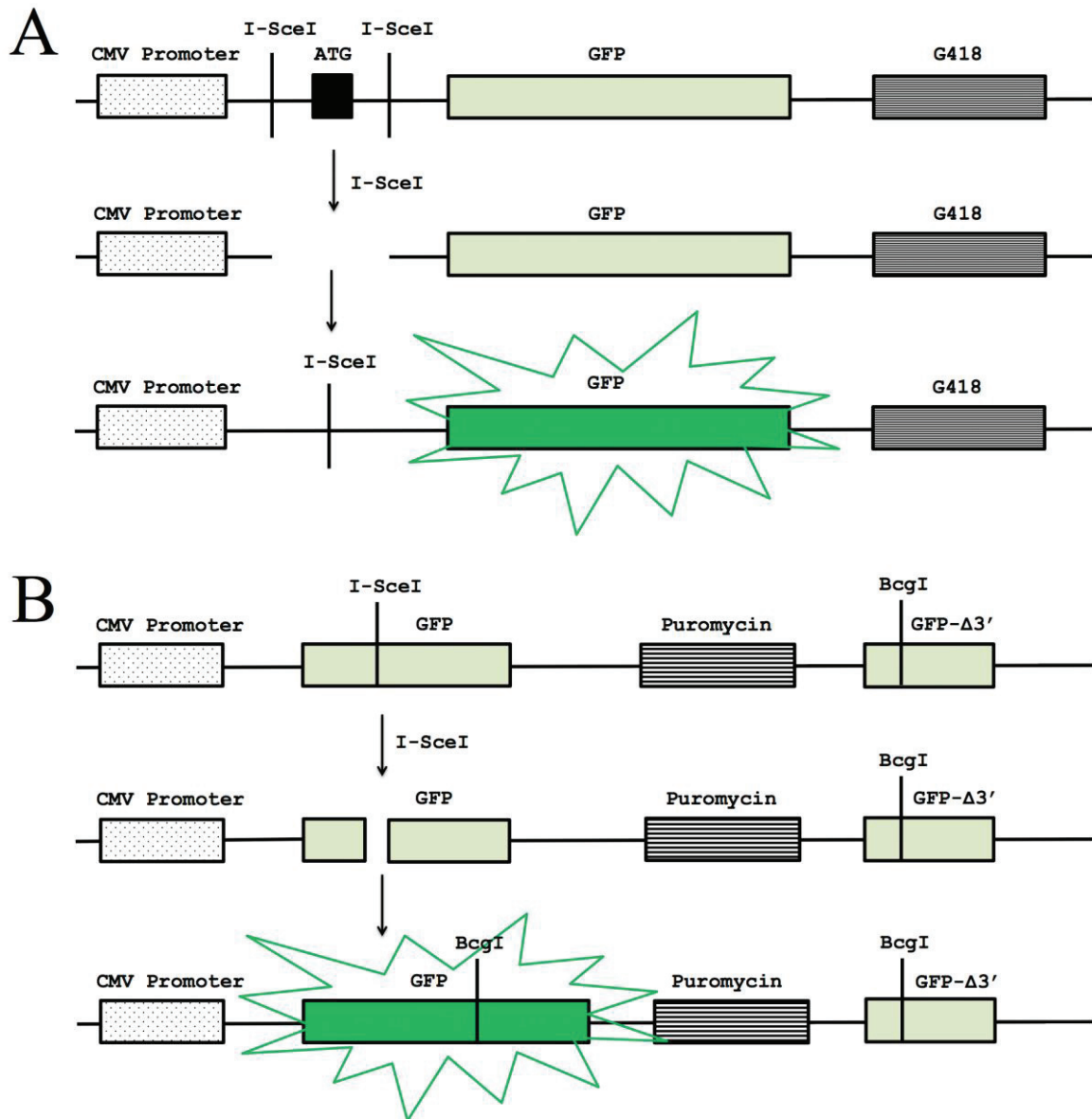
Figure 2.2. Linearized depictions of reporter plasmids used to study DNA repair.
(A) The NHEJ reporter plasmid pEJ. An out-of-frame start codon placed between two
recognition sites for I-SceI separates a CMV promoter from a GFP gene. I-SceI
expression results in DSB formation and removal of the codon. DSB repair by NHEJ
leads to GFP expression. The G418-resistance gene allows for selection of cells
containing stably integrated NHEJ reporter DNA through treatment with the protein
synthesis inhibitor G418 **(B)** The HR reporter plasmid pGC. Two GFP fragments, one
containing an I-SceI recognition site, are separated by a puromycin-resistance gene. The
puromycin-resistance gene allows for selection of cells containing stably integrated HR
reporter DNA through treatment with the protein synthesis inhibitor puromycin. I-SceI
expression creates a DSB that, if repaired by HR using homologous sequence from the 3'
truncated GFP fragment, results in reconstitution of the GFP gene and GFP expression.

2.3.1.3 Flanking NHEJ and HR reporters with loxP-loxPM sites

To create an NHEJ reporter flanked with loxP and loxPM sites, a 2184-bp fragment (termed pEJ fragment 1) spanning the CMV promoter, I-SceI sites and the GFP gene was amplified from pEJ using a forward primer containing an ApaI restriction site (pEJ1 ApaI F and pEJ1R; see **Table 2.4** for primer sequences). The PCR product was digested with ApaI and HincII and cloned into ApaI/HincII-digested BSK to generate BSK-pEJ1. A linker oligonucleotide containing a loxP site was then introduced into ApaI/NsiI-digested BSK-pEJ1 (upstream to the CMV promoter) to create BSK-pEJ1-loxP (pEJ loxP linker; see **Table 2.3** for oligonucleotide sequences). A second 2943-bp fragment (termed pEJ fragment 2), spanning the kanamycin/neomycin-resistance gene and overlapping with pEJ fragment 1 (past the HincII restriction site) was then PCR amplified from pEJ using a reverse primer containing an EcoRV site (pEJ 2F and pEJ2 EcoRV R; **Table 2.4**). The pEJ fragment 2 PCR product was then digested with HincII and EcoRV, and ligated into HincII/EcoRV-cut BSK-loxP-pEJ1 to generate BSK-loxP-pEJfull. The loxPM site was introduced into SacII/SacI-digested BSK-loxP-pEJfull (3' to the kanamycin/neomycin-resistance gene) through an oligonucleotide linker (pEJ loxPM linker; **Table 2.3**) to generate the final loxP-flanked, or Floxed-pEJ (**Figure 2.3A**).

To flank the HR reporter from the pGC vector with loxP and loxPM sites, oligonucleotide linkers containing each lox site were sequentially integrated into an empty pcDNA3.1(-) vector. The loxPM linker was incorporated into EcoRI/HindIII-digested pcDNA3.1(-) (pGC loxPM linker; see **Table 2.3** for oligonucleotide linker sequences) to generate pcDNA3.1-loxPM. The loxP site was then incorporated as an annealed oligonucleotide linker upstream of loxPM in MunI/NruI-digested pcDNA3.1-loxPM (pGC loxP linker; **Table 2.3**), creating pcDNA3.1-loxP-loxPM. A 2868-bp fragment (termed pGC fragment 1) was then PCR amplified from the pGC vector with primers containing NruI and MluI sites (pGC1 NruI F and pGC1 MluI R; **Table 2.4**). pGC fragment 1 (spanning a region containing the CMV promoter, I-SceI site and the 5' GFP sequence) was digested with NruI and MluI and ligated into NruI/MluI-digested pcDNA3.1-loxP-loxPM between the lox sites. A second fragment of 1867 bp, which slightly overlapped in sequence with pGC fragment 1, up to an SfII restriction site (spanning the puromycin-resistance gene and the 3'-truncated GFP sequence), was then

PCR amplified from the pGC vector using a reverse primer containing an MluI restriction site (pGC2 F and pGC2 MluI R; **Table 2.4**). The pGC fragment 2 PCR product was digested with SflI and MluI and cloned into SflI/MluI-cut pcDNA3.1-loxP-pGC1-loxPM to generate the final loxP flanked, or Floxed-pGC (**Figure 2.3B**).

PCR amplifications were performed as described in section 2.3.1.1. All cloning steps to generate Floxed-pEJ and Floxed-pGC were done in MAX efficiency Stbl2 competent *E. coli* cells and all cloning intermediates as well as the final products were verified at every stage by sequencing to ensure all sequences were correct and in frame.

2.3.1.4 Generation of pFlexible-LacO-pBLR5 clustered regularly interspaced short palindromic repeats (CRISPR) donor plasmids for pre-determined locus targeting

Homology arms for targeting an intergenic region of Chromosome 15 (Chr15) and exon 1 of the human transporter associated with antigen processing (TAP1) gene (**Figures 2.4 and 2.5**) were amplified from U2OS genomic DNA using primers shown in **Table 2.4**. The reverse primers for the 5'-homology arms as well as the forward primers for the 3'-homology arms were designed to include AflII and MluI restriction sites, respectively, to allow the pFlexible-LacO-pBLR5 construct to be cloned between the two arms. These primers also contained compatible overhangs long enough to be annealed together, allowing the 5'-and 3'-homology arms to be joined in a second round of PCR amplification. All Chr15 and TAP1 homology arms were PCR amplified as described in section 2.3.1.1 and cloned into pCR4-TOPO using a TOPO-TA Cloning Kit (Thermo Fisher Scientific). pFlexible-LacO-pBLR5 was digested with AflII and MluI and the 11-kb targeting construct isolated and ligated between the 5' and 3' homology arms of AflII/MluI-digested Chr15-TOPO4 or TAP-TOPO4 to generate the final pFlexible-LacO-pBLR5 CRISPR donor plasmids for Ch15/TAP targeting (termed Chr15-pFlexible-LacO-pBLR5-TOPO4 and TAP-pFlexible-LacO-pBLR5-TOPO4, respectively). All PCR amplicons and final donor plasmids were verified by sequencing.
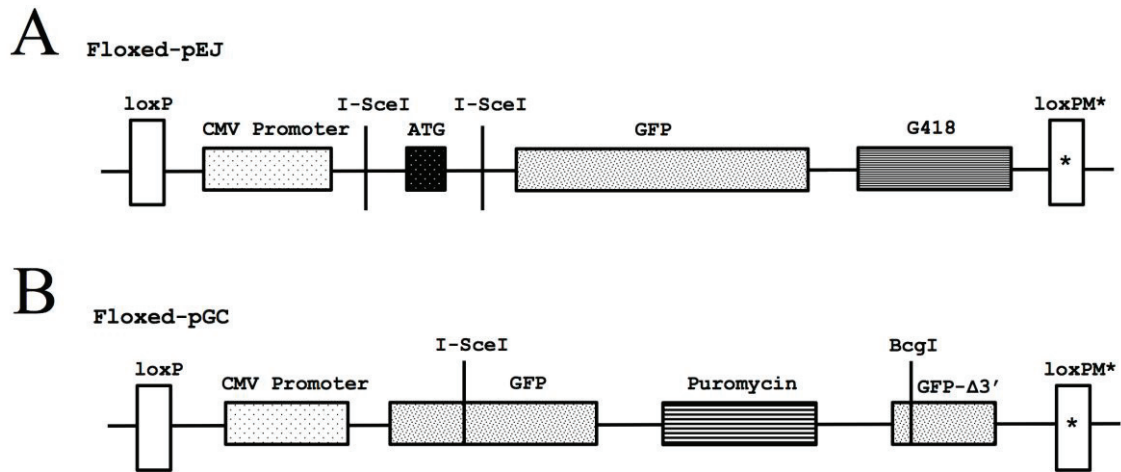
Figure 2.3. **Linearized depictions of loxP-loxPM flanked (floxed) pEJ and pGC vectors. (A)** The Floxed-pEJ vector contains a reporter for DNA repair by NHEJ. The NHEJ reporter is flanked with a loxP and a loxPM site. **(B)** The Floxed-pGC vector contains a reporter for DNA repair by HR. The HR reporter is flanked with a loxP and a loxPM site. The reporters from Floxed-pEJ and Floxed-pGC can be exchanged with the pFlexible-LacO-pBLR5 construct present in the U2OS genome through Cre-lox directional recombination across matching lox sites.

Legend:

Blue Text = Sequence used for 5'-homology template
Red Text = Sequence used for 3'-homology template
Yellow Highlight = Sequence of guide RNAs
Underlined Text = Sequenced PCR amplicon from wild-type U2OS genomic DNA

```
GGACAAAGATTAGATGCATCTTTTTGTTGTGAAATTTTGGTAAACTACTTACTCTTTCTCAGCCTCAGTTC
TTTGAACTATGAAATGGAGACAATAGTAATAGTATCAACCTCAAAGGGCTGGTGAGAAAACTAACCAAGAC
AATTCACACAAAGTTTCAGAACAGTCCCGGGCAGGTGCGTGACTTACGCATTTGGCTTTTGTTCACCACTA
TTACTACTTGCTTATTGAAGCTGAGCCAGGTGGCTGAGCAATGTCCCTTTCTGGCAAGGAGGGTGGAGGCA
AGTGTCACATTTCAGAAAGATCCCTGGGCTCCTGTTGAATCTGTCCCCACACCAAAACATGCCCGTGGGGG
CTCTAGCTCCTGCCCCAGCAGCGAAAGGGGCTCCTCCTTCTCTGGTGCCCAGTCCTAGCTCACCTGCTCTT
CACAAGCCTCCTCCCAGCACAGCCTGCACCACACAGGTGCTCAGTAAGGGGGTTGCTCTGAACAGGGAGCA
GGCCCACATGCTGAGAGTGGTGGAGGCGTGCAGGCTCTGATGACCACCTGAACCCAGACTCCAGGGCAGGA
CAGGTCCTTACAGACCGTAAGGGCTTCCTGCCTACCCTCTTCCCATGCAGTTACCTCAACCCTGGGACACC
AGGAAGGTTGAGCATTCCAGGAAAGCCCCGACCCACCCAGGAAACCCAAGTACCTGGTGGGGCCTCATCTG
GCCCATTGTCCTGAAAGGACAGGAATAAAGGCTCTCTCCTCATGGCCACACACCCTAGGGACGTCCAGCCT
CCAGCTTTCTGTGGGTGGGGCAAATGACTGAGGAGGCTTCCCTCCCTGCAGGCGCCTCCCTCTGGGGCCTC
CTGTGGTCCAGTCGTCCCTGGTCCCCAGCTCTCAGGTGGGTCATAGGGCATCTCAGCAGGACCACCAGGAA
GAGCATCAGGAGGGGAAGGAGCCAGAGAGCCCTCCAGGCCAGTGCACTGCTAACTCAACATCTCATCTTCC
TATCTCGTCCCTTCTGCTCACCTCCGGAGACTCCCCCTCCCCTCTCATGCTCTTCACTGGCAGGTTATGAT
GGCCCAGAGATCCCCACCAGAGTCCCAGATATCAGTGGGGATCCCAGCCTATTCCTCCAAGCTCCCAGTTG
CCAGTGACAGGGAGGCAGAAACAGCCTGGAAATTAACTGTGGGTTCTCCCTGAGCCTGTGGATACATGGAA
AGAGAGCTTCACCACCACCCCCTTCTCTGAATATACATACAGGATCTGAGGAGGGAGGATTCTGTGTGGAT
GCATGTGTGCACAGATGTGCATGTTTGTACGTGTGTATGGGTGAGCAGGTCATACGTGTGGTCCCATGTGC
CCACCTGTTGTATATATGCATGCTTGTTTTGTGTAAGTGAGCATAAGAGGTCAAGCCAGAGAGAGAAATAG
GAACAAGGAGAGACAGAGAGAGAGAGAATAGAAACAGAGACCAACAGGGAAACAGAATGAGACTGAGACAG
AGAACAACAGAAGGCCAGACAGGTAGACAAGCCACAGTTCCATCTTCCCTGGTGCTGGCTGCCAAGGCAGA
CAACTCTCCTCTCACTTCATTGATGTTCTGCCTGTGTTTATACCCATGATTGGGGTGGAGTTCAGGAAAGG
ATGTATCAGGGCTAGGACGCCCCCACCTCCACACTCACAGGGCCAGTCAGGGCCCTCTGCAGGGGCTGCCA
TTTCCTCAAGCTGAGGAATGGGCTTGGATCCCTCGGATGCCTTCCAGGGTGCAGGGGCGCTCCCAGTGACT
GGGCTCTTGTGGTGGCTGGGGAGGGGGAGCTCCTCTGACAGGCCCCATGCTGGGGGAAACGTCCTGAGACT
GACCTATCACGGGCTGACATGCACACCAAGGAGGTCTCACATCTGCTGGGAAATGAGGGGCTGGTGGAGGT
GAGAAAACCTCAAGTTCTAATGCCTTCCCAACACCTTCACCTCACCTGAGAAGCTTCTAGATTCCACCCAC
CCCTGTTTCCTTGGGGGAGGGTGTTGTGTGGAGGTGGGAAGAGGCAGGAGTCCAGGTTCTAGGCCAGGCTC
TGAAGGGGCAGGTAGCTCAG
```

Figure 2.4. **Reference sequence for a 2079-bp intergenic region of Chr15 targeted for CRISPR genome editing.** Genomic Location: (GRCh37.p.13 primary assembly chr15:74696007-74698086). Guide RNAs targeting Chr15 are highlighted in yellow. The sequences used to generate the homology arms of the donor vectors are shown in blue (5' homology) and red (3' homology). Underlined text denotes the region of the PCR amplicon from wild-type U2OS genomic DNA that was verified through Sanger sequencing.

Legend:

Blue Text = Sequence used for 5'-homology template
Red Text = Sequence used for 3'-homology template
`Yellow Highlight` = Sequence of guide RNAs
Underlined Text = Sequenced PCR amplicon from wild-type U2OS genomic DNA

```
GGTGCTGCGGGGCTGCTTTGCGCGCGGCGCTAACGTGTGTAGGGCAGATCTGCCCCGAGACAAGTGACGAG
GCAGCCCCGCCCTGAGGCTGGGGTGGGAAAACTGGTGCAAGTGGAAAGGCAGGAGGCAGGGAGAGGCGAGA
AGGGTGTGCGTGATGGAGAAAATTGGGCACCAGGGCTGCTCCCGAGATTCTCAGATCTGATTTCCACGCTT
GCTACCAAAATAGTCTGGGCAGGCCACTTTTGGAAGTAGGCGTTATCTAGTGAGCAGGCGGCCGCTTTCGA
TTTCGCTTTCCCCTAAATGGCTGAGCTTCTCGCCAGCGCAGGATCAGCCTGTTCCTGGGACTTTCCGAGAG
CCCCGCCCTCGTTCCCTCCCCCAGCCGCCAGTAGGGGAGGACTCGGCGGTACCCGGAGCTTCAGGCCCCAC
CGGGGCGCGGAGAGTCCCAGGCCCGGCCGGGACCGGGACGGCGTCCGAGTGCCAATGGCTAGCTCTAGGTG
TCCCGCTCCCCGCGGGTGCCGCTGCCTCCCCGGAGCTTCTCTCGCATGGCTGGGGACAGTACTGCTACTTC
TCGCCGACTGGGTGCTGCTCCGGACCGCGCTGCCCCGCATATTCTCCCTGCTGGTGCCCACCGCGCTGCCA
CTGCTCCGGGTCTGGGCGGTGGGCCTGAGCCGCTGGGCCGTGCTCTGGCTGGGGGCCTGCGGGGTCCTCAG
GGCAACGGTTGGCTCCAAGAGCGAAAACGCAGGTGCCCAGGGCTGGCTGGCTGCTTTGAAGCCATTAGCTG
CGGCACTGGGCTTGGCCCTGCCGGGACTTGCCTTGTTCCGAGAGCTGATCTCATGGGGAGCCCCCGGGTCC
GCGGATAGCACCAGGCTACTGCACTGGGGAAGTCACCCTACCGCCTTCGTTGTCAGTTATGCAGCGGCACT
GCCCGCAGCAGCCCTGTGGCACAAACTCGGGAGCCTCTGGGTGCCCGGCGGTCAGGGCGGCTCTGGAAACC
CTGTGCGTCGGCTTCTAGGCTGCCTGGGCTCGGAGACGCGCCGCCTCTCGCTGTTCCTGGTCCTGGTGGTC
CTCTCCTCTCTTGGTAAGGGGAACGCAGGGCAAGAGGGGAGGACACAAGGGGACTGGGACAGGAATCAAAG
GTAATTGTCAGTAAGGTAGAGTAGCGTGGGTTCTGGGAAATGTGGAGCAGGAGAAGGACTCCTAGCGTGGG
TCTTGGAACACCACTTCGGTGTAGAAGAAACGGCACTGGACTGGCGGGGGCCAGAGGTTCTGGGCTCCATT
GCTGACCGGGTCTTGATTCTTTGGGCCACGCCGGAAGCGGGGAAATCCTTTGCTCTGGGGCCGAAGGGCGG
GGCATCCTCATCTCTAACAGGAGGCTTTTCTACTTCATGATCTCCAGCCTTCCTAATAAAATCCTGAAAGT
TCTGGTAGAGCAACCACAGGGTAGTGAGTTCCAGGGCAGCCTATTTAGGTTCGGGATTGAGACGTCAGTGT
TTCCTTTCTGCTGATGCCCTCCAGGATAATGGTGAGGGGGAGGAGGCGTGGTGGGGCCAGT
```

Figure 2.5. Reference sequence for a 1552-bp region around exon 1 of the human TAP1 gene targeted for CRISPR genome editing. Genomic Location: (GRCh37.p.13 primary assembly chr6:32821893-32823445). Guide RNAs targeting TAP1 are highlighted in yellow. The sequences used to generate the homology arms of the donor vectors are shown in blue (5' homology) and red (3' homology). Underlined text denotes the region of the PCR amplicon from wild-type U2OS genomic DNA that was verified through Sanger sequencing.

2.3.1.5 Generation of NHEJ/HR CRISPR donor plasmids for targeting genome-integrated pFlexible-LacO-pBLR5

To target the NHEJ and HR reporters into the pFlexible-LacO-pBLR5 construct that had been integrated into U2OS cells at Chr15 or TAP1 loci, 5'-and 3'-homology arms were amplified by PCR using the pFlexible plasmid as a template (**see Figure 2.6** and **Table 2.4** for primer sequences). The reverse primers for the 5'-homology arms as well as the forward primers for 3'-homology arms were designed to include either SalI/SacII or AvrII/SspI restriction sites to allow the NHEJ reporter from pEJ or the HR reporter from pGC, respectively, to be cloned between the pFlexible homology arms. These primers also contained compatible overhangs long enough in sequence to be annealed together, allowing the 5'-and 3'-homology arms to be joined in a second round of PCR amplification. pFlexible homology arms were PCR amplified using Phusion high-fidelity DNA polymerase (as described above) and cloned into pCR2.1-TOPO using a TOPO-TA Cloning Kit (Thermo Fisher Scientific). The NHEJ reporter was PCR amplified from the pEJ vector using primers containing SalI and SacII restriction sites and cloned into SalI/SacII-digested pFlexible-TOPO2.1(N) to create a CRISPR NHEJ donor plasmid termed pFlexible-pEJ-TOPO2.1. The HR reporter was isolated from the pGC vector through a digest with AvrII and SspI and ligated into AvrII/SspI-digested pFlexible-pGC-TOPO2.1(H) to generate a CRISPR HR donor plasmid termed pFlexible-pGC-TOPO2.1. All PCR amplicons and final donor plasmids were verified by sequencing.

Legend:

Blue Text = Sequence used for 5'-homology template

Red Text = Sequence used for 3'-homology template

`Yellow Highlight` = Sequence of guide RNAs

`Green Highlight` = I-SceI restriction site

`Blue Highlight` = loxP and loxPM sites

```
TTAACCCTAGAAAGATAGTCTGCGTAAAATTGACGCATGCATTCTTGAAATATTGCTCTCTCTTTCTAAAT
AGCGCGAATCCGTCGCTGTGCATTTAGGACATCTCAGTCGCCGCTTGGAGCTCCCGTGAGGCGTGCTTGTC
AATGCGGTAAGTGTCACTGATTTTGAACTATAACGACCGCGTGAGTCAAAATGACGCATGATTATCTTTTA
CGTGACTTTTAAGATTTAACTCATACGATAATTATATTGTTATTTCATGTTCTACTTACGTGATAACTTAT
TATATATATATTTTCTTGTTATAGATATCGATCATGGCATCTTAAGCAAGCTCGAAATTAACCCTCACTAA
AGGGAACAAAAGCTGGTACCGGGCCCCCCCTCGAGGTCGAGACGGTATCGATGGCGCGGAATTCAAAAAGT
TTAAACAAAAAAGGCGCGCCATAACTTCGTATAATGTATGCTATACGAAGTTATAAGCTTAGTTACGCTAG
GGATAACAGGGTAATATAGTTAATTAAGAAGTTCCTATTCCGAAGTTCCTATTCTCTAGAAAGTATAGGAA
CTTCGAAGTTCCTATTCCGAAGTTCCTATTCTCTAGAAAGTATAGGAACTTCATAACTTCGTATAAAGTAT
CCTATACGAAGTTATATGCAGGGCGGCCGCAAAAAAAAGGCCAAAAAGGCCAAAAAAAAGGCCGGCCAAGG
CCGCCACCGCGGTGGAGCTCCAATTCGCCCTATAGTGAGTCGTATTACAATTCACTGGCCGTCGTTTTACA
ACGTCGTGACTGGGAAAACCCTGGCGTTACCCAACTTAATCGCCTTGCAGCACATCCCCCTTTCGCCAGCT
GGCGTAATAGCGAAGAGGCCCGCACCGATCGCCCTTCCCAACAGTTGCGCAGCCTGAATGGCGAATGGAAA
TTGTAAGCGTTAATATTTTGTTAAAATTCGCGTTAAATTTTTGTTAAATCAGCTCATTTTTTAACCAATAG
GCCGAAA
```

Figure 2.6. Reference sequence for a 1000-bp region of pFlexible-LacO-pBLR5 integrated at Chr15 or TAP1 in U2OS cells. U2OS cells containing pFlexible-LacO-pBLR5 integrated at Chr15/TAP1 had previously undergone FLP recombination to remove the puroΔTK selectable marker prior to CRISPR genome editing to introduce the NHEJ or HR reporter. Guide RNAs targeting pFlexible-LacO-pBLR5 are highlighted in yellow. Guide RNAs were designed to target the 5' end of pFlexible-LacO-pBLR5 adjacent to the I-SceI restriction site (green highlight) and the lox sites (blue highlight). The sequences used to generate the homology arms of the donor vectors are shown in blue (5' homology) and red (3' homology).

2.3.1.6 CRISPR guide RNA design and cloning

Guide RNA (gRNA) sequences used in this study were selected and analyzed using the COSMID (CRISPR Off-target Sites with Mismatches, Insertions and Deletions) website (http://crispr.bme.gatech.edu/) to check for any potential off-target sites (256) and are listed in **Table 2.5**. For the expression of CRISPR guide RNAs targeting various protospacer sequences in the genome of U2OS cells, oligonucleotides were annealed (oligonucleotides termed A and B in **Table 2.5** were annealed together, creating a duplex with BbsI restriction enzyme-compatible overhangs) and cloned into BbsI-digested px330-U6-Chimeric_BB-CBh-hSpCas9 (CRISPR-associated protein-9 (Cas9) nuclease expression vector, termed px330) or BbsI-cut px335-U6-Chimeric_BB-CBh-hSpCas9n(D10A) (Cas9 nickase expression vector, termed px335). Cas9/gRNA expression vectors were verified by sequencing.

Table 2.5. CRISPR gRNA oligonucleotide sequences

CRISPR gRNA	Oligonucleotide sequence (5'-3')
Chr15 5' Oligo A	CACCGTCACTGGCAACTGGGAGCT
Chr15 5' Oligo B	AAACAGCTCCCAGTTGCCAGTGAC
Chr15 3' Oligo A	CACCGAACAGCCTGGAAATTAACTG
Chr15 3' Oligo B	AAACCAGTTAATTTCCAGGCTGTTC
TAP 5' Oligo A	CACCGTCAAAGCAGCCAGCCAGCCC
TAP 5' Oligo B	AAACGGGCTGGCTGGCTGCTTTGAC
TAP 3' Oligo A	CACCGGGCACTGGCTTGGCCCTGC
TAP 3' Oligo B	AAACGCAGGGCCAAGCCCAGTGCCC
pFlex Oligo A	CACCGTCAAAAAGTTTAAACAAAAA
pFlex Oligo B	AAACTTTTTGTTTAAACTTTTTGAC

2.3.2 Transfection of targeting constructs for cell line generation

2.3.2.1 PiggyBac (PB) transposition

For the random integration of the pFlexible-LacO-pBLR5 construct into the genome of U2OS cells using PB transposition, cells were co-transfected with pFlexible-LacO-pBLR5 and the PB transposase expression vector, mPB (252). A total of 12 μg of DNA was transfected with lipofectamine 2000 (Thermo Fisher Scientific) according to manufacturer's protocol at a ratio of 1:2, 1:5 or 1:10 of pFlexible-LacO-pBLR5 construct to transposase. Cells were allowed to recover for 48 h before selection with 1 μg/mL puromycin (Thermo Fisher Scientific). Cells were seeded at a low density to allow individual colony formation with 12 puromycin-resistant clones for each transfection ratio being picked for characterization (see **Table 2.1** for list of cell lines generated).

2.3.2.2 CRISPR/Cas9 genome editing of Chr15 and TAP1 loci

To target the pFlexible-LacO-pBLR5 construct to the Chr15 or TAP1 locus using CRISPR/Cas9, a total of 12 μg of DNA consisting of equal parts Chr15/TAP1 pFlexible-LacO-pBLR5 donor vectors and CRISPR Cas9/gRNA vectors were transfected into a total of 2×10^6 U2OS cells using the Neon transfection system (Thermo Fisher Scientific) according to manufacturer's protocol for U2OS cells (see **Table 2.6** for transfection details). Cells were allowed to recover for 48 h before selection with 1 μg/mL puromycin. Cells were seeded at a low density to allow individual colony formation with 6 puromycin-resistant clones for each transfection condition being picked for characterization (for a total of 24 clones-see **Table 2.1**).

Table 2.6. Transfections for the CRISPR/Cas9 mediated integration of pFlexible-LacO-pBLR5 at specific genomic loci in U2OS cells. CRISPR donor vectors carrying the pFlexible-LacO-pBLR5 construct flanked by homology arms targeting a specific locus on Chr15 or the TAP1 gene were co-transfected with Cas9/Cas9D10A nickase (px330/px335, respectively) expression vectors (which also contain locus-specific gRNAs) into U2OS cells. For the Cas9D10A nickase, two gRNA-containing vectors were transfected simultaneously to achieve effective targeting.

Transfection	CRISPR donor vector	Cas9/gRNA vector 1	Cas9/gRNA vector 2
1	6 µg Chr15-pFlexible-LacO-pBLR5-TOPO4	6 µg px330-Chr15 5' gRNA	–
2	6 µg Chr15-pFlexible-LacO-pBLR5-TOPO4	6 µg px330-Chr15 3' gRNA	–
3	4 µg Chr15-pFlexible-LacO-pBLR5-TOPO4	4 µg px335-Chr15 5' gRNA	4 µg px335-Chr15 3' gRNA
4	6 µg TAP-pFlexible-LacO-pBLR5-TOPO4	6 µg px330-TAP 5' gRNA	–
5	6 µg TAP-pFlexible-LacO-pBLR5-TOPO4	6 µg px330-TAP 3' gRNA	–
6	4 µg TAP-pFlexible-LacO-pBLR5-TOPO4	4 µg px335-TAP 5' gRNA	4 µg px335-TAP 3' gRNA

2.3.2.3 FLP /FRT and Cre/lox recombination

One Chr15 and one TAP1 clone (U2OS Chr15 5' px330 pFlexible col. 6 and U2OS TAP 5' px330 pFlexible col. 1) were selected for DNA repair reporter integration. For the removal of the puroΔTK selectable marker, these cells were transfected with a human-codon-optimized FLP recombinase expression vector, pPGK-FLPobpA (6 µg pPGK-FLPobpA and 6 µg BSK as a carrier for a total of 12 µg DNA) using lipofectamine 2000. Cells were allowed to recover for 48 h before selection with 5 µg/mL ganciclovir (Sigma-Aldrich). These cells were termed U2OS Chr15 5' px330 pFlexible col. 6 FLP and U2OS TAP 5' px330 pFlexible col. 1 FLP. Ganciclovir-resistant cells were then co-transfected with 6 µg of a Cre recombinase expression vector (pBS513 EF1 alpha-Cre) and either 6 µg of Floxed-pEJ or Floxed-pGC (as above). Cells were allowed to recover for 48 h before selection with either 1 µg/mL puromycin (for cells transfected with Floxed-pGC) or 400 µg/mL G418 (for cells transfected with Floxed-pEJ). Cells were seeded at a low density to allow individual colony formation with six drug-resistant clones for each transfection being picked for characterization. These cells were termed: U2OS Chr15 pFlexible Cre-NHEJ col. 1-6; U2OS Chr15 pFlexible Cre-HR col 1-6;

U2OS TAP pFlexible Cre-NHEJ col 1-6; U2OS TAP pFlexible Cre-HR col 1-6 (see **Table 2.1**).

2.3.2.4 CRISPR/Cas9 genome editing of Chr15/TAP1-integrated pFlexible-LacO-pBLR5

Alternatively, the NHEJ and HR reporters were integrated into the pFlexible-LacO-pBLR5 construct of U2OS Chr15 5' px330 pFlexible col. 6 FLP and U2OS TAP 5' px330 pFlexible col. 1 FLP cell lines using CRISPR/Cas9 targeting. A total of 2 x 10^6 cells from each cell line were co-transfected using Neon with 6 µg of either pFlexible-pEJ-TOPO2.1 or pFlexible-pGC-TOPO2.1 CRISPR donor vector (which carry the NHEJ or HR reporter respectively, flanked by homology arms targeting pFlexible-LacO-pBLR5) and 6 µg of a Cas9/gRNA vector (see **Table 2.7** for transfection details). Cells were allowed to recover for 48 h before selection with either 1 µg/mL puromycin (for cells transfected with pFlexible-pGC-TOPO2.1) or 400 µg/mL G418 (for cells transfected with pFlexible-pEJ-TOPO2.1). Cells were seeded at a low density to allow individual colony formation with six drug-resistant clones for each transfection being picked for characterization. These cells were termed: U2OS Chr15 pFlexible CRISPR-HR col 1-6; U2OS Chr15 pFlexible CRISPR-NHEJ col 1-6; U2OS TAP pFlexible CRISPR-HR col 1-6; U2OS TAP pFlexible CRISPR-NHEJ col 1-6 (see **Table 2.1**).

Table 2.7. Transfections for the CRISPR/Cas9 mediated integration of NHEJ and HR DNA repair reporters into U2OS cells containing the pFlexible-LacO-pBLR5 construct at Chr15/TAP1. CRISPR donor vectors carrying either the NHEJ or HR reporter flanked by homology arms targeting pFlexible-LacO-pBLR5 were co-transfected with a Cas9/gRNA expression vector into U2OS Chr15 5' px330 pFlexible col.6 FLP and U2OS TAP 5' px330 pFlexible col. 1 FLP cell lines.

Transfection	Transfected cell line	CRISPR donor vector	Cas9/gRNA vector
1	U2OS Chr15 pFlexible 5' px330 col. 6 FLP	6 µg pFlexible-pEJ-TOPO2.1	6 µg px330-pFlex gRNA
2	U2OS Chr15 pFlexible 5' px330 col. 6 FLP	6 µg pFlexible-pGC-TOPO2.1	6 µg px330-pFlex gRNA
3	U2OS TAP pFlexible 5' px330 col. 1 FLP	6 µg pFlexible-pEJ-TOPO2.1	6 µg px330-pFlex gRNA
4	U2OS TAP pFlexible 5' px330 col. 1 FLP	6 µg pFlexible-pGC-TOPO2.1	6 µg px330-pFlex gRNA

2.4 Cell line characterization

2.4.1 Southern blot analysis

Southern blot analysis was used to determine the number of copies of pFlexible-LacO-pBLR5 integrated in U2OS pFlexible PB clones. A 300-bp fragment of the puromycin-resistance gene was amplified by PCR using the pFlexible plasmid as a template (using primers: PuroF: 5'-CACATCGGCAAGGTGTGGGT-3' and PuroR: 5'-CGCTCGTAGAAGGGGAGGTT-3') to serve as the probe to detect pFlexible-LacO-pBLR5 insertions. A 560-bp high-copy-number telomere-associated repeat control probe (detecting a series of fragments ranging from 29 to 1.5 kb in EcoRI-digested human genomic DNA; M. Dobson, Dalhousie University, personal communication) was isolated from the pMD35 plasmid through digestion with EcoRI and SacI.

For Southern blot analysis, genomic DNA was isolated from each U2OS pFlexible PB cell line using the Wizard Genome DNA Purification Kit (Promega) according to the manufacturer's protocol. A total of 50 µg genomic DNA from each cell

line along with a Lambda DNA/HindIII Marker (Thermo Fisher Scientific) were digested with 20 units of EcoRI overnight at 37°C. Following digestion, DNA was phenol extracted and ethanol precipitated to ensure high DNA quality and quantity for analysis. Briefly, DNA was diluted 5-fold by addition of TE buffer (10 mM Tris, pH 8.0, 1 mM ethylenediaminetetraacetic acid (EDTA)), mixed and centrifuged at 11000 rpm for 10 min at room temperature. An equal volume of TE-saturated phenol was added and each sample was mixed and centrifuged again (as above). The aqueous layer was removed and 1/10 volume of 3 M sodium acetate pH 5.2 along with 2.5 volumes of 100% ethanol was added, mixed by inversion and samples incubated at -20°C for 1 h. Samples were centrifuged at 14000 rpm for 15 min at 4°C, pellets were washed in 70% ethanol and centrifuged at 15000 rpm for 5 min at 4°C. Pellets were then air dried and resuspended in 20 μL TE and concentrations determined on an Eppendorf BioPhotometer D30. A total of 20 μg purified EcoRI-digested genomic DNA per lane along with 100 ng of Lambda DNA/HindIII Marker (ladder) were resolved in 0.8% agarose gels (25 x 20 cm) in duplicate, using a Horizon gel apparatus (Biometra), to allow hybridization with a single-copy or high-copy probe. Gels were run at 25 mA, 43 V overnight (16-24 h) at 4°C. The following day, gels were stained with 0.5 μg/mL ethidium bromide with shaking for 30 min and imaged on a VersaDoc imaging system MP4000 (BioRad) to visually confirm complete digestion. Gels were subsequently destained in distilled water (dH$_2$O) for 1 h, followed by depurination in 0.25 M HCl for 15 min with shaking. Gels were rinsed for 5 min in dH$_2$O, denatured for 30 min in 1.5 M NaCl, 0.5 M NaOH, rinsed again in dH$_2$O and neutralized for 30 min in 1.5 M NaCl, 0.5 M Tris HCl pH 7.5 all while shaking. Finally, gels were rinsed briefly in dH$_2$O and incubated in 20X saline sodium citrate (SSC) transfer buffer (3 M NaCl, 300 mM Na$_3$C$_6$H$_5$O$_7$ pH 7.0). Resolved DNA was then transferred to pre-cut Zeta-Probe GT Charged Nylon membranes (BioRad) (that had been pre-rinsed in dH$_2$O for 10 min followed by 10 min in 10X SSC) overnight by Southern blotting (257). The following day, membranes were dried for 30 min and DNA crosslinked using a UV-Stratalinker 1800 (Stratagene) (1200 x 100 μJoule for 1 min). To prepare for probe hybridization, membranes were neutralized for 15 min in 2X SSC and then incubated for 1-2 h at 65°C in 6X saline-sodium phosphate-EDTA pre-hybridization solution (3 M NaCl, 200 mM NaH$_2$PO$_4$, 20 mM EDTA pH 7.4, 5x Denhardt's (Thermo

Fisher Scientific), 10% sodium dodecyl sulphate (SDS), 100 mg/mL denatured salmon sperm DNA (Thermo Fisher Scientific)).

To generate radioactively-labeled probes, probe DNA (described above) was boiled at 95°C for 10 min and placed on ice. Probes were immediately labeled with P^{32}-dCTP (Perkin Elmer) using a Random-Primed DNA Labeling Kit (Roche) according to the manufacturer's protocol. The labeling reaction was stopped with EDTA and the probes diluted 10-fold in TE buffer. Probe mixtures were then loaded onto a spin column consisting of packed dry Sephadex G50 beads (Sigma-Aldrich) and centrifuged for 5 min. One mL of pre-hybridization solution was added to the eluted labeled DNA which was then boiled for 10 min at 95°C. Probes were then added to the pre-hybridization solution containing the membrane and incubated overnight at 65°C with shaking. The following day, membranes were washed twice in 2X SSC for 30 min, exposed for 24-72 h at -80°C to autoradiographic film (Thermo Fisher Scientific) with Kodak intensifier screens, and then developed on a Kodak X-OMAT processor.

2.4.2 Inverse PCR

Inverse PCR was used to map the integration sites of pFlexible-LacO-pBLR5 in U2OS pFlexible PB clones. First, genomic DNA was extracted from each clone as described in section 2.4.1. Purified genomic DNA was then digested with either EcoRI (which cuts the pFlexible-LacO-pBLR5 insert 50 times starting at the 414th nucleotide from the 5' end and ending at the 10820th nucleotide) or PstI (which cuts the pFlexible-LacO-pBLR5 insert 18 times starting at the 1100th nucleotide from the 5' end and ending at the 10792nd nucleotide) for 2 h at 37°C, followed by heat inactivation for 20 mins (65°C for EcoRI digests and 80°C for PstI digests). Digested genomic DNA was then self-ligated using T4 DNA ligase (New England Biolabs) according to the manufacturer's protocol and subsequently used as a template for inverse PCR. Eight sets of primers were designed to amplify the genomic sequence flanking both sides of the insertion site separately (see **Table 2.8** for inverse PCR primer sequences and binding positions within pFlexible-LacO-pBLR5). PCR amplification was performed as described in section 2.3.1.1 (with various primer combinations and various adjustments made to annealing

temperature).

Table 2.8. Primers for mapping integration sites of U2OS pFlexible PB clones using inverse PCR.

Primer name	Sequence (5'-3')	Binding position*
EcoRI 5A R	CAAGCGGCGACTGAGATGT	118-100
EcoRI 5B R	CAGTGACACTTACCGCATTGACA	161-139
EcoRI 5C F	GGCATCTTAAGCAAGCTCGAA	320-340
EcoRI 5D F	CACTAAAGGGAACAAAAGCTGGTA	350-373
EcoRI 3A F	CACAATATGATTATCTTTCTAGGG	100056-10079
EcoRI 3B F	GATATACACACCGATAAAACACAT	9996-10019
EcoRI 3C R	AAAACTCAAAATTTCTTCTATAAAG	10880-9856
EcoRI 3D R	GTAACAAAACTTTTAACTAGTATGTCG	9856-9830
PstI 5C F	CTCGCACACATTCCACATCCA	822-845
PstI 5D F	CAAATGGAAGTAGCACGTCTCACT	688-708

*As measured from the 5' end of the pFlexible-LacO-pBLR5 construct

2.4.3 Fluorescence *in-situ* hybridization (FISH) and immuno-FISH

FISH and 3D immuno-FISH protocols were adapted from Zinner *et al*., 2007 and Ching *et al*., 2013 (230, 258). Cells were seeded onto sterile frosted glass microscope slides (Thermo Fisher Scientific) so that they would be at a confluency of 70-80% the next day. Slides were rinsed twice in PBS at 37°C and cells fixed in 4% PFA for 10 min at room temperature. Cells were washed three times in 0.01% Triton X-100 for 3 min, followed by a 15 min wash in 0.5% Triton X-100 and an overnight incubation in 20% glyercol, all at room temperature. The next day, slides were frozen in liquid nitrogen for 30 s, allowed to thaw completely, and then immersed back into 20% glycerol; this was repeated four times. Cells were subsequently washed three times in PBS for 10 min at room temperature followed by a 5 min incubation in 0.1 M HCl. Cells were then washed twice in 2X SSC for 3 min and incubated overnight in a 50% formamide-SSC solution, all at room temperature.

In preparation for probe hybridization, 0.5 µg Spectrum Orange-labeled Chr15, TAP1 or BCL2 probe (BAC reference: RP11105M14, RP111A19 and RP11-160M23,

61

respectively) along with 0.5 μg pFlexible-LacO-pBLR5 digoxigenin (DIG)-labeled probe (Sick Kids Centre for Applied Genomics, Toronto) was mixed in a 2:1 ratio with human Cot1 DNA (Thermo Fisher Scientific) in 10 μL pre-hybridization buffer (50% formamide, 10% dextran sulfate, 50 mM sodium phosphate buffer, pH 7.0 in 2X SSC). The probe mixture was added to a coverslip, placed onto the target area of the slide and sealed with rubber cement (Fixogum). Cellular and probe DNA was denatured for 3 min at 75°C and probe hybridization was performed at 37°C for 3 days. Following hybridization, coverslips and rubber cement were gently removed and slides were washed three times in 2X SSC for 5 min at 37°C followed by three washes in 0.1X SSC for 5 min at 65°C, all with shaking. Cells were rinsed briefly in SSC/Tween (4X SSC, 0.2% Tween 20), blocked in 4% (w/v) (bovine serum albumin) BSA (BioShop) in SSC/Tween for 15 min at 37°C. Cells were subsequently incubated with mouse anti-DIG antibodies (Abcam) (to detect the pFlexible-LacO-pBLR5 specific probe) diluted to 0.8 μg/mL final concentration or for immuno-FISH, with rabbit-anti-PML antibodies (Bethyl) diluted 1:1000 in 1% BSA SSC/Tween for 1 h at 37°C. Following incubation with the primary antibody, cells were washed 3 times in SSC/Tween for 3 min each wash at 37°C with shaking and incubated with Alexa Fluor 488 donkey anti-mouse or donkey anti-rabbit antibody (Thermo Fisher Scientific) diluted 1:1000 in 1% BSA SSC/Tween for 45 min at 37°C. Cells were washed 3 times in SSC/Tween for 3 min at 37°C and incubated with 4',6-diamidino-2-phenylindole (DAPI) (Sigma-Aldrich) at a final concentration of 1 μg/mL in PBS for 10 minutes at room temperature to visualize nuclei, followed by three 5 min room temperature washes in PBS. Coverslips were then mounted on slides using VECTASHIELD antifade mounting medium (Vector Laboratories). Fluorescent images were captured on a Zeiss Axioobserver Z1 inverted microscope (as described above) under a 63x immersion oil objective lens and processed using Slidebook and Adobe Photoshop CS8. For 3D immuno-FISH, image stacks were exported to Imaris software, where quantification of distances between PML nuclear bodies and the Chr15, TAP1 and BCL2 FISH probes were determined. The 3D positions of the nuclei were first defined using DAPI fluorescence signal, while the 3D positions of PML nuclear bodies in the nuclei were defined using Alexa Fluor 488 signal from the anti-PML immunostaining and the 3D positions of the Chr15/TAP1/BCL2 locus defined using signal from the Spectrum

Orange-labeled probes. The distances between the centres of the defined FISH probe objects and closest PML body in each defined nucleus were calculated and exported to Excel for analysis. At least 50 nuclei were analyzed for TAP1 and BCL2 probes while 9 were analyzed for Chr15. The average closest distance between a PML nuclear body and FISH signal was calculated for each probe. Statistical analyses (two-tailed t-test) were conducted using Excel.

2.4.4 Genomic PCR

PCR was used to confirm that the pFlexible-LacO-pBLR5 construct was integrated as predicted at the Chr15 or TAP1 locus of U2OS cells. Each end of the integrated construct was mapped separately by PCR. To map the 5' end of the construct, forward primers were designed to bind in the Chr15 or TAP1 locus upstream of the edited region and reverse primers were designed to bind within the 5' end of pFlexible-LacO-pBLR5 (see **Table 2.9** for primer sequences). Similarly, to map the 3' end of the construct, forward primers were designed to bind within the extreme 3' end of pFlexible-LacO-pBLR5 and reverse primers were designed to bind in the Chr15 or TAP1 locus downstream of the edited region (see **Figure 2.7A**). Genomic DNA was isolated from each U2OS Chr15/TAP1 pFlexible clone (as described in section 2.4.1) and used as a template for PCR amplification (as described in section 2.3.1.1). Genomic DNA isolated from wild-type U2OS cells was used as a control. Resulting PCR amplicons of the correct size were then gel purified and verified by Sanger sequencing.

To confirm correct integration of the NHEJ or HR reporter into U2OS Chr15 5' px330 pFlexible col. 6 FLP or U2OS TAP 5' px330 pFlexible col. 1 FLP cells, a forward primer was designed to bind the 5' end of pFlexible-LacO-pBLR5 (5' to the edited region) and a reverse primer designed to bind within the CMV promoter of the NHEJ/HR reporter as shown in **Figure 2.7B** (refer to **Table 2.9** for primer sequences). Genomic DNA was isolated from each U2OS Chr15 pFlexible CRISPR NHEJ/HR or U2OS TAP pFlexible CRISPR NHEJ/HR set of clones and used as a template for PCR amplification. Genomic DNA isolated from wild-type U2OS cells as well as from U2OS Chr15 5'

px330 pFlexible col. 6 FLP and U2OS TAP 5' px330 pFlexible col 1 FLP cells were used as controls. Resulting PCR amplicons of the correct size were then gel purified and verified by sequencing.

Table 2.9. Primers used for genomic PCR verification of CRISPR/Cas9 generated cell lines.

Primer name	Sequence (5'-3')	Region used to verify
C15 SEQ 5 F1	CTGGGCTCCTGTTGAATCTGT	5'end of Chr15 pFlexible-LacO-pBLR5 insertion
TAP SEQ 5 F5	CGCATATTCTCCCTGCTGGT	5'end of TAP1 pFlexible-LacO-pBLR5 insertion
pFlex SEQ 5 R1	TGGATGTGGAATGTGTGCGA	5'end of Chr15/TAP1 pFlexible-LacO-pBLR5 insertion
C15 SEQ 3 R1	CTCCACCAGCCCCTCATTT	3'end of Chr15 pFlexible-LacO-pBLR5 insertion
TAP SEQ 3 R1	ACCTTTGATTCCTGTCCCAGTC	3 end of TAP1 pFlexible-LacO-pBLR5 insertion
pFlex SEQ 3 F1	CGTACGTCACAATATGATTATCTTTCTA	3'end of Chr15/TAP1 pFlexible-LacO-pBLR5 insertion
pFlex N/H F	GCTCGAAATTAACCCTCACTAAAG	Insertion of NHEJ/HR reporter in pFlexible-LacO-pBLR5
CMV Pro N/H R	CGTTACTATGGGAACATACGTCATT	Insertion of NHEJ/HR reporter in pFlexible-LacO-pBLR5
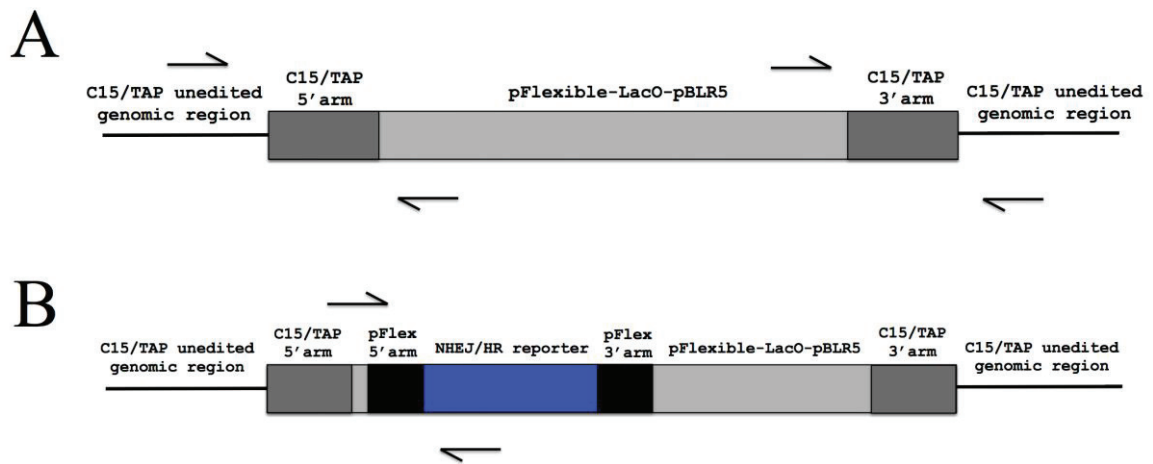
Figure 2.7. Strategy for verifying CRISPR insertions in U2OS cells by genomic PCR. (A) To verify correct insertion of pFlexible-LacO-pBLR5 at the Chr15 or TAP1 locus in U2OS cells, primers (depicted by half arrows) were designed to sequence both sites of the insertion separately as shown. **(B)** To verify correct insertion of NHEJ or HR reporter DNA within integrated-pFlexible-LacO-pBLR5, a forward primer was designed to bind the pFlexible-LacO-pBLR5 sequence downstream of the 5' homology arm and a reverse primer was designed to bind within the CMV promoter of NHEJ/HR reporter DNA as shown.

2.4.5 I-SceI assays

To test the functionality of integrated NHEJ/HR reporters in U2OS Chr15 pFlexible CRISPR NHEJ/HR and U2OS TAP pFlexible CRISPR NHEJ/HR clones, 3 μg of an I-SceI expression vector, β-Actin-SceI, was transfected along with 3 μg of a Far-Red protein expression vector, pNLS-IRFP670 (transfection control) and 6 μg BSK (carrier) into each clone using the Neon transfection system. Cells were then analyzed for GFP expression by flow cytometry (section 2.5.2) 72 h post-transfection.

2.5 DNA repair assays

HR repair assays were performed as previously described (259). Briefly, a total of 2×10^6 U2OS and U2OS PML knockout (ΔPML) cells were transfected with equal amounts of Clover-lamin CRISPR donor, empty FLAG vector (CMV-FLAG-J1) or a plasmid that would express a single FLAG-tagged PML isoform (PML I-VI) along with one expressing Far-Red protein fused to an NLS (pNLS-IRFP670; transfection control) +/- px330-lamin 5' gRNA (12 μg total DNA) using the Neon transfection system. In transfections without px330-lamin 5' gRNA, BSK was used as a replacement. Cells were plated into separate 9-cm plates (each containing a sterile coverslip) and harvested for flow cytometry (an aliquot was removed for cell cycle analysis) and immunofluorescence analysis after 72 h.

For NHEJ repair assays, a total of 2×10^6 U2OS and U2OS ΔPML cells were transfected with equal amounts of the NHEJ repair reporter vector EJ5-GFP, empty FLAG vector (CMV-FLAG-J1) or an individual FLAG-tagged PML isoform (I-VI) expression vector and pNLS-IRFP670 +/- a β-Actin-SceI expression vector (12 μg total DNA) using Neon. In transfections without β-Actin-SceI, BSK was used instead. Cells were plated and harvested as above.

For chromosomal HR/NHEJ repair assays, a total of 2×10^6 U2OS Chr15 pFlexible CRISPR HR col.2, U2OS TAP CRISPR HR col. 6 and U2OS TAP pFlexible CRISPR NHEJ col. 4 cells were transfected with equal amounts of an empty FLAG vector (CMV-FLAG-J1) or an individual FLAG-tagged PML isoform (I-VI) expression

vector, pNLS-IRFP670 (transfection control) and BSK (carrier) +/- a β-Actin-SceI expression vector (12 µg total DNA) using Neon. In transfections without β-Actin-SceI, additional BSK was added to achieve 12 µg total DNA. Cells were plated and harvested as described above.

2.5.1 Immunofluorescence

Cells were transfected and plated as described above. On the day of analysis, coverslips were removed from each 9-cm plate, placed into an individual well of a 6-well dish and washed briefly with PBS. Cells were fixed in 2% PFA for 10 min, washed 3 times for 5 min each wash in PBS, permeabilized in 0.5% Triton X-100 for 5 min and washed again 3 times in PBS for 5 min. Cells were blocked in 3% BSA in PBS for 20 min followed by a 1 h incubation with antibodies specific for PML (rabbit anti-PML) and FLAG (mouse anti-FLAG M2, Sigma-Aldrich), both diluted 1:1000 in 3% BSA in PBS. Following incubation with the primary antibody, cells were washed 3 times in PBS for 5 min per wash and incubated for 30 min with Alexa-Fluor 649 donkey anti-rabbit and Alexa-Fluor 555 donkey anti-mouse (Thermo Fisher Scientific) secondary antibodies both diluted 1:1000 in 3% BSA in PBS. Cells were washed again three times in PBS for 5 min, nuclei were stained with DAPI for 10 min at a final concentration of 1 µg/ml, and washed again 3 times in PBS for 5 min. Coverslips were mounted on frosted glass microscope slides using Dako fluorescent mounting medium (Dako Agilent Pathology Solutions) and fluorescent images were captured as described in section 2.4.3.

2.5.2 Flow cytometry

For determining the percent of Clover- or GFP-positive cells, cells were trypsinized from 9-cm plates and resuspended in PBS. Cell suspensions were fixed in 2% PFA for 20 minutes at room temperature with constant inversion. Cells were then pelleted by centrifugation at 2000 rpm for 5 minutes at 4°C, washed in 25 mM ammonium citrate in PBS, centrifuged (as above) and resuspended in 1 mL PBS.

For cell cycle analysis, cells were trypsinized from 9-cm plates and 1×10^6 cells were pelleted by centrifugation at 1200 rpm for 6 minutes at room temperature. Pellets were resuspended in 0.5 mL PBS and fixed with the dropwise addition of 4.5 mL of 70% ice-cold ethanol with mild vortexing. Ethanol-fixed cell suspensions were incubated for at least 24 h at -20°C. On the day of cell cycle analysis, samples were pelleted by centrifugation at 1200 rpm for 5 min at room temperature, washed in PBS, collected by centrifugation, and resuspended in 0.5 mL of a PBS-propidium iodide (PI) solution (0.1% Triton X-100, 0.2 mg/mL RNaseA, 1mg/mL PI) for 30 minutes at room temperature.

Flow cytometry was performed using a FACSCalibur flow cytometer (BD Biosciences) and analysis performed using Flowing Software (Cell Imaging Core, Turku Centre for Biotechnology, Finland; version 2.5.1). For DNA repair assays, cells were first gated for intact cell population using forward-scatter *versus* side-scatter plots and then gated for transfected cells based on the expression of the transfection control, Far-Red protein IRFP-670 using side-scatter versus IRFP-670 plots. Transfected cells were then gated for GFP or Clover-positive cells on the side-scatter *versus* GFP/Clover plots such that the percentage of IRFP-670-transfected control cells (cells transfected with a specific PML isoform but without β-Actin-SceI or px330-lamin 5' gRNA) that were designated as GFP/Clover positive was 1%. The mean and standard deviation from three independent replicates were calculated. Statistical analyses (two-tailed t-test) were conducted using Excel 2007 software. For cell cycle analysis, cells were gated for intact cell population (as above) and percentage of cells in each cell cycle phase determined from plots of counts versus PI. Cell cycle analysis was done in triplicate for each experimental condition in each cell line. Statistical analysis was performed as above.

CHAPTER 3. RESULTS

This chapter contains material (Figures 3.1, 3.2) originally published in:

"Andrin C, McDonald D, Attwood KM, Rodrigue A, Ghosh S, Mirzayans R, Masson JY, Dellaire G, and Hendzel MJ. 2012. A requirement for polymerized actin in DNA double-strand break repair. Nucleus 3:384-395"

and material (Figure 3.3) originally published in:

"Lemaitre C, Grabarz A, Tsouroula K, Andronov L, Furst, A, Pankotai, T, Heyer V, Rogier M, Attwood KM, Kessler R, Delliare G, Klaholz, B, Reina-San-Martin B, and Soutoglou E. 2014. Nuclear position dictates DNA repair pathway choice. Genes and Development 28:2450-2463"

3.1 The role of polymerized nuclear actin in DNA repair

As discussed in section 1.4.1, nuclear actin, particularly in the polymerized state, has been implicated in the cellular response to DNA damage. Specifically, overexpression of an actin-depolymerization factor was found to alter nuclear actin dynamics and to consequently sensitize cells to IR (182, 183). However the exact contribution of polymeric nuclear actin to DNA repair or the DDR was never examined. In collaboration with Dr. Michael Hendzel and his group at the University of Alberta, I investigated the role of polymerized nuclear actin in DSB repair (13).

As an initial determination of whether a relationship exists between actin polymerization and DSB repair, Dr. Hendzel's group examined the dynamics of several DDR factors after IR-induced DNA damage in cells pre-treated with the actin-disrupting drug latrunculin. It was found that certain DDR proteins, notably Ku70/Ku80, MRE11, NBS1, ATM and CHK2, displayed a lower association with chromatin in nuclei extracted from these cells, compared to nuclei extracted from irradiated but untreated cells. However, not all of these factors were found to associate with polymeric actin *in vitro*.

Using an F-actin pull-down assay, which separates polymeric actin and its interaction partners from monomeric actin and other smaller complexes by high-speed centrifugation, it was shown that Ku70/Ku80, MRE11 and RAD51, but not CHK2, associate with polymeric actin. While this assay cannot separate direct interactions with nuclear actin from indirect associations mediated by other factors, it was interesting to note that polymeric actin was found to associate specifically with proteins involved in the recognition and processing of DSBs (Ku80, MRE11, RAD51) rather than DSB signaling (CHK2). This was the initial suggestion that actin plays a role at the level of DNA repair itself, as opposed to downstream DDR signaling events. To determine whether polymerized actin does in fact impact the DNA repair process, Dr. Hendzel's group used an *in vitro* NHEJ assay based on the repair of a linearized plasmid containing non-homologous ends. Briefly, nuclear soluble extracts from control or latrunculin-treated cells were incubated with plasmid DNA and repair, as visualized by bands of increasing size on an agarose gel, was evaluated. Through this assay, it was determined that disruption of actin polymerization by latrunculin treatment did in fact result in a reduction of DNA repair by NHEJ. To extend these results and determine if polymerized actin plays a physiologically relevant role in DNA repair, two *in vivo* DNA repair assays, the comet assay and the fraction-of-activity released (FAR) assay, were used to determine repair efficiency in the presence or absence of latrunculin. The comet and FAR assays are similar, highly sensitive methods used to measure the amount of DNA damage (both DSBs and SSBs) present in a cell at various time points following irradiation, thus serving as an indicator of the overall level of DNA repair (260). Both *in vivo* assays revealed a delay in the repair of IR-induced DSBs when actin polymerization was disrupted by treatment with latrunculin. Subsequent western blot analysis revealed that disruption of actin polymerization does not affect the overall phosphorylation of H2AX in irradiated cells, nor does it impact the phosphorylation and thus activation of ATM or CHK2. DNA damage signaling and checkpoint pathways therefore appear to be unaffected following disruption of actin polymerization, reinforcing the notion that polymeric actin is important during the DNA repair process itself.

3.1.1 Altering the polymerization state of nuclear actin affects retention of the DNA repair factor Ku80 at DNA breaks

Given the data showing that polymeric actin interacts with the Ku70/Ku80 heterodimer, and in an attempt to further understand the manner in which polymeric actin contributes to DNA repair, I examined the effects of altering actin polymerization on Ku80 recruitment and retention kinetics at UV laser-induced DNA damage sites. Human osteosarcoma U2OS cells were co-transfected with plasmids that would express GFP-tagged Ku80 and either a polymerization-incompetent actin mutant, NLS-actin G13R (261), or NLS-wild-type actin. Cells were then subjected to UV laser micro-irradiation, generating tracks of DNA damage across transfected nuclei (248). Ku80-GFP recruitment to these laser tracks was then followed by live-cell fluorescent imaging. As a control, cells transfected with Ku80-GFP alone were micro-irradiated to establish baseline Ku recruitment kinetics without any alterations to the nuclear actin pool (**Figure 3.2A**). Ku80-GFP was recruited rapidly (within seconds) to DNA damage tracks, consistent with previously published results (12). Importantly, co-transfection with nuclear-targeted wild-type actin did not appear to alter Ku80-GFP recruitment kinetics (compare **Figure 3.1A** top panel with **Figure 3.2A** top panel). Co-transfection with the NLS-actin G13R mutant also had no discernible effect on Ku80-GFP recruitment to UV laser-induced DNA damage tracks; however, Ku80-GFP retention at damage sites was significantly reduced as determined by measuring fluorescence intensity within the damage track relative to an outside nuclear region (**Figure 3.1A** bottom panel and **B**). To further support these results, Ku80-GFP transfected cells were treated with another actin-disrupting drug, cytochalasin D. In the presence of cytochalasin D, Ku80-GFP was rapidly recruited to DNA damage tracks, and its retention at damage sites was reduced to a similar degree as in NLS-actin G13R transfected cells (**Figure 3.2A** bottom panel and **B**). Therefore it appears that polymerized nuclear actin is playing an important role in the repair process itself by facilitating the retention of the Ku heterodimer to DNA break sites during NHEJ.
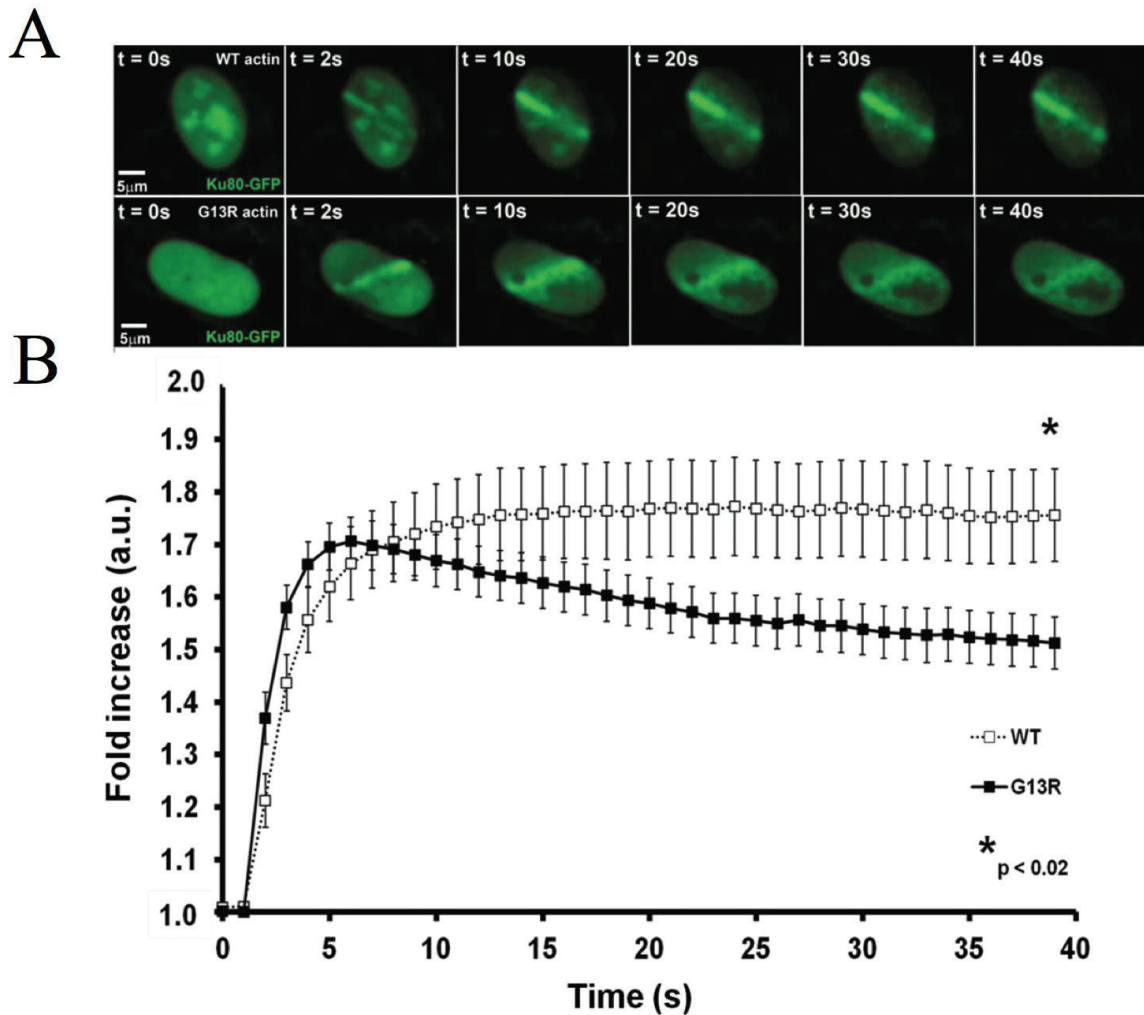
Figure 3.1. **Recruitment and retention of Ku80-GFP to sites of micro-irradiation-induced DNA damage in the presence actin mutants**. **(A)** UV laser micro-irradiated U2OS cells expressing Ku80-GFP and either wild-type or G13R mutant actin. Cells were imaged every second for 40 s by live-cell spinning-disc confocal microscopy. **(B)** Fold increase of GFP fluorescence intensity within UV laser-induced DNA damage tracks relative to nuclear regions outside of the tracks. Relative fluorescence intensity was measured for each wild-type or G13R actin-transfected cell every second for 40 s. Error bars represent standard error. n = 30. Two-tailed t-test indicates the differences in fold increase of GFP fluorescence intensity in wild-type *versus* G13R actin-transfected cells were significant (p < 0.02).
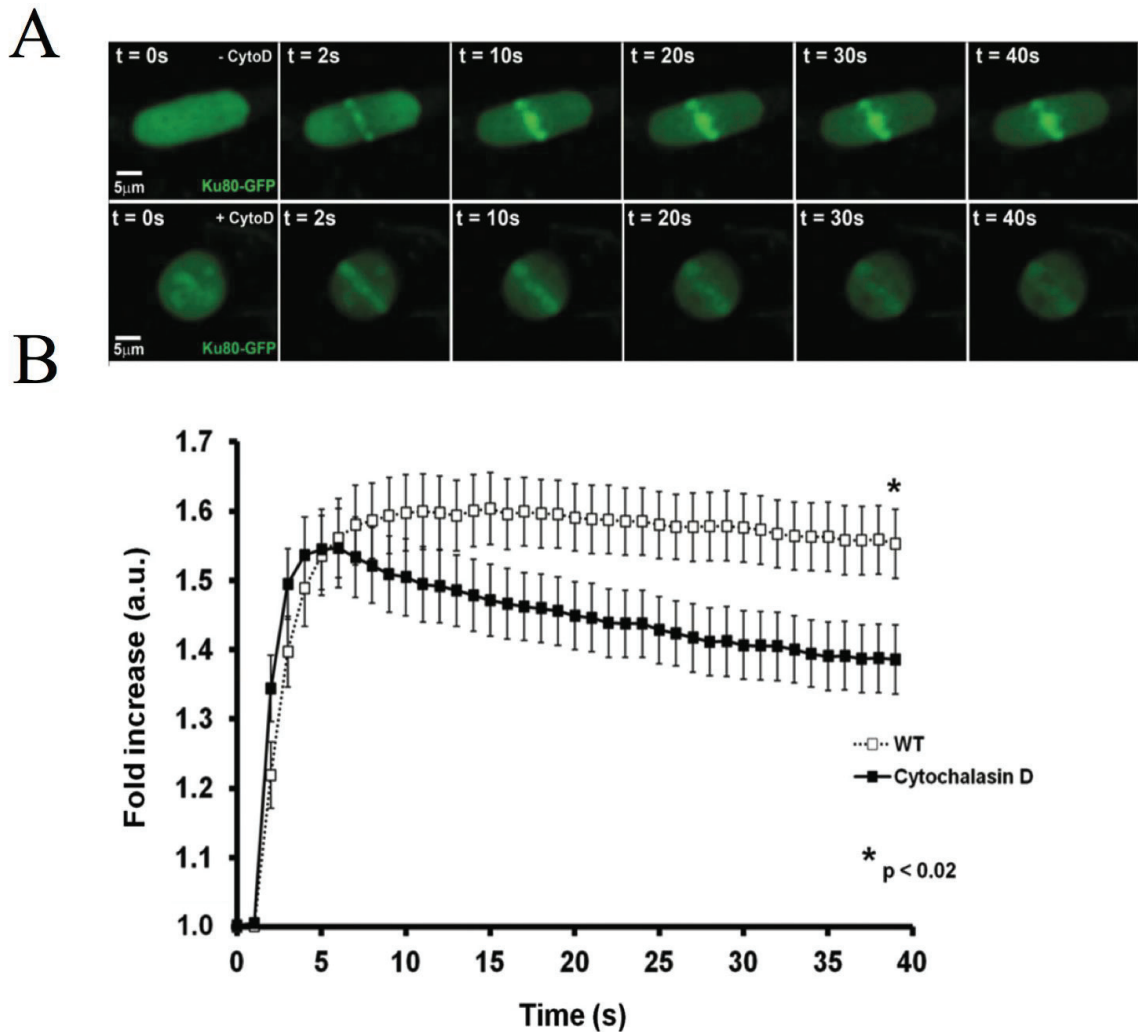
Figure 3.2. Recruitment and retention of Ku80-GFP to sites of micro-irradiation-induced DNA damage in the presence of the actin-polymerization inhibitor cytochalasin D. (A) UV laser micro-irradiated U2OS cells expressing Ku80-GFP with and without cytochalasin D treatment. Cells were imaged every second for 40 s by live-cell spinning-disc confocal microscopy. **(B)** Fold increase of GFP fluorescence intensity within UV laser-induced DNA damage tracks relative to nuclear regions outside of the tracks. Relative fluorescence intensity was measured for each untreated or cytochalasin D-treated cell every second for 40 s. Error bars represent standard error. n = 30. Two tailed t-test indicates the differences in fold increase of GFP fluorescence intensity in untreated *versus* cytochalasin D treated cells were significant (p < 0.02).

3.2 DNA repair at the nuclear lamina

As discussed in section 1.4, the nuclear location in which a DNA break occurs with respect to particular nuclear subdomains has the potential to influence its subsequent repair. In collaboration with Dr. Evi Soutoglou and her group at the Institut Génétique Biologie Moléculaire Cellulaire, I investigated DNA repair at the nuclear periphery, specifically the nuclear lamina (262).

To study DNA repair at the nuclear lamina, Dr. Soutoglou's group created U2OS cells in which a single DSB could be induced in a temporally and spatially defined manner. Specifically, these U2OS cells contained a stably integrated restriction site for the rare-cutting endonuclease I-SceI, flanked by a 256x LacO array. The LacO/I-SceI chromosomal locus could then be visualized in the nucleus through expression of a GFP-tagged Lac repressor (LacI). Additionally, to allow temporal control of DSB induction, these cells were engineered to express I-SceI under the control of a doxycycline-inducible promoter. Sequestration of the LacO/I-SceI locus to the nuclear lamina could then be induced in these cells through expression of an emerin C-terminal deletion (ΔEMD) protein that has been previously shown to localize to the nuclear lamina (264), fused to GFP-LacI (GFP-LacI-ΔEMD). Relocalization of the LacO/I-SceI locus to the nuclear periphery is confirmed by its colocalization with the nuclear lamina component, lamin B through immuno-FISH. To assess the impact of the nuclear lamina on DDR efficiency, the kinetics of γ-H2AX formation were compared at the I-SceI-induced DSB in cells expressing either GFP-LacI (nuclear interior), or GFP-LacI-ΔEMD (nuclear lamina) by immuno-FISH. Delayed γ-H2AX accumulation at the I-SceI-induced DSB was observed in GFP-LacI-ΔEMD expressing cells, with maximal γ-H2AX colocalization with the LacO/I-SceI locus occurring at 24 h after doxycycline addition, relative to only 14 h in cells expressing GFP-LacI. A similar delay in recruitment of another DDR factor, 53BP1, was also observed in these cells, suggesting that the nuclear lamina is generally a repressive microenvironment for DDR. To investigate if this delay in the DDR at the nuclear lamina is related to DNA repair itself, the degree of colocalization of two key NHEJ factors, Ku80 and XRCC4, with the LacO/I-SceI locus in GFP-LacI or GFP-LacI-ΔEMD expressing cells was examined. No observable difference in Ku80 or XRCC4 recruitment was found following DSB induction at the nuclear interior relative to the

nuclear lamina, suggesting that NHEJ can occur with equal efficiency in both compartments. However, when the recruitment kinetics of HR factors such as BRCA1 and RAD51 were examined, there appeared to be a marked defect in factor recruitment when the DSB was localized at the nuclear periphery, suggesting that the nuclear lamina is a particularly repressive environment for HR but not NHEJ.

3.2.1 Histone deacetylase inhibitor trichostatin A alleviates homologous recombination repression at the nuclear lamina

As discussed in section 1.4.2, the nuclear lamina is one of the main sites of heterochromatin in mammalian nuclei. Therefore, one possible explanation for the delay in HR and DDR factor recruitment to DSBs at the nuclear periphery is that the highly structured nature of the chromatin normally associated with this nuclear compartment is acting as a barrier for effective HR. To investigate this possibility, cells were treated with the HDAC inhibitor TSA to increase histone acetylation and subsequently induce global chromatin decondensation. TSA treatment was confirmed to cause relaxation of chromatin structure at the nuclear periphery as visualized by EM (**Figure 3.3**) and to alleviate the delay in DDR (γ-H2AX) and HR (BRCA1 and RAD51) factor recruitment to DSBs induced in GFP-LacI-ΔEMD expressing cells (without impacting sequestration of the LacO/I-SceI locus to the nuclear lamina). This finding therefore points to an inhibitory role of heterochromatin in HR and the DDR occurring at the nuclear lamina. This effect was also confirmed by Dr. Soutoglou's group through direct tethering of the chromatin remodeler BRG1 to the LacO/I-SceI locus by expressing it as a fusion protein with cherry-LacI (cherry-LacI-BRG1). Tethering BRG1 to the LacO/I-SceI array in GFP-LacI-ΔEMD expressing cells induced chromatin relaxation around the break site and alleviated the defect in DDR and HR factor recruitment to a similar degree as TSA treatment. Altogether these results demonstrate that the reduced DDR and HR occurring at the nuclear lamina is due to the highly compacted chromatin associated with this nuclear compartment.
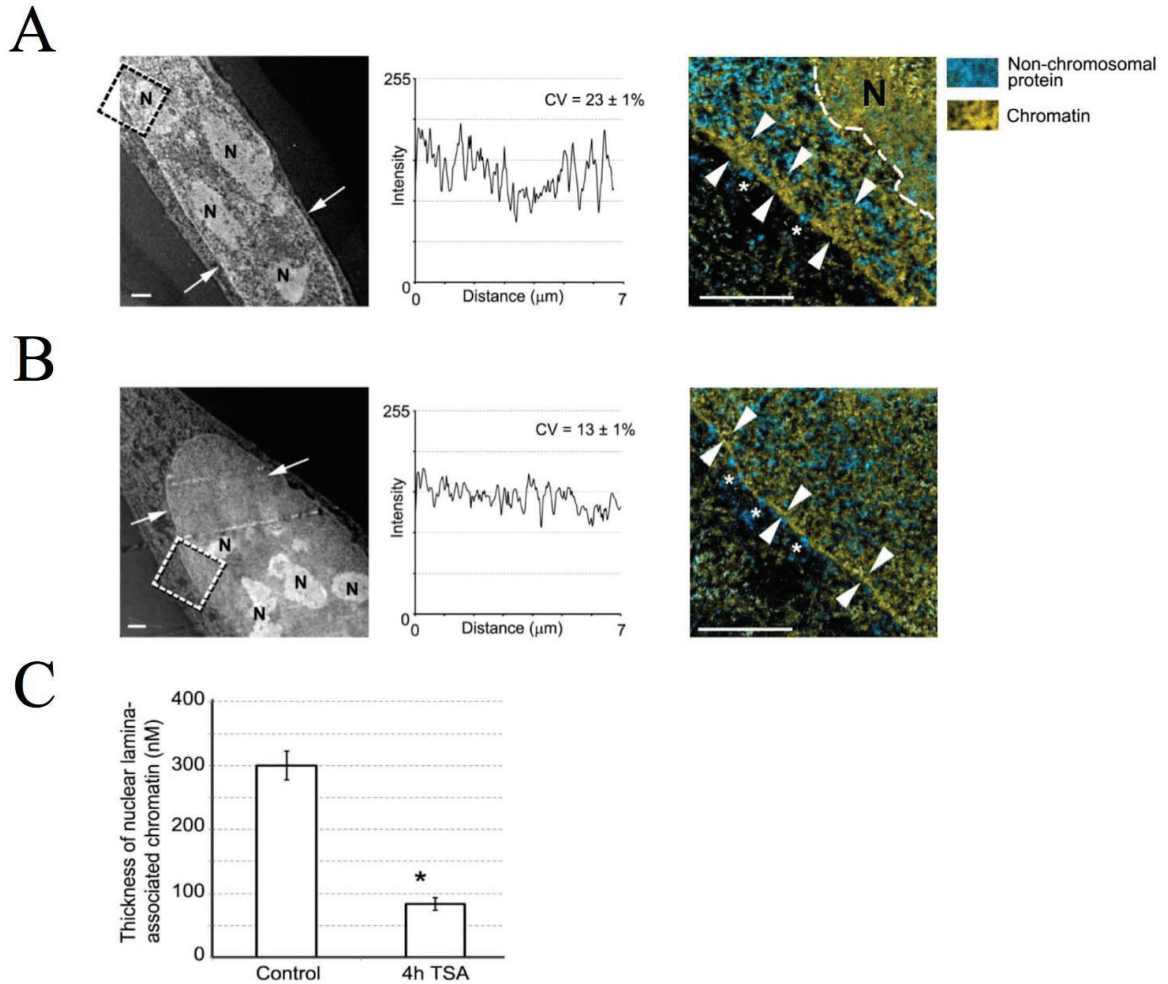
Figure 3.3. Chromatin ultrastructural changes following DMSO or TSA treatment.
U2OS cells were treated with **(A)** vehicle (0.1% DMSO) or **(B)** with 500 nM TSA for 4 h before fixation and processing for ESI. In each row a low magnification phosphorus-enriched (155 KeV) electron micrograph is shown at the left, a line-scan of phosphorus intensity across the cell nucleus (between the white arrows) is shown in the middle panel, and on the far right a high magnification ESI electron micrograph is shown of the region outlined by a dashed box in the low-magnification micrograph. The CV is also shown for the phosphorus intensity across the nuclei of vehicle- and TSA-treated cells (n=5; ± SEM), and represents the degree of variability in chromatin density as a percentage, where a lower percentage indicates a more homogeneous chromatin density. The ESI micrographs have been false coloured such that chromatin appears yellow and non-chromosomal protein (e.g. nucleopores, marked by white asterisks) appears cyan. The thickness of the nuclear lamina-associated chromatin is demarcated by white arrowheads, N = nucleoli, and the scale bars = 1 micron. **(C)** The mean thickness of condensed chromatin associated with the nuclear lamina for cells treated with vehicle or with 500 nM TSA and depicted as a bar graph. Error bars = SEM, n=10. *p < 0.001.

3.3 Generation of cell lines containing reporters to study DSB repair at single defined nuclear positions

The major aim of this study was to follow the repair of single defined DSBs induced at various nuclear positions to further our understanding of the influence of nuclear architecture on DNA repair. As a means of monitoring DNA repair, reporter plasmids based on the reconstitution of a defective GFP gene (as described in section 2.3.1.2 and **Figure 2.2**) were used to measure DNA repair by either NHEJ or HR at a single defined DSB induced by the I-SceI endonuclease. To study DNA repair in differing nuclear positions, an initial strategy was devised using a combination of directional Cre/loxP recombination and PiggyBac transposition to randomly integrate a single copy of either the NHEJ or HR reporter into the genome of U2OS cells. Cellular clones containing reporter DNA integrated in different chromosomes and chromatin environments would then be selected. An alternative strategy was later employed to specifically target reporter DNA to pre-determined genomic loci by CRISPR/Cas9 genome editing. In both strategies, a 128x LacO array integrated adjacent to reporter DNA would allow locus visualization in these cells. The effect of nuclear position on DNA repair could then be determined by directly comparing rates of DNA repair (as measured by detecting GFP fluorescence following I-SceI DSB induction) between different cell lines.

3.3.1 PiggyBac transposition

The PiggyBac transposon is a mobile genetic element originally isolated from the genome of the cabbage looper moth *Trichoplusia ni*. PiggyBac transposase efficiently transposes a DNA sequence flanked by PiggyBac terminal repeat sequences by a "cut and paste" mechanism, inserting the DNA at target sites containing TTAA sequences, with only modest preference for gene-rich genomic regions (264, 265). The PiggyBac transposon system was chosen as the means for engineering the cell lines in this study due to its ability to mediate stable, long-term expression in mammalian cells and its capacity to transpose large-size cargo (up to 100 kb) (265, 266). To generate these cell lines, the following strategy was initially devised (see **Figure 3.4**). Firstly, a 14-kb

targeting construct termed pFlexible-LacO-pBLR5 that contains the LacO array as well as the components for FLP/FRT and Cre/lox recombination in addition to the terminal repeats required for PiggyBac transposition, was created (see section 2.3.1.1 and **Figure 2.1**). The pFlexible-LacO-pBLR5 construct can then be integrated into the genome of U2OS cells by expressing a human-codon-optimized PiggyBac transposase, with integration being selected for by cellular resistance to puromycin. Individual puromycin-resistant colonies can then be screened for pFlexible-LacO-pBLR5 integration number and genomic position, with only those colonies containing a single integration selected for further genome engineering. Transfection of these cells with a FLP recombinase expression vector results in recombination across FRT sites and ultimate deletion of the intervening puroΔTK selectable marker (which is selected for by cellular resistance to ganciclovir). Removal of puroΔTK is crucial, as the HR reporter contains a puromycin-resistance gene that is used to select for its subsequent integration. Finally, co-transfection of a Cre recombinase expression vector, along with vectors containing loxP flanked or "floxed" NHEJ or HR reporter DNA (Floxed-pEJ and Floxed-pGC, respectively; **Figure 2.3**), results in directional insertion of reporter DNA into the U2OS genome adjacent to the LacO array. Resistance to G418 selects for integration of the NHEJ reporter, while resistance to puromycin selects for integration of the HR reporter. Ultimately this strategy leads to the generation of a series of cell lines containing NHEJ and HR reporters integrated at the exact same genetic locus, allowing rates of DNA repair by both pathways to be followed in parallel. In addition, comparison of DNA repair rates between cell lines containing reporters in different chromosomes and nuclear positions allows the contribution of nuclear architecture on DNA repair to be studied.
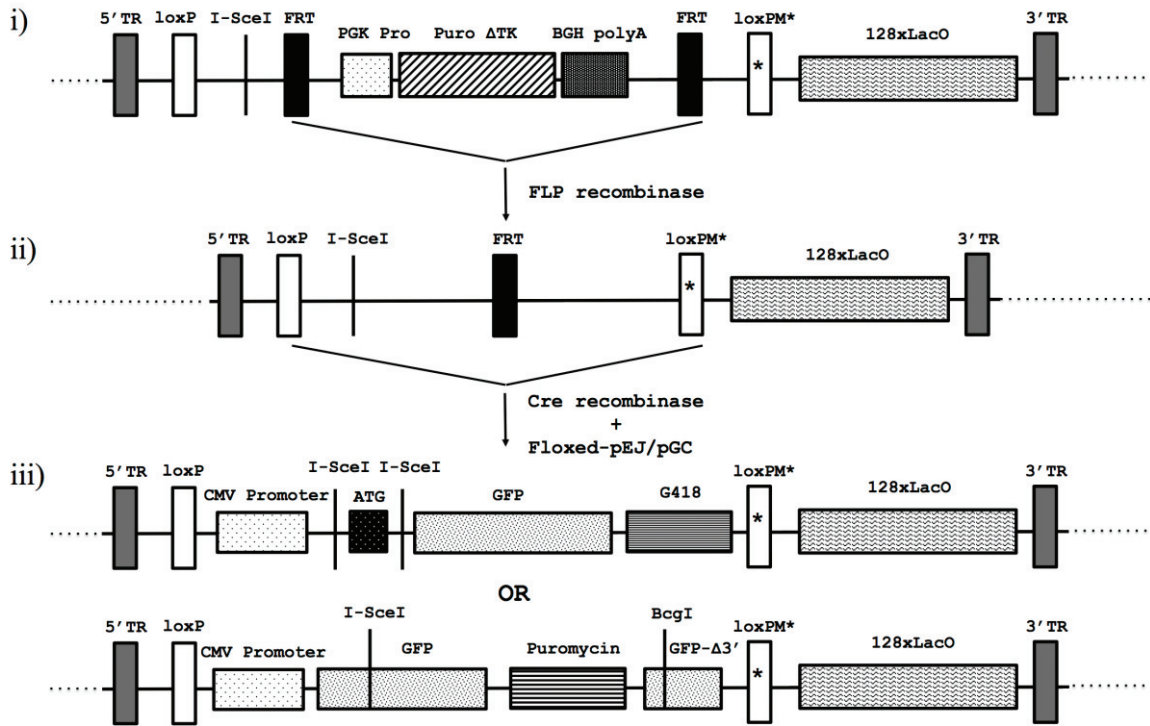
Figure 3.4. Strategy for cell line generation by PiggyBac transposition. **(i)** The pFlexible-LacO-pBLR5 construct is integrated into the genome of U2OS cells by PiggyBac transposition, with integration being selected for by resistance to puromycin. Clones generated from cells containing a single integration of this construct are then selected for further engineering. **(ii)** FLP recombinase expression results in recombination across FRT sites and deletion of the puroΔTK selectable marker. **(iii)** Transfection with a Cre recombinase expression vector and floxed NHEJ or HR reporter-containing vectors results in recombination across loxP sites and directional integration of reporter DNA adjacent to the LacO array in the U2OS genome. Dashed lines indicate genomic sequence flanking the construct integration site.

3.3.1.1 Characterization of U2OS pFlexible PB colonies by Southern blot analysis

U2OS cells were co-transfected with the pFlexible-LacO-pBLR5 targeting construct and a PiggyBac transposase expression vector at varying ratios (1:2, 1:5 and 1:10). This was done to determine the optimal ratio required to promote a single integration event per cellular genome. Resistance to puromycin was then used to select for cells with genomic integration of pFlexible-LacO-pBLR5. A total of 36 individual puromycin-resistant U2OS pFlexible PB colonies (12 colonies per transfection ratio-see **Table 2.1**) were selected for characterization by Southern blot (integration number) and inverse PCR (genomic position). To determine pFlexible-LacO-pBLR5 integration number, genomic DNA was isolated from individual U2OS pFlexible PB colonies, digested with EcoRI and subjected to Southern blot analysis using a probe against a portion of the puromycin-resistance gene from pFlexible-LacO-pBLR5. Additionally, a high-copy number probe that would recognize a telomere-associated repeat in the human genome generated from pMD35 plasmid DNA was used as a control to ensure DNA quality and protocol effectiveness. A representative autoradiograph from Southern blot analysis of three U2OS pFlexible PB colonies is presented in **Figure 3.5** (additional results are presented in **Appendix Figure 1**). Through Southern blot analysis, a total of 11 U2OS pFlexible PB colonies were determined to contain a single genomic integration of pFlexible-LacO-pBLR5, while 7 others were found to have multiple (two or more) integrations. It was also determined that a ratio of 1:2 (construct to PB transposase expression plasmid) was optimal for achieving single genomic integration.
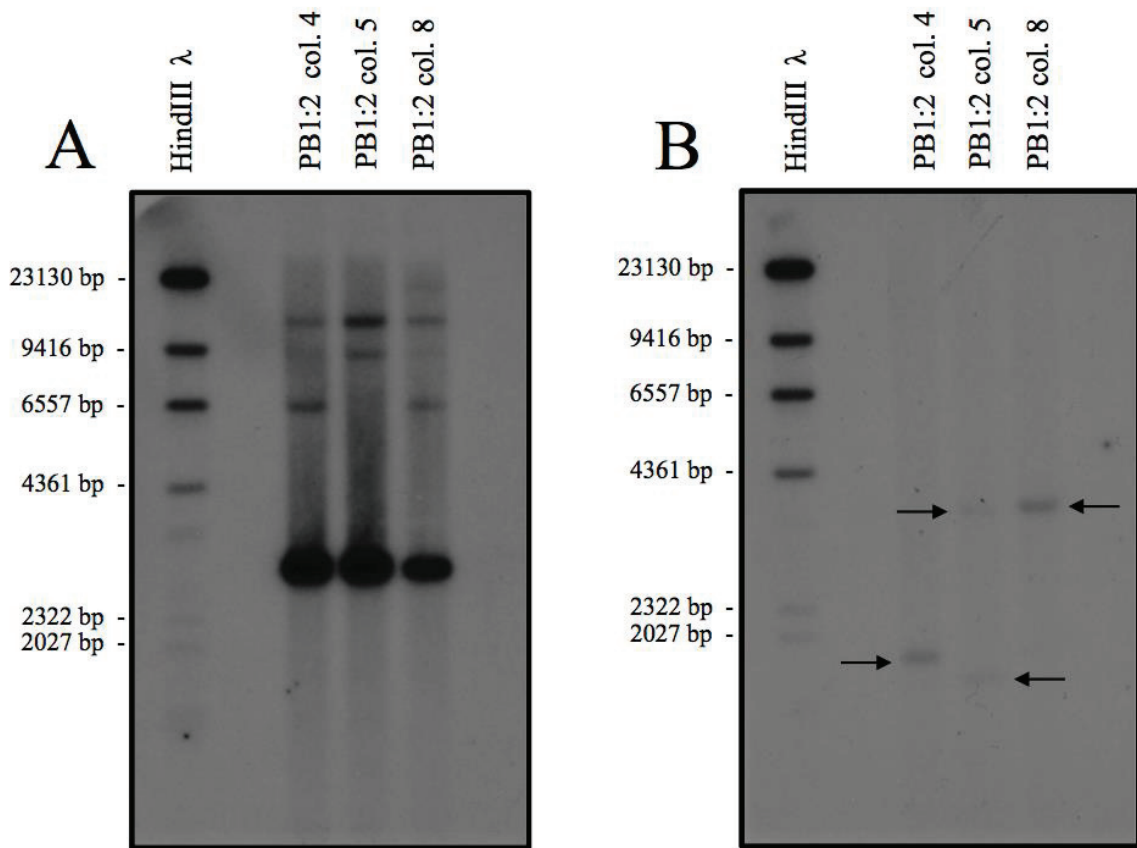
Figure 3.5. Southern blot analysis of genomic DNA isolated from three U2OS pFlexible PB colonies. Genomic DNA was isolated from U2OS pFlexible PB 1:2 colonies 4, 5 and 8, digested with EcoRI and hybridized with **(A)** a high-copy number control probe generated from pMD35 plasmid DNA or **(B)** a probe against a portion of the puromycin-resistance gene from pFlexible-LacO-pBLR5 plasmid DNA. HindIII λ phage DNA ladder resolved in the first lane of each blot was detected by hybridization with radiolabeled lambda DNA. A single hybridization fragment is observed in DNA derived from U2OS pFlexible PB colonies 4 and 8 (approximately 1800 bp and 4000 bp in size, respectively; denoted by arrows), indicating a single integration of pFlexible-LacO-pBLR5 in each of these cell lines. Two faint hybridization fragments are observed in DNA derived from U2OS pFlexible PB 1:2 col. 5 (approximately 4000 bp and 1500 bp in size; denoted by arrows), indicating two integrations of pFlexible-LacO-pBLR5.

3.3.1.2 Characterization of U2OS pFlexible PB colonies by inverse PCR

To determine the genomic integration position in colonies with single pFlexible-LacO-pBLR5 insertions, genomic DNA from each colony was digested with either EcoRI or PstI and self-ligated to form circular DNA containing a portion of the pFlexible-LacO-pBLR5 construct and a portion of adjacent genomic DNA. This external flanking genomic DNA was then amplified by inverse PCR using primer sets listed in **Table 2.8**, and the resulting products were sequenced and compared to the NCBI human nucleotide database to map the integration site. Due to the large size of the integrated pFlexible-LacO-pBLR5 construct (approximately 11 kb) the 5' and 3' ends of the integration site were mapped in separate inverse PCR reactions. Representative inverse PCR agarose gels for several U2OS pFlexible PB clones are presented in **Appendix Figure 2**. This technique proved to be extremely challenging, as PCR reactions often yielded no discernible products and were particularly susceptible to contamination. While tentative genomic integration locations were identified for two colonies, these could not be effectively confirmed by repeat sequencing. Ultimately, it was decided that this was an ineffective technique and overall strategy for cell line generation. As an alternative, CRISPR/Cas9 genome engineering was used to integrate the pFlexible-LacO-pBLR5 construct into U2OS cells. However, unlike PiggyBac transposition, pFlexible-LacO-pBLR5 integration would be at pre-determined genomic positions.

3.3.2 CRISPR/Cas9 genome engineering

The bacterially-derived CRISPR/Cas9 system is a powerful tool for targeted genome editing. It makes use of the Cas9 nuclease from *Streptococcus pyrogenes* to introduce DSBs at precise genomic locations using complementary gRNAs. HR using a repair template containing sequences that are homologous to regions flanking the break site then leads to insertion of the repair template (267). In this manner, the CRISPR/Cas9 system can be used to effectively generate targeted genomic deletions, base substitutions and insertions. One limitation with CRISPR/Cas9 is the potential for off-target effects caused by promiscuous gRNA binding. To minimize off-target mutations and enhance CRISPR/Cas9 specificity, a Cas9D10A nickase mutant can be used as an alternative.

Expression of Cas9D10A along with two gRNAs that bind in close proximity to one another but target opposite DNA strands create a DSB at the target site, while individual gRNAs would only create single nicks in off-target locations, thereby minimizing off-target DNA DSBs and unintended insertions or mutations (268).

The CRISPR/Cas9 system was used to integrate the pFlexible-LacO-pBLR5 construct into U2OS cells into pre-determined genomic loci. The same overall strategy as that presented in **Figure 3.4** was adopted for cell-line generation, with the exception of the use of CRISPR/Cas9 for initial integration of pFlexible-LacO-pBLR5 instead of PiggyBac transposition. Two genomic loci were chosen to target with CRISPR/Cas9: an intergenic region of chromosome 15 (GRCh37.p.13 primary assembly chr15:74696007-74698086; **Figure 2.4**) and exon 1 of the human TAP1 gene (GRCh37.p.13 primary assembly chr6:32821893-32823445; **Figure 2.5**). The TAP1 gene is located within the MHC class 1 gene-cluster region, which as discussed in section 1.4.3 has been found to be significantly associated with PML nuclear bodies (227). 3D immuno-FISH was then used to measure the respective distance between PML nuclear bodies and either the Chr15 or TAP1 locus. It was confirmed that the TAP1 locus is significantly associated with PML bodies when compared to a known unassociated locus, BCL2. In contrast, Chr15 was found to be significantly unassociated with bodies (**Figure 3.6**). By choosing these two genomic regions, a comparison of DNA DSB repair can be made between chromatin known to be associated with PML nuclear bodies (TAP1) and chromatin unassociated with bodies (Chr15).

Figure 3.6 3D immuno-FISH measuring association of the BCL2, Chr15 and TAP1 loci with PML nuclear bodies. Distances between PML nuclear bodies and the BCL2, Chr15 and TAP1 FISH probes were measured from 3D immuno-FISH image stacks. The 3D positions of the nuclei were defined using DAPI fluorescent signal, while the 3D positions of PML nuclear bodies in the nuclei were defined using signal from PML immunostaining, and 3D positions of the BCL2/Chr15/TAP1 were loci defined using signal from Spectrum Orange-labeled probes. The distance between the centres of the defined FISH probe objects and closest PML body (depicted by arrows) in each defined nucleus was calculated. At least 50 nuclei were analyzed for TAP1 and BCL2 probes while 9 were analyzed for Chr15 and are presented in a box-and-whisker plot. The average closest distance between a PML nuclear body and FISH signal was calculated for each probe. Two tailed t-test indicates the differences in PML nuclear body association between TAP1/BCL2 and TAP1/Chr15 are significant ** $p < 0.01$.
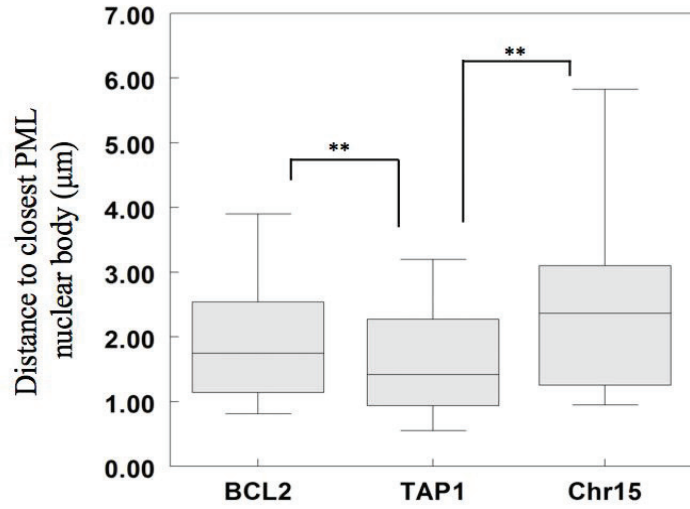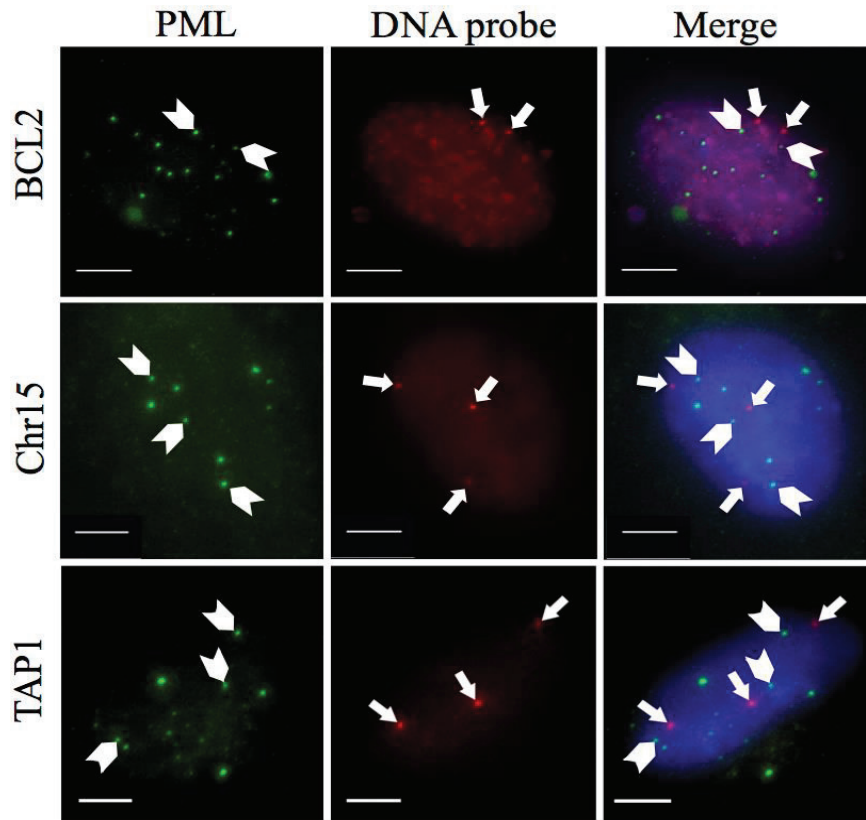
3.3.2.1 Characterization U2OS Chr15/TAP pFlexible clones by FISH

The pFlexible-LacO-pBLR5 construct was cloned into a CRISPR donor vector containing homology arms for targeting Chr15 or TAP1 (termed Chr15-pFlexible-LacO-pBLR5-TOPO4 and TAP-pFlexible-LacO-pBLRT5-TOPO4, respectively). Two separate gRNAs were designed to target each locus (Chr15 5' oligo A+B, Chr15 3' oligo A+B. TAP 5' oligo A+B, and TAP 3' oligo A+B) to maximize the effectiveness of CRISPR/Cas9 targeting. U2OS cells were then co-transfected with Chr15/TAP1 pFlexible-LacO-pBLR5 donor vectors and either wild-type Cas9 or Cas9D10A nickase expression vector (termed px330 and px335, respectively) carrying different gRNAs (see **Table 2.6** for transfection details). Both wild-type and nickase Cas9 were used to determine which version of Cas9 would result in the most accurate genomic editing events. Cellular resistance to puromycin was then used to select for genomic integration of pFlexible-LacO-pBLR5. A total of 18 individual puromycin-resistant U2OS Chr15 pFlexible clones and 18 U2OS TAP pFlexible clones (6 clones per transfection condition: see **Table 2.1** and **Table 2.6**) were selected for characterization by FISH and genomic PCR.

To confirm successful pFlexible-LacO-pBLR5 targeting to the Chr15 or TAP1 locus, individual clones were analyzed by FISH using Spectrum Orange-labeled Chr15 or TAP1 DNA probes and a DIG-labeled LacO array probe. FISH revealed exact co-localization of the LacO array of pFlexible-LacO-pBLR5 with the Chr15 locus in U2OS Chr15 pFlexible cells and with the TAP1 locus in U2OS TAP pFlexible cells (**Figure 3.7**). U2OS cells are aneuploid and contain three copies of chromosomes 6 and 15, and it was therefore expected that pFlexible-LacO-pBLR5 would be integrated at all three alleles. Interestingly, in the majority of clones analyzed by FISH, only a single LacO hybridization spot was observed. The exception seemed to be the clones generated by the Cas9D10A nickase, some of which had two hybridization spots detected by FISH. In no cellular clone was the pFlexible-LacO-pBLR5 construct observed to have been integrated at all three Chr15 or TAP1 alleles. The integration of pFlexible-LacO-pBLR5 at one or two alleles as opposed to all three present in the U2OS genome may be due to the inefficiency of integrating such a large construct (approximately 11 kb) by HR.
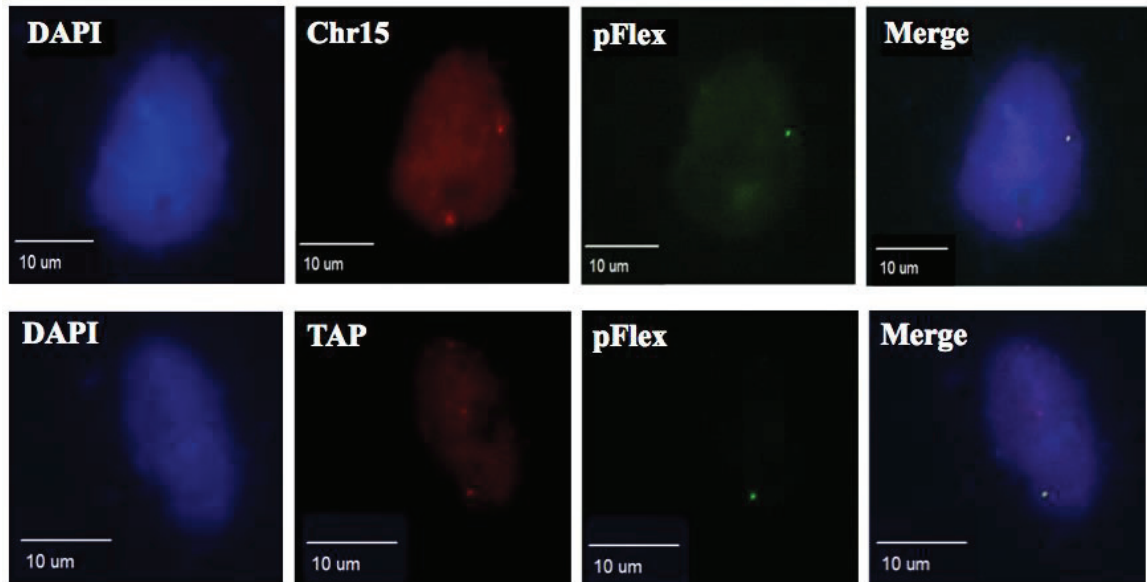
Figure 3.7. Representative FISH of U2OS Chr15 pFlexible and U2OS TAP pFlexible clones. Immuno-FISH single-Z confocal images of the LacO array of the pFlexible-LacO-pBLR5 construct at the CRISPR/Cas9-targeted Chr15 or TAP1 loci of U2OS cells. The DIG-labeled LacO array probe is detected by an anti-DIG antibody (green), and Chr15 and TAP1 loci are detected using BAC DNA probes (red) specific to each locus. Nuclei are stained blue with DAPI. Three hybridization spots are observed for Chr15 and TAP1 loci (the third spot in the Chr15 image is outside of the focal plane). A single LacO hybridization spot is observed that co-localizes exactly with one of the Chr15 alleles in the U2OS Chr15 pFlexible clone and one of the TAP1 alleles in the U2OS TAP pFlexible clone.

3.3.2.2 Characterization of U2OS Chr15/TAP pFlexible clones by genomic PCR

As further confirmation, the pFlexible-LacO-pBLR5 integration sites within the Chr15 and TAP1 loci in U2OS Chr15/TAP pFlexible clones were mapped by genomic PCR. Primers were designed to bind outside of the edited genomic region of the Chr15 or TAP1 locus as well as within the pFlexible-LacO-pBLR5 sequence (see **Table 2.9**). Due to the large size of pFlexible-LacO-pBLR5, the 5' and 3' ends of the insertion site were mapped in separate PCR reactions. Genomic PCR mapping of U2OS Chr15 pFlexible clones is shown in **Figure 3.8A-B** and that of U2OS TAP pFlexible clones is shown in **Figure 3.9A-B**. Genomic DNA isolated from the majority of clones yielded 5' and 3' PCR amplification products of the expected size (in the cases where some clones yielded a product only in one of the two PCR reactions, this was likely due to a PCR failure rather than incorrect integration). PCR amplification products were then verified by Sanger sequencing (representative sequences are presented in **Appendix Figure 3A-B** and **Appendix Figure 4A-B**). Additionally, a control PCR was performed using the external PCR primers that bind outside of the edited genomic region of Chr15 and TAP1. If pFlexible-LacO-pBLR5 had been integrated at all three alleles, no PCR product would be expected using these primers, as the large size of pFlexible-LacO-pBLR5 makes PCR amplification impossible. However, if pFlexible-LacO-pBLR5 had been integrated at one or two alleles, leaving at least one site unedited, PCR amplification products of approximately 1700 bp for Chr15 and 500 bp for TAP1 would be expected. Products consistent with this were observed (**Figure 3.8C** and **Figure 3.9C**), which is in full correlation with FISH data. At these unedited alleles, although the donor plasmid is not incorporated, Cas9 still makes a DSB that requires repair, which is expected to be primarily through NHEJ. As discussed in section 1.2.1, NHEJ is inherently error prone, often resulting in nucleotide deletions at the break site. Sequencing of these amplification products confirmed this expectation. Sequencing revealed that the unedited allele(s) of these clones had deletions at the predicted break site ranging in size from 12 bp up to several hundred (which is observed most visibly in the U2OS Chr15 pFlexible clones of **Figure 3.8C**), consistent with repair by NHEJ. As a control in these PCR reactions, DNA isolated from wild-type U2OS was used (**Figure 3.8D** and **Figure 3.9D**). No

amplification products were observed using the primers designed to map the 5' and 3' integration sites of pFlexible-LacO-pBLR5, as expected, while a product of correct size is observed in PCR amplifications using the external set of primers.

Ultimately, the unexpected result of obtaining clones with just a single genomic integration of pFlexible-LacO-pBLR5 at the Chr15 or TAP1 locus was in line with the initial aim of this study, which was to create cell lines containing single copies of reporter DNA. One Chr15 clone (U2OS Chr15 5' px330 pFlexible col. 6) and one TAP1 clone (U2OS TAP 5' px330 pFlexible col. 1) that contained a single genomic pFlexible-LacO-pBLR5 integration as determined by FISH, and that had the smallest deletion in the unedited alleles (12 bp for Chr15 and 28 bp for TAP1- see **Appendix Figures 3C** and **4C**, respectively) as determined by genomic PCR and subsequent sequencing were chosen for further engineering (insertion of DNA repair reporters).

Figure 3.8. Confirmation of successful CRISPR/Cas9 Chr15 targeting by genomic PCR. PCR amplification of template DNA isolated from 18 individual U2OS Chr15 pFlexible clones or wild-type U2OS cells using various primer sets. **(A)** PCR amplification of the 5' integration junction. PCR using a forward primer designed to bind externally to the CRISPR/Cas9 edited region and a reverse primer designed to bind the 5' end of pFlexible-LacO-pBLR5 is expected to yield products of 1100 bp in size. **(B)** PCR amplification of the 3' integration junction. PCR using a forward primer designed to bind the 3' end of pFlexible-LacO-pBLR5 and a reverse primer designed to bind externally to the CRISPR/Cas9 edited region is expected to yield products of 800 bp in size. **(C)** External PCR amplification. PCR using forward and reverse primers designed to bind externally to the CRISPR/Cas9 edited genomic region is expected to yield products of 1700 bp in size. **(D)** Control PCR amplification. 5' junction, 3' junction and external PCR amplifications using wild-type U2OS genomic DNA as a template. The primer-binding regions and expected product sizes are depicted in the cartoon adjacent to each agarose gel. The grey bars represent integrated pFlexible-LacO-pBLR5 while the bold black bars represent homology arms used in Chr15 genomic targeting, and the thin black bars represent Chr15 genomic sequence external to the edited region. 5' px330 and 3' px330 are the wild-type Cas9 expression plasmids containing the 5' Chr15 gRNA and 3' Chr15 gRNA, respectively. 5' 3' px335 is the nickase mutant Cas9D10A expression plasmid containing both 5' and 3' Chr15 gRNAs. The red arrow indicates the clone used for further engineering.

91
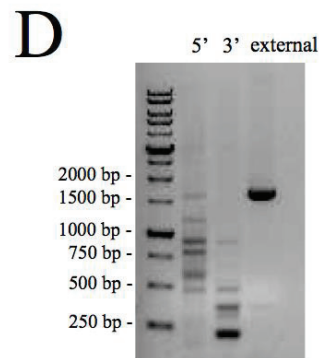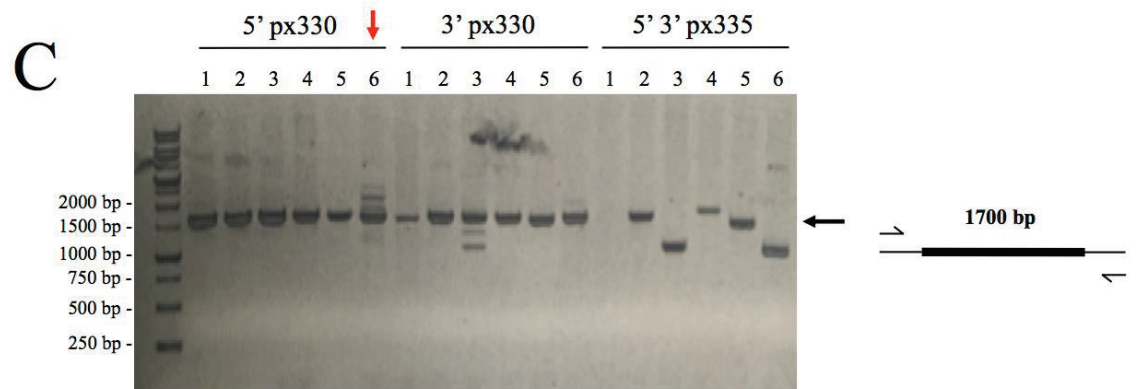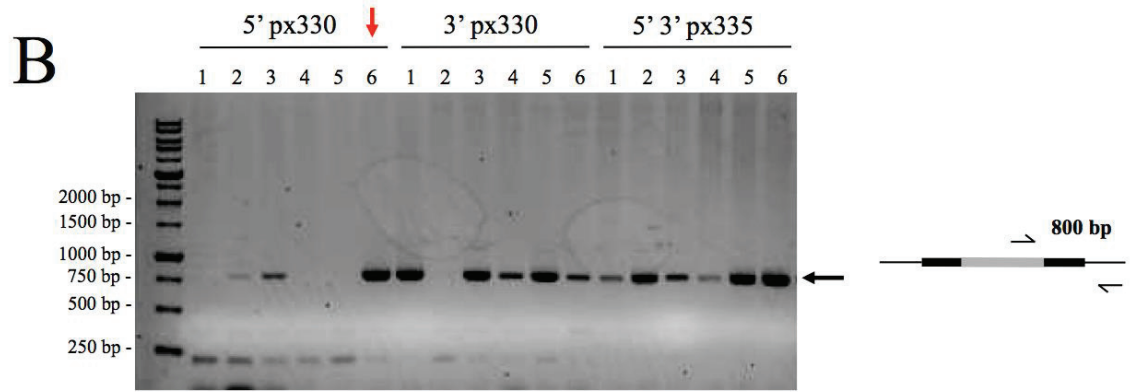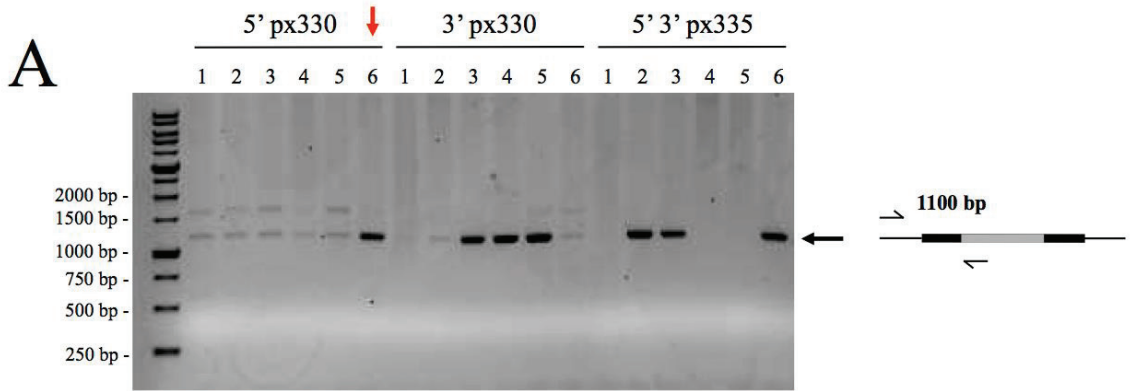
Figure 3.9. Confirmation of successful CRISPR/Cas9 TAP1 targeting by genomic PCR. PCR amplification of template DNA isolated from 18 individual U2OS TAP pFlexible clones or wild-type U2OS cells using various primer sets. **(A)** PCR amplification of the 5' integration junction. PCR using a forward primer designed to bind externally to the CRISPR/Cas9 edited region and a reverse primer designed to bind the 5' end of pFlexible-LacO-pBLR5 is expected to yield products 200 bp in size. **(B)** PCR amplification of the 3' integration junction. PCR using a forward primer designed to bind the 3' end of pFlexible-LacO-pBLR5 and a reverse primer designed to bind externally to the CRISPR/Cas9 edited region is expected to yield products 300 bp in size. **(C)** External PCR amplification. PCR using forward and reverse primers designed to bind externally to the CRISPR/Cas9 edited genomic region is expected to yield products 500 bp in size. **(D)** Control PCR amplification. 5' junction, 3' junction and external PCR amplifications using wild-type U2OS genomic DNA as a template. The primer binding regions and expected product sizes are depicted in the cartoon adjacent to each agarose gel. The grey bars represent integrated pFlexible-LacO-pBLR5 while the bold black bars represent homology arms used in TAP1 genomic targeting, and the thin black bars represent TAP1 genomic sequence external to the edited region. 5' px330 and 3' px330 are the wild-type Cas9 expression plasmids containing the 5' TAP1 gRNA and 3' TAP1 gRNA, respectively. 5' 3' px335 is the nickase mutant Cas9D10A expression plasmid containing both 5' and 3' TAP1 gRNAs. The red arrow indicates the clone used for further engineering.
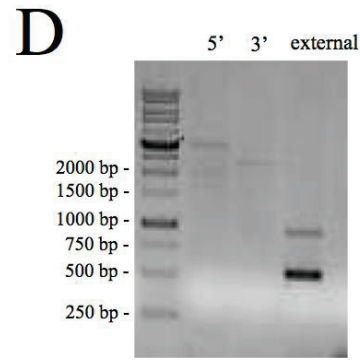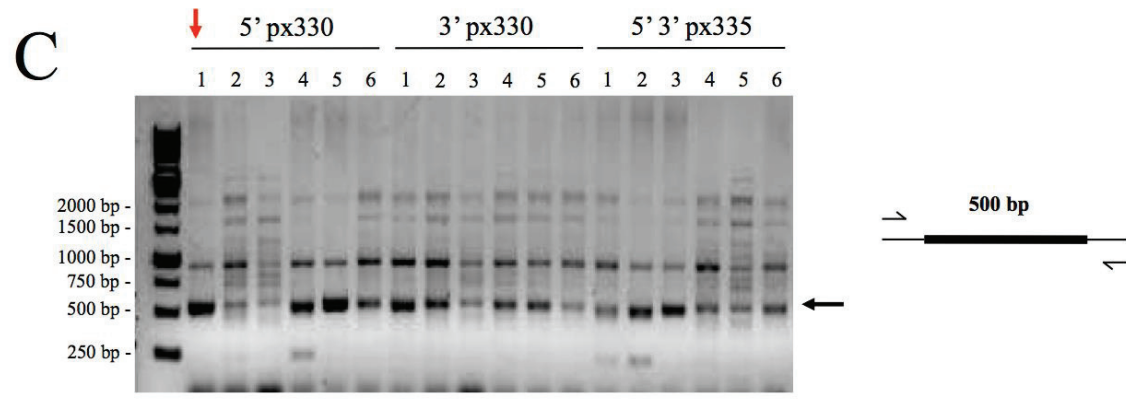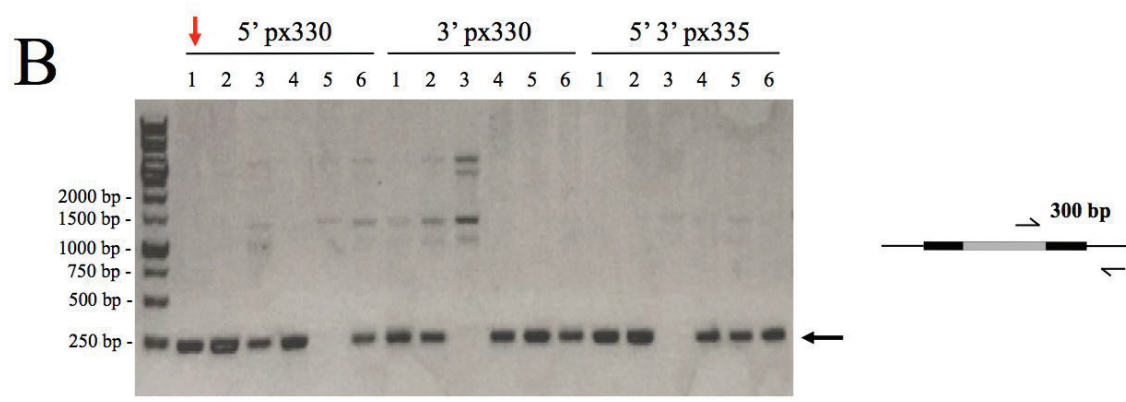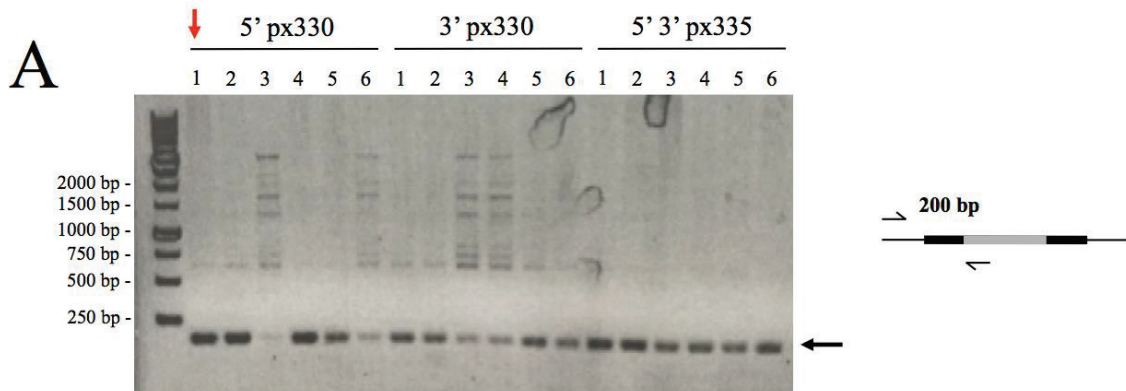
3.3.2.3 FLP/FRT and Cre/loxP recombination

As a next step in cell line generation, following the strategy presented in **Figure 3.4**, U2OS Chr15 5' pFlexible px330 col. 6 and U2OS TAP 5' px330 pFlexible col. 1 cells were transfected with a FLP recombinase expression vector. FLP/FRT recombination results in deletion of the puroΔTK selectable marker, the removal of which is selected for by cellular resistance to ganciclovir. Ganciclovir-resistant cells were then co-transfected with a Cre recombinase expression vector and either Floxed-pEJ or Floxed-pGC vectors (carrying a loxP-flanked NHEJ or HR reporter, respectively). Integration of the NHEJ or HR reporter vector into the genome of U2OS Chr15 5' px330 pFlexible col. 6 FLP and U2OS TAP 5' px330 pFlexible col. 3 FLP cells was then selected for by cellular resistance to G418 or puromycin, respectively. A total of 12 individual puromycin-resistant U2OS Chr15 pFlexible Cre-HR and U2OS TAP pFlexible Cre-HR clones (6 clones each: see **Table 2.1**) were screened for successful HR reporter integration. Likewise, a total of 12 individual G418-resistant U2OS Chr15 pFlexible Cre-NHEJ and U2OS TAP pFlexible Cre-NHEJ clones (6 clones each: see **Table 2.1**) were screened for successful NHEJ reporter integration.

Genomic PCR was then used to confirm successful Cre/lox-mediated insertion of NHEJ or HR reporter DNA in these clones. Forward and reverse primers specific to the NHEJ or HR reporter sequence were used to detect the presence of reporter DNA in genomic DNA isolated from individual clones. In addition, to confirm reporter DNA had been inserted at the correct genomic position (between the loxP/loxPM sites of pFlexible-LacO-pBLR5 at the Chr15 or TAP1 locus), the insertion site was mapped using a reverse primer specific to NHEJ/HR reporter DNA and a forward primer specific to Chr15 or TAP1 genomic DNA. While PCR using primers specific to NHEJ and HR reporter DNA yielded amplicons of the correct size and sequence, PCR to confirm successful insertion of reporter DNA within the pFlexible-LacO-pBLR5 construct at either Chr15 or TAP1 did not yield any discernible products. Furthermore, when individual clones were transfected with an I-SceI expression vector to test reporter functionality there was no detectable green fluorescence in these cells. Therefore, although genomic DNA isolated from these clones contained NHEJ or HR reporter DNA, the lack of green fluorescence suggest these reporters may have been misincorporated by Cre/lox recombination,

ultimately impacting reporter function. Therefore, rather than integrating NHEJ or HR reporter DNA using Cre/lox recombination another strategy was adopted, again based on CRISPR/Cas9 genome editing. Briefly, a gRNA was designed to target the 5' end of the pFlexible-LacO-pBLR5 construct and CRISPR donor vectors carrying NHEJ or HR reporter DNA flanked by homology arms targeting pFlexible-LacO-pBLR5 were constructed (**Figure 2.6**).

3.3.2.4 Characterization of U2OS Chr15 pFlexible CRISPR NHEJ/HR and U2OS TAP CRISPR NHEJ/HR clones by genomic PCR

NHEJ and HR reporters were integrated into the pFlexible-LacO-pBLR5 construct present in U2OS Chr15 5' px330 pFlexible col. 6 FLP and U2OS TAP 5' px330 pFlexible col. 1 FLP cell lines. This was achieved through co-transfection with CRISPR donor vectors carrying reporter DNA flanked by homology arms targeting pFlexible-LacO-pBLR5 along with a wild-type Cas9/gRNA expression vector (see **Table 2.7** for transfection details). Integration of the NHEJ or HR reporter vector was then selected for by cellular resistance to G418 or puromycin, respectively. A total of 12 individual puromycin-resistant U2OS Chr15 pFlexible CRISPR HR and U2OS TAP pFlexible CRISPR HR clones (6 clones each- see **Table 2.1**) were screened for HR reporter integration. Likewise, a total of 12 individual G418-resistant U2OS Chr15 pFlexible CRISPR NHEJ and U2OS TAP pFlexible CRISPR NHEJ clones (6 clones each- see **Table 2.1**) were screened for NHEJ reporter integration.

Genomic PCR was used to verify successful CRISPR/Cas9-mediated insertion of NHEJ or HR reporter DNA within the pFlexible-LacO-pBLR5 construct of each individual clone. A forward primer was designed to bind within the pFlexible-LacO-pBLR5 sequence and a reverse primer was designed to bind within the CMV promoter of reporter DNA. Proper insertion of NHEJ or HR reporter DNA results in an amplification product of approximately 350 bp. Genomic DNA isolated from two U2OS Chr15 pFlexible CRISPR NHEJ clones and five U2OS Chr15 pFlexible CRISPR HR clones yielded amplification products of the expected size (**Figure 3.10A and B**, left panels), while DNA isolated from three U2OS TAP pFlexible CRISPR NHEJ clones and five

U2OS TAP pFlexible CRISPR HR clones also yielded correctly sized PCR products (**Figure 3.11A and B**, left panels). All PCR amplicons were sequenced, confirming that reporter DNA had been correctly integrated within pFlexible-LacO-pBLR5 in these clones (representative sequences are presented in **Appendix Figures 5, 6, 7 and 8**). Genomic DNA isolated from unedited U2OS Chr15 5' px330 pFlexible col. 6 FLP and U2OS TAP 5' px330 pFlexible col. 1 FLP cells along with wild-type U2OS served as negative controls in these PCR amplifications.

For further confirmation, I wanted to verify that these clones still contained the pFlexible-LacO-pBLR5 construct stably integrated at the correct genomic position (Chr15 or TAP1). As described in section 3.3.2.2, primers were designed to amplify the 5' and 3' genomic insertion site of pFlexible-LacO-pBLR5 within Chr15 or TAP1. As expected, PCR using genomic DNA from each clone as a template, resulted in amplification products of the correct size and sequence (**Figures 3.10 and 3.11**, middle and right panels; **Appendix Figures 5, 6, 7, and 8**).
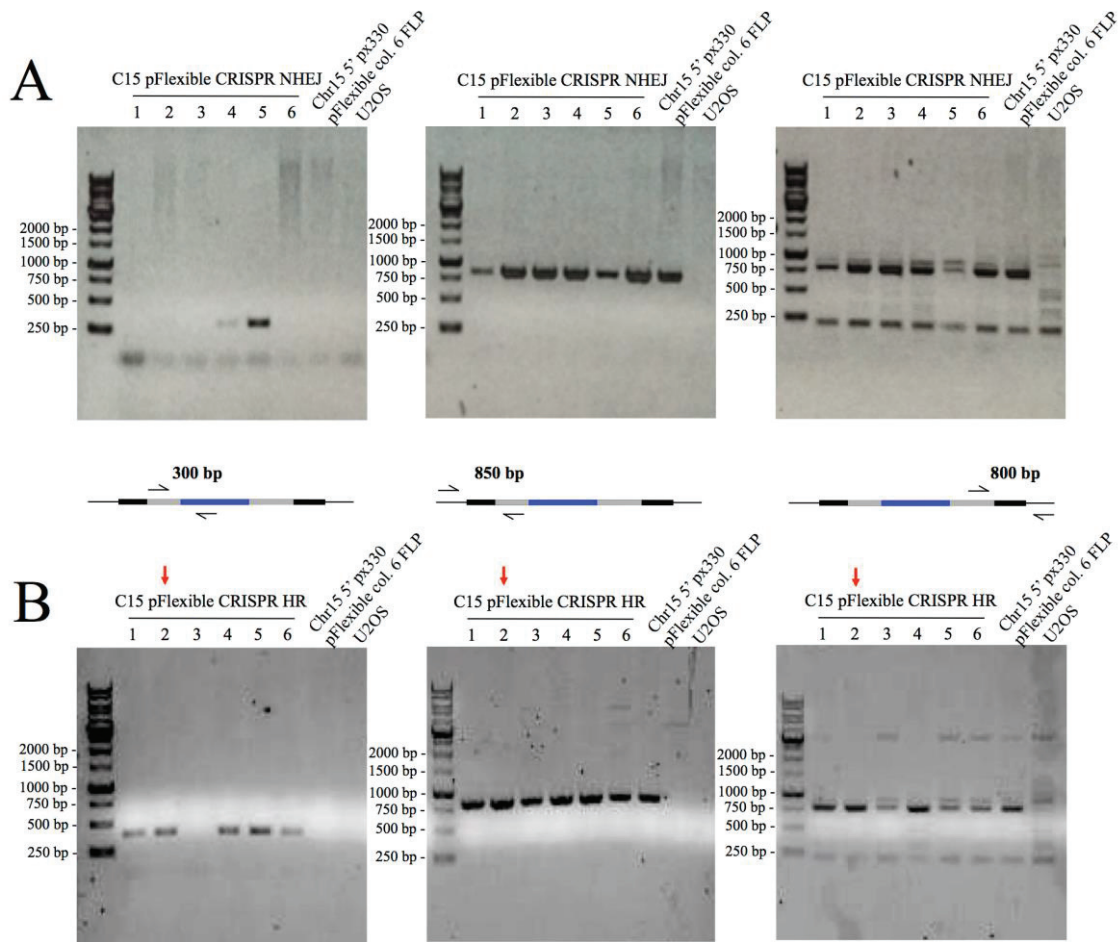
Figure 3.10. Characterization of U2OS Chr15 pFlexible CRISPR NHEJ and U2OS Chr15 pFlexible CRISPR HR clones by genomic PCR. (A) PCR amplification of genomic DNA isolated from 6 individual U2OS Chr15 pFlexible CRISPR NHEJ clones, U2OS Chr15 5' px330 pFlexible col. 6 FLP cells and wild-type U2OS cells using various primer sets. Binding locations of the primer pairs used in each PCR reaction, as well as the expected product sizes, are depicted below each agarose gel. The blue bar represents NHEJ or HR reporter DNA integrated within the pFlexible-LacO-pBLR5 construct (grey bar). The bold black bars represent homology arms used in Chr15 genomic targeting, while the thin black bars represent Chr15 genomic sequence external to the edited region. **(B)** PCR amplification of template DNA isolated from 6 individual U2OS Chr15 pFlexible CRISPR HR clones, U2OS Chr15 5' px330 pFlexible col. 6 FLP cells and wild-type U2OS cells using various primer sets. Primer pairs and expected product sizes are same as those in (A). The red arrow indicates the final clone used in all further experiments.
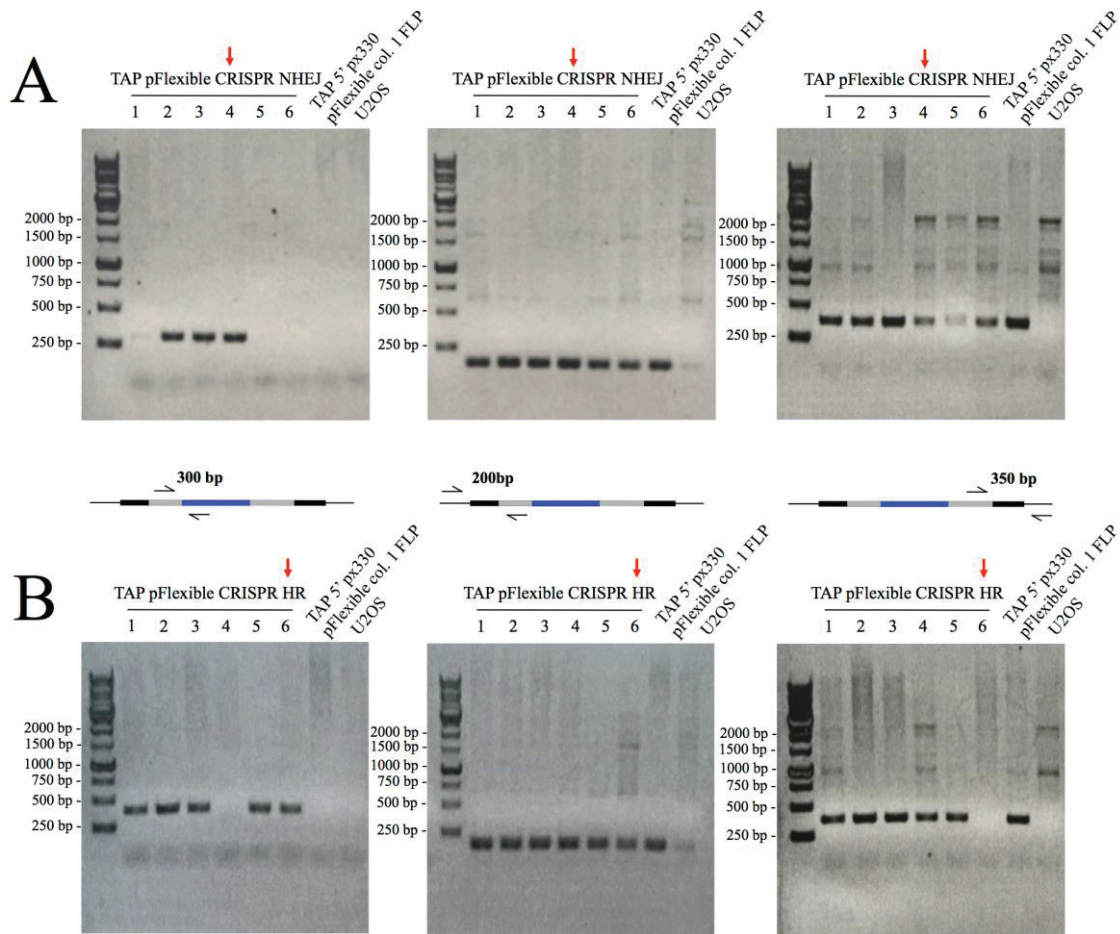
Figure 3.11. Characterization of U2OS TAP pFlexible CRISPR NHEJ and U2OS TAP pFlexible CRISPR HR clones by genomic PCR. (A) PCR amplification of genomic DNA isolated from 6 individual U2OS TAP pFlexible CRISPR NHEJ clones, U2OS TAP 5' px330 pFlexible col. 1 FLP cells and wild-type U2OS cells using various primer sets. Binding locations of the primer pairs used in each PCR reaction, as well as the expected product size, are depicted below each agarose gel. The blue bar represents NHEJ or HR reporter DNA integrated within the pFlexible-LacO-pBLR5 construct (grey bar). The bold black bars represent homology arms used in TAP1 genomic targeting, while the thin black bars represent TAP1 genomic sequence external to the edited region. **(B)** PCR amplification of template DNA isolated from 6 individual U2OS TAP pFlexible CRISPR HR clones, U2OS TAP 5' px330 pFlexible col. 1 FLP cells and wild-type U2OS cells using various primer sets. Primer pairs and expected product sizes are same as those in (A). The red arrows indicate the final clones used in all further experiments.

98

3.3.2.5 Characterization of U2OS Chr15 pFlexible CRISPR NHEJ/HR and U2OS TAP CRISPR NHEJ/HR clones by I-SceI assays

As a final validation, to test reporter functionality these clones were transfected with an I-SceI expression vector and analyzed by fluorescence microscopy for GFP expression. Based on these I-SceI assays, two suitable TAP1 clones (U2OS TAP pFlexible CRISPR HR col. 6 and U2OS TAP pFlexible CRISPR NHEJ col. 4, which will be called U2OS TAP HR 6 and U2OS TAP NHEJ 4 from now on for simplicity) and one Chr15 clone (U2OS Chr15 pFlexible CRISPR HR col.2, henceforth called U2OS Chr15 HR 2 for simplicity) were chosen for all future experiments (**Figure 3.12**). Unexpectedly however, despite PCR supporting integration of the NHEJ reporter at the correct genomic location, the Chr15 NHEJ clones that were tested did not produce GFP upon I-SceI DSB induction. This lack of response may have been due to unforeseen errors during CRISPR/Cas9 reporter integration that could have impacted reporter functionality. More U2OS Chr15 pFlexible CRISPR NHEJ clones need to be selected and screened to identify those containing a functional NHEJ reporter. For this study however, I proceeded with the three clones that had been successfully characterized (**Figure 3.12; Appendix Figures 5, 6, 7 and 8**).
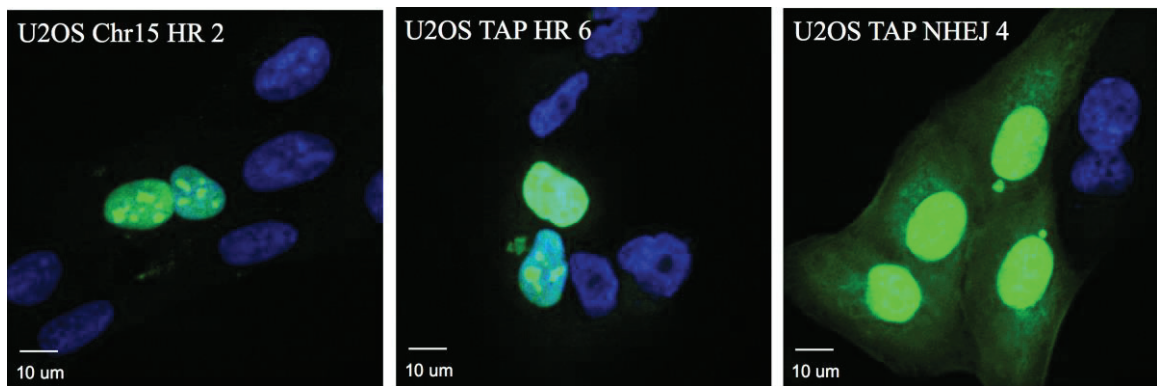
Figure 3.12. Representative I-SceI assays to determine DSB repair reporter functionality. U2OS Chr15 HR 2, U2OS TAP HR 6 and U2OS TAP NHEJ 4 cells were transiently transfected with a vector encoding the I-SceI endonuclease. Seventy-two hours post-transfection, cells were fixed and examined by confocal fluorescence microscopy for GFP expression. Nuclei were stained blue with DAPI.

3.4 Effect of PML nuclear bodies and PML isoforms on rates of DSB repair

As discussed in section 1.4.3, PML nuclear bodies have been implicated as playing a role in DSB repair, particularly HR (244-246). To determine the effect of PML nuclear bodies on DNA repair, rates of HR repair were compared between the Chr15 and TAP1 HR cell lines as well as between wild-type U2OS cells and U2OS cells in which PML had been stably knocked out. The contribution of the PML protein itself to DSB repair by both NHEJ and HR was examined by monitoring DNA repair levels following overexpression of individual PML isoforms in the Chr15, TAP1, wild-type U2OS and PML-knockout cell lines.

3.4.1 HR at the TAP1 locus is significantly lower than at Chr15

The cell lines generated in this study were used to compare rates of HR at DSBs induced within chromatin more-closely associated with PML nuclear bodies (TAP1) and chromatin unassociated with bodies (Chr15). U2OS Chr15 HR 2 and U2OS TAP HR 6 cells were transiently transfected with an I-SceI expression vector to induce a DSB in HR reporter DNA, along with a vector expressing IRFP as a transfection control. Cells were then analyzed by flow cytometry to determine the percentage of transfected cells (red) that were GFP positive (green) and had therefore undergone repair by HR (**Figure 3.13A**). Spontaneous HR repair events were corrected for by normalizing to cells transfected with IRFP alone. The percentage of transfected cells expressing GFP was higher in cells in which the HR reporter was integrated at Chr15 (approximately 9% of transfected cells) relative to TAP1 (5% of transfected cells) (**Figure 3.13A**). DSB repair by HR is cell cycle dependent, occurring in S or G2 phases. To determine if the difference in HR repair rates observed between these two cell lines was due to differences in cell cycle distribution, I analyzed cell cycle profiles of each cell line by flow cytometry (**Figure 3.13B**). No significant differences in cell cycle profiles were observed between the two cell lines, indicating that the difference in HR can likely be attributed to the difference in nuclear positioning of the reporter DNA.

Figure 3.13. **Comparison of HR rates and cell cycle profiles of Chr15 and TAP1 cell lines. (A)** U2OS Chr15 HR 2 and U2OS TAP HR 6 cells were transfected with an IRFP expression vector with or without an I-SceI endonuclease expression vector. Seventy-two hours post-transfection, cells were fixed and analyzed by flow cytometry. Shown are representative IRFP versus GFP plots and the mean percentage of GFP-positive cells from three independent experiments ($\pm$ s.d.) counting at least 50 000 events per experiment. Data are normalized to cells expressing IRFP alone. Two-tailed t-test indicates the difference in percentage of transfected Chr15 *versus* TAP1 cells expressing GFP is significant (**$p < 0.01$). **(B)** Cell cycle analysis of U2OS Chr15 HR 2 and U2OS TAP HR 6 cells using PI staining and flow cytometry. Data represent the mean values of three replicate experiments ($\pm$ s.d.) counting at least 10 000 events per experiment.

A

Untransfected   IRFP   I-SceI

Chr15

TAP1

IRFP ↑
GFP →

B
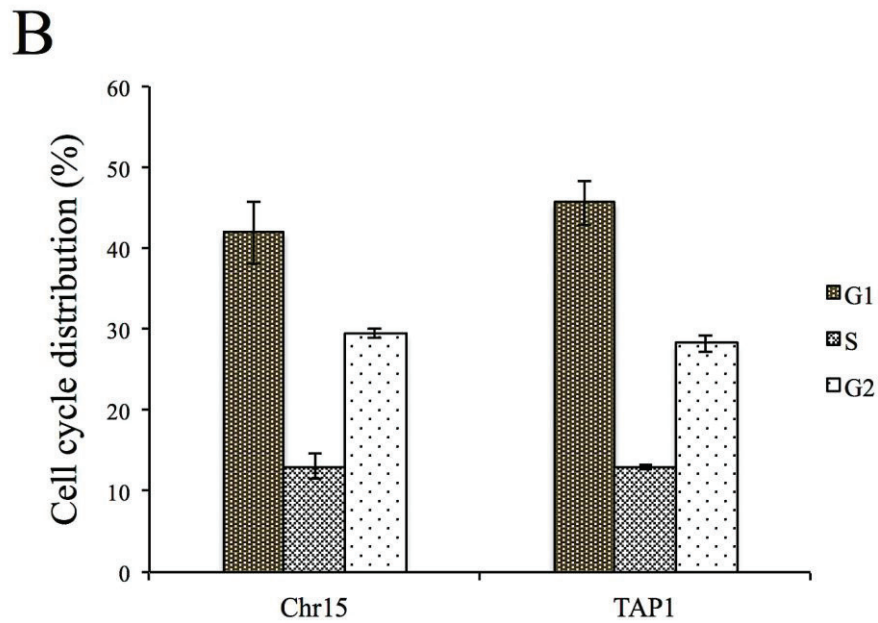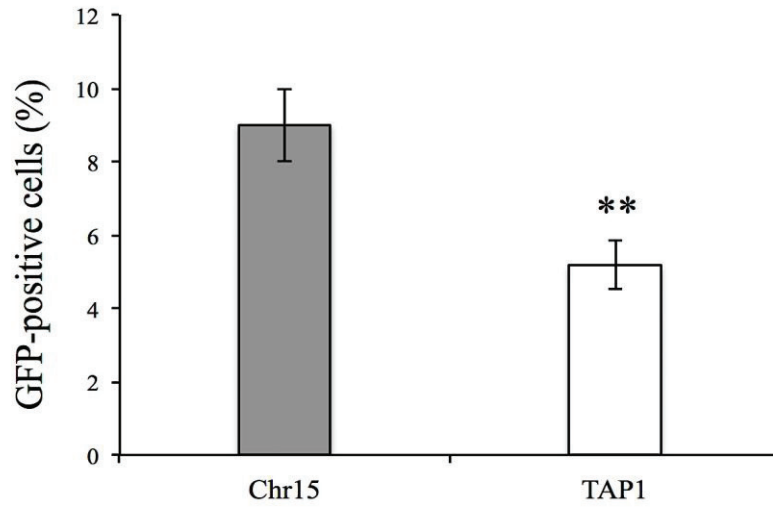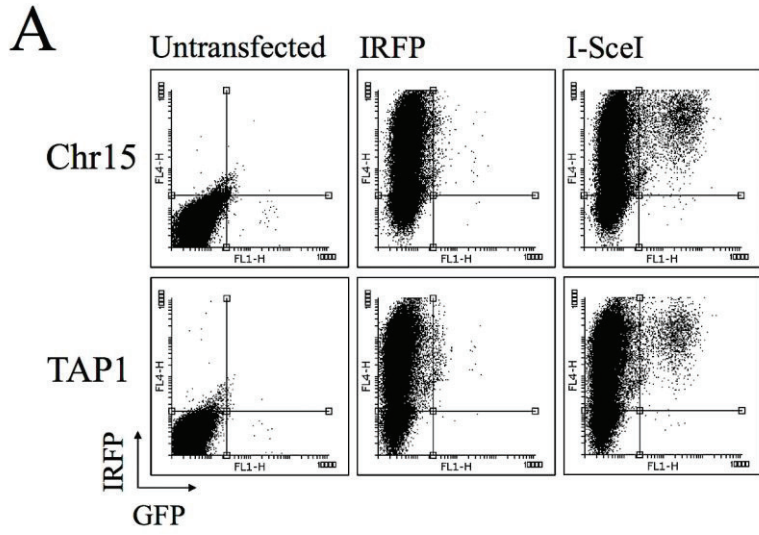
3.4.2 HR is decreased in stable PML-knockout cells

Due to the observed decrease in HR when a DSB occurs in chromatin significantly associated with PML nuclear bodies, I wanted to determine whether the absence of PML nuclear bodies also impacted the process of HR. To accomplish this, I compared the rates of HR in wild-type U2OS and a U2OS cell line in which the PML coding region had been deleted by CRISPR/Cas9 gene editing (termed ΔPML). These cells do not express PML or form PML nuclear bodies (**Figure 3.15A**, bottom panel, left-most image). To measure HR in these cells, a novel assay developed by our laboratory (described in detail in reference 259) based on CRISPR/Cas9 gene targeting was used. Briefly, cells were co-transfected with a CRISPR donor vector carrying the gene for a GFP variant, Clover, along with a vector expressing Cas9 and a gRNA targeting the second codon of the *LMNA* gene. Productive incorporation of Clover by CRISPR/Cas9-mediated homology-directed repair results in cells expressing fluorescent nuclear lamin A/C and thus a green nuclear lamina (see **Figure 3.14A**).

U2OS and ΔPML cells were transfected with the Clover-lamin CRISPR donor plasmid with or without the Cas9/gRNA expression vector, along with a vector expressing IRFP as a transfection control. Cells were then analyzed by flow cytometry to determine the percentage of transfected cells (red) that were Clover positive (green) and had therefore undergone CRISPR/Cas9-mediated HR (**Figure 3.14B**). Background fluorescence was corrected for by normalizing to cells transfected with the Clover-lamin CRISPR donor plasmid alone. The percentage of transfected, Clover expressing cells was slightly lower in ΔPML cells relative to wild-type U2OS, but significant, indicating a decrease in HR when PML is absent. Importantly, there was also no difference in cell cycle profiles between wild-type U2OS and ΔPML cells indicating that eliminating the PML protein does not impact cell cycle position and consequently HR capacity (**Figure 3.14C**).

Figure 3.14. **Comparison of HR rates and cell cycle profiles of wild-type U2OS and ΔPML cells. (A)** CRISPR Clover lamin 'knock-in' HR assay. Wild-type U2OS and ΔPML cells were co-transfected with a Clover-lamin CRISPR donor plasmid and a Cas9/gRNA expression vector. Seventy-two hours post-transfection cells were fixed and examined by confocal fluorescence microscopy for fluorescent nuclear lamina structures. **(B)** Wild-type U2OS and ΔPML cells were transfected with a Clover-lamin CRISPR donor plasmid with or without the Cas9/gRNA expression vector, along with a vector expressing IRFP as a transfection control. Seventy-two hours post-transfection, cells were fixed and analyzed by flow cytometry. Shown are representative IRFP *versus* Clover plots and the mean percentage of Clover-positive cells from three independent experiments (± s.d.) counting at least 50 000 events per experiment. Data are normalized to cells expressing Clover-lamin CRISPR donor without Cas9/gRNA. Two-tailed t-test indicates the difference in percentage of transfected U2OS *versus* ΔPML cells expressing Clover is significant (*$p < 0.05$). **(C)** Cell cycle analysis of wild-type U2OS and ΔPML cells using PI staining and flow cytometry. Data represent the mean values of three replicate experiments (± s.d.) counting at least 10 000 events per experiment.

A

U2OS   ΔPML

10 um   10 um

B

Untransfected   Clover donor   Clover donor + gRNA

U2OS

ΔPML

IRFP

Clover
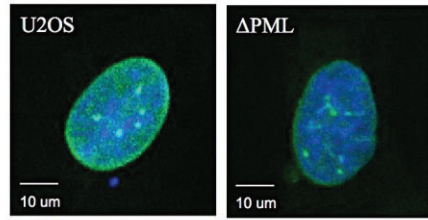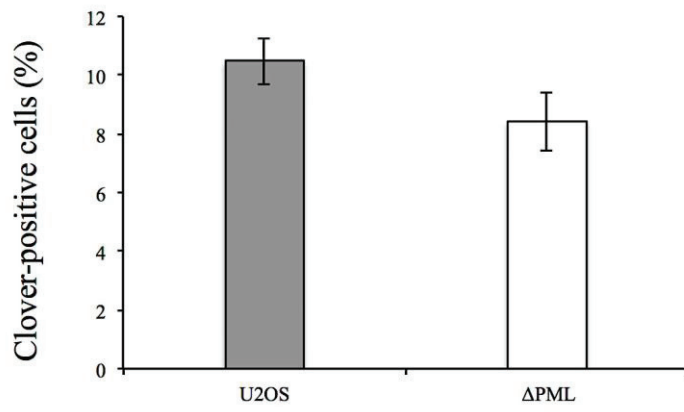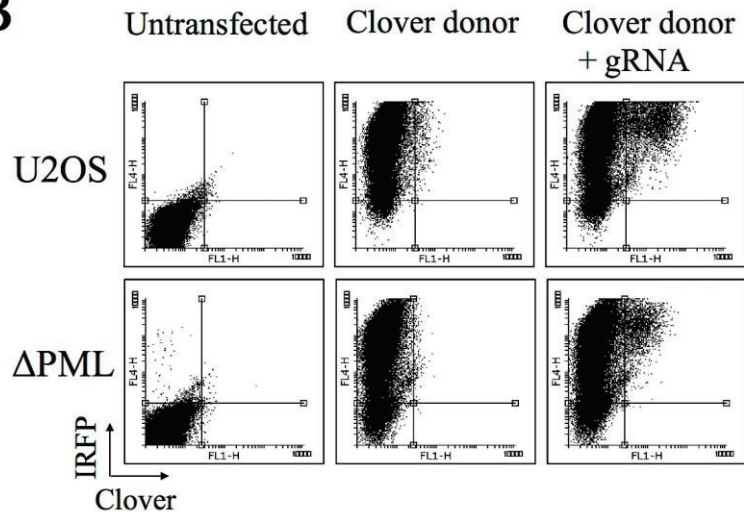
C

3.4.3 Effect of individual PML isoform overexpression on rates of DSB repair by HR and NHEJ

The positioning of a DNA break in close proximity to PML nuclear bodies appears to impact HR (**Figure 3.13**), but there is only a minor effect on HR levels when PML nuclear bodies are absent from cells by deletion of PML (**Figure 3.14**). Since it is known that individual PML protein isoforms may differentially affect cellular processes including cell fate decisions following DNA damage (269), I decided to further explore the role of PML on DNA repair by investigating the effects of each PML isoform. To accomplish this, I individually overexpressed each of the six nuclear PML isoforms (PMLI-VI) in wild-type U2OS, ΔPML cells and in each of the three cell lines generated in this study (U2OS Chr15 HR 2, U2OS TAP HR 6, U2OS TAP NHEJ 4; sections 3.3.2.4, 3.3.2.5). PMLVII has a primarily cytoplasmic localization and as such was not chosen for use in these experiments.

3.4.3.1 PML overexpression is inhibitory to HR in an isoform-specific manner

To determine the effects of PML isoform overexpression on rates of CRISPR/Cas9-mediated HR, U2OS and ΔPML cells were transiently co-transfected with the Clover-lamin CRISPR donor plasmid and either an empty FLAG vector or an individual FLAG-tagged PML isoform expression vector, either with or without the Cas9/gRNA expression vector. Again, IRFP served as a transfection control. PML isoform overexpression was confirmed by immunofluorescence microscopy using anti-PML and anti-FLAG antibodies (**Figure 3.15A**). As previously reported, PML isoform overexpression results in changes in PML body size and number that are isoform specific (217-219), as can be seen in **Figure 3.15A** and **Figure 3.16A**. Additionally, in a PML-knockout background, overexpression of individual PML isoforms is sufficient to cause *de novo* nuclear body formation (270), as can be seen in ΔPML cells (**Figure 3.15A**, bottom panel). Cells were then analyzed by flow cytometry to determine the percentage of transfected cells that were Clover positive and thus the levels of HR following individual PML-isoform overexpression (**Figure 3.15B**). The levels of Clover fluorescence were normalized to those of cells transfected without the Cas9/gRNA

vector. In both U2OS and ΔPML cells, PML isoform overexpression resulted in an overall reduction in HR to varying degrees. The most notable effect on HR was observed upon overexpression of PMLI, II and IV. Importantly, these effects on HR were not due to alterations in cell cycle caused by PML isoform overexpression (**Figure 3.15C**).

To further analyze the possible effects of PML isoform overexpression on HR, I used the U2OS Chr15 HR 2 and U2OS TAP HR 6 cells generated in this study that contain a chromosomal copy of the HR reporter. These cells were transfected with an empty FLAG vector or an individual FLAG-tagged PML-isoform expression vector either with or without a vector expressing I-SceI, to initiate chromosomal HR. PML isoform overexpression was confirmed by immunofluorescence microscopy (**Figure 3.16A**). Similar to the results of the Clover-lamin HR assay, the chromosomal HR assay in U2OS Chr15 HR 2 cells indicated that PML isoform overexpression produced an overall reduction (**Figure 3.16B**), which was not due to alterations in cell cycle profiles (**Figure 3.16C**). Interestingly however, in U2OS TAP HR 6 cells, HR levels did not significantly differ upon PML isoform overexpression, with the exception of PMLI (**Figure 3.16B**).

Figure 3.15. PML isoform overexpression leads to a decrease in HR in wild-type and ΔPML cells that is not related to changes in cell cycle. (A) Wild-type U2OS and ΔPML cells were transfected with vectors expressing individual FLAG-tagged PML isoforms. Transfected cells were fixed and analyzed by immunofluorescent staining with anti-PML and anti-FLAG polyclonal antibodies, followed by Alexa-Fluor 649-conjugated (red) or Alexa-Fluor 555-conjugated (artificially coloured yellow) secondary antibodies, respectively. Cell nuclei were stained with DAPI. **(B)** Wild-type U2OS and ΔPML cells were co-transfected with the Clover-lamin CRISPR donor plasmid and an empty FLAG vector or an individual FLAG-tagged PML-isoform expression vector, either with or without Cas9/gRNA. Cells were also transfected with an IRFP expression vector as a transfection control. Seventy-two hours post-transfection, cells were fixed and analyzed by flow cytometry. Shown are representative IRFP *versus* Clover plots and the mean percentage of Clover-positive cells from three independent experiments (± s.d.) counting at least 50 000 events per experiment. Data are normalized to cells expressing Clover-lamin CRISPR donor and specific PML isoforms without Cas9/gRNA. Two-tailed t-tests indicate the differences in percentage of Clover-expressing cells between empty-FLAG and FLAG-tagged PML isoform vector-transfected cells is significant (** $p < 0.01$, for wild-type U2OS cells and * $p < 0.05$ for ΔPML cells) **(C)** Cell cycle analysis of wild-type U2OS and ΔPML cells using PI staining and flow cytometry. Data represent the mean values of three replicate experiments (± s.d.) counting at least 10 000 events per experiment.
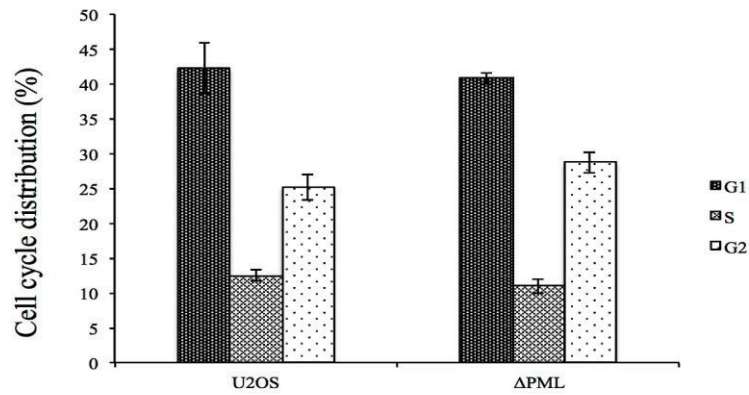
A

B

C

U2OS   ΔPML
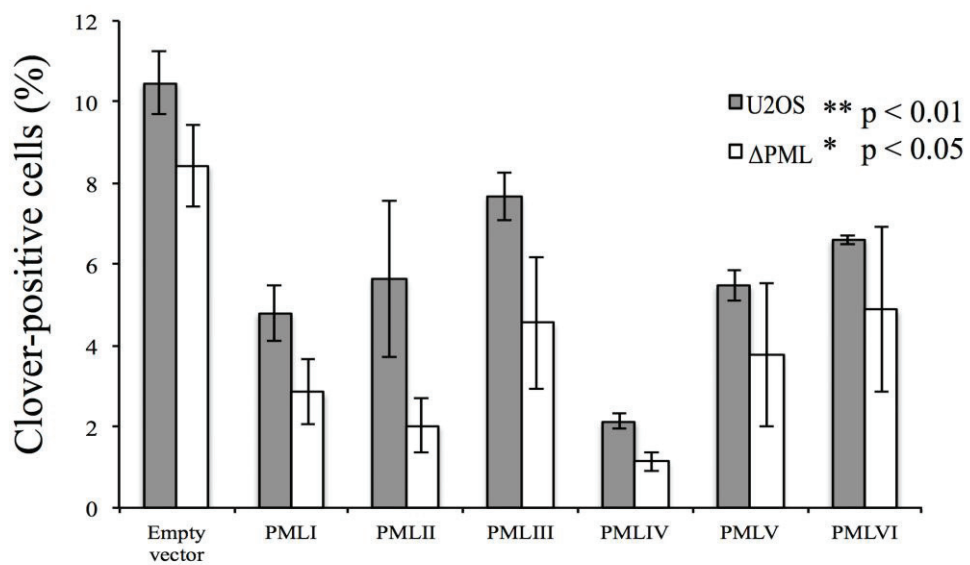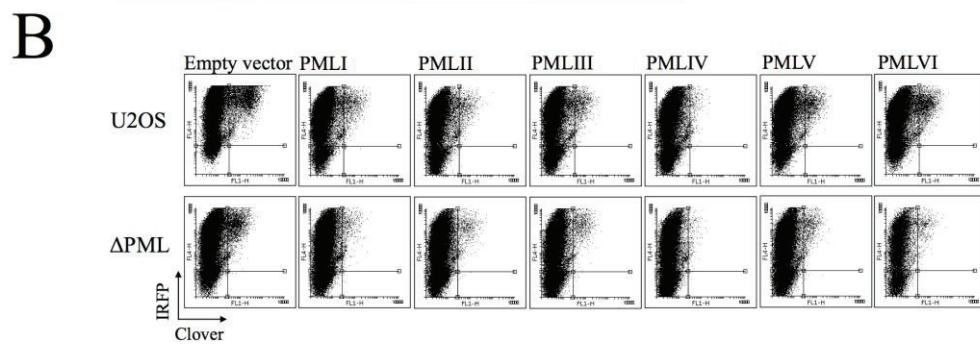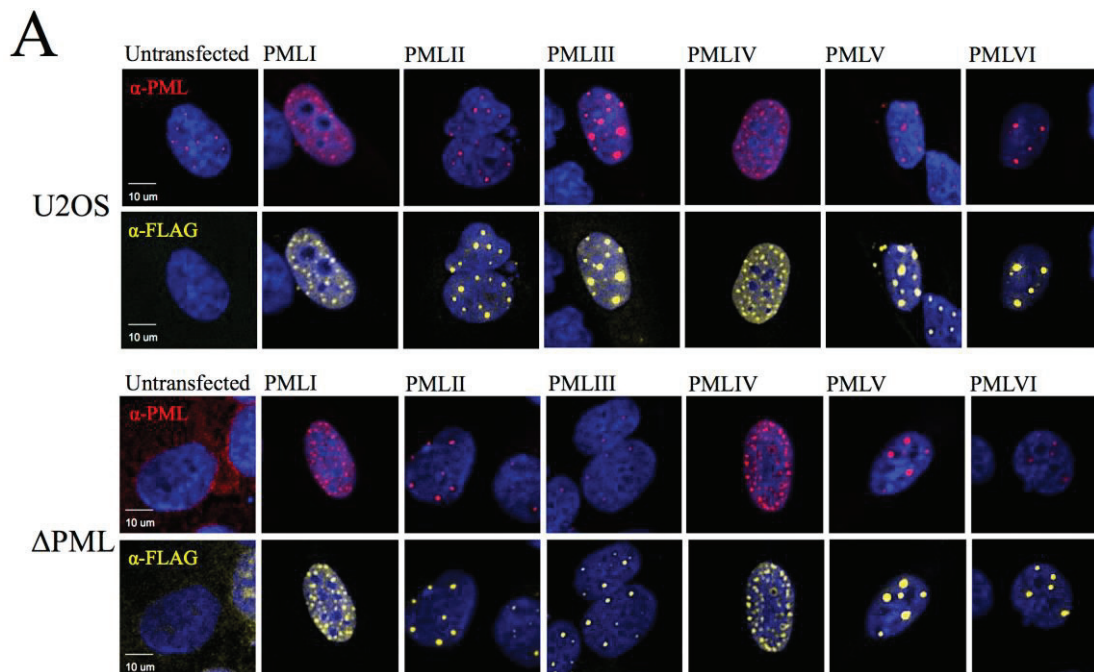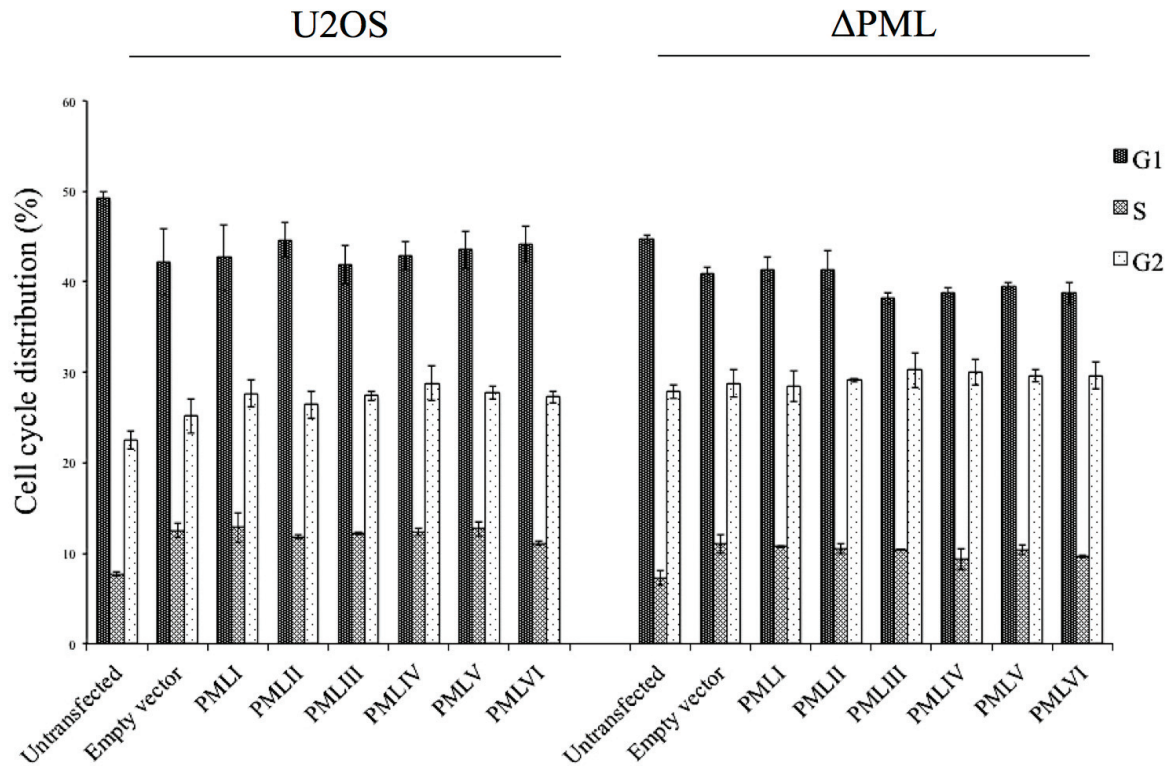
Figure 3.16. PML isoform overexpression leads to a decrease in HR in U2OS Chr15 HR 2 cells but not U2OS TAP HR 6 cells, with the exception of PMLI. (A) Cells were transfected with vectors expressing individual FLAG-tagged PML isoforms. Transfected cells were fixed and analyzed by immunofluorescent staining with anti-PML and anti-FLAG polyclonal antibodies, followed by Alexa-Fluor 649-conjugated (red) or Alexa-Fluor 555-conjugated (artificially coloured yellow) secondary antibodies, respectively. Cell nuclei were stained with DAPI. **(B)** U2OS Chr15 HR 2 and U2OS TAP HR 6 cells were co-transfected with an empty FLAG vector or an individual FLAG-tagged PML-isoform expression vector, either with or without an I-SceI expression vector. Cells were also transfected with an IRFP expression vector as a transfection control. Seventy-two hours post-transfection, cells were fixed and analyzed by flow cytometry. Shown are representative IRFP *versus* GFP plots and the mean percentage of GFP-positive cells from three independent experiments (± s.d.) counting at least 50 000 events per experiment. Data are normalized to cells expressing specific PML isoforms without I-SceI. Two-tailed t-tests indicate the differences in percentage of GFP-expressing cells between empty-FLAG vector and FLAG-tagged PML isoform vector-transfected U2OS Chr15 HR 2 cells are significant   (* p <0.05). Two-tailed t-tests indicate the differences in percentage of GFP-expressing cells between empty-FLAG and FLAG-tagged PML vetor-transfected U2OS TAP HR 6 cells, with the exception of PMLI (* p <0.05), were non-significant. **(C)** Cell cycle analysis of U2OS Chr15 HR 2 and U2OS TAP HR 6 cells using PI staining and flow cytometry. Data represent the mean values of three replicate experiments (± s.d.) counting at least 10 000 events per experiment.

A

| | Untransfected | PMLI | PMLII | PMLIII | PMLIV | PMLV | PMLVI |

Chr15
α-PML
α-FLAG

TAP1
α-PML
α-FLAG

B

Empty vector PMLI PMLII PMLIII PMLIV PMLV PMLVI

Chr15

TAP1

IRFP
GFP

C

Chr15   TAP1

60

Cell cycle distribution (%)

50

40

30

20

10

0

Untransfected Empty vector PMLI PMLII PMLIII PMLIV PMLV PMLVI   Untransfected Empty vector PMLI PMLII PMLIII PMLIV PMLV PMLVI

■ G1
▨ S
□ G2
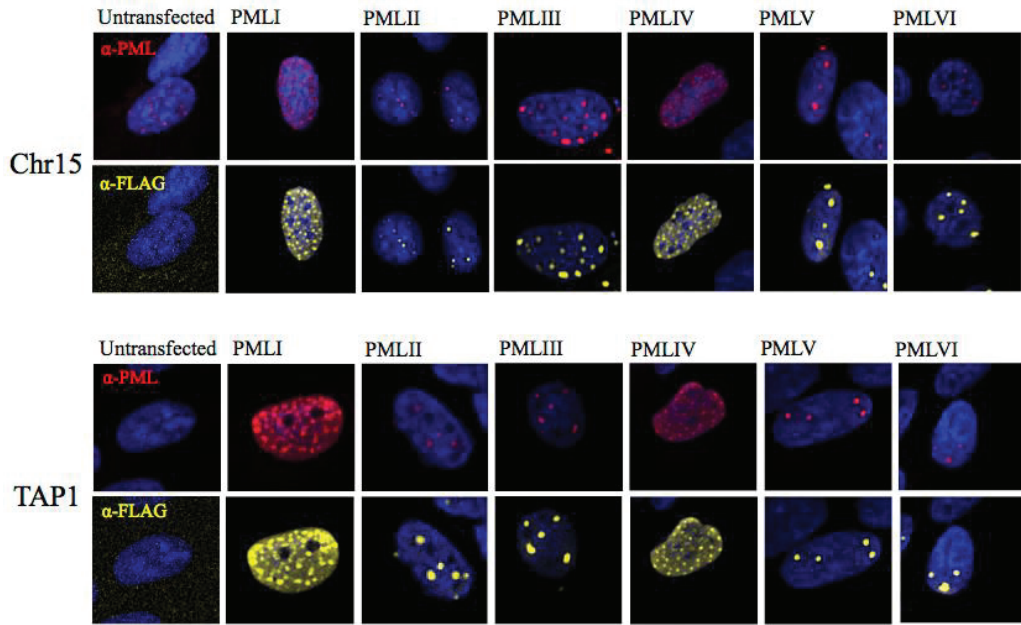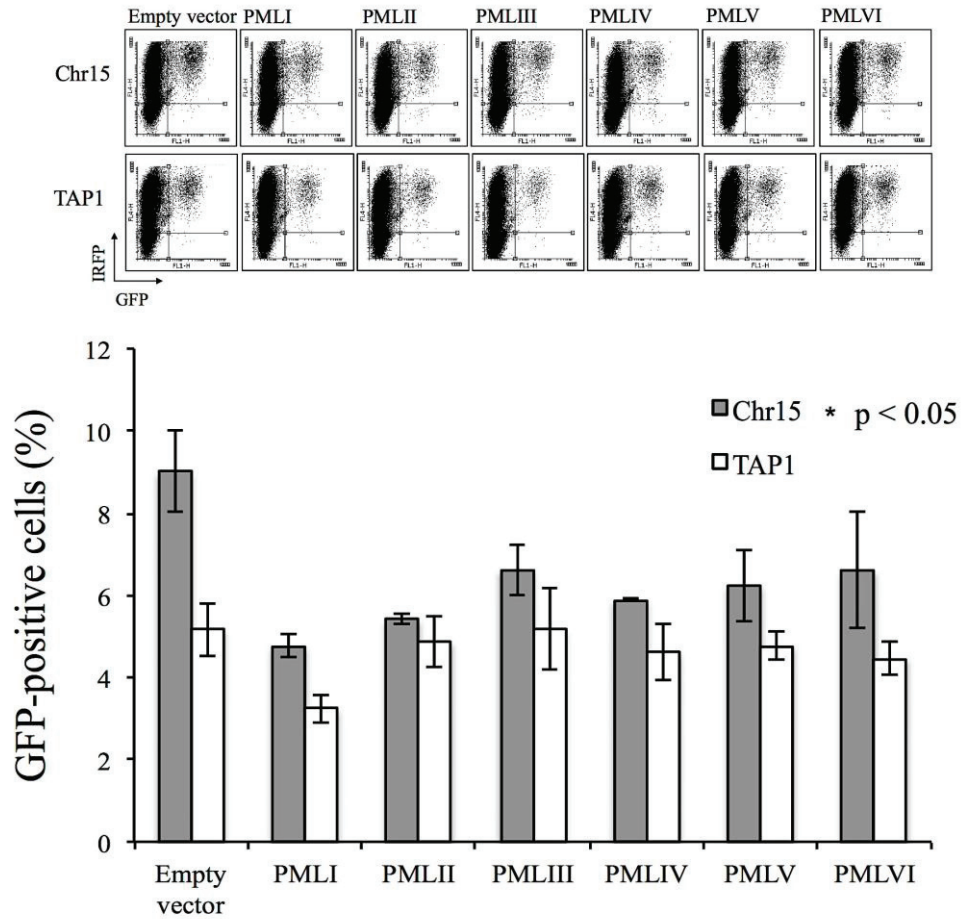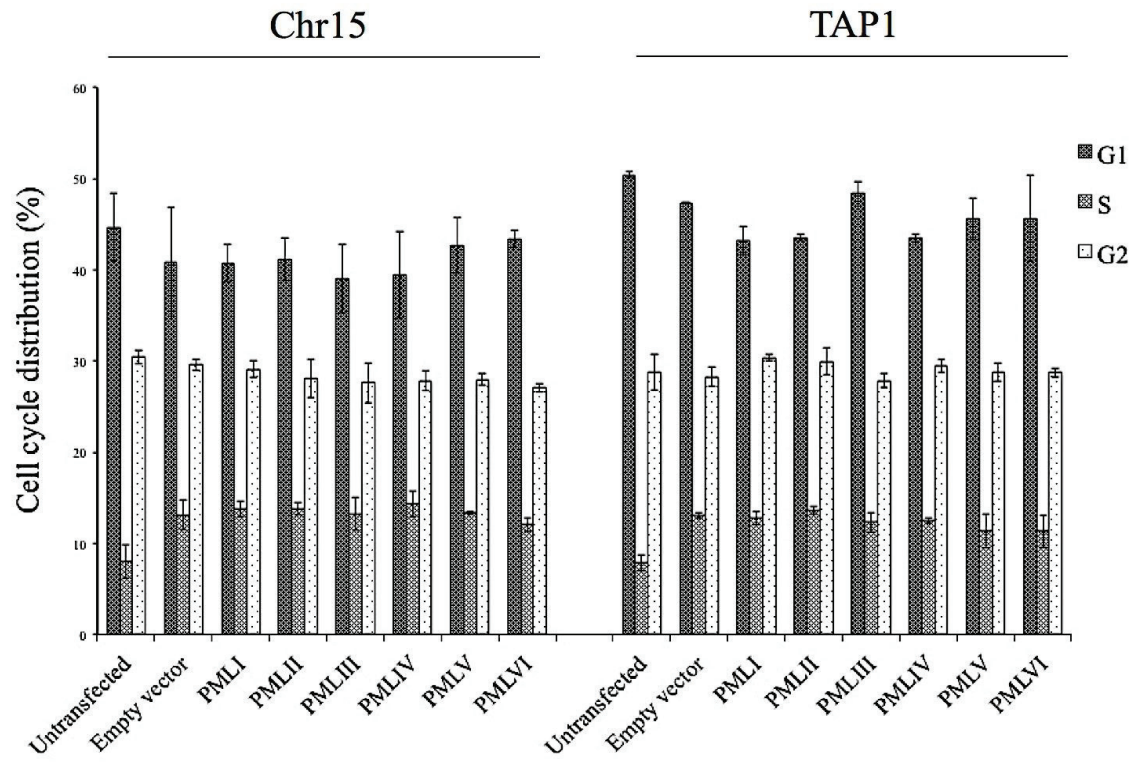
3.4.3.2 PML overexpression is inhibitory to NHEJ in an isoform-specific manner

Having observed an inhibitory effect of PML isoform overexpression on HR efficiency in wild-type U2OS, ΔPML and U2OS Chr15 HR 2 cell lines, I next assessed the effect of PML isoform overexpression on DSB repair by NHEJ. Wild-type U2OS and ΔPML cells were transiently co-transfected with the EJ5-GFP NHEJ reporter vector (255) and an empty FLAG vector or individual FLAG-tagged PML-isoform expression vector, either with or without an I-SceI expression vector. Similar to what was seen for HR, there was an overall reduction in levels of DSB repair by NHEJ upon PML isoform overexpression, in particular PML isoforms II and IV, (**Figure 3.17**) as measured by flow cytometry. However, this effect appeared to be less prominent in ΔPML cells compared to wild-type U2OS cells, suggesting that other PML isoforms might contribute together to the observed inhibition of NHEJ. Finally, in contrast to the inhibitory effect of PML loss on HR (**Figure 3.15**), knockout of PML appeared to modestly enhance NHEJ (**Figure 3.17**).

To further assess the inhibitory effects of PML isoform overexpression, I employed the U2OS TAP NHEJ 4 cell line carrying a single copy of the NHEJ reporter integrated into the TAP1 locus. Using these cells, PML isoform overexpression also resulted in reduced NHEJ efficiency, with the most pronounced effect being again in cells transiently overexpressing PMLII and IV (**Figure 3.18**). This serves as an indication that PML, notably isoforms I, II and IV may be playing an early role in DSB repair, being involved in both major pathways, NHEJ and HR.
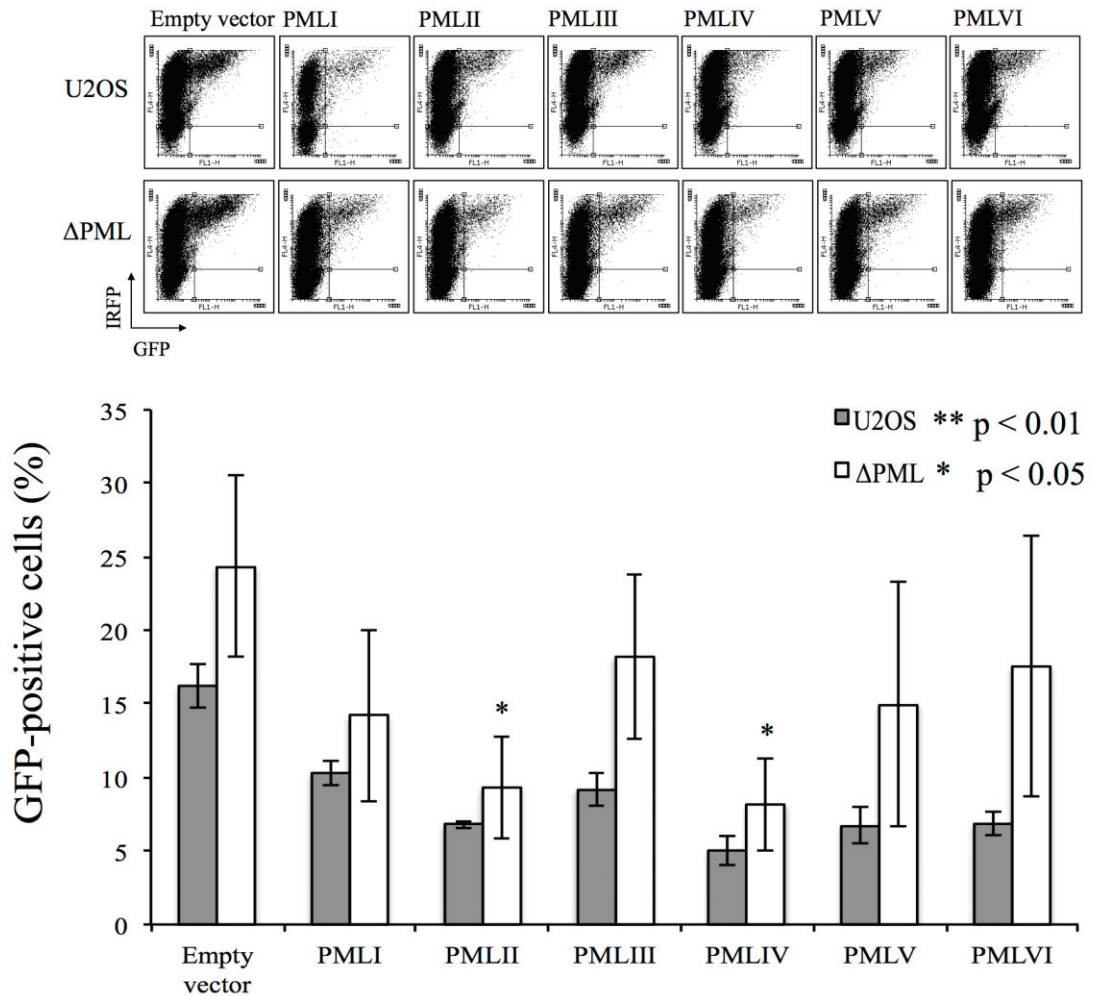
Figure 3.17. PML overexpression leads to a decrease in NHEJ levels in wild-type and ΔPML cells. Wild-type U2OS and ΔPML cells were transiently co-transfected with the EJ5-GFP NHEJ reporter vector and empty FLAG vector or individual FLAG-tagged PML-isoform expression vectors, either with or without an I-SceI endonuclease expression vector. Cells were also transfected with an IRFP expression vector as a transfection control. Seventy-two hours post-transfection, cells were fixed and analyzed by flow cytometry. Shown are representative IRFP *versus* GFP plots and the mean percentage of GFP-positive cells from three independent experiments ($\pm$ s.d.) counting at least 50 000 events per experiment. Data are normalized to cells expressing the NHEJ plasmid and specific PML isoform without I-SceI. Two-tailed t-tests indicate the differences in percentage of GFP-expressing cells between empty-FLAG vector and FLAG-tagged PML isoform vector-transfected wild-type U2OS cells are significant (* p <0.01). Two-tailed t-tests indicate the differences in the percentage of GFP-expressing cells between empty-FLAG vector and FLAG-tagged PML isoform vector-transfected ΔPML cells (* p <0.05) were non-significant.
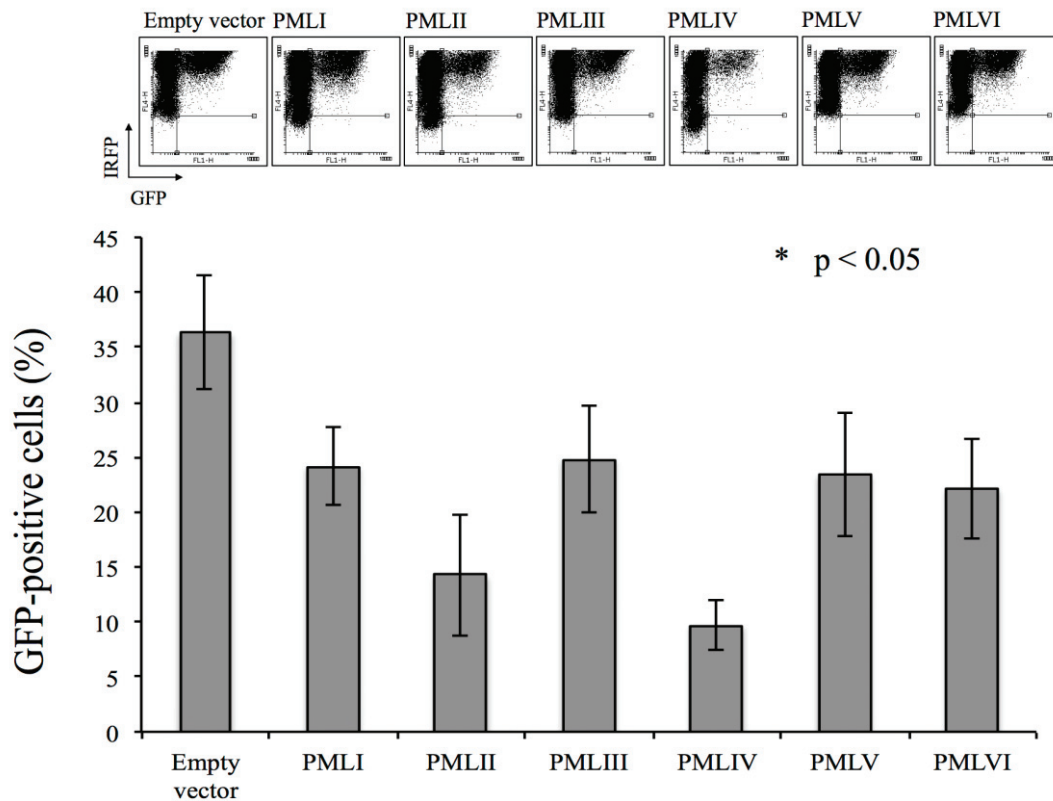
Figure 3.18. Effects of PML isoform overexpression on levels of NHEJ in U2OS TAP NHEJ 4 cells. U2OS TAP NHEJ 4 cells were transiently co-transfected with an empty FLAG vector or individual FLAG-tagged PML-isoform expression vector, either with or without an I-SceI endonuclease expression vector. Cells were also transfected with an IRFP expression vector as a transfection control. Seventy-two hours post-transfection, cells were fixed and analyzed by flow cytometry. Shown are representative IRFP versus GFP plots and the mean percentage of GFP-positive cells from three independent experiments ($\pm$ s.d.) counting at least 50 000 events per experiment. Data are normalized to cells expressing a specific PML isoform without I-SceI. Two-tailed t-tests indicate the differences in percentage of GFP-expressing cells between empty-FLAG vector and FLAG-tagged PML isoform vector-transfected U2OS NHEJ TAP 4 cells are significant (* $p < 0.05$).

CHAPTER 4. DISCUSSION

4.1 General overview

In this thesis, I have investigated DSB repair in the context of nuclear architecture. I determined how a major contributing factor to nuclear organization and mechanical stability (polymerized nuclear actin) is involved in DNA DSB repair. Specifically, I identified a novel role for polymeric nuclear actin in NHEJ, through retention of the Ku heterodimer at DNA break sites. I also investigated the reason behind the delay in HR observed at the nuclear lamina, finding that it is the structure of the chromatin associated with the nuclear periphery that is responsible. Finally, I generated cell lines to study NHEJ and HR in a biologically-relevant context. One cell line contained reporter DNA inserted within a locus that is significantly associated with PML nuclear bodies and in another, the reporter DNA was integrated in a locus not associated with bodies. I investigated the impact of a DNA break at these loci on repair efficiency, finding that HR is decreased at the locus more closely associated with PML bodies. I also examined the role of individual PML isoforms on DNA DSB repair, finding that PML isoform overexpression, notably of PML I, II and IV, resulted in decreased levels of both HR and NHEJ, suggesting a role for PML early in the DNA repair process.

4.2 A novel role for polymerized nuclear actin in DNA repair

Nuclear actin had previously been implicated in DNA repair, but a precise role had not been elucidated. In collaboration with Dr. Hendzel's group I demonstrated a role of polymerized nuclear actin in DNA repair, specifically in NHEJ. Dr. Hendzel's group found that several DNA repair proteins, including the Ku70/80 heterodimer, MRE11 and RAD51, interact with nuclear actin *in vitro*. Additionally, they demonstrated that disruption of actin polymerization inhibits DNA repair *in vitro* and *in vivo*. Importantly, this inhibition was not due to altered H2AX, CHK2 or ATM phosphorylation, implying that polymeric nuclear actin exerts its effects on the DNA repair process itself rather than at the level of DDR signaling.

To further understand the contributions of polymeric nuclear actin to DNA repair, I investigated its role in the recruitment and retention of one of its newly identified interaction partners, Ku80, to DNA damage sites in live cells. I demonstrated that disruption of actin polymerization, either through introduction of a polymerization-incompetent actin mutant or treatment with the drug cytochalasin D, significantly reduced retention of GFP-tagged Ku80 to UV laser-induced DNA damage tracks (**Figure 3.1** and **Figure 3.2**). Notably, however, initial Ku80 recruitment to damage sites was unaffected by these alterations to the polymeric nuclear actin pool.

The Ku heterodimer is one of the earliest factors recruited in response to a DSB and is extremely important in mediating DSB repair through NHEJ (12, 13, 271). Upon DSB formation, Ku70/Ku80 binds the damaged DNA ends, helping to maintain end stability while simultaneously facilitating exposure of DNA ends to the end-processing and ligation machineries (28). In fact, the Ku heterodimer is proposed to function as a "tool belt," remaining associated with DNA breaks throughout the entire repair process and facilitating recruitment of a variety of factors to DNA ends, depending on the break complexity (10, 42). Following DNA damage, broken DNA ends have been shown to remain relatively stationary within the nucleus (248, 272). Importantly, it has been demonstrated that Ku80 specifically is responsible for restricting the mobility of damaged DNA ends (272) yet the exact manner in which Ku80 acts in maintaining DSB positional stability is largely unknown.

In this study it was demonstrated that the polymerization state of nuclear actin impacts Ku80 retention at DNA damage sites. These findings indicate that nuclear actin may be the factor responsible for the immobilization of DNA breaks mediated by Ku80. Nuclear actin serves a well-established structural role in the nucleus, contributing to the stabilization of several nuclear compartments (163, 166-170). Another such role may be in providing structural integrity and support through maintaining the Ku heterodimer at DNA break sites. It would then be expected that loss of polymeric nuclear actin could lead to increased levels of chromosomal translocations and overall genomic instability. Interestingly, a recent study has found that levels of polymerized nuclear actin increased in cells subjected to DNA damage by MMS and IR, and that these actin filaments promote DSB repair (273). Increasing the pool of polymeric actin in response to DNA

damage may be a way to ensure proper stability of broken DNA ends, thereby preventing inappropriate end-joining and genomic instability. In line with this idea, it has previously been found that over-expression of an actin-depolymerization factor increases cellular sensitivity to IR (182). Overall, these findings provide the first evidence of a direct role of nuclear actin in DNA repair: maintaining the key NHEJ factor Ku80 at DNA damage sites. Whether nuclear actin also plays a role in other aspects of the repair process remains to be determined.

4.3 DDR and HR delays at the nuclear lamina are due to nuclear periphery-associated heterochromatin

Early evidence from yeast suggested that following damage, DNA migrates to dedicated nuclear repair centres that provide an optimal environment for DNA repair (274). A similar situation was postulated to occur in mammalian cells; however, it has since been demonstrated that DSBs are repaired individually and DNA break ends remain immobile in the nucleus (272). Restricting DNA DSB motility may be an important strategy for protecting genomic integrity, as spatial proximity has been proven to be a key determinant of chromosomal translocation frequency in mammalian cells (275, 276). Moreover, increasing evidence has suggested a role of nuclear compartmentalization in the maintenance of genomic stability (277). This then leads to the question of whether DNA breaks occurring throughout the nucleus are repaired with equal efficiency, or whether their repair is position specific. To further understand the contributions of nuclear architecture to DNA repair, Dr. Soutoglou's group investigated DNA repair at the nuclear lamina. In conjunction with their group, I specifically examined the role of chromatin structural changes with respect to HR efficiency at the nuclear periphery.

Using a U2OS cell line containing a stably integrated I-SceI restriction site flanked by a 256x LacO array, Dr. Soutoglou's group was able to sequester the I-SceI/LacO locus to the nuclear lamina through expression of a GFP-LacI-ΔEMD fusion protein, and then induce DSBs and study repair at this position relative to that in the nuclear interior. Delayed γH2AX and 53BP1 recruitment kinetics were observed when a DSB was induced at the nuclear lamina relative to the nuclear interior, suggesting an overall reduction in DDR signaling. However, when the two major DSB repair pathways were

investigated, it was found that I-SceI/LacO relocalization to the nuclear lamina did not impact recruitment of NHEJ proteins Ku80 and XRCC4, but rather significantly delayed the recruitment of HR factors BRCA1, RAD51, and RAD54. This data suggested that the nuclear lamina is generally a repressive microenvironment for the DDR, and specifically for DNA repair by HR. Treating cells with TSA resulted in decondensation of chromatin associated with the nuclear lamina (**Figure 3.3**) with subsequent alleviation of the delay in DDR and HR factor recruitment to nuclear lamina-associated DSBs. These results suggest that the reason for the reduced DDR and HR in particular is due to the highly condensed heterochromatin associated with the nuclear lamina.

Increasing evidence points to chromatin and its compaction state as playing a key role in the regulation of the DDR and DSB repair (278-281). The findings that lamina-associated heterochromatin is responsible for the observed delay in DDR and HR factor recruitment at the nuclear periphery is in agreement with other studies that have found that DSBs formed within heterochromatin are processed with slower kinetics than those in euchromatin (153, 282). The delay in HR within heterochromatin may be due to altered accessibility of the underlying DNA DSB to repair factors. Alternatively, repressing HR in favor of NHEJ may represent a means to prevent inappropriate recombination events that could easily occur across highly repetitive heterochromatic sequences, a mechanism proposed for heterochromatin DSB repair in *Drosophila* cells (203, 283).

Based on the findings presented in section 3.2 it can be suggested that the nuclear lamina may be functioning to sequester highly repetitive heterochromatin at the nuclear periphery, thereby playing a role in maintaining genome stability. In agreement with this, the heterochromatin associated with the nuclear lamina has been shown to be particularly immobile in the nucleus, in part due to the actions of the A-type lamins (201, 284). Additionally, depletion of A-type lamins leads to increased sensitivity to IR, defects in repair foci assembly and an overall increase in genomic instability (197, 201). Therefore, the nuclear lamina may not only play a role in the structural integrity of the nucleus but also in maintaining genomic stability by compartmentalizing certain heterochromatic regions.

4.4 The use of diverse genetic engineering techniques in cell line generation

Much of my doctoral work was focused on generating cell lines containing single genomic insertions of NHEJ or HR reporter DNA adjacent to a 128x LacO array to study DNA DSB repair at varying nuclear locations. Several genetic engineering techniques were employed, with varying degrees of efficacy, in the generation of these cell lines, including PiggyBac transposition and CRISPR/Cas9 targeted gene editing in conjunction with FLP/FRT and Cre/loxP recombination (**Figure 3.4**).

Initially, PiggyBac transposition was used to randomly integrate the pFlexible-LacO-pBLR5 construct, created for cell-line generation in this study, into the genome of U2OS cells. The PiggyBac transposon is a mobile genetic element that transposes DNA flanked by specific terminal repeat sequences into target TTAA sequences by a "cut and paste" mechanism. PiggyBac transposition is also reversible: DNA can be excised from the genome without leaving 'footprint' mutations at the excision site (285). The high transposition efficiency exhibited by PiggyBac in a wide range of cell lines and organisms, in addition to its propensity for mediating stable, long-term expression of large DNA cargo, have led to its broad use for a variety of genetic engineering applications (265). For these reasons, the PiggyBac transposon system was initially chosen as the major method for cell line engineering in this study.

Following transposition of the pFlexible-LacO-pBLR5 construct into the genome of U2OS cells, 11 colonies were shown by Southern blot analysis to contain a single genomic integration. While the random transposition of pFlexible-LacO-pBLR5 DNA was at one point thought to be beneficial for the creation of cell lines in which DNA repair could be studied at an array of diverse genomic locations, ultimately it was this exact feature of PiggyBac that proved most problematic. Due to the fact that the integration sites of pFlexible-LacO-pBLR5 were unknown, their genomic position had to be mapped by inverse PCR. This technique is particularly challenging, as it is unknown which restriction enzyme will be most appropriate to generate recircularized products of a size amenable to PCR amplification, and as such multiple enzymes must be tried for each individual cell line. Additionally, if no products are generated following PCR amplification, it is unknown if this absence is due to inefficiency in the self-ligation reaction, or if the primer pairs utilized are simply not optimal. Consequently, the

pFlexible-LacO-pBLR5 integration location could not be effectively determined, which was a vital criterion for studying the effects of genomic positioning of DNA breaks on repair.

As a result of these limitations, the newly available CRISPR/Cas9 technique for targeted gene editing was employed as an alternative strategy. The CRISPR/Cas9 system is a means of introducing precise DSBs in the genome by targeting the Cas9 endonuclease to specific loci using complementary gRNAs (267). These breaks can be repaired by NHEJ resulting in deletions at the break site and locus disruption, or they can be repaired by HR using a homology-containing donor repair template, resulting in precise replacement mutations. This method of genetic engineering was employed to target the pFlexible-LacO-pBLR5 construct to two specific loci that were strategically chosen to study the influence of PML nuclear body proximity on DNA repair efficiency (Chr15 and TAP1).

Integration of pFlexible-LacO-pBLR5 at either the Chr15 or TAP1 locus in U2OS cells was verified by FISH and genomic PCR (**Figures 3.7-3.9**). In my studies, two different Cas9 endonucleases were employed, the wild-type and D10A nickase mutant (268). Both were used for cell line generation as it was uncertain which would result in the most effective targeting. Use of wild-type Cas9 yielded individual clones containing pFlexible-LacO-pBLR5 integrated at a single Chr15/TAP1 allele rather than at all three alleles present in the U2OS genome. Sequence data from PCR amplicons revealed small deletions of 12-43 bp at the Chr15/TAP1 loci not targeted by HR in these clones. Conversely, Cas9D10A nickase yielded individual clones containing pFlexible-LacO-pBLR5 integrated primarily at two of the three Chr15/TAP1 alleles in the U2OS genome. Sequence data also revealed significantly larger deletions in non-HR targeted alleles (up to several hundred base pairs). The increased insertional efficiency of Cas9D10A is likely due to the fact that an increased amount of Cas9D10A, as compared to wild-type Cas9, was used in each transfection, as the two gRNAs required to make a DNA DSB are expressed from individual Cas9D10A expression vectors (**Table 2.6**). While there is increased potential for off-target effects using wild-type Cas9 (286), ultimately Chr15 and TAP1 clones generated by wild-type Cas9 were chosen for further engineering. This

is because they contained a single genomic integration of pFlexible-LacO-pBLR5, and had the smallest deletions in unedited alleles as determined by FISH and PCR.

There are specific benefits but also significant disadvantages to each of the major genetic engineering techniques used in this study. The PiggyBac system, which encodes its own DNA transposase, is extremely efficient for integrating DNA sequences into cellular genomes, much more so than CRISPR/Cas9. This difference might arise in part from the fact that CRISPR/Cas9 relies on host-cell machinery and HR for DNA integration, and as such is cell cycle dependent. Additionally, on a surface level, PiggyBac transposition appears to be less labour intensive; all that is required is to flank donor DNA by terminal repeat sequences and to perform a single transfection. PiggyBac is also reversible: at any time, any desired construct can be eliminated from the genome with no excision footprint mutation by simple re-transfection with the transposase. In experiments where integration number and location are unimportant PiggyBac is a powerful technique. However, in the context of this study, knowledge of the exact genomic position was vital, making the PiggyBac system less desirable: mapping integration sites is extremely time consuming and must be performed with great care, as each step of inverse PCR must be meticulously tested and optimized.

Targeted integration at pre-determined genomic sites by CRISPR/Cas9 editing is extremely powerful. Confirmation of successful integration is achieved with greater ease; however, integration efficiency is not as high as with PiggyBac, and despite being precise there is still the potential for off-target mutations. Additionally, as was found in this study, non-HR targeted genomic loci (depending on the type of Cas9 endonuclease used) can have deletions up to a few hundred base pairs, which may result in unintended locus disruption (286). Finally, while screening for successful integration is faster and easier, in the context of this study the cloning steps required for CRISPR/Cas9-mediated HR are initially more time consuming than using PiggyBac to integrate DNA into a genome. For example, individual gRNAs targeting each desired locus must be designed and cloned into individual Cas9 expression vectors. In addition, DNA homology arms flanking desired donor DNA must be constructed for each targeted locus and multiple separate transfections are required to generate individual cell lines. Due to this complexity, I

strategically focused on only two genomic loci (Chr15 and TAP1) for CRISPR/Cas9-mediated HR integration of pFlexible-LacO-pBLR5.

Other genome engineering techniques used in this study for cell line generation were FLP/FRT and Cre/loxP site-specific DNA recombination. FLP and Cre recombinases catalyze DNA exchange reactions between short recombinase-specific target sequences (287). FLP-catalyzed recombination across identical FRT sites resulted in the successful removal of the puroΔTK selectable marker within the pFlexible-LacO-pBLR5 construct integrated at either the Chr15 or TAP1 locus of U2OS cells. The Cre/lox system, which was designed in this study to mediate directional recombination across heterospecific loxP sites, was then used to incorporate floxed reporter DNA between the lox sites of the pFlexible-LacO-pBLR5 construct. While FLP/FRT recombination worked well, Cre/loxP directional recombination was problematic: correct integration of reporter DNA could not be confirmed by genomic PCR.

While Cre/loxP recombination is a widely used technique, caution must be taken as mammalian genomes have been found to contain multiple cryptic lox sites, which can lead to inappropriate recombination (288). Several groups have demonstrated a relatively high frequency of non-specific recombination events when using similar heterospecific loxP sites to those used in this study (289, 290). Additionally, to obtain recombination efficiencies similar to those of wild-type loxP sites, mutant loxP sites have to be exposed to much greater concentrations of Cre recombinase, which can be cytotoxic (291). Finding an appropriate balance between the level of Cre expression and recombination frequency is extremely important when using this system for genome engineering. Equally important is accurately screening for inappropriate recombination events.

Due to the inefficiency experienced incorporating NHEJ and HR reporter DNA using Cre/loxP recombination, I again employed CRISPR/Cas9 to target reporter DNA to the previously integrated pFlexible-LacO-pBLR5 construct. Incorporation of reporter DNA sequences was confirmed by genomic PCR and by transfection with I-SceI (**Figures 3.10-3.12**). This strategy worked well for the TAP1 locus, but I had more difficulty with the Chr15 locus. Although genomic PCR indicated the presence of NHEJ reporter DNA in a few Chr15 cellular clones, no GFP expression was detectable upon I-SceI transfection. Thus, more clones will need to be selected and screened to identify one

containing a functional NHEJ reporter.

Overall, several different genome engineering techniques were used in this study for cell line generation, each offering specific advantages and disadvantages. The original aim of this study was to produce a series of cell lines, each one containing a single copy of a NHEJ or HR repair reporter adjacent to a LacO array integrated at a different distinct genomic position to study DNA repair throughout the nucleus. Several different genome engineering techniques were employed to varying degrees of success, ultimately yielding three different cell lines: two containing the NHEJ and HR reporter/LacO array integrated at the TAP1 locus and one containing the HR reporter/LacO array at the Chr15 locus. These cell lines are versatile tools for studying DNA repair. The NHEJ and HR reporters described in this study can be used as a sensitive and highly quantitative assay for the measurement of DNA DSB repair efficiency. Genomic integration of reporter DNA provides the advantage of analyzing DNA repair in a chromosomal context. Furthermore, having reporter DNA integrated at single defined nuclear locations allows direct comparison between NHEJ and HR efficiencies at the exact same genetic locus. Additional versatility is provided by the 128x LacO array located adjacent to reporter DNA in these lines. Although useful for locus visualization by FISH, the LacO array can also be used in a manner similar to that described in section 3.2 to sequester reporter DNA to different subnuclear compartments through expression of a nuclear domain-targeting peptide fused to LacI. Alternatively, different proteins can be fused to LacI and recruited and tethered to the LacO array to determine their influence on NHEJ or HR repair pathways. Beyond simply addressing the question of whether DSB positioning relative to PML nuclear bodies influences DNA DSB repair, these cell lines represent versatile tools allowing a number of different aspects of DNA repair to be examined in the future.

4.5 The role of PML and PML nuclear bodies on DSB repair

PML nuclear bodies and, to a lesser extent, the PML protein itself have long been implicated as playing a role in the cellular response to DNA damage. Several DDR factors are known to associate constitutively with PML bodies, while others associate

only transiently, being specifically recruited to or released from bodies after damage (236). These include DNA damage sensing and transducing factors such as the MRN complex, ATM, ATR, TOPBP1 and CHK2 and multiple proteins involved in HR (RAD51, BLM, RPA, WRN, BRCA1) (234, 237, 238). The PML protein itself is a target of phosphorylation by ATM, ATR and CHK2, an event that is thought to regulate protein stability and nuclear body integrity in response to DNA damage (204, 240). One of the many theorized functions for PML bodies is as a cellular storage depot (292). In the context of DNA repair, bodies may play a temporally important role, sequestering or releasing factors as necessary following damage. Due to the large number of repair factors associated with bodies it is thought that DNA breaks occurring close to bodies may be repaired with increased efficiency, as PML nuclear bodies may be providing a favorable environment for DNA repair. However, repair within PML body-associated DNA has not been investigated. Additionally while the PML protein has been implicated in DNA repair, its specific role, as well as the contribution of individual PML isoforms, has not been extensively examined. To study the role of PML nuclear bodies in DNA repair, specifically HR, the levels of repair were compared between the two cell lines generated in this study containing the HR reporter integrated at Chr15 or the TAP1 locus (U2OS Chr15 HR 2 and U2OS TAP HR 6 cell lines). Additionally, a novel assay based on CRISPR/Cas9-mediated HR developed in our laboratory (259) was used to compare rates of HR between wild-type and PML-depleted cells. Furthermore, the effects of individual PML isoforms on both HR and NHEJ were investigated through transient overexpression in U2OS Chr15 HR 2, U2OS TAP HR 6, U2OS TAP NHEJ 4, wild-type U2OS and a PML-knockout cell line.

4.5.1 Association of a DNA break with PML nuclear bodies can impact its repair by HR

The TAP1 locus has been previously shown to be significantly associated with PML nuclear bodies (225). This was confirmed in this study by measuring TAP1 locus proximity to PML bodies by immuno-FISH. Importantly, when proximity of the Chr15 locus to bodies was examined, Chr15 was found to be significantly unassociated with

PML bodies, at a level higher than the known negative control locus, BCL2 (**Figure 3.6**). Analysis of I-SceI transfected U2OS TAP HR 6 cells revealed a significant decrease in GFP expression, and hence HR, in cells where the HR reporter was integrated at TAP1 compared to U2OS Chr15 HR 2 cells (**Figure 3.13A**). This effect was not due to differences in cell cycle distribution between these two cell lines (**Figure 3.13B**). This marks the first time the effect of DSB location relative to PML nuclear bodies on DNA repair efficiency has been examined. As a variety of repair factors are known to be located constitutively or transiently with PML bodies, this is somewhat of a surprising finding. If this apparent decrease in HR is really due to proximity of the break to PML bodies, an important experiment would be to physically sequester the HR reporter in U2OS Chr15 HR 2 cells to PML bodies. This can be done using the adjacent LacO array in a similar manner to that described in section 3.2. Briefly, expression of a known PML nuclear body component protein such as SP100 (292), fused to LacI, would result in relocalization of the LacO array and adjacent HR reporter in Chr15 to PML bodies. Levels of HR could then be compared in cells expressing SP100, SP100-LacI or LacI alone followed by I-SceI DSB induction. This will be an important future experiment to confirm the observations of this study and to determine if PML nuclear bodies are somehow creating local environments that are repressive to HR.

4.5.2 HR is dependent on the presence of PML/PML nuclear bodies

To determine if HR is affected when PML nuclear bodies are completely absent, a CRISPR-based assay was used to compare levels of HR between wild-type and PML knockout (ΔPML) U2OS cells (demonstration of PML knockout is found in **Figure 3.15A**, bottom panel, left). A modest but significant decrease in HR was observed in ΔPML cells relative to U2OS wild-type cells (10.5% in wild-type and 8.4% in ΔPML cells) (**Figure 3.14B**), which was not attributed to differences in cell cycle distributions between these two cell lines (**Figure 3.14C**). This is in relative agreement with what was observed in two previous studies (243, 244). Both studies reported a drastic inhibition of HR upon PML knockdown. However, based on the observations in this study the effect of PML depletion on HR may be subtler than what has been previously reported (245,

246). For instance, Biochuk *et al*, 2011 (245) transiently knocked down PML and followed HR through a similar I-SceI-based HR reporter assay. They reported a decrease in GFP-positive cells, from 3.82% to 0.29%, after PML knockdown as measured by flow cytometry (245). However, they did not correct for transfection efficiency in these experiments, which may have affected their error calculations and thus the significance of their results. Yeung *et al*, 2012 (246) used a similar I-SceI-based HR reporter assay with the exception that reconstitution of a puromycin-resistance gene rather than a fluorescent gene was being measured. Puromycin-resistant cellular colony formation following I-SceI DSB induction then served as an indication of HR, with shRNA-mediated PML knockdown resulting in 3-fold or 21-fold reduction in HR events (depending on the shRNA used) (246). This method is very low throughput and can be biased by clonal expansion in tissue culture, which may lead to amplification of HR events scored in the assay. Depletion of PML does indeed impact HR repair efficiency; however, the data presented in this study suggest this decline may not be to the extent previously described. Based on the data presented here, closer association of a DNA DSB with PML nuclear bodies appears to negatively influence HR, yet ultimately PML or PML nuclear bodies are required in at least some capacity for DNA repair by HR.

4.5.3 PML isoforms are inhibitory to both HR and NHEJ

Although the PML protein has been implicated in DNA repair (205, 242), the contribution of each individual PML isoform has not been investigated. The effect of individually overexpressing each of the six nuclear-located PML isoforms on HR was examined in wild-type U2OS, ΔPML, U2OS Chr15 HR 2 and U2OS TAP HR 6 cells. Transient overexpression of PML isoforms induced formation of bodies that are altered in size and number, and an overall repression of HR, but did not significantly affect cell cycle progress (**Figures 3.15 and 3.16**). This is in agreement with Yeung *et al*, 2012 (246) who overexpressed PML isoforms IV and VI only, finding that both lead to a reduction in HR. The most notable decrease in this study was observed upon overexpression of PMLI, II and IV, an effect that was consistent across wild-type, ΔPML and U2OS Chr15 HR 2 cell lines. It is interesting to note that the isoforms whose

overexpression results in a drastic increase in PML body number: PMLI and IV, and to a lesser extent PMLII (**Figures 3.15A and 3.16A**), resulted in the highest HR inhibition. Based on the findings that HR was decreased at a locus significantly associated with PML nuclear bodies, an increase in PML body number could therefore lead to an increased likelihood of a DSB occurring in proximity to a body, negatively impacting its repair. Along these lines, it is intriguing that PML isoform overexpression (with the exception of PMLI) in TAP HR 6 cells did not result in a significant change in HR levels. This begs the question as to whether the pre-existing proximity of the DSB to PML bodies in these cells precludes additional inhibitory effects of PML overexpression on HR.

To gain a more complete understanding of the role of PML in DNA repair, the effect of PML on NHEJ was examined. Yeung *et al,* 2012 suggested that PML does not play a role in NHEJ, as only a modest increase in NHEJ was observed following PML knockdown (246). That finding was confirmed in this study, as NHEJ reporter assays in ΔPML cells resulted in a slight increase in percentage of GFP-expressing cells compared to wild-type U2OS cells. However, I decided to further extend these studies by investigating the role of individual PML isoforms on NHEJ in U2OS, ΔPML and U2OS TAP NHEJ 4 cells. Due to the apparent inhibitory role of PML isoforms on HR, one would expect a compensatory increase in NHEJ. Surprisingly, however, this was not what was observed. NHEJ levels were decreased in all three cell lines in a similar fashion, with the greatest inhibitory effect being due to PML isoforms II and IV (**Figures 3.17,** and **3.18**), the same isoforms with the greatest impact on HR when overexpressed.

The exact role of PML and PML nuclear bodies on DNA repair is not fully understood. Previous studies have focused on primarily linking PML/PML bodies specifically to HR, with conflicting reports as to the exact involvement of PML. Biochuk *et al*, 2011 (245) demonstrated a potential role of PML in early stages of HR. Knockdown of PML was found to cause a decrease in HR with subsequent loss of RPA, RAD51, and BRCA1 in DNA repair foci, suggesting that PML is required for DNA break processing (245). However, Yeung *et al*, 2012 (246) also found PML depletion to be inhibitory to HR, yet found no effect on RAD51 foci formation and demonstrated a

normal induction of γ-H2AX, indicating PML involvement at later steps in the HR pathway (246).

In my studies, I have demonstrated that PML and/or PML nuclear bodies are playing a role not only in HR but also NHEJ. Due to the fact that PML overexpression has been found to be inhibitory to both repair pathways, it is likely that PML is playing a role at a very early stage in repair, possibly through sequestration and/or inactivation of damage-sensing proteins. Important future work will be to investigate through immunofluorescence whether PML overexpression leads to increased sequestration of early DDR factors such as MRE11 or NBS1 within PML bodies. Moreover, PML may have a hitherto unexplored association with NHEJ factors. Experiments, similar to those described in section 3.1, could be used to examine the effect of PML overexpression on Ku80 recruitment or retention to laser tracks of DNA damage.

An important caveat of these experiments is that U2OS cells are alternative lengthening of telomeres (ALT)-positive. ALT is a mechanism that enables cancerous cells to become immortalized by circumventing the process that leads to telomere shortening at every cell division (293). The molecular mechanism of ALT is not fully understood, but in a portion (5-10%) of ALT-positive cells, PML nuclear bodies associate with telomeres, forming what are called ALT-associated PML nuclear bodies (APBs) (294, 295). These bodies are composed of regular PML nuclear body components such as PML, SP100 and SUMO, but also contain a significantly higher proportion of DDR factors such as γ-H2AX, BLM, RPA, RAD51, BRCA1 and the MRN complex (293, 296-299), presumably aiding in regulating recombination at telomeres. Thus the observations in this study of decreased HR upon PML knockout or isoform overexpression may be due in some capacity to the effects attributed to the ALT pathway and APBs. It will be important to repeat DNA repair assays with PML knockdown or overexpression in non-ALT cells such as normal human diploid fibroblasts.

Overall in this study, the role of PML and PML nuclear bodies in DNA repair has been investigated in multiple ways. Repair was studied in the context of PML knockout, PML isoform overexpression, as well as DSB-PML body proximity. PML depletion was found to be inhibitory to HR but not NHEJ, while PML isoform overexpression was found to be repressive to both pathways. Additionally, decreased HR repair was observed

at a DNA break located within chromatin significantly associated with PML bodies. Investigating the role of PML can be complicated. PML nuclear bodies are complex subnuclear domains that are associated with a large number of seemingly unrelated proteins, spanning a broad functional spectrum. It can be difficult to separate the activities attributed to the PML protein with those associated with PML nuclear bodies, as the formation and function of PML bodies is greatly impacted when the intracellular levels of PML protein are altered through depletion or overexpression (222). Even when PML is knocked out and then reintroduced as a single isoform, *de novo* PML bodies are formed. It is clear through this study that PML and PML nuclear bodies have a complex relationship with both DSB repair pathways, a relationship that requires further investigation.

4.6 Concluding remarks

Despite some recent advances, we still know very little about how nuclear structure affects DNA repair in mammalian cells. Using advanced microscopy techniques and a combination of genetic engineering systems, I examined the role of polymerized nuclear actin, the nuclear lamina and PML nuclear bodies in DNA repair.

First I investigated the role of the important structural protein polymeric nuclear actin on DNA repair. I found that when actin polymerization was disrupted, the retention of the key NHEJ factor Ku80 to DNA damage sites was impaired, which led to a corresponding decrease in NHEJ. I also examined DNA DSB repair efficiency at the nuclear lamina in relation to chromatin ultrastructure using electron microscopy. These results contributed to the findings that the DDR, and specifically HR, is delayed at the nuclear periphery due to the dense heterochromatin associated with that compartment.

I also examined the role of PML isoforms and nuclear bodies in DNA DSB repair. Using genome engineering, I created cell lines containing a single copy of an HR or NHEJ DNA DSB reporter integrated at a chromosomal locus significantly associated with PML nuclear bodies (TAP1) or at a locus unassociated with bodies (Chr15). In addition to the DNA repair reporter, these cell lines contain an adjacent array of Lac repressor binding sites that permits locus visualization and provides a manner for targeted

locus relocalization upon expression of the Lac repressor fused to nuclear domain structural proteins. These cell lines are valuable and versatile tools for studying DSB repair in a biologically relevant context. Using these cell lines, I determined that HR is significantly decreased at the PML nuclear body-associated TAP1 locus compared to Chr15. Additionally, using these cell lines along with wild-type U2OS and a U2OS PML knockout cell line, I demonstrated that PML isoform overexpression, notably that of PML I, II and IV, leads to significant inhibition of DNA DSB repair by HR and, for the first time, NHEJ. These data, and recent studies in the literature, suggest an early role for PML in DNA repair.

Disruption of nuclear domains such as the nuclear lamina, or PML nuclear bodies, as well as depletion of structural protein components of the nucleus such as polymeric nuclear actin, can lead to impaired DNA repair and increased genomic instability. Overall, my findings enable a further understanding of how nuclear architecture and organization contribute to DNA repair, and as such, to the maintenance of genomic integrity.

REFERENCES

1. Lindahl, T. (1993) Instability and decay of the primary structure of DNA. *Nature* **362**, 709-715

2. Mehta, A., and Haber, J.E. (2014) Sources of DNA double-strand breaks and models of recombinational DNA repair. *Cold Spring Harb Perspect Biol* **6**, a016428

3. De Bont, R., and van Larebeke. (2004) Endogenous DNA damage in humans: a review of quantitative data. *Mutagenesis* **19**, 169-185

4. Hoeijmakers, J.H. (2009) DNA damage, aging, and cancer. *N Engl J Med* **361**, 1475-1485

5. Malu, S., Malshetty, V., Francis, D., and Cortes, P. (2012) Role of non-homologous end joining in V(D)J recombination. *Immunol Res* **54**, 233-246

6. Murakami, H., and Keeney, S. (2008) Regulating the formaton of DNA double-strand breaks in meiosis. *Genes Dev* **22**, 286-292

7. Wyman, C., and Kanaar, R. (2006) DNA double-strand break repair: all's well that ends well. *Annu Rev Genet* **40**, 363-383

8. Soulas-Sprauel, P., Le Guyader, G., Rivera-Munoz. P., Abramowski, V., Olivier-Martin, C., Goujet-Zalc, C., Charneau, P., and de Villartay, J-P. (2007) Role for DNA repair factor XRCC4 in immunoglobulin class switch recombination. *JEM* **204**, 1717-1727

9. Woodbine, L., Gennery, A.R., and Jeggo, P.A. (2014) The clinical impact of deficiency in DNA non-homologous end-joining. *DNA Repair (Amst)* **16**, 84-96

10. Davis, A.J., and Chen, D.J. (2013) DNA double strand break repair via non homologous end joining. *Transl Cancer Res* **2**, 130-143

11. Mao, Z., Bozzella, M., Seluanov, A., and Gorbunova, V. (2008) DNA repair by nonhomologous end joining and homologous recombination during cell cycle in human cells. *Cell Cycle* **7**, 2902-2906

12. Mari, P.O., Florea, B.I, Persengiev, S.P., Verkaik, N.S., Bruggenwirth, H.T., Modesti, M., Giglia-Mari, G., Bezstarosti, K., Demmers, J.A., Luider, T.M., Houtsmuller, A.B., and van Gent, D.C. (2006) Dynamic assembly of end-joining complexes requires interaction between Ku70/80 and XRCC4. *Proc Natl Acad Sci USA* **103**, 18597-18602

13. Andrin, C., McDonald, D., Attwood, K.M., Rodrigue, A., Ghosh, S., Mirzayans, R., Masson, J.Y., Dellaire, G., and Hendzel, M.J. (2012). A requirement for polymerized actin in DNA double-strand break repair. *Nucleus* **3**, 384-395

14. Mimori, T., Hardin, J.A., and Steitz, J.A. (1986) Characterization of the DNA-binding protein antigen Ku recognized by autoantibodies form patients with rheumatic disorders. *J Biol Chem* **261**, 2274-2278

15. Blier, P.R., Griffith, A.J., Craft, J., and Hardin, J.A. (1993) Measurement of affinity for ends and demonstration of binding to nicks. *J Biol Chem* **268**, 7594-7601

16. Paillard, S., and Strauss, F. (1991) Analysis of the mechanism of interaction of simian Ku protein with DNA. *Nucleic Acids Res* **19**, 5619-5624

17. Walker, J.R., Corpina, R.A., and Goldberg, J. (2001) Structure of the Ku heterodimer bound to DNA and its implications for double-strand break repair. *Nature* **412**, 607-614

18. Uematsu, N., Weterings, E., Yano, K., Morotomi-Yano, K., Jakob, B., Taucher-Scholz, G., Mari, P.O., van Gent, D.C., Chen, B.P., and Chen, D.J. (2007) Autophosphorylation of DNA-PKCS regulates its dynamics at DNA double-strand breaks. *J Cell Biol* **177**, 219-229

19. Costantini, S., Woodbine, L., Andreoli, L., Jeggo, P.A., and Vindigni, A. (2007) Interaction of the Ku heterodimer with the DNA ligase IV/Xrcc4 complex and its regulation by DNA-PK. *DNA Repair (Amst)* **6**, 712-722

20. Nick McElhinny, S.A., Snowden, C.M., McCarville, J., and Ramsden, D.A. (2000) Ku recruits the XRCC4-ligase IV complex to DNA ends. *Mol Cell Biol* **20**, 2996-3003

21. Yano, K., Morotomi-Yano, K., Wang, S-Y., Uematsu, N., Lee, K-J., Asaithamby, A., Weterings, E., and Chen, D.J. (2008) Ku recruits XLF to DNA double-strand breaks. *EMBO Rep* **9**, 91-96

22. Grundy, G.J., Rulten, S.L., Zeng, Z., Arribas-Bosacoma, R., Iles, N., Manley, K., Oliver, A., and Caldecott, K.W. (2013) APLF promotes the assembly and activity of non-homologous end joining protein complexes. *EMBO J* **32**, 112-125

23. Kanno, S., Kuzuoka, H., Sasao, S., Hong, Z., Lan, L., Nakajima, S., and Yasui, A. (2007) A novel human AP endonuclease with conserved zinc-finger-like motifs involved in DNA strand break responses. *EMBO J* **26**, 2094-2103

24. Macrae, C.J., McCulloch, R.D., Ylanko, J., Durocher, D., and Koch, C.A. (2008) APLF (C2orf13) facilitates nonhomologous end-joining and undergoes ATM-dependent hyperphosphorylation following ionizing radiation. *DNA repair (Amst)* **7**, 292-302

25. Ochi, T., Blackford, A.N., Coates, J., Jhujh, S., Mehmood, S., Tamura, N., Travers, J, Wu, Q., Draviam, V.M., Robinson, C.V., Blundell, T.L., and Jackson, S.P. (2015) PAXX, a paralog of XRCC4 and XLF, interacts with Ku to promote DNA double-strand break repair. *Science* **347**, 185-188

26. Xing, M., Yang, M., Huo, W., Feng, F., Wei, L., Jiang, W., Ning, S., Yan, Z., Li, W., Wang, Q., Hou, M., Dong, C., Guo, R., Gao, G., Ji, J., Zha, S., Lan, L., Liang, H., and Xu, D. (2015) Interactome analysis identifies a new paralogue of XRCC4 in non-homologous end joining DNA repair pathway. *Nat Commun* **6**:6233.

27. Meek, K., Dang, V., and Lees-Miller, S.P. (2008) DNA-PK: the means to justify the ends? *Adv Immunol* **99**, 33-58

28. Yoo, S., and Dynan, W.S. (1999) Geometry of a complex formed by double strand break repair proteins at a single DNA end: recruitment of DNA-PKcs induces inward translocation of Ku protein. *Nucleic Acids Res*. **27**, 4679-4686

29. Williams, D.R., Lee, K.J., Shi, J., Chen, D.J., and Stewart, P.L. (2008) Cryoelectron microscopy structure of the DNA-dependent protein kinase catalytic subunit (DNA-PKcs) at subnanometer resolution reveals α-helices and insight into DNA binding. *Structure* **16**, 468-477

30. DeFazio, L.G., Stansel, R.A., Griffith, J.D., and Chu, G. (2002) Synapsis of DNA ends by DNA-dependent protein kinase. *EMBO J* **21**, 3192-3200

31. Ma, Y., Pannicke, U., Schwarz, K., and Lieber, M.R. (2002) Hairpin opening and overhang processing by an Artemis/DNA-dependent protein kinase complex in nonhomologous end joining and V(D)J recombination. *Cell* **108**, 781-794

32. Povirk, L.F., Zhou, T., Zhou, R., Cowan, M.J., and Yannone, S.M. (2007) Processing of 3'-phosphoglycolate-terminated DNA double strand breaks by Artemis nuclease. *J Biol Chem* **282**, 3547-3558

33. Perry, J.J., Yannone, S.M., Holden, L.G., Hitomi, C., Asaithamby, A., Han, S., Cooper, P.K., Chen, D.J., and Tainer, J.A. (2006) WRN exonuclease structure and molecular mechanism imply an editing role in DNA end processing. *Nat Struct Mol Biol* **13**, 414-422

34. Li, S., Kanno, S., Watanabe, R., Ogiwara, H., Kohno, T., Watanabe, G., Yasui, A., and Lieber, M.R. (2011) Polynucleotide kinase and aprataxin-like forkhead-associated protein (PALF) acts as both a single-stranded DNA endonuclease and a single-stranded DNA 3' exonuclease and can participate in DNA end joining in a biochemical system. *J Biol Chem* **286**, 36368-36377

35. Bernstein, N.K., Williams, R.S., Rakovszky, M.L., Cui, D., Green, R., Karimi-Busheri, F., Mani, R.S., Galicia, S., Koch, C.A., Cass, C.E., Durocher, D., Weinfield, M., and Glover, J.N. (2005) The molecular architecture of the mammalian DNA repair enzyme, polynucleotide kinase. *Mol Cell* **17**, 657-670

36. Ahel, I., Rass, U., El-Khamisy, S.F., Katyal, S., Clements, P.M., McKinnon, P.J., Caldecott, K.W., and West, S.C. (2006) The neurodegenerative disease protein aprataxin resolves abortive DNA ligation intermediates. *Nature* **443**, 713-716

37. Nick McElhinny, S.A., Havener, J.M., Garcia-Diaz, M., Juarez, R., Bebenek, K,. Kee, B.L., Blanco, L., Kunkel, T.A., and Ramsden, D.A. (2005) A gradient of template dependence defines distinct biological roles for family X polymerases in nonhomologous end joining. *Mol Cell* **19**, 357-366

38. Grawunder, U., Wilm, M., Wu, X., Kulesza, P., Wilson, T.E., Mann, M., and Lieber, M.R. (1997) Activity of DNA ligase IV stimulated by complex formation with XRCC4 protein in mammalian cells. *Nature* **388**, 492-495

39. Lu, H., Pannicke, U., Schwarz, K., and Lieber, M.R. (2007) Length-dependent binding of human XLF to DNA and stimulation of XRCC4.DNA ligase IV activity. *J Biol Chem* **282**, 11155-11162

40. Yano, K., and Chen, D.J. (2008) Live cell imaging of XLF and XRCC4 reveals a novel view of protein assembly in the non-homologous end-joining pathway. *Cell Cycle* **7**, 1321-1325

41. Rulten, S.L., Fisher, A.E., Robert, I., Zuma, M.C., Rouleau, M., Ju, L., Poirier, G., Reina-San-Martin, B., and Caldecott, K.W. (2011) PARP-3 and APLF function together to accelerate nonhomologous end-joining. *Mol Cell* **41**, 33-45

42. Reynolds, P., Anderson, J.A., Harper, J.V., Hill, M.A., Botchway, S.W., Parker, A.W., and O'Neill, P. (2012) They dynamics of Ku70/80 and DNA-PKcs at DSBs induced by ionizing radiation is dependent on the complexity of damage. *Nucleic Acids Res* **40**, 10821-10831

43. Jasin, M., and Rothstein, R. (2013) Repair of strand breaks by homologous recombination. *Cold Spring Harb Perspect Biol* **5**, a012740

44. Lam, I., and Keeney, S. (2014) Mechanism and regulation of meiotic recombination initiation. *Cold Spring Harb Perspect Biol* **7**, a016634

45. Helleday, T. (2010) Homologous recombination in cancer development, treatment and development of drug resistance. *Carcinogenesis* **31**, 955-960

46. Karanam, K., Kafri, R., Loewer, A., and Lahav, G. (2012) Quantitative live cell imaging reveals a gradual shift between DNA repair mechanisms and a maximal use of HR in mid S phase. *Mol Cell* **47**, 320-329

47. de Jager, M., van Noort, J., van Gent, D.C., and Kanaar, R. (2001) Human Rad50/Mre11 is a flexible complex that can tether DNA ends. *Mol Cell* **8**, 1129-1135

48. Williams, R.S., Dodson, G.E., Limbo, O., Yamada, Y., Williams, J.S, Guenther, G., Classen, S., Glover, J.N., Iwasaki, H., Russell, P., and Tainer, J.A. (2009) Nbs1 flexibility tethers Ctp1 and Mre11-Rad50 to coordinate DNA double-strand break processing and repair. *Cell* **139**, 87-99

49. Kim, J.S., Krasieva, T.B., Kurumizaka, H., Chen, D.J., and Taylor, A.M. (2005) Independent and sequential recruitment of NHEJ and HR factors to DNA damage sites in mammalian cells. *J Cell Biol* **170**, 341-347

50. Sartori, A.A., Lukas, C., Coates, J., Mistrik, M., Fu, S., Bartek, J., Baer, R., Lukas, J., and Jackson, S.P. (2007) Human CtIP promotes DNA end resection. *Nature* **450**, 509-514

51. Zhong, Z., Chen, C.F., Li, S., Chen, Y., Wang, C.C., Xiao, J., Chen, P.L., Sharp, Z.D., and Lee, W.H. (1999) Association of BRCA1 with the hRad50-hMre11-p95 complex and the DNA damage response. *Science* **285**, 747-750

52. Yu, X., Wu, L.C., Bowcock, A.M., Aronheim, A., and Baer, R. (1998) The C-terminal (BRCT) domains of BRCA1 interact in vivo with CtIP, a protein implicated in the CtBP pathway of transcriptional repression. *J Biol Chem* **273**, 25388-25392

53. Cruz-Garcia, A., Lopez-Saavedra, A., and Huertas, P. (2014) BRCA1 accelerates CtIP-mediated DNA-end resection. *Cell Rep* **9**, 451-459

54. Nimokar, A.V., Genschel, J., Kinoshita, E., Polaczek, P., Campbell, JL., Wyman, C., Modrich, P., and Kowalczykowski, S.C. (2011) BLM-DNA2-RPA-MRN and EXO1-BLM-RPA-MRN constitute two DNA end resection machineries for human DNA break repair. *Genes Dev* **25**, 350-362

55. Zhang, Y., Hefferin, M.L., Chen, L., Shim, E.Y., Tseng, H.M., Kwon, Y., Sung, P., Lee, S.E., and Tomkinson, A.E. (2007) Role of Dnl4-Lif1 in nonhomologous end-joining repair complex assembly and suppression of homologous recombination. *Nat Struct Mol Biol* **14**, 639-646

56. Pierce, A.J., Hu, P., Han, M., Ellis, N., and Jasin, M. (2001) Ku DNA end-binding protein modulates homologous repair of double-strand breaks in mammalian cells. *Genes Dev* **15**, 3237-3242

57. Wold, M.S. (1997) Replication protein A: a heterotrimeric, single-stranded DNA-binding protein required for eukaryotic DNA metabolism. *Annu Rev Biochem* **66**, 61-92

58. Eggler, A.L., Inman, R.B., and Cox, M.M. (2002) The Rad51-dependent pairing of long DNA substrates is stabilized by replication protein A. *J Biol Chem* **277**, 39280-39288

59. Sugiyama, T., Zaitseva, E.M., and Kowalczykowski, S.C. (1997) A single-stranded DNA-binding protein is needed for efficient presynaptic complex formation by the *Saccharomyces cerevisiae* Rad51 protein. *J Biol Chem* **272**, 7940-7945

60. Conway, A.B., Lynch, T.W., Zhang, Y., Fortin, G.S., Fung, C.W., Symingotn, L.S., and Rice, P.A. (2004) Crystal structure of a Rad51 filament. *Nat Struct Mol Biol* **11**, 791-796

61. Zaitseva, E.M., Zaitsev, E.N., and Kowalczykowski, S.C. (1999) The binding properties of *Saccharomyces cerevisiae* Rad51 protein. *J Biol Chem* **274**, 2907-2915

62. Yang, H.J., Li, Q.B., Fan, J., Holloman, W.K., and Pavletich, N.P. (2005) The BRCA2 homologue Brh2 nucleates RAD51 filament formation at a dsDNA-ssDNA junction. *Nature* **433**, 653-657

63. San Filippo, J., Chi, P., Sehorn, M.G., Etchin, J., Krejci, L., and Sung, P. (2006) Recombination mediator and Rad51 targeting activities of a human BRCA2 polypeptide. *J Biol Chem* **281**, 11649-11657

64. Yonetani, Y., Hochegger, H., Sonoda, E., Shinya, S., Yoshikawa, H., Takeda, S., and Yamazoe, M. (2005) Differential and collaborative actions of Rad51 paralog proteins in cellular response to DNA damage. *Nucleic Acids Res* **33**, 4544-4552

65. Chen, J., Morrical, M.D., Donigan, K.A., Weidhaas, J.B, Sweasy, J.B., Averill, A.M., Tomczak, J.A., and Morrical, S.W. (2015) Tumor-associated mutations in a conserved structural motif alter physical and biochemical properites of human RAD51 recombinase. *Nucleic Acids Res* **43**, 1098-1111

66. Yu, X., Jacobs, S.A., West, S.C., Ogawa, T., and Egelman, E.H. (2001) Domain structure and dynamics in the helical filaments formed by RecA and Rad51 on DNA. *Proc Natl Acad Sci USA* **98**, 8419-8425

67. Gupta, R.C., Fotla-Stogniew, E., O'Malley, S., Takahashi, M., and Radding, C.M. (1999) Rapid exchange of A:T base pairs is essential for recognition of DNA homology by human Rad51 recombination protein. *Mol Cell* **4**, 705-714

68. Renkawitz, J., Ldemann, C.A., Kalocsay, M., and Jentsch, S. (2013) Monitoring homology search during DNA double-strand break repair in vivo. *Mol Cell* **50**, 261-272

69. Solinger, J.A., Lutz, G., Sugiyama, T., Kowalczykowski, S.C., and Heyer, W.D. (2001) Rad54 protein stimulates heteroduplex DNA formation in the synaptic phase of DNA strand exchange via specific interactions with the presynaptic Rad51 nucleoprotein filament. *J Mol Biol* **307**, 1207-1221

70. Mazin, O.M., and Mazin, A.W. (2004) Human Rad54 protein stimulates DNA strand exchange activity of hRad51 protein in the presence of Ca2+. *J Biol Chem* **279**, 52041-52051

71. Alexeev, A., Mazin, A., and Kowalczykowski, S.C. (2003) Rad54 protein possesses chromatin-remodeling activity stimulated by a Rad51-ssDNA nucleoprotein filament. *Nature Struct Biol* **10**, 182-186

72. Plank, J.L., Wu, J.H., and Hsieh, T.S. (2006) Topoisomerase III alpha and Bloom's helicase can resolve a mobile double Holliday junction substrate through convergent branch migration. *Proc Natl Acad Sci USA* **103**, 11118-11123

73. Li, X., and Heyer, W.D. (2008) Homologous recombination in DNA repair and DNA damage tolerance. *Cell Research* **18**, 99-113

74. Fekairi, S., Scaglione, S., Chahwan, C., Taylor, E.R., Tissier, A., Coulon, S., Dong, M.Q., Ruse, C., Yates, J.R., Russell, R., Fuchs, R.P., McGowan, C.H., and Gaillard, P.H. (2009) Human SLX4 is a Holliday junction resolvase subunit that binds multiple DNA repair/recombination endonucleases. *Cell* **138**, 78-89

75. Ip, S.C.Y., Rass, U., Blanco, M.G., Flynn, H.R., Skehel, J.M., and West, C. (2008) Identificaiton of Holliday junction resolvases from humans and yeast. *Nature* **456**, 357-361

76. Munoz, I.P., Hain, K., Declais, A.C., Gardiner, M., Toh, G.W., Sanchez-Pulido, L., Heukmann, J.M., Toth, R., Macartney, T., Eppink, B., Kanaar, R., Ponting, C.P., Lilley, D.M., and Rouse, J. (2009) Coordination of structure-specific nucleases by human SLX4/BTBD12 is required for DNA repair *Mol Cell* **35**, 116-127

77. Van Brabant, A.J., Ye, T., Sanz, M., German, J.L., Ellis, N.A., and Holloman, W.K. (2000) Binding and melting of D-loops by the Bloom syndrome helicase. *Biochemistry* **39**, 14617-14625

78. Orren, D.K., Theodore, S., and Machwe, A. (2002) The Werner syndrome helicase/exonuclease (WRN) disrupts and degrades D-loops *in vitro*. *Biochemistry* **41**, 13483-13488

79. Malkova, A., and Grzegorz, I. (2013) Break-induced replication: functions and molecular mechanism. *Curr Opin Genet Dev* **23**, 271-279

80. Huang, L.C., Clarkin, K.C., and Wahl, G.M. (1996) Sensitivity and selectivity of the DNA damage sensor responsible for activating p53-dependent G1 arrest. *Proc Natl Acad Sci USA* **93**, 4827-4832

81. Pinder, J.B., Attwood, K.M., and Dellaire, G. (2013) Reading, writing, and repair: the role of ubiquitin and the ubiquitin-like proteins in DNA damage signaling and repair. *Front Genet* **4**:45

82. Bekker-Jensen, S., and Mailand, N. (2010) Assembly and function of DNA double-strand break repair foci in mammalian cells. *DNA Repair (Amst)* **9**, 1219-1228

83. Polo, S.E., and Jackson, S.P. (2011) Dynamics of DNA damage response proteins at DNA breaks: a focus on protein modifications. *Genes Dev* **25**, 409-433

84. Rogakou, E.P., Pilch, D.R., Orr, A.H., Ivanova, V.S., and Bonner, W.M. (1998) DNA double-stranded breaks induce histone H2AX phosphorylation on serine 139. *J Biol Chem* **273**, 5858-5868

85. Paull, T.T., Rogakou, E.P. Yamazaki, V., Kirchgessner, C.U., Gellert, M., and Bonner, W.M. (2000) A critical role for histone H2AX in recruitment of repair factors to nuclear foci after DNA damage. *Curr Biol* **10**, 886-895

86. Ward, I.M., and Chen, J. (2001) Histone H2AX is phosphorylated in an ATR-dependent manner in response to replicational stress. *J Biol Chem* **276**, 47759-47762

87. Stiff, T., O'Driscoll, M., Rief, N., Iwabuchi, K., Lobrich, M., and Jeggo, P.A. (2004) ATM and DNA-PK function redundantly to phosphorylate H2AX after exposure to ionizing radiation. *Cancer Res* **64**, 2390-2396

88. Lukas, C., Melander, F., Stucki, M., Falck, J., Bekker-Jensen, S., Goldberg, M., Lerenthal, Y., Jackson, S.P., Bartek, J., and Lukas, J. (2004) Mdc1 couples DNA double-strand break recognition by Nbs1 with its H2AX-dependent chromatin retention. *EMBO J* **23**, 2674-2683

89. Stucki, M., Clapperton, J.A., Mohammad, D., Yaffe, M.B., Smerdon, S.J., and Jackson, S.P. (2005) MDC1 directly binds phosphorylated H2AX to regulate cellular responses to DNA double-strand breaks. *Cell* **123**, 1213-1226

90. Rogakou, E.P., Boon, C., Redon, C., and Bonner, W.M. (1999) Megabase chromatin domains involved in DNA double-strand breaks *in vivo*. *J Cell Biol* **146**, 905-916

91. Meier, A., Fiegler, H., Munoz, P., Ellisa, P., Rigler, D., Langford, C., Blasco, M.A., Carter, N., and Jackson, S.P. (2007) Spreading of mammalian DNA-damage response factors studied by ChIP-chip at damaged telomeres. *EMBO J* **26**, 2707-2718

92. Iacovoni, J.S., Caron, P., Lassadi, I., Nicolas, E., Massip, L., Trouche, D., and Legube, G. (2010) High-resolution profiling of γ-H2AX around DNA double strand breaks in the mammalian genome. *EMBO J* **29**, 1446-1457

93. Uziel, T., Lerenthal, Y., Moyal, L., Andegeko, Y., Mittelman, L., and Shiloh, Y. (2003) Requirement of the MRN complex for ATM activation by DNA damage. *EMBO J* **22**, 5612-5621

94. Lee, J.H., and Paull, T.T. (2005) ATM activation by DNA double-strand breaks through the Mre11-Rad50-Nbs1 complex. *Science* **308**, 551-554

95. Paull, T.T., Rogakou, E.P., Yamazaki, V., Kirchgessner, C.U., Gellert, M., and Bonner, W.M. (2000) A critical role for histone H2AX in recruitment of repair factors to nuclear foci after DNA damage. *Curr Biol* **10**, 886-895

96. Nakamura, A.J., Rao, V.A., Pommier, Y., and Bonner, W.M. (2010) The complexity of phosphorylated H2AX foci formation and DNA repair assembly at DNA double-strand breaks. *Cell Cycle* **9**, 389-397

97. Downs, J.A., Allard, S., Jobin-Robitaille, O., Javaheri, A., Auger, A., Bouchard, N., Kron, S.J., Jackson, S.P., and Cote, J. (2004) Binding of chromatin-modifying activities to phosphorylated histone H2A at DNA damage sites. *Mol Cell* **16**, 979-990

98. Morrison, A.J., Highland, J., Krogan, N.J., Arbel-Eden, A., Greebblatt, J.F., Haber, J.E., and Shen, X. (2004) INO80 and γ-H2AX interaction links ATP-dependent chromatin remodeling to DNA damage repair. *Cell* **119**, 767-775

99. van Attikum, H., Fritsch, O., Hohn, B., and Gasser, S.M. (2004) Recruitment of the INO80 complex by H2A phosphorylation links ATP-dependent chromatin remodeling with DNA double-strand break repair. *Cell* **119**, 777-788

100. Bonilla, C.Y., Melo, J.A., and Toczyski, D.P. (2008). Colocalization of sensors is sufficient to activate the DNA damage checkpoint in the absence of damage. *Mol Cell* **30**, 267-276

101. Soutoglou. E., and Misteli, T. (2008) Activation of the cellular DNA damage response in the absence of DNA lesions. *Science* **320**, 1507-1510

102. Haince, J-F., McDonald, D., Rodrigue, A., Dery, U., Masson, J-Y., Hendzel, M.J., and Poirier, G.G. (2008) PARP1-dependent kinetics of recruitment of MRE11 and NBS1 proteins to multiple DNA damage sites. *J Biol Chem* **283**, 1197-1208

103. Matsuoka, S., Ballif, B.A., Smogorzeska, A., McDonald, E.R., Hurov, K.E., Luo, J., Bakalarski, C.E., Zhao, Z., Solimini, N., Lerenthal, Y., Shiloh, Y., Gygi, S.P., and Elledge, S.J. (2007) ATM and ATR substrate analysis reveals extensive protein networks responsive to DNA damage. *Science* **316**, 1160-1166

104. Kaidi, A., and Jackson, S.P. (2013) KAT5 tyrosine phosphorylation couples chromatin sensing to ATM signaling, *Nature* **498**, 70-74

105. Nam, E.A., and Cortez, D. (2011) ATR signaling: more than meeting at the fork. *Biochem J* **436**, 527-536

106. Cortez, D., Guntuku, S., Qin, J., and Elledge, S.J. (2001) ATR and ATRIP: partners in checkpoint signaling. *Science* **294**, 1713-1716

107. Zou, L., and Elledge, S.J. (2003) Sensing DNA damage through ATRIP recognition of RPA-ssDNA complexes. *Science* **300**, 1542-1548

108. Shiotani, B., and Zou, L. (2009) Single-stranded DNA orchestrates an ATM-to ATR switch at DNA breaks. *Mol Cell* **33**, 547-558

109. Spycher, C., Miller, E.S., Townsend, K., Pavic, L., Morrice, N.A., Janscak, P., Stewart, G.S., and Stucki, M. (2008) Constitutive phosphorylation of MDC1 physically links the MRE11-RAD50-NBS1 complex to damaged chromatin. J *Cell Biol* **181**, 227-240

110. Lou, Z., Minter-Dykhouse, K., Franco, S., Gostissa, M., Rivera, M.A., Celeste, A., Manis, J.P., van Deursen, J., Nussenzweig, A., Paull, T.T., Alt, F.W., and Chen, J. (2006) MDC1 maintians genomic stability by participating in the amplification of ATM-dependent DNA damage signals. *Mol Cell* **21**, 187-200

111. Mailand, N., Beker-Jensen, S., Faustrup, H., Melander, F., Bartek, J., Lukas, C., and Lukas, J. (2007) RNF8 ubiquitylates histones at DNA double-strand breaks and promotes assembly of repair proteins. *Cell* **131**, 887-900

112. Huen, M.S., Grant, R., Manke, I., Minn, K., Yu, X., Yaffe, M.B., and Chen, J. (2007) RNF8 transduces the DNA-damage signal via histone ubiquitylation and checkpoint protein assembly. *Cell* **131**, 901-914

113. Doil, C., Mailand, N., Bekker-Jensen, S., Menard, P., Larsen, D.H., Peperkok, R., Ellenberg, J., Panier, S., Durocher, D., Bartek, J., Lukas, J., and Lukas, C. (2009) RNF168 binds and amplifies ubiquitin conjugates on damaged chromosomes to allow accumulation of repair proteins. *Cell* **136**, 435-446

114. Stewart, G.S., Panier, S., Townsend, K., Al-Hakim, A.K., Kolas, N.K., Miller, E.S., Nakada, S., Ylanko, J., Olivarius, S., Mendez, M., Oldreive, C., Wildenhain, J., Tagliaferro, A., Pelletier, L., Taubenheim, N., Durandy, A., Byrd, P.J., Stankovic, T., Taylor, A.M., and Durocher, D. (2009) The RIDDLE syndrome protein mediates a ubiquitn-dependent signaling cascade at sites of DNA damage. *Cell* **136**, 420-434

115. Gatti, M., Pinato, S., Maspero, E., Soffientini, P., Polo, S., and Penengo, L. (2012) A novel ubiquitin mark at the N-terminal tail of histone H2As targeted by RNF168 ubiquitin ligase. *Cell Cycle* **11**, 2538-2544

116. Mattiroli, F., Vissers, J.H., van Dijk, W.J., Ikpa, P., Citterio, E., Vermeulen, W., Marteijn, J.A., and Sixma, T.K. (2012) RNF168 ubiquitinates K13-15 on H2A/H2AX to drive DNA damage signaling. *Cell* **150**, 1182-1195

117. Plans, V., Scheper, J., Soler, M., Loukili, N., Okano, Y., and Thomson, T.M. (2006) The RING finger protein RNF8 recruits UBC13 for lysine 63-based self polyubiquitylation. *J Cell Biochem* **97**, 572-582

118. Bekker-Jensen, S., Rendtlew Danielson, J., Fugger, K., Gromova, I., Nerstedt, A., Lukas, C., Bartek, J., Lukas, J., and Mailand, N. (2010) HERC2 coordinates ubiquitin-dependent assembly of DNA repair factors on damaged chromosomes. *Nat Cell Biol* **12**, 80-86

119. Kolas, N.K., Chapman, J.R., Nakada, S., Ylanko, J., Chahwan, R., Sweeney, F.D., Panier, S., Mendez, M., Wildenhain, J., Thomson, T.M., Pelletier, L., Jackson, S.P., and Durocher, D. (2007) Orchestration of the DNA-damage response by the RNF8 ubiquitin ligase. *Science* **318**, 1637-1640

120. Botuyan, M.V., Lee, J., Ward, I.M., Kim, J-E., Thompson, J.R., Chen, J., and Mer, G. (2006) Structural basis for the methylation state-specific recognition of histone H2-K20 by 53BP1 and Crb2 in DNA repair. *Cell* **127**, 1361-1373

121. Mallette, F.A., Mattiroli, F., Cui, G., Young, L.C., Hendzel, M.J., Mer, G., Sixma, T.K., and Richard, S. (2012) RNF8- and RNF168-dependent degradation of KDM4A/JMJD2A triggers 53BP1 recruitment to DNA damage sites. *EMBO J* **31**, 1865-1878

122. Zimmermann, M., and de Lange, T. (2014) 53BP1: pro choice in DNA repair. *Trends Cell Biol* **24**, 108-117

123. Escribano-Diaz, C., Orthwein, A., Fradet-Turcotte, A., Xing, M., Young, J.T.F., Tkac, J., Cook, M.A., Rosebrock, A.P., Munro, M., Canny, M.D., Xu, D., and Durocher, D. (2013) A cell cycle-dependent regulatory circuit composed of 53BP1-RIF1 and BRCA1-CtIP controls DNA repair pathway choice. *Mol Cell* **49**, 872-883

124. Bunting, S.F., Callen, E., Wong, N., Chen, H-T., Polato, F., Gunn, A., Bothmer, A., Feldhahn, N., Fernandez-Capetillo, O., Cao, L., Xu, X., Deng, C-X., Finkel, T., Nussenzweig, M., Stark, J.M., and Nussenzweig, A. (2010) 53BP1 inhibits homologous recombination in BRCA1-deficient cells by blocking resection of DNA breaks. *Cell* **141**, 243-254

125. Dimitrova, N., Chen, Y.C., Spector, D.L., and de Lange, T. (2008) 53BP1 promotes non-homologous end joining of telomeres by increasing chromatin mobility. *Nature* **456**, 524-528.

126. Wang, B, and Elledge, S.J. (2007) Ubc13/Rnf8 ubiquitin ligases control foci formation of the Rap80/Abraxas/Brca1/Brcc36 complex in response to DNA damage. *Proc Natl Acad Sci USA* **104**, 20759-20763

127. Galanty, Y., Beloserkovskaya, R., Coates, J., Polo, S., Miller, K.M., and Jackson, S.P. (2009) Mammalian SUMO E3-ligases PIAS1 and PIAS4 promote responses to DNA double-strand breaks. *Nature* **462**, 935-939

128. Morris, J.R. Boutell, C., Keppler, M., Densham, R., Weekes, D., Alamshah, A., Butler, L., Galanty, Y., Pangon, L., Kiuchi, T., Ng, T., and Solomon, E. (2009) The SUMO modification pathway is involved in the BRCA1 response to genotoxic stress. *Nature* **462**, 886-890

129. Shibata, A., and Jeggo, P.A. (2014) DNA double-strand break repair in a cellular context. *Clin Oncol (R Coll Radiol)* **26**, 243-249

130. Hochegger, H., Takeda, S., and Hunt, T. (2008) Cyclin-dependent kinases and cell cycle transitions: does one fit all? *Nat Rev Mol Cell Biol* **9**, 910-916

131. Matsuoka, S., Rotman, G., Ogawa, A., Shiloh, Y., Tamai, K., and Elledge, S.J. (2000) Ataxia telangiectasia-mutated phosphorylates Chk2 in vivo and in vitro. *Proc Natl Acad Sci USA* **97**, 10389-10394

132. Liu, Q., Guntuku, S., Cui, X-S., Matsuoka, S., Cortez, D., Tamai, K., Luo, G., Carattini-Rivera, S., DeMayo, F., Bradley, A., Donehower, L.A., and Elledge, S.J. (2000) Chk1 is an essential kinase that is regulated by Atr and required for the G2/M DNA damage checkpoint. *Genes Dev* **14**, 1448-1459

133. Zhao, H., and Piwnca-Worms, H. (2001) ATR-mediated checkpoint pathways regulate phosphorylation and activation of human Chk1. *Mol Cell Biol* **21**, 4129-4139

134. Liu, S., Bekker-Jensen, S., Mailand, N., Lukas, C., Bartek, C., Bartek, J., and Lukas, J. (2006) Claspin operates downstream of TopBP1 to direct ATR signaling towards Chk1 activation. *Mol Cell Biol* **26**, 6056-6064

135. Delacroix, S., Wagner, J.M., Kobayashi, M., Yamamoto, K., and Karnitz, L.M. (2007) The Rad9-Hus1-Rad1 (9-1-1) clamp activates checkpoint signaling via TopBP1. *Genes Dev* **21**, 1472-1477

136. Christiano Silva Chini, C., and Chen, J. (2003) Human claspin is required for replication checkpoint control. *J Biol Chem* **278**, 30057-30062

137. Smith, J., Tho, T.M., Xu, N., and Gillespie, D.A. (2010) The ATM-Chk2 and ATR-Chk1 pathways in DNA damage signaling and cancer. *Adv Cancer Res* **108**, 73-112

138. Luger, K., Dechassa, M.L., and Tremethick, D.J. (2012) New insights into nucleosome and chromatin structure: an ordered state or a disordered affair? *Nat Rev Mol Cell Biol* **13**, 436-447

139. Groth, A., Rocha, W., Verreault, A., and Almouzni, G. (2007) Chromatin challenges during DNA replication and repair. *Cell* **128**, 721-733

140. Li, B., Carey, M., and Workman, J.L. (2007) The role of chromatin during transcription. *Cell* **128**, 707-719

141. Price, B.D., and D'Andrea, A.D. (2013) Chromatin remodeling at DNA double strand breaks. *Cell* **152**, 1344-1354

142. Gelato, K.A., and Fischle, W. (2008) Role of histone modifications in defining chromatin structure and function. *Biol Chem* **389**, 353-363

143. Saha, A., Wittmeyer, J., and Cairns, B.R. (2006) Chromatin remodeling: the industrial revolution of DNA around histones. *Nat Rev Mol Cell Biol* **7**, 437-447

144. Ikura, T., Ogryzko, VV., Grigoriev, M., Groisman, R., Wang, J., Horkikoshi, M., Scully, R., Qin, J., and Nakatani, Y. (2000) Involvement of the TIP60 histone acetylase complex in DNA repair and apoptosis. *Cell* **102**, 463-473

145. Downs, J.A., Allard, S., Jobin-Robitaille, O., Javaheri, A., Auger, A., Bouchard, N., Kron, S.J., Jackson, S.P., and Cote, J. (2004) Binding of chromatin-modifying activities to phosphorylated histone H2A at DNA damage sites. *Mol Cell* **16**, 979-990

146. Murr, R., Loizou, J.I., Yang, Y.G., Cuenin, C., Li, H., Wang, Z.Q., and Herceg, Z. (2006) Histone acetylation by Trrap-Tip60 modulates loading of repair proteins and repair of DNA double-strand breaks. *Nat Cell Biol* **8**, 91-99

147. Doyon, Y., and Cote, J. (2004) The highly conserved and multifunctional NuA4 HAT complex. *Curr Opin Genet Dev* **14**, 147-154

148. Gorrini, C., Squatitro, M., Luise, C., Syed, N., Perna, D., Wark, L., Martinato, F., Sardella, D., Verrecchia, A., Bennet, S., Confalonierei, S., Cesaroni, M., Marchesi, F., Gasco, M., Scanziani, E., Capra, M., Mai, S., Nuciforo, P., Crook, T., Lough, J., and Amati, B. (2007) Tip60 is a haplo-insufficient tumor suppressor required for an oncogene-induced DNA damage response. *Nature* **448**, 1063-1067

149. Xu, Y., Sun, Y., Jian, X., Ayrapetov, M.K., Moskwa, P., Yang, S., Weinstock, D.M., and Price, B.D. (2010) The p400 ATPase regulates nucleosome stability and chromatin ubiquitination during DNA repair. *J Cell Biol* **191**, 31-43

150. Kusch, T., Florens, L., Macdonald, W.H., Swanson, S.K., Glaser, R.L., Yates, J.R., Abmayr, S.M., Washburn, M.P., and Work, J.L. (2004) Acetylation by Tip60 is required for selective histone variant exchange at DNA lesions. *Science* **306**, 2084-2087

151. Xu, Y., Ayrapetov, M.K., Xu, C., Gursoy-Yuzugullu, O., Hu, Y., and Price, B.D. (2012) Histone H2A.Z controls a critical chromatin remodeling step required for DNA double-strand break repair. *Mol Cell* **48**, 723-733

152. Jacquet, K., Fradet-Turcotte, A., Avvakumov, N., Lambert, J.P., Roques, C., Pandita, R.K., Pacquet, E., Herst, P., Gingras, A.C., Pandita, T.K., Legube, G., Doyon, Y., Durocher, D., and Cote, J. (2016) The TIP60 complex regulates bivalent chromatin recognition by 53BP1 through direct H4K20me binding and H2AK15 acetylation. *Mol Cell* **62**, 409-421

153. Goodarzi, A.A., Noon, A.T., Deckbar, D., Ziv, Y., Shiloh, Y., Lobrich, M., and Jeggo, P.A. (2008) ATM signaling facilitates repair of DNA double-strand breaks associated with heterochromatin. *Mol Cell* **31**, 167-177

154. Noon, A.T., Shibata, A., Rief, N., Lobrich, M., Stewart, G.S., Jeggo, P.A., and Goodarzi, A.A. (2010) 53BP1-dependent robust localized KAP-1 phosphorylation is essential for heterochromatic DNA double-strand break repair. *Nat Cell Biol* **12**, 177-184

155. Kim, J.A., Kruhlak, M., Dotiwala, F., Nussenzweig, A., and Haber, J.E. (2007) Heterochromatin is refractory to gamma-H2AX modification in yeast and mammals. *J Cell Biol* **178**, 209-218

156. Savic, V., Yin, B., Maas, N.L., Bredemeyer, A.L., Carpenter, A.A., Helmink, B.A., Yang-lott., K.S., Sleckman, B.P., and Bassing, C.H. (2009) Formation of dynamic gamma-H2AX domains along broken DNA strands is distinctly regulated by ATM and MDC1 and dependent upon H2AX densities in chromatin. *Mol Cell* **34**, 298-310

157. Schultz, D.C., Friedman, J.R., and Rauscher, F.J. (2001) Targeting histone deacetylase complexes via KRAB-zinc finger proteins: the PHD and bromodomains of KAP-1 form a cooperative unit that recruits a novel isoform of the Mi-2α subunit of NuRD. *Genes Dev* **15**, 428-443

158. Goodarzi, A.A., Kurka, T., and Jeggo, P.A. (2011) KAP-1 phosphorylation regulates CHD3 nucleosome remodeling during the DNA double-strand break response. *Nat Struct Mol Biol* **18**, 831-839

159. Ziv, Y., Bielopolski, D., Galantry, Y., Lukas, C., Taya, Y., Schultz, D.C., Lukas, J., Bekker-Jensen, S., Bartek, J., and Shiloh, Y. (2006) Chromatin relaxation in response to DNA double-strand breaks is modulated by a novel ATM and KAP-1 dependent pathway. *Nat Cell Biol* **8**, 810-876

160. Croft, J.A., Bridger, J.M., Boyle, S., Perry, P., Teague, P., and Bickmore, W.A. (1999) Differences in the localization and morphology of chromosomes in the human nucleus. *J Cell Biol* **145**, 1119-1131

161. Misteli, T., and Soutoglou, E. (2009) The emerging role of nuclear architecture in DNA repair and genome maintenance. *Mol Cell Biol* **10**, 243-254

162. Dellaire, G., and Bazett-Jones, D.P. (2007) Beyond repair foci: subnuclear domains and the cellular response to DNA damage. *Cell Cycle* **6**, 1864-1872

163. Grosse, R., and Vartiainen, M.K. (2013) To be or not to be assembled: progressing into nuclear actin filaments. *Nat Rev Mol Cell Biol* **14**, 693-697

164. Sasseville, A.M., and Lagnelier, Y. (1998) *In vitro* interaction of the carboxy terminal domain of lamin A with actin. *FEBS Lett* **425**, 485-489

165. Fairley, E.A., Kendrick-Jones, J., and Ellis, J.A. (1999) The Emery-Dreifuss muscular dystrophy phenotype arises from aberrant targeting and binding of emerin at the inner nuclear membrane. *J Cell Sci* **112**, 2571-2582

166. Holaska, J.M., Kowalski, A.K., and Wilson, K.L. (2004) Emerin caps the pointed end of actin filaments: Evidence for an actin cortical network at the nuclear inner membrane. *PLoS Biol* **2**, E231

167. Holaska, J.M., and Wilson, K.L. (2007) An emerin "proteome:" Purification of distinct emerin-containing complexes from HeLa cells suggests molecular basis for diverse roles including gene regulation, mRNA splicing, signaling, mechanosensing, and nuclear architecture. *Biochemistry* **46**, 8897-8908

168. Dundr, M., Ospina, J.K., Sung, M-H., John, S., Upender, M., Ried, T., Hager, G.L., and Matera, A.G. (2007) Actin-dependent intranuclear repositioning of an active gene locus in vivo. *J Cell Biol* **179**, 1095-1103

169. Chuang, C.H., Carpenter, A.E., Fuchsova, B., Johnson, T., de Lanerolle, P., and Belmont, A.S. (2006) Long-range directional movement of an interphase chromosome site. *Curr Biol* **16**, 825-831

170. Muratani, M., Gerlich, D., Janicki, S.M., Gebhard, M., Eils, R., and Spector, D.L. (2002) Metabolic-energy-dependent movement of PML bodies within the mammalian cell nucleus. *Nat Cell Biol* **4**, 106-110

171. Hofmann, W.A., Stojiljkovic, L., Fuchsova, B., Vargas, G.M., Mavrommatis, E., Philimoneko, V., Kysela, K., Goodrich, J.A., Lessard, J.L., Hope, T.J., Hozak, P., and de Lanerolle, P. (2004) Actin is part of pre-initiation complexes and is necessary for transcription by RNA polymerase II. *Nat Cell Biol* **6**, 1094-1101

172. Hu, P., Wu, S., and Hernandez, N.A. (2004) A role for beta-actin in RNA polymerase III transcription. *Genes Dev* **18**, 3010-3015

173. Philimonenko, V.V., Zhao, J., Iben, S., Dingova, H., Kysela, K., Kahle, M., Zentgraf, H., Hofmann, W.A., de Lanerolle, P., Hozak, P., and Grummt, I. (2004) Nuclear actin and myosin I are required for RNA polymerase I transcription. *Nat Cell Biol* **6**, 1165-1172

174. Fomproix, N., and Percipalle, P. (2004) An actin-myosin complex on actively transcribing genes. *Exp Cell Res* **294**, 140-148

175. Vartianinen, M.K., Guettier, S., Larijani, B., and Treisman, R. (2007) Nuclear actin regulates dynamic subcellular localization and activity of the SRF cofactor MAL. *Science* **316**, 1749-1752

176. Qi, T., Tang, W., Wang, L., Zhai, L., Guo, L., and Zeng, X. (2011) G-actin participates in RNA polymerase II-dependent transcription elongation by recruiting positive transcription elongation factor b (P-TEFb). *J Biol Chem* **286**, 15171-15181

177. Zhao, K., Wang, E., Rando, O.J., Xue, Y., Swiderek, K., Kuo, A., and Crabtree, G.R. (1998) Rapid and phosphoinositol-dependent binding of the SWI/SNF-like BAF complex to chromatin after T lymphocyte receptor signaling. *Cell* **95**, 625 636

178. Farrants, A.K. (2008) Chromatin remodeling and actin organization. *FEBS Lett* **582**, 2041-2050

179. Kapoor, P., Chen, M., Winkler, D.D., Luger, K., and Shen, X. (2013) Evidence for monomeric actin function in INO80 chromatin remodeling. *Nature Struct Mol Biol* **20**, 426-432

180. Hofmann, W., Reichart, B., Ewald, A., Muller, E., Schmitt, I., Stauber, R.H., Lottspeich, F., Jockusch, B.M., Scheer, U., Hauber, J., and Dabauvaille, M.C. (2001) Cofactor requirements for nuclear export of Rev response element (RRE)- and constitutive transport element (CTE)-containing retroviral RNAs. An unexpected role for actin. *J Cell Biol* **152**, 895-910

181. Coutts, A.S., Boulahbel, H., Graham, A., and La Thangue, N.B. (2007) Mdm2 targets the p53 transcription cofactor JMY for degradation. *EMBO Rep* **8**, 84-90

182. Yahara, I., Aizawa, H., Moriyama, K., Iida, K., Yoneazwa, N., Nishida, E., Hatanaka, H., and Inagaki, F. (1996) A role of cofilin/destrin in reorganization of actin cytoskeleton in response to stresses and cell stimuli. *Cell Struct Funct* **21**, 421-424

183. Lee, Y.J., Sheu, T.J., and Keng, P.C. (2005) Enhancement of radiosensitivity in H1299 cancer cells by actin-associated protein cofilin. Biochem Biophys *Res Commun* **335**, 286-291

184. Burke, B., and Stewart, C.L. (2013) The nuclear lamins: flexibility in function. *Nat Rev Mol Cell Biol* **14**, 13-24

185. Fisher, D.Z., Chaudhary, N., and Blobel, G. (1986) cDNA sequencing of nuclear lamins A and C reveals primary and secondary structural homology to intermediate filament proteins. *Proc Natl Acad Sci USA* **83**, 6450-6454

186. Dhe-Paganon, S., Werner, E.D., Chi, Y.I., and Shoelson, S.E. (2002) Structure of the globular tail of nuclear lamin. *J Biol Chem* **277**, 17381-17384

187. Furukawa, K., Inagaki, H., and Hotta, Y. (1994) Identificaiton and cloning of an mRNA coding for a germ cell-specific A-type lamin in mice. *Exp Cell Res* **212**, 426-430

188. Lin, F., and Worman, H.J. (1996) Structural organization of the human gene encoding nuclear lamin A and nuclear lamin C. *J Biol Chem* **268**, 16321-16326

189. Machiels, B.M., Zorenc, A.H., Endert, J.M., Kuijpers, H.J., van Eys, G.J., Ramaekers, F.C., and Broers, J.L. (1996) An alternative splicing product of the lamin A/C gene lacks exon 10. *J Biol Chem* **271**, 9249-9253

190. Vorburger, K., Lehner, C.F., Kitten, G.T., Eppenberger, H.M., and Nigg, E.A. (1989) A second higher vertebrate B-type lamin. cDNA sequence determination and *in vitro* processing of chicken lamin B2. *J Mol Biol* **208**, 405-415

191. Lin, F., and Worman, H.J. (1995) Structural organization of the human gene (LMNB1) encoding nuclear lamin B1. *Genomics* **27**, 230-236

192. Stierle, V., Couperie, J., Ostlund, C., Krimm, I., Zinn-Justin, S., Hossenlopp, P., Worman, H.J., Courvalin, J,C., and Duband-Goulet, I. (2003) The carboxyl terminal region common to lamins A and C contains a DNA binding domain. *Biochemistry* **42**, 4819-4828

193. Goldberg, M., Harel, A., Brandeis, M., Rechsteiner, T., Richmond, T.J., Weiss, A.M., and Gruenbaum, Y. (1999) The tail domain of lamin Dm0 binds histones H2A and H2B. *Proc Natl Acad Sci USA* **96**, 2852-2857

194. Mattout, A., Cabianca, D.S., and Gasser, S.M. (2015) Chromatin states and nuclear organization in development- a view from the nuclear lamina. *Genome Biol* **16**, 174-189

195. Goldman, R.D., Shumaker, D.K., Erdos, M.R., Eriksson, M., Goldman, A.E., Gordon, L.B., Gruenbaum, Y., Khoun, S., Mendez, M., Varga, R., and Collins, F.S. (2004) Accumulation of mutant lamin A causes progressive changes in nuclear architecture in Hutchinson-Gilford progeria syndrome. *Proc Natl Acad Sci USA* **101**, 8963-8968

196. Sullivan, T., Escalante-Alcalde, D., Bhatt, H., Anver, M., Bhat, N., Nagashima, K., Stewart, C.L., and Burke, B. (1999) Loss of A-type lamin expression compromises nuclear envelope integrity leading to muscular dystrophy. *J Cell Biol* **147**, 913-920

197. Gonzalez-Suarez, I., Redwood, A.B., and Gonzalo, S. (2009) Loss of A-type lamins and genomic instability. *Cell Cycle* **8**, 3860-3865

198. Spann, T.P., Moir, R.D., Goldman, A.E., Stick, R., and Goldman, R.D. (1997) Disruption of nuclear lamin organization alters the distribution of replication factors and inhibits DNA synthesis. *J Cell Biol* **136**, 1201-1212

199. Spann, T.P., Goldman, A.E., Wang, C., Huang, S., and Goldman, R.D. (2002) Alteration of nuclear lamin organization inhibits RNA polymerase II-dependent transcription. *J Cell Biol* **13**, 603-608

200. Dorner, D., Gotzmann, J., and Foisner, R. (2007) Nucleoplasmic lamins and their interaction partners, LAP2α, Rb, and BAF, in transcriptional regulation. *FEBS J* **274**, 1362-1373

201. Mahen, R., Hattori, H., Lee, M., Sharma, P., Jeyasekharan, A.D., and Venkitaraman, A.R. (2013) A-type lamins maintain the positional stability of DNA damage repair foci in mammalian nuclei. *PLoS One* **8**, e61893

202. Redwood, A.B., Perkins, S.M., Vaderwaal, R.P., Feng, Z., Biehl, K.J., Gozalez Suarez, I., Morgado-Palacin, L., Shi, W., Sage, J., Roti-Roti, J.L., Stewart, C.L., Zhang, J., and Gonzalo, S. (2011) A dual role for A-type lamins in DNA double strand break repair. *Cell Cycle* **10**, 2549-2560

203. Gonzalo, S. (2014) DNA damage and lamins. *Adv Exp Med Biol* **773**, 377-399

204. Dellaire, G., Farrall, R., and Bickmore, W.A. (2003) The nuclear protein database (NPD): sub-nuclear localization and functional annotation of the nuclear proteome. *Nucleic Acids Res* **31**, 328-330

205. Lallemand-Breitenbach, V., and de The, H. PML nuclear bodies. (2010) *Cold Spring Harb Perspect Biol* **2**, a000661

206. Zhong, S., Salomoni, P., and Pandolfi, P.P. (2000) The transcriptional role of PML and the nuclear body. *Nat Cell Biol* **2**, 85-90

207. Salomoni, P., and Pandolfi, P.P. (2002) The role of PML in tumor suppression. *Cell* **108**, 165-170

208. Maul, G.G. (1998) Nuclear domain 10, the site of DNA virus transcription and replication. *Bioessays* **20**, 660-667

209. Block, G.J., Eskiw, C.H, Dellaire, G., and Bazett-Jones, D.P. (2006) Transcriptional regulation is affected by subnuclear targeting of reporter plasmids to PML nuclear bodies. *Mol Cell Biol* **26**, 8814-8825

210. Haupt, S., Mitchell, C., Corneille, V., Shortt, J., Fox, S., Pandolfi, P.P., Castillo Martin, M., Bonal, D.M., Cordon-Cardo, C., Lozano, G., and Haupt, Y. (2013) Loss of PML cooperates with mutant p53 to drive more aggressive cancers in a gender-dependent manner. *Cell Cycle* **12**, 1722-1731

211. Reineke, E.L., and Kao, H-Y. (2009) PML: An emerging tumor suppressor and a target with therapeutic potential. *Cancer Ther* **7**, 219-226

212. Wang, A.G., Delva, L., Gaboli, M., Rivi, R., Giorgio, M., Cordon-Cardo, C., Grosveld, F., and Pandolfi, P.P. (1998) Role of PML in cell growth and the retinoic acid pathway. *Science* **279**, 1547-1551

213. Reymond, A., Meroni, G., Fantozzi, A., Merla, G., Cairo, S., Luzi, L., Riganelli, D., Zanaria, E., Messali, S., Cainarca, S., Guffanti, A., Minucci, S., Pelicci, P.G., and Ballabio, A. (2001) The tripartite motif family identifies cell compartments. *EMBO J* **20**, 2140-2151

214. Meroni, G., and Diez-Roux, G. (2005) TRIM/RBCC, a novel class of 'single protein RING finger' E3 ubiquitin ligases. *Bioessays* **27**, 1147-1157

215. Jensen, K., Shiels, C., and Freemont, P.S. (2001) PML protein isoforms and the RBCC/TRIM motif. *Oncogene* **20**, 7223-7233

216. Fagioli, M., Alcalay, M., Pandolfi, P.P., Venturini, L., Mencarelli, A., Simeone, A., Acampora, D., Grignani, F., and Pelicci, P.G. (1992) Alternative splicing of PML transcripts predicts coexpression of several carboxy-terminally different protein isoforms. *Oncogene* **7**, 1083-1091

217. Beech, S.J., Lethbridge, K.J., Killick, N., McGilncy, N., and Leppard, K.N. (2005) Isoforms of the promyelocytic leukemia protein differ in their effects on ND10 organization. *Exp Cell Res* **307**, 109-117

218. Condemine, W., Takahashi, Y., Zhu, J, Puvion-Dutilleul, F., Guegan, S., Janin, A., and de The, H. (2006) Characterization of endogenous human promyelocytic leukemia isoforms. Cancer Res. **66**, 6192-6198

219. Weidtkamp-Peters, S., Lenser, T., Negorev, D., Gerstner, N., Hofmann, T.G., Schwanitz, G., Hoischen, C., Maul, G., Dittrich, P., and Hemmerich, P. (2008) Dynamics of component exchange at PML nuclear bodies. *J Cell Sci* **121**, 2731 2743

220. Lallemand-Breitenbach, V., Zhu, J., Puvioon, F., Koken, M., Honore, N., Doubeikovsky, A., Duprez, E., Pandolfi, P.P., Puvion, E., Freemont, P., and de The, H. (2001) Role of promyelocytic leukemia (PML) sumolation in nuclear body formation, 11S proteasome recruitment, and As(2)O(3)-induced PML or PML/retinoic acid receptor α degradation. *J Exp Med* **193**, 1361-1372

221. Duprez, E., Saurin, A.J., Desterro, J.M., Lallemand-Breitenbach, V., Howe, K., Boddy, M.N., Soloman, E., de The, H., Hay, R.T., and Freemont, P.S. (1999) SUMO-1 modification of the acute promyelocytic leukaemia protein PML: implications for nuclear localization. *J Cell Sci* **112**, 381-393

222. Shen, T.H., Lin, H.K., Scaglioni, P.P., Yung, T.M., and Pandolfi, P.P. (2006) The mechanisms of PML-nuclear body formation. *Mol Cell* **24**, 331-339

223. Nacreddine, K., Lehembre, F., Bhaumik, M., Artus, J., Cohen-Tannoudji, M., Babinet, C., Pandolfi, P.P., and Dejean, A. (2005) The SUMO pathway is essential for nuclear integrity and chromosome segregation in mice. *Dev Cell* **9**, 769-779

224. Boisvert, F.M., Hendzel, M.J., and Bazett-Jones, D.P. (2000) Promyelocytic leukemia (PML) nuclear bodies are protein structures that do not accumulate RNA. *J Cell Biol* **148**, 283-292

225. Eskiw, C.H., Dellaire, G., and Bazett-Jones, D.P. (2004) Chromatin contributes to structural integrity of promyelocytic leukemia bodies through a SUMO-1 independent mechanism. *J Biol Chem* **279**, 9577-9585

226. Wang, J., Shiels, C., Sasieni, P., Wu, P.J., Islam, S.A., Freemont, P.S., and Sheer, D. (2004) Promyelocytic leukemia nuclear bodies associate with transcriptionally active genomic regions. *J Cell Biol* **164**, 515-526

227. Shiels, C., Islam, S.A., Vatcheva, R., Sasieni, P., Sternberg, M.J., Freemont, P.S., and Sheer, D. (2001) PML bodies associate specifically with the MHC gene cluster in interphase nuclei. *J Cell Sci* **114**, 3705-3716

228. Kumar, P.P., Bischof, O., Purbey, P.K., Notani, D., Urlaub, H., Dejean, A., and Galande, S. (2007) Functional interaction between PML and SATB1 regulates chromatin-loop architecture and transcription of the MHC class I locus. *Nature Cell Biol* **9**, 45-56

229. Sun, Y., Durrin, L.K., and Krontiris, T.G. (2003) Specific interaction of PML bodies with the TP53 locus in Jurkat interphase nuclei. *Genomics* **82**, 250-252

230. Ching, R.W., Ahmed K., Boutros, P.C., Penn, L.Z., and Bazett-Jones, D.P. (2013) Identifying gene locus associations with promyelocytic leukemia nuclear bodies using immune-TRAP. *J Cell Biol* **201**, 325-335

231. Dellaire, G., Ching, R.Q., Dehghani, H., Ren, Y., and Bazett-Jones, D.P. (2006) the number of PML nuclear bodies increases in early S phase by a fission mechanism. *J Cell Sci* **119**, 1026-1033

232. Dellaire, G., Eskiw, C.H., Dehghani, H., Ching, R.W., and Bazett-Jones, D.P. (2006) Mitotic accumulations of PML protein contribute to the re-establishment of PML nuclear bodies in G1. *J Cell Sci* **119**, 1034-1042

233. Chen, Y.C., Kappel, C., Beaudouin, J., Eils, R., and Spector, D.L. (2008) Live cell dynamics of promyelocytic leukemia nuclear bodies upon entry into and exit from mitosis. *Mol Biol Cell* **19**, 3147-3162

234. Eskiw, C.H., Dellaire, G., Mymryk, J.S., and Bazett-Jones, D.P. (2003) Size, position and dynamic behavior of PML nuclear bodies following cells stress as a paradigm for supramolecular trafficking and assembly. *J Cell Sci* **116**, 4455 4466

235. Dellaire, G., Ching, R.W., Ahmed, K., Jalali, F., Tse, K.C., Bristow, R.G., and Bazett-Jones, D.P. (2006) Promyelocytic nuclear bodies behave as DNA damage sensors whose response to DNA double-strand breaks is regulated by NBS1 and the kinases ATM, Chk2, and ATR. *J Cell Biol* **175**, 55-66

236. Dellaire, G., and Bazett-Jones, D.P. (2004) PML nuclear bodies: dynamic sensors of DNA damage and cellular stress. *Bioessays* **26**, 963-977

237. Kepkay, R., Attwood, K.M., Ziv, Y., Shiloh, Y., and Dellaire, G. (2011) KAP1 depletion increases PML nuclear body number in concert with ultrastructural changes in chromatin. *Cell Cycle* **10**, 308-322

238. Nefkens, I., Negorev, D.G., Ishov, A.M., Michaelson, J.S., Yeh, E.T., Tanguay, R.M., Muller, W.E., and Maul, G.G. (2003) Heat shock and Cd2+ exposure regulate PML and Daxx release from ND10 by independent mechanisms that modify the induction of heat shock proteins 70 and 25 differentially. *J Cell Sci* **116**, 512-524

239. Bischof, O., Kim, S.H., Irving, J., Beresten, S., Ellis, N.A., and Campisi, J. (2001) Regulation and localization of the bloom syndrome protein in response to DNA damage. *J Cell Biol* **153**, 367-380

240. Carbone, R., Pearson, M., Minucci, S., and Pelicci, P.G. (2002) PML NBs associate with the hMre11 complex and p53 at sites of irradiation induced DNA damage. *Oncogene* **21**, 1633-1640

241. Eladad, S., Ye, T.Z., Hu, P., Leversha, M., Beresten, S., Matunis, M.J., and Ellis, N.A. (2005) Intra-nuclear trafficking of the BLM helicase to DNA damage induced foci is regulated by SUMO modification. *Hum Mol Genet* **14**, 1351 1365

242. Yang, S., Kuo, C., Bisi, J., and Kim, M.K. (2002) PML-dependent apoptosis after DNA damage is regulated by the checkpoint kinase hCds1/Chk2. *Nature Cell Biol* **4**, 865-870

243. Boe, S.O., Haave, M., Jul-Larsen, A., Grudic, A., Bjerkvig, R., and Lonning, P.E. (2006) Promyelocytic leukemia nuclear bodies are predetermined processing sites for damaged DNA. *J Cell Sci* **119**, 3284-3295

244. Munch, S., Weidtkamp-Peters, S., Klement, K., Grigaravicius, P., Monajembashi, S., Salomoni, P., Pandolfi, P.P., Weihart, K., and Hemmerich, P. (2014) The tumor suppressor PML specifically accumulates at RPA/Rad51-containing DNA damage repair foci but is nonessential for DNA damage-induced fibroblast senescence. *Mol Cell Biol* **34**, 1733-1746

245. Boichuk, S., Hu, L., Makielski, K., Pandolfi, P.P., Gjoerup, O.V. (2011) Functional connection between Rad51 and PML in homology-directed repair. *PLoS One* **6**, e25814

246. Yeung, P.L., Denissova, N.G., Nasello, C., Hakhverdyan, Z., Chen, J..D., and Brenneman, M.A. (2012) Promyelocytic leukiemia nuclear bodies support a late step in DNA double-strand break repair by homologous recombination. *J Cell Biochem* **113**, 1787-1799

247. Zhong, S., Hu, P., Ye, T-Z., Stan, R., Ellis, N.A., and Pandolfi, P.P. (1999) A role for PML and the nuclear body in genomic stability. *Oncogene* **18**, 7941 7947

248. Kruhlak, M.J., Celeste, A., Dellaire, G., Fernandez-Capetillo, O., Muller W.G., and McNally, J.G. (2006) Changes in chromatin structure and mobility in living cells at sites of DNA double-strand breaks. *J Cell Biol* **172**, 823-834

249. Dellaire, G, Nisman, R., and Bazett-Jones, D.P. (2004) Correlative light and electron spectroscopic imaging of chromatin in situ. *Methods Enzymol* **375**, 456-478

250. Dellaire, G., Kepkay, R., and Bazett-Jones, D.P. (2009) High resolution imaging of changes in the structure and spatial organization of chromatin, γ-H2A.X and the MRN comples within etoposide-induced DNA repair foci. *Cell Cycle* **8**, 3750-3769

251. van der Weyden, L., Adams, D.J., Harris, L.W., Tannahill, D., Arends, M.J., and Bradley, A. (2005) Null and conditional semaphorin 3B alleles using a flexible puroDeltatk loxP/FRT vector. *Genesis* **41**, 171-178

252. Cadinanos, J., and Bradley, A. (2007) Generation of an inducible and optimized piggyBac transposon system. *Nucleic Acids Res* **35**, e87

253. Lee, G., and Saito, J. (1998) Role of nucleotide sequences of loxP spacer region in Cre-mediated recombination. *Gene* **216**, 55-65

254. Mansour, W.Y., Schumacher, S., Rosskopf, R., Rhein, T., Schmidt-Petersen, F., Gatzemeier, F., Haag, F., Borgmann, K., Willers, H., and Dahm-Daphi, J. (2008) Hierarchy of nonhomologous end-joining, single-strand annealing and gene converstion at site-directed DNA double-strand breaks. *Nucleic Acids Res* **36**, 4088-4098

255. Bennardo, N., Cheng, A., Huang, N., and Stark, J.M. (2008) Alternative-NHEJ is a mechanistically distinct pathway of mammalian chromosome break repair. *PLoS Genet* **4**, e1000110.

256. Cradick, T.J., Qui, P., Lee, C.M., Fine, E.J., and Bao, G. (2014) COSMID: A web-based tool for identifying and validating CRISPR/Cas off-target sites. *Mol Ther Nucleic Acids* **3**, e214

257. Southern, E.M. (1975) Detection of specific sequences among DNA fragments separated by gel electrophoresis. *J Mol Biol* **98**, 503-517

258. Zinner, R., Teller, K., Versteegm R., Cremer, T., and Cremer, M. (2007) Biochemistry meets nuclear architecture: multicolor immuno-FISH for colocalization analysis of chromosome segments and differentially expressed gene loci with various histone methylations. *Adv Enzyme Regul* **47**, 223-241

259. Pinder, J., Salsman, J., and Dellaire, G. (2015) Nuclear domain 'knock-in' screen for the evaluation and identification of small molecule enhancers of CRISPR-based genome editing. *Nucleic Acids Res* **43**, 9379-9392

260. Azqueta, A., Slyskova, J., Langie, S.A.S., O'Neill Gaivao, I., and Collins, A. (2014) Comet assay to measure DNA repair: approach and applications. *Front Genet* **5**, 288-296

261. Posern, G., Sotiropoulos, A., and Treisman, R. (2002) Mutant actins demonstrate a role for unpolymerized actin in control of transcription by serum response factor. *Mol Biol Cell* **13**, 4167-4178

262. Lemaitre, C., Grabarz, A., Tsouroula, K., Andronov, L., Furst, A., Pankotai, T., Heyer, V., Rogier, M, Attwood, K.M., Kessler, R., Delliare, G., Klaholz, B., Reina-San-Martin, B., and Soutoglou, E. (2014) Nuclear position dictates DNA repair pathway choice. *Genes Dev* **28**, 2450-2463

263. Reddy, K.L., Zullo, J.M., Bertolino, E., and Singh, H. (2008) Transcriptional repression mediated by repositioning of genes to the nuclear lamina. *Nature* **452**, 243-247

264. Galvan, D.L., Nakazawa, Y., Kaja, A., Kettlun, C., Cooper, L.J.N., Rooney, C.M., and Wilson, M.H. (2009) Genome-wide mapping of *piggyBac* transposon integrations in primary human T cells. *J Immunother* **32** 837-844

265. Li, X., Burnight, E.R., Cooney, A.L., Malani, N., Bradley, T., Sander, J.D., Staber, J., Wheelan, S.J., Joung, J.K., McCray, P.B., Bushman, F.D., Sinn, P.L., and Craig, N.L. (2013) *piggyBac* transposase tools for genome engineering. *Proc Natl Acad Sci USA* **110**, E2279-87

266. Li, X., Ewis, H., Hice, R.H., Malani, N., Parker, N., Zhou, L., Feschotte, C., Bushman, F.D., Atkinson, P.W., and Craig, N.L. (2012) A resurrected mammalian *hAT* transposable element and a closely related insect element are highly active in human cell culture. *Proc Natl Acad Sci USA* **110**, E478-E487

267. Mali, P., Yang, L., Esvelt, K.M., Aach, J., Guell, M., DiCarlo, J.E., Norville, J.E., and Church, G.M. (2013) RNA-guided human genome engineering via Cas9. *Science* **339**, 823-826

268. Ran, F.A., Hsu, P.D., Lin, C-Y., Gootenberg, J.S., Konermann, S., Trevino, A., Scott, D.A., Inoue, A., Matoba, S., Zhang, Y., and Zhang, F. (2013) Double nicking by RNA-guided CRISPR Cas9 for enhanced genome editing specificity. *Cell* **154**, 1380-1389

269. Bernardi, R., and Pandolfi, P.P. (2007) Structure, dynamics and functions of promyelocytic leukaemia nuclear bodies. *Nat Rev Mol Cell Biol* **8**, 1006-1016

270. Ishov, A.M., Sotnikov, A.G., Negorev, D., Vladimirova, O.V., Neff, N., Kamitani, T., Yeh, E.T.H., Strauss, J.F., and Maul, G.G. (1999) Pml is critical for ND10 formation and recruits the Pml-interacting protein Daxx to this nuclear structure when modified by Sumo-1. *J Cell Biol* **147**, 221-234

271. Nussenzweig, A., Chen, C., da Costa Soares, V., Sanchez, M., Sokol, K., Nussenzweig, MC., and Li, G.C. (1996) Requirement for Ku80 in growth and immunoglobulin V(D)J recombination. *Nature* **382**, 551-555

272. Soutoglou, E., Dorn, J.F., Sengupta, K., Jasin, M., Nusenzweig, A., Ried, T., Danuser, G., and Misteli, T. (2007) Positional stability of single double-strand breaks in mammalian cells. *Nat Cell Biol* **9**, 675-682

273. Belin, B.J., Lee, T., and Dyche Mullins, R. (2015) DNA damage induces nuclear actin filament assembly by Formin-2 and Spire-1/2 that promotes efficient DNA repair. *eLife* **4**, e07735

274. Lisby, M., Mortensen, U.H., and Rothstein, R. (2003) Colocalization of multiple DNA double-strand breaks at a single Rad52 repair centre. *Nat Cell Biol* **5**, 572-577

275. Roukos, V., Voss, T.C., Schmidt, C.K., Lee, S., Wangsa, D., and Misteli, T. (2013) Spatial dynamics of chromosome translocations in living cells. *Science* **341**, 660-664

276. Roukos, V., and Misteli, T. (2014) The biogenesis of chromosome translocations. *Nat Cell Biol* **16**, 293-300

277. Misteli, T., and Soutoglou, E. (2009) The emerging role of nuclear architecture in DNA repair and genome maintenance. *Nat Rev Mol Cell Biol* **10**, 243-254

278. Clouaire, T., and Legube, G. (2015) DNA double strand break repair pathway choice: a chromatin based decision? *Nucleus* **6**, 107-113

279. Murray, J.M., Stiff, T., and Jeggo, P.A. (2012) DNA double-strand break repair within heterochromatin regions. *Biochem Soc Trans* **40**, 173-178

280. Jha, D.K., and Strahl, B.D. (2014) An RNA polymerase II-coupled function for histone H3K36 methylation in checkpoint activation and DSB repair. *Nat Commun* **5**, 3965

281. Pai, C.C., Deegan, R.S., Subramanian, L., Gal, C., Sarkar, S., Blaikley, E.J., Walker, C., Hulme, L., Bernhard, E., Codlin, S., Bahler, J., Allshire, R., Whitehall, S., and Humphrey, T.C. (2014) A histone H3K36 chromatin switch coordinates DNA double-strand break repair pathway choice. *Nat Commun* **5**, 4091

282. Lorat, Y., Schanz. S., Schuler, N., Wennemuth, G., Rube, C., and Rube, C.E. (2012) Beyond repair foci: DNA double-strand break repair in euchromatic and heterochromatic compartments analyzed by transmission electron microscopy. *PLoS One* **7**, e38165

283. Chiolo, I., Minoda, A., Colmenares, S.U., Polyzos, A., Costes, S.V., and Karpen, G.H. (2011) Double-strand breaks in heterochromatin move outside of a dynamic HP1a domain to complete recombinational repair. *Cell* **144**, 732-744

284. Chubb, J.R., Boyle, S., Perry, P., and Bickmore, W.A (2002) Chromatin motion is constrained by association with nuclear compartments in human cells. *Curr Biol* **12**, 439-445

285. Fraser, M.J., Ciszczon, T., Elick, T., and Bauser, C. (1996) Precise excision of TTAA-specific lepidopteran transposons piggyBac (IFP2) and tagalong (TFP3) from the baculovirus genome in cell lines from two species of Lepidoptera. *Insect Mol Biol* **5**, 141-151

286. Cho, S.W., Kim, S., Kim, Y., Kweon, J., Kim, H.S., Bae, S., and Kim, J-S. (2014) Analysis of off-target effects of CRISPR/Cas-derived RNA guided endonucleases and nickases. *Genome Res* **24**, 132-141

287. Turan, S., Zehe, C., Kuehle, J., Qiao, J., and Bode, J. (2013) Recombinase mediated cassette exchange (RCME)- a rapidly-expanding toolbox for targeted genomic modifications. *Gene* **515**, 1-27

288. Semprini, S., Troup, T.J., Kotelevtseva, N., King, K., Davis, J.R.E., Mullins, L.J., Chapman, K.E., Dunbar, D.R., and Mullins, J.J. (2007) Cryptic loxP sites in mammalian genomes: genome-wide distribution and relevance for the efficiency of BAC/PAC recombineering techniques. *Nucleic Acids Res* **35**, 1402-1410

289. Araki, K., Araki, M., and Yamamura, K. (2002) Site-directed integration of the cre gene mediated by Cre recombinase using a combination of mutant *lox* sites. *Nucleic Acids Res* **30**, e103

290. Soukharev, S., Miller, J.L., Sauer, B. (1999) Segmental genomic replacement in embryonic stem cells by double lox targeting. *Nucleic Acids Res* **27**, e21

291. Loonstra, A., Vooijs, M., Beverloo, B., Allak, B.A., van Drunen, E., Kanaar, R., Berns, A., and Jonkers, J. (2001) Growth inhibition and DNA damage induced by Cre recombinase in mammalian cells. *Proc Natl Acad Sci USA* **98**, 9209-9214

292. Negorev, D., and Maul, G.G. (2001) Cellular proteins localized at and interacting within ND10/PML nuclear bodies/PODs suggest functions of a nuclear depot. *Oncogene* **20**, 7234-7242

293. Chung, I., Osterwald, S., Deeg, K.I., and Rippe, K. (2012) PML body meets telomere: The beginning of an ALTernate ending. *Nucleus* **3**, 263-275

294. Yeager, T.R., Neumann, A.A., Englezou, A., Huschtscha, L.I., Noble, J.R., and Reddel, R.R. (1999) Telomerase-ngative immortalized human cells contain a novel type of promyelocytic leukemia (PML) body. *Cancer Res* **59**, 4175-4179

295. Henson, J.D., Hannay, J.A., McCarthy, S.W., Royds, J.A., Yeager, T.R., Robinson, R.A., Wharton, S.B., Jellnek, D.A., Arbuckle, S.M., Yoo, J., Robinson, B.G., Learoyd, D.L., Stalley, P.D., Bonar, S.F., Yu, D., Pollock, R.E., Reddel, R.R. (2005) A robust assay for alternative lengthening of telomeres in tumors shows the significance of alternative lengthening of telomeres in sarcomas and astrocytomas. *Clin Cancer Res* **11**, 217-225

296. Stavropoulos, D.J., Bradshaw, P.S., Li, X., Pasic, I., Truong, K., Ikura, M., Ungrin, M., and Meyn, M.S. (2002) The Bloom syndrome helicase BLM interacts with TRF2 in ALT cells and promotes telomeric DNA synthesis. *Hum Mol Genet* **11**, 3135-3144

297. Potts, P.R., and Yu, H. (2007) The SMC5/6 complex maintains telomere length in ALT cancer cells through SUMOylation of telomere-biding proteins. *Nat Struct Mol Biol* **14**, 581-590

298. Wu, G., Jiang, X., Lee, W.H., and Chen, P.L. (2003) ALT-associated promyelocytic leukemia bodies requires Nijmegen Breakage Syndrome 1. *Cancer Res* **63**, 2589-2595

299. Wu, G., Lee, W.H., and Chen, P.L. (2000) NBS1 and TRF1 colocalize at promyelocytic leukemia bodies during late S/G2 phases in immortalized telomerase-negative cells. Implication of NBS1 in alternative lengthening of telomeres. *J Biol Chem* **275**, 30618-30622

APPENDIX A: Supplementary Data
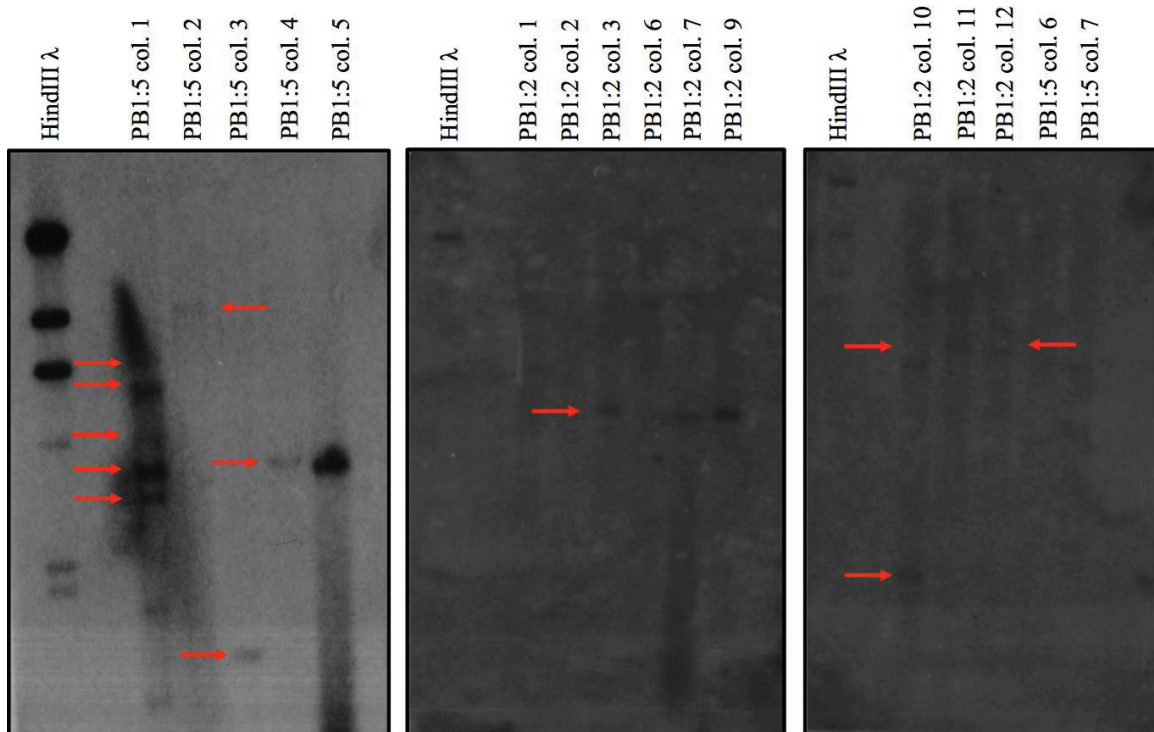
Appendix A Figure 1. Southern blot analysis of genomic DNA isolated from U2OS pFlexible PB colonies. Genomic DNA was isolated from U2OS pFlexible PB colonies, digested with EcoRI and hybridized with probe against a portion of the puromycin-resistance gene from pFlexible-LacO-pBLR5 plasmid DNA. HindIII λ phage DNA ladder resolved in the first lane of each blot was detected by hybridization with radiolabeled lambda DNA. Arrows denote position of hybridization bands.
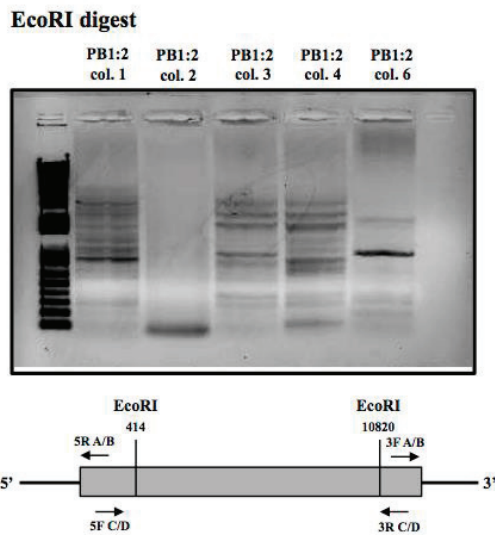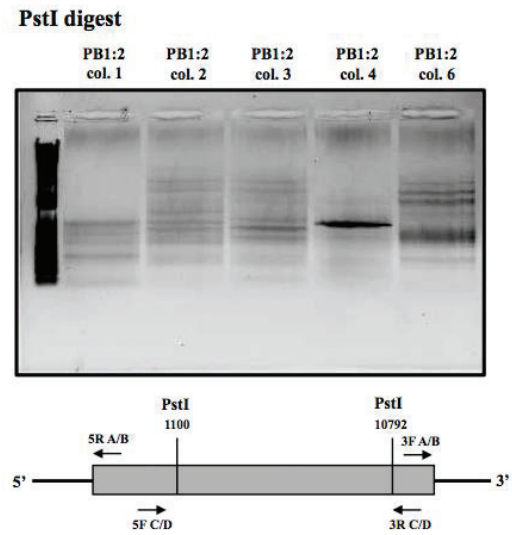
Appendix A Figure 2. **Representative inverse PCR to map genomic pFlexible-LacO-pBLR5 integration position of U2OS pFlexible PB colonies**. Agarose gel of 5' end inverse PCR carried out on **(A)** EcoRI digested or **(B)** PstI digested, recircularized genomic DNA isolated from U2OS pFlexible PB colonies. The bottom cartoons depict where EcoRI and PstI cleave within the pFlexible-LacO-pBLR5 construct and arrows indicate the primers used for amplification.

**Appendix A Figure 3. Sequenced PCR amplicons from U2OS Chr15 pFlexible 5'
px330 col. 6. (A)** PCR amplicon sequence confirming the 5' end of the pFlexible-LacO-
pBLR5 integration site at the Chr15 locus. **(B)** PCR amplicon sequence confirming the
3'end of the pFlexible-LacO-pBLR5 integration site at the Chr15 locus. **(C)** PCR
amplicon sequence of unedited Chr15 loci. A 12 bp deletion resulting from NHEJ repair
of CRISPR/Cas9 induced DSBs was found when this sequence was compared to wild-
type U2OS and its location is indicated by a slash mark (/). Sequence of the Chr15 locus
is highlighted in grey, with the sequences used to generate the homology arms of the
pFlexible-LacO-pBLR5 donor vector shown in blue (5' homology) or red (3' homology).
pFlexible-LacO-pBLR5 sequence is shown in bold text, with its various components
being highlighted in different colours.

Legend:

`Grey highlight` = Chr15 genomic sequence

`Blue text` = Sequence used for Chr15 5' homology template

`Red text` = Sequence used for Chr15 3' homology template

`Bold text` = pFlexible-LacO-pBLR5 sequence

`Green highlight` = loxP site of pFlexible-LacO-pBLR5

`Yellow highlight` = I-SceI site of pFlexible-LacO-pBLR5

`Blue highlight` = FRT site of pFlexible-LacO-pBLR5

`Pink highlight` = PGK Pro of pFlexible-LacO-pBLR5

(/) = Deletion

A

GGGGGCTCTAGCTCCTGCCCCAGCAGCGAAAGGGGCTCCTCCTTCTCTGGTGCCCAGTCCTAGCTCACCTG
CTCTTCACAAGCCTCCTCCCAGCACAGCCTGCACCACACAGGTGCTCAGTAAGGGGGTTGCTCTGAACAGG
GAGCAGGCCCACATGCTGAGAGTGGTGGAGGCGTGCAGGCTCTGATGACCACCTGAACCCAGACTCCAGGG
CAGGACAGGTCCTTACAGACCGTAAGGGCTTCCTGCCTACCCTCTTCCCATGCAGTTACCTCAACCCTGGG
ACACCAGGAAGGTTGAGCATTCCAGGAAAGCCCCGACCCACCCAGGAAACCCAAGTACCTGGTGGGGCCTC
ATCTGGCCCATTGTCCTGAAAGGACAGGAATAAAGGCTCTCTCCTCATGGCCACACACCCTAGGGACGTCC
AGCCTCCAGCTTTCTGTGGGTGGGGCAAATGACTGAGGAGGCTTCCCTCCCTGCAGGCGCCTCCCTCTGGG
GCCTCCTGTGGTCCAGTCGTCCCTGGTCCCCAGCTCTCAGGTGGGTCATAGGGCATCTCAGCAGGACCACC
AGGAAGAGCATCAGGAGGGGAAGGAGCCAGAGAGCCCTCCAGGCCAGTGCACTGCTAACTCAACATCTCAT
CTTCCTATCTCGTCCCTTCTGCTCACCTCCGGAGACTCCCCCTCCCCTCTCATGCTCTTCACTGGCAGGTT
ATGATGGCCCAGAGATCCCCACCAGAGTCCCAGATATCAGTGGGGATCCCAGCCTATTCCTTCTTAAGCAA
GCTCGAAATTAACCCTCACTAAAGGGAACAAAAGCTGGTACCGGGCCCCCCCTCGAGGTCGAGACGGTATC
GATGGCGCGGAATTCAAAAAGTTTAAACAAAAAAGGCGCGCCATAACTTCGTATAATGTATGCTATACGAA
GTTATAAGCTTAGTTACGCTAGGGATAACAGGGTAATATAGTTAATTAAGAAGTTCCTATTCCGAAGTTCC
TATTCTCTAGAAAGTATAGGAACTTCAGCTTGATATCGAATTAATTCTACCGGGTAGGGGAGGCGCTTTTC
CCAAGGCAGTCTGGAGCATGCGCTTTAGCAGCCCCGCTGGGCACT

B

ATGATTATCTTTCTAGGGTTAATCTAGTATACGCGTAGTTCTCCCTGAGCCTGTGGATACATGGAAAGAGA
GCTTACCACCACCCCCTTCTCTGAATATACATACAGGATCTGAGGAGGGAGGATTCTGTGTGGTAGCATGT
GTGCACAGATGTGCATGTTTGTACGTGTGTATGGGTGAGCAGGTCATACGTGTGGTCCCATGTGCCCACCT
GTTGTATATATGCATGCTTGTTTTGTGTAAGTGAGCATAAGAGGTCAAGCCAGAGAGAGAAATAGGAACAA
GGAGAGACAGAGAGAGAGAGAGAATAGAAACAGAGAGACCAAGAGGGAAACAGAATGAGACTGAGACAGAG
AACAACAGAAGGCCAGACAGGTAGACAAGCCACAGTTCCATCTTCCCTGGTGCTGGCTGCCAAGGCAGACA
ACTCTCCTCTCACTTCATTGTTGTTCTGCCTGTGTTTATACCCATGATTGGGGTGGAGTTCAGGAAAGGAT
GTATCAGGGCTAGGACGCCCCCACCTCCACACTCACAGGGCCAGTCAGGGCCCTCTGCAGGGGCTGCCATT
TCCTCAAGCTGAGGAATGGGCTTGGATCCCTCGGATGCCTTCCAGGGTGCAGGGGCGCTCCCAGTGACTGG
GCACTTGTGGTGGCTGGGGAGGGGGAGCTCCTCNGACAGGCCCCATGCTGGGGGAAACGTCCTGAGACTGA
CCTATGACGGGCTGACATGCACACCAAGGAGGTCTCACATCTGCTGGGAAATGAGGG

C

CACCTGCTCTTCACAAGCCTCCTCCCAGCACAGCCTGCACCACACAGGTGCTCAGTAAGGGGGGTTGCTCTG
AACAGGGAGCAGGCCCACATGCTGAGAGTGGTGGAGGCGTGCAGGCTCTGATGACCACCTGAACCCAGACT
CCAGGGCAGGACAGGTCCTTACAGACCGTAAGGGCTTCCTGCCTACCCTCTTCCCATGCAGTTACCTCAAC
CCTGGGACACCAGGAAGGTTGAGCATTCCAGGAAAGCCCCGACCCACCCAGGAAACCCAAGTACCTGGTGG
GGCCTCATCTGGCCCATTGTCCTGAAAGGACAGGAATAAAGGCTCTCTCCTCATGGCCACACACCCTAGGG
ACGTCCAGCCTCCAGCTTTCTGTGGGTGGGGCAAATGACTGAGGAGGCTTCCCTCCCTGCAGGCGCCTCCC
TCTGGGGCCTCCTGTGGTCCAGTCGTCCCTGGTCCCCAGCTCTCAGGTGGGTCATAGGGCATCTCAGCAGG
ACCACCAGGAAGAGCATCAGGAGGGGAAGGAGCCANATAGCCCTCCAGGCCAGTGCACTGCTAACTCAACA
TCTCATCTTCCTATCTCGTCCCTTCTGCTCACCTCCGGAGACTCCCCCTCCCCTCTCATGCTCTTCACTGG
CAGGTTATGATGGCCCAGAGATCCCCACCANANTCCCAGATATCAGTGGGGATCCCAGCCTATTCCTCCAA
GCTCCCAGTTGCCAGTGACANGGAGGCAGAAACAGC(/)CTGTGGGTTCTCCCTGAGCCTGTGGATACATG
GAAAGAGAGCTTCACCACCACCCCCTTCTCTGAATATACATACAGGATCTGAGGAGGGAGGATTCTGTGTG
GATGCATGTGTGCACAGATGTGCATGTTTGTACGTGTGTATGGGTGAGCAGGTCATACGTGTGGTCCCATG
TGCCCACCTGTTGTATATATGCATGCTTGTTTTGTGTAAGTGAGCATAAGAGGTCAAGCCAGAGAGAGAAA
TAGGAACAAGGAGAGACAGAGAGAGAGAGAATAGAAACAGAGACCAACAGGGAAACAGAATGAGACTGAGA
CAGAGAACAACAGAAGGCCAGACAGGTAGACAAGCCACAGTTCCATCTTCCCTGGTGCTGGCTGCCAAGGC
AGACAACTCTCCTCTCACTTCATTGATGTTCTGCCTGTGTTTATACCCATGATTGGGGTGGAGTTCAGGAA
AGGATGTATCAGGGCTAGGACGCCCCCACCTCCACACTCACAGGGCCAGTCAGGGCCCTCTGCAGGGGCTG
CCATTTCCTCAAGCTGAGGAATGGGCTTGGATCCCTCGGATGCCTTCCAGGGTGCAGGGGCGCTCCCAGTG
ACTGGGCACTTGTGGTGGCTGGGGAGGGGGAGCTCCTCNGACAGGCCCCATGCTGGGGGAAACGTCCTGAG

Legend:

`Grey highlight` = TAP1 genomic sequence

`Blue text` = Sequence used for TAP1 5' homology template

`Red text` = Sequence used for TAP1 3' homology template

`Bold text` = pFlexible-LacO-pBLR5 sequence

`(/)` = Deletion

A

CAGTACTGCTACTTCTCGCCGACTGGGTGCTGCTCCGGACCGCGCTGCCCCGCATATTCTCCCTGCTGGTG
CCCACCGCGCTGCCCACTGCTCCGGGTCTGGGCGGTGGGCCTGAGCCGCTGGGCCGTGCTCTGGCTGGGGGC
CTGCNGGGTCCTCAGGGCAACGGTTGGCTCCAAGAGCGAAAAC**TCTTAAGCAAGC**

B

GATTATCTTTCTAGGGTTAATTCTAGTATACGCGTACGAGAGCTGATCTCATGGGGAGCCCCCGGGTCCGC
GGATAGCACCAGGCTACTGCNCNGGGGGAAGTCACCCTACCGCCTTCGTTGTCAGTTATGCAGCGGCACTGC
CCGCAGCAGCCCTGTGGCACAAACTCGGGAGCCTCTGGGTGCCCGGCGGTCAGGGCGGCTCTGGAAACCCT
GTGCGTCGGCTTCTAGGCTGCCTGGGCTCGGAGACGCGCCGCCTCTCGCTGTTCCTGGTCCTGGTGGTCCT
CTCCTCTCTTGGTAAGGGG

C

GACAGTACTGCTACTTCTCGCCGACTGGGTGCTGCTCCGGACCGCGCTGCCCCGCATATTCTCCCTGCTGG
TGCCCACCGCGCTGCCCACTGCTCCGGGTCTGGGCGGTGGGCCTGAGCCGCTGGGCCGTGCTCTGGCTGGGG
GCCTGCNGGGTCCTCAGGGCAACGGTTGGCTCCAAGAGCGAAAACGCAGGTGCCCAGGGCTGGCTGGCTGC
TTTGAAGCCATTAGCTGCGGCACTGGGC**(/)**GAGAGCTGATCTCATGGGGAGCCCCCGGGTCCGCGGATAG
CACCAGGCTACTGCNCNGGGGAAGTCACCCTACCGCCTTCGTTGTCAGTTATGCAGCGGCACTGCCCGCAG
CAGCCCTGTGGCACAAACTCGGGAGCCTCTGGGTGCCCGGCGGTCAGGGCGGCTCTGGAAACCCTGTGCGT
CGGCTTCTAGGCTGCCTGGGCTCGGAGACGCGCCGCCTCTCGCTGTTCCTGGTCCTGGTGGTCCTCTCCTC
TCTTGGTAAGGGGGAA

**Appendix A Figure 4. Sequenced PCR amplicons from U2OS TAP pFlexible 5'
px330 col. 1. (A)** PCR amplicon sequence confirming the 5' end of the pFlexible-LacO-
pBLR5 integration site at the TAP1 locus. **(B)** PCR amplicon sequence confirming the
3'end of the pFlexible-LacO-pBLR5 integration site at the TAP1 locus. **(C)** PCR
amplicon sequence of unedited TAP1 loci. A 28 bp deletion resulting from NHEJ repair
of CRISPR/Cas9 induced DSBs was found when this sequence was compared to wild-
type U2OS and its location is indicated by a slash mark (/). Sequence of the Chr15 locus
is highlighted in grey, with the sequences used to generate the homology arms of the
pFlexible-LacO-pBLR5 donor vector shown in blue (5' homology) or red (3' homology).
pFlexible-LacO-pBLR5 sequence is shown in bold text.

Appendix A Figure 5. Sequenced PCR amplicons from U2OS Chr15 HR 2. (A) PCR amplicon sequence confirming the integration of HR reporter DNA within the pFlexible-LacO-pBLR5 construct **(B)** PCR amplicon sequence confirming the 5' end of the pFlexible-LacO-pBLR5 integration site at the Chr15 locus. **(C)** PCR amplicon sequence confirming the 3'end of the pFlexible-LacO-pBLR5 integration site at the Chr15 locus. Sequence of the Chr15 locus is highlighted in grey, with the sequences used to generate the homology arms of the pFlexible-LacO-pBLR5 donor vector shown in blue (5' homology) or red (3' homology). pFlexible-LacO-pBLR5 sequence is shown in bold text, and the CMV promoter of the HR reporter in pink highlight.

Legend:
`Grey highlight` = Chr15 genomic sequence
`Blue text` = Sequence used for Chr15 5' homology template
`Red text` = Sequence used for Chr15 3' homology template
`Bold text` = pFlexible-LacO-pBLR5 sequence
`Pink highlight` = CMV Pro of HR reporter

A

CCGGGCCATGGTCGAAAACAAGGGAAATCACTCCCAATTAAAGCTCCCCCCCTCGAGGTCGAGACGGTATC
GATGGCGCGGAATTCAAAAAGTTTAAACAAAAAAGGCGCTAATATTATTGAAGCATTTATCAGGGTTATTG
TCTCATGAGCGGATACATATTTGAATGTATTTAGTAGTAATCAATTACGGGGTCATTAGTTCATAGCCCAT
ATATGGAGTTCCGCGTTACATAACTTACGGTAAATGGCCCGCCTGGCTGACCGCCCAACGACCCCCGCCCA
TTGACGTCAATAATGACGTATGTTCCCATAGTAACGACGTATGTTCCC

B

GGGGCTCTAGCTCCTGCCCCAGCAGCGAAAGGGGCTCCTCCTTCTCTGGTGCCCAGTCCTAGCTCACCTGC
TCTTCACAAGCCTCCTCCCAGCACAGCCTGCACCACACAGGTGCTCAGTAAGGGGGTTGCTCTGAACAGGG
AGCAGGCCCACATGCTGAGAGTGGTGGAGGCGTGCAGGCTCTGATGACCACCTGAACCCAGACTCCAGGGC
AGGACAGGTCCTTACAGACCGTAAGGGCTTCCTGCCTACCCTCTTCCCATGCAGTTACCTCAACCCTGGGA
CACCAGGAAGGTTGAGCATTCCAGGAAAGCCCCGACCCACCCAGGAAACCCAAGTACCTGGTGGGGCCTCA
TCTGGCCCATTGTCCTGAAAGGACAGGAATAAAGGCTCTCTCCTCATGGCCACACACCCTAGGGACGTCCA
GCCTCCAGCTTTCTGTGGGTGGGGCAAATGACTGAGGAGGCTTCCCTCCCTGCAGGCGCCTCCCTCTGGGG
CCTCCTGTGGTCCAGTCGTCCCTGGTCCCCAGCTCTCAGGTGGGTCATAGGGCATCTCAGCAGGACCACCA
GGAAGAGCATCAGGAGGGGAAGGAGCCAGAGAGCCCTCCAGGCCAGTGCACTGCTAACTCAACATCTCATC
TTCCTATCTCGTCCCTTCTGCTCACCTCCGGAGACTCCCCCTCCCCTCTCATGCTCTTCACTGGCAGGTTA
TGATGGCCCAGAGATCCCCACCAGAGTCCCAGATATCAGTGGGGATCCCAGCCTATTCCT**TCTTAAGCAAG**
CTCGAAATTAACCCTCACTAAAGGGAACAAAAGCTGGTACCGGGCCCCCCCTCGAGGTCGAGACGGTATCG

C

CGTACGTCACAATATGATTATCTTTCTAGGGTTAATTCTAGTATACGCGTAGTTCTCCCTGAGCCTGTGGA
TACATGGAAAGAGAGCTTCACCACCACCCCCTTCTCTGAATATACATACAGGATCTGAGGAGGGAGGATTC
TGTGTGGATGCATGTGTGCACAGATGTGCATGTTTGTACGTGTGTATGGGTGAGCAGGTCATACGTGTGGT
CCCATGTGCCCACCTGTTGTATATATGCATGCTTGTTTTGTGTAAGTGAGCATAAGAGGTCAAGCCAGAGA
GAGAAATAGGAACAAGGAGAGACAGAGAGAGAGAGAATAGAAACAGAGACCAACAGGGAAACAGAATGAGA
CTGAGACAGAGAACAACAGAAGGCCAGACAGGTAGACAAGCCACAGTTCCATCTTCCCTGGTGCTGGCTGC
CAAGGCAGACAACTCTCCTCTCACTTCATTGATGTTCTGCCTGTGTTTATACCCATGATTGGGGTGGAGTT
CAGGAAAGGATGTATCAGGGCTAGGACGCCCCCACCTCCACACTCACAGGGCCAGTCAGGGCCCTCTGCAG
GGGCTGCCATTTCCTCAAGCTGAGGAATGGGCTTGGATCCCTCGGATGCCTTCCAGGGTGCAGGGGCGCTC
CCAGTGACTGGGCTCTTGTGGTGGCTGGGGAGGGGGAGCTCCTCTGACAGGCCCCATGCTGGGGGAAACGT
CCTGAGACTGACCTATCACGGGCTGACATGCACACCAAGGAGGTCTCACATCTGCTGGGAAATGAGGGGCT

Appendix A Figure 6. Sequenced PCR amplicons from U2OS Chr15 NHEJ 5. (A)
PCR amplicon sequence confirming the integration of NHEJ reporter DNA within the
pFlexible-LacO-pBLR5 construct **(B)** PCR amplicon sequence confirming the 5' end of
the pFlexible-LacO-pBLR5 integration site at the Chr15 locus. **(C)** PCR amplicon
sequence confirming the 3'end of the pFlexible-LacO-pBLR5 integration site at the
Chr15 locus. Sequence of the Chr15 locus is highlighted in grey, with the sequences used
to generate the homology arms of the pFlexible-LacO-pBLR5 donor vector shown in blue
(5' homology) or red (3' homology). pFlexible-LacO-pBLR5 sequence is shown in bold
text, and the CMV promoter of the NHEJ reporter in pink highlight.

Legend:

`Grey highlight` = Chr15 genomic sequence

`Blue text` = Sequence used for Chr15 5' homology template

`Red text` = Sequence used for Chr15 3' homology template

`Bold text` = pFlexible-LacO-pBLR5 sequence

`Pink highlight` = CMV Pro of NHEJ reporter

A

GGCCATGGTCGAAAACAAGGGAAATCACTCCCAATTAAAGCTCCCCCCCTCGAGGTCGAGACGGTATCGAT
GGCGCGGAATTCAAAAAGTTTAAACAAAAAAGGCGCTAATATTATTGAAGCATTTATCAGGGTTATTGTCT
CATGAGCGGATACATATTTGAATGTATTTAG<mark>TAGTAATCAATTACGGGGTCATTAGTTCATAGCCCATATA
TGGAGTTCCGCGTTACATAACTTACGGTAAATGGCCCGCCTGGCTGACCGCCCAACGACCCCCGCCCATTG
ACGTCAATAATGACGTATGTTCCCATAGTAACGACGTATGTTCCCATAGTA</mark>

B

GGGGCTCTAGCTCCTGCCCCAGCAGCGAAAGGGGCTCCTCCTTCTCTGGTGCCCAGTCCTAGCTCACCTGC
TCTTCACAAGCCTCCTCCCAGCACAGCCTGCACCACACAGGTGCTCAGTAAGGGGGTTGCTCTGAACAGGG
AGCAGGCCCACATGCTGAGAGTGGTGGAGGCGTGCAGGCTCTGATGACCACCTGAACCCAGACTCCAGGGC
AGGACAGGTCCTTACAGACCGTAAGGGCTTCCTGCCTACCCTCTTCCCATGCAGTTACCTCAACCCTGGGA
CACCAGGAAGGTTGAGCATTCCAGGAAAGCCCCGACCCACCCAGGAAACCCAAGTACCTGGTGGGGCCTCA
TCTGGCCCATTGTCCTGAAAGGACAGGAATAAAGGCTCTCTCCTCATGGCCACACACCCTAGGGACGTCCA
GCCTCCAGCTTTCTGTGGGTGGGGCAAATGACTGAGGAGGCTTCCCTCCCTGCAGGCGCCTCCCTCTGGGG
CCTCCTGTGGTCCAGTCGTCCCTGGTCCCCAGCTCTCAGGTGGGTCATAGGGCATCTCAGCAGGACCACCA
GGAAGAGCATCAGGAGGGGAAGGAGCCAGAGAGCCCTCCAGGCCAGTGCACTGCTAACTCAACATCTCATC
TTCCTATCTCGTCCCTTCTGCTCACCTCCGGAGACTCCCCCTCCCCTCTCATGCTCTTCACTGGCAGGTTA
TGATGGCCCAGAGATCCCCACCAGAGTCCCAGATATCAGTGGGGATCCCAGCCTATTCCT**TCTTAAGCAAG**
CTCGAAATTAACCCTCACTAAAGGGAACAAAAGCTGGTACCGGGCCCCCCC

C

ACGTCACAATATGATTATCTTTCTAGGGTTAATTCTAGTATACGCGTAGTTCTCCCTGAGCCTGTGGATAC
ATGGAAAGAGAGCTTCACCACCACCCCCTTCTCTGANTATACATACAGGATCTGAGGAGGGAGGATTCTGT
GTGGATGCATGTGTGCACAGATGTGCATGTTTGTACGTGTGTATGGGTGAGCAGGTCATACGTGTGGTCCC
ATGTGCCCACCTGTTGTATATATGCATGCTTGTTTTGTGTAAGTGAGCATAAGAGGTCAAGCCAGAGAGAG
AAATAGGAACAAGGAGAGACAGAGAGAGAGAGAATAGAAACAGAGACCAACAGGGAAACAGAATGAGACTG
AGACAGAGAACAACAGAAGGCCAGACAGGTAGACAAGCCACAGTTCCATCTTCCCTGGTGCTGGCTGCCAA
GGCAGACAACTCTCCTCTCACTTCATTGATGTTCTGCCTGTGTTTATACCCATGATTGGGGTGGAGTTCAG
GAAAGGATGTATCAGGGCTAGGACGCCCCCACCTCCACACTCACAGGGCCAGTCAGGGCCCTCTGCAGGGG
CTGCCATTTCCTCAAGCTGAGGAATGGGCTTGGATCCCTCGGATGCCTTCCAGGGTGCAGGGGCGCTCCCA
GTGACTGGGCTCTTGTGGTGGCTGGGGAGGGGGAGCTCCTCTGACAGGCCCCATGCTGGGGGAAACGTCCT
GAGACTGACCTATCACGGGCTGACATGCAC

Legend:
Grey highlight = TAP1 genomic sequence
Blue text = Sequence used for TAP1 5' homology template
Red text = Sequence used for TAP1 3' homology template
Bold text = pFlexible-LacO-pBLR5 sequence
Pink highlight = CMV Pro of HR reporter

A

TGGTCGAAAACAAGGGAAATCACTCCCAATTAAAGCTCCCCCCCTCGAGGTCGAGACGGTATCGATGGCGC
GGAATTCAAAAAAGGCGCTAATATTATTGAAGCATTTATCAGGGTTATTGTCTCATGAGCGGATACATATT
TGAATGTATTTAGTAGTAATCAATTACGGGGTCATTAGTTCATAGCCCATATATGGAGTTCCGCGTTACAT
AACTTACGGTAAATGGCCCGCCTGGCTGACCGCCCAACGACCCCCGCCCATTGACGTCAATAATGACGTAT
GTTCCCATAGTAACGACGTATGTTCCCATAGTAA

B

AGTACTGCTACTTCTCGCCGACTGGGTGCTGCTCCGGACCGCGCTGCCCCGCATATTCTCCCTGCTGGTGC
CCACCGCGCTGCCACTGCTCCGGGTCTGGGCGGTGGGCCTGAGCCGCTGGGCCGTGCTCTGGCTGGGGGCC
TGCGGGGTCCTCAGGGCAACGGTTGGCTCCAAGAGCGAAAAC**TCTTAAGCAAGCTCGAAATTAACC**

C

CACAATATGATTATCTTTCTAGGGTTAATTCTAGTATACGCGTACGAGAGCTGATCTCATGGGGAGCCCCC
GGGTCCGCGGATAGCACCAGGCTACTGCNCNGGGGAAGTCACCCTACCGCCTTCGTTGTCAGTTATGCAGC
GGCACTGCCCGCAGCAGCCCTGTGGCACAAACTCGGGAGCCTCTGGGTGCCCGGCGGTCAGGGCGGCTCTG
GAAACCCTGTGCGTCGGCTTCTAGGCTGCCTGGGCTCGGAGACGCGCCGCCTCTCGCTGTTCCTGGTCCTG
GTGGTCCTCTCCTCTCTTGGTAAGGGGAACGCAGGGCAAGAGGGGAGGACACAAGGGG

Appendix A Figure 7. Sequenced PCR amplicons from U2OS TAP HR 6. (A) PCR
amplicon sequence confirming the integration of HR reporter DNA within the pFlexible-
LacO-pBLR5 construct **(B)** PCR amplicon sequence confirming the 5' end of the
pFlexible-LacO-pBLR5 integration site at the TAP1 locus. **(C)** PCR amplicon sequence
confirming the 3'end of the pFlexible-LacO-pBLR5 integration site at the TAP1 locus.
Sequence of the TAP1 locus is highlighted in grey, with the sequences used to generate
the homology arms of the pFlexible-LacO-pBLR5 donor vector shown in blue (5'
homology) or red (3' homology). pFlexible-LacO-pBLR5 sequence is shown in bold text,
and the CMV promoter of the HR reporter in pink highlight.

Legend:

`Grey highlight` = TAP1 genomic sequence

`Blue text` = Sequence used for TAP1 5' homology template

`Red text` = Sequence used for TAP1 3' homology template

`Bold text` = pFlexible-LacO-pBLR5 sequence

`Pink highlight` = CMV Pro of NHEJ reporter

A

CATGGTCGAAAACAAGGGAAATCACTCCCAATTAAAGCTCCCCCCCCTCGAGGTCGAGACGGTATCGATGGC
GCGGAATTCAAAAAGTTTAAACAAAAAAGGCGCTAATATTATTGAAGCATTTATCAGGGTTATTGTCTCAT
GAGCGGATACATATTTGAATGTATTTAG`TAGTAATCAATTACGGGGTCATTAGTTCATAGCCCATATATGG`
`AGTTCCGCGTTACATAACTTACGGTAAATGGCCCGCCTGGCTGACCGCCCAACGACCCCCGCCCATTGACG`
`TCAATAATGACGTATGTTCCCATAGTAACGACGTATGTTCCCATAG`

B

`GCTACT`**`TCTCGCCGACTGGGTGCTGCTCCGGACCGCGCTGCCCCGCATATTCTCCCTGCTGGTGCCCACCG`**
`CGCTGCCCACTGCTCCGGGTCTGGGCGGTGGGCCTGAGCCGCTGGGCCGTGCTCTGGCTGGGGGCCTGCGGG`
`GTCCTCAGGGCAACGGTTGGCTCCAAGAGCGAAAAC`**TCTTAAGCAAGCTCGAAATTAACC**

C

GATTATCTTTCTAGGGTTAATTCTAGTATACGCGTAC`GAGAGCTGATCTCATGGGGAGCCCCCGGGTCCGC`
`GGATAGCACCAGGCTACTGCNCNGGGGGAAGTCACCCTACCGCCTTCGTTGTCAGTTATGCAGCGGCACTGC`
`CCGCAGCAGCCCTGTGGCACAAACTCGGGAGCCTCTGGGTGCCCGGCGGTCAGGGCGGCTCTGGAAACCCT`
`GTGCGTCGGCTT`CTAGGCTGCCTGGGCTCGGAGACGCGCCGCCTCTCGCTGTTCCTGGTCCTGGTGGTCCT
CTCCTCTCTTGGTAAGGGGAACGCAGGGCAAGAGGGGAGGACACAAGGGGACTGGGACAGGAATCAA

Appendix Figure 8. Sequenced PCR amplicons from U2OS TAP NHEJ 4. (A) PCR
amplicon sequence confirming the integration of NHEJ reporter DNA within the
pFlexible-LacO-pBLR5 construct **(B)** PCR amplicon sequence confirming the 5' end of
the pFlexible-LacO-pBLR5 integration site at the TAP1 locus. **(C)** PCR amplicon
sequence confirming the 3'end of the pFlexible-LacO-pBLR5 integration site at the
TAP1 locus. Sequence of the TAP1 locus is highlighted in grey, with the sequences used
to generate the homology arms of the pFlexible-LacO-pBLR5 donor vector shown in blue
(5' homology) or red (3' homology). pFlexible-LacO-pBLR5 sequence is shown in bold
text, and the CMV promoter of the NHEJ reporter in pink highlight.

APPENDIX B: Copyright Agreements

Taylor & Francis
Taylor & Francis Group

Permissions

7/6/2016

Kathleen M Attwood
Dalhousie University
5850 College Street
Halifax B3H 4R2
Canada
kattwood@dal.ca

Dear Ms. Attwood,

We are in receipt of your request to reproduce Figure 8 and Figure 9 from your Open Access article

> Christi Andrin, Darin McDonald, Kathleen M. Attwood et al (2012)
> A requirement for polymerized actin in DNA double-strand break repair
> *Nucleus* 3 (4): 384-395.
> DOI: 10.4161/nucl.21055

For use in your dissertation

Permission is granted for print and electronic use.

We will be pleased to grant you permission free of charge on the condition that:

This permission is for non-exclusive English world rights.

This permission does not cover any third party copyrighted work which may appear in the material requested.

Full acknowledgment must be included showing article title, author, and full Journal title, reprinted by permission Taylor & Francis LLC, (http://www.tandfonline.com).

Thank you very much for your interest in Taylor & Francis publications. Should you have any questions or require further assistance, please feel free to contact me directly.

Sincerely,

Mary Ann Muller

Permissions Coordinator

E-mail: maryann.muller@taylorandfrancis.com

Telephone: 215.606.4334

Genes & Development

From:	Kathleen Attwood <KAttwood@Dal.Ca>
Sent:	Tuesday, June 28, 2016 9:26 AM
To:	Genes & Development
Subject:	Copyright agreement request

Good morning,

I'm am a doctoral student requesting copyright permission to include a manuscript in my thesis. While I understand you provide this permission as indicated on your website, my institution requires official documentation prior to final thesis submission. Would you be so kind to provide me with written notice of permission for the following document:

Nuclear position dictates DNA repair pathway choice
28(22):2450-2463 doi:10.11011gad.248369.114

Sincerely,

Kathleen Attwood, B.Sc.
PhD Candidate
Dalhousie University
Sir Charles Tupper Medical Building
5850 College St, Rm 11G1

1

Nuclear position dictates DNA repair pathway choice

- Charlène Lemaître,
- Anastazja Grabarz,
- Katerina Tsouroula,
- Leonid Andronov,
- Audrey Furst,
- Tibor Pankotai,
- Vincent Heyer,
- Mélanie Rogier,
- Kathleen M. Attwood,
- Pascal Kessler,
- Graham Dellaire,
- Bruno Klaholz,
- Bernardo Reina-San-Martin,
- and Evi Soutoglou

Re: Copyright agreement request

Frontiers Editorial Office <editorial.office@frontiersin.org>

Mon 2016-06-27 11:01 AM

To: Kathleen Attwood <KAttwood@Dal.Ca>;

Dear Ms Attwood,

Thank you for your email.

Under the Frontiers Terms and Conditions, authors retain the copyright to their work. Furthermore, all Frontiers articles are Open Access and distributed under the terms of the Creative Commons Attribution License (CC-BY 3,0), which permits the use, distribution and reproduction of material from published articles, provided the original authors and source are credited, and subject to any copyright notices concerning any third-party content.

You can therefore freely reuse an article published at Frontiers without having to ask for permission. More information about CC-BY can be found here: http://creativecommons.org/licenses/by/4.0/

Please also make sure to properly acknowledge, in your manuscript, the original authors and source of the figures that you intend to reproduce.

We recommend to use the format below:
"As originally published in Pinder JB, Attwood KM and Dellaire G (2013) Reading, writing, and repair: the role of ubiquitin and the ubiquitin-like proteins in DNA damage signaling and repair. Front. Genet. 4:45. doi: 10.3389/fgene.2013.00045".

Please let me know if you have any other questions.

Kind Regards,

Damaris

Damaris Critchlow
Editorial Operations Specialist

Frontiers | London Office
www.frontiersin.org
WeWork, 1 Fore St
London, UK
Office T +44(0)7934464749

Registered in England (number 9952345)
Registered Office: Munro House, Portsmouth Road, Cobham, Surrey KT11 1PP, United Kingdom
Directors: Kamila Markram, Roger Biggs, Michael Kenyon

Loop | Twitter | Facebook